

Deciphering the BH3 code for the neutralization of pro-survival Bcl-2 proteins in membranes

Dissertation

der Mathematisch-Naturwissenschaftlichen Fakultät

der Eberhard Karls Universität Tübingen

zur Erlangung des Grades eines

Doktors der Naturwissenschaften

(Dr. rer. nat.)

vorgelegt von

Kushal Kumar Das

aus Purnea, India

Tübingen

2017

Gedruckt mit Genehmigung der Mathematisch-Naturwissenschaftlichen Fakultät der Eberhard Karls Universität Tübingen.

Tag der mündlichen Qualifikation:

12.04.2018

Dekan:

Prof. Dr. Wolfgang Rosenstiel

1. Berichterstatter:

Prof. Dr. Ana J. García Sáez

2. Berichterstatter:

Prof. Dr. Erik Schäffer

Summary

The proteins of Bcl-2 family, the pro-survival and the pro-apoptotic tightly regulates the process of apoptosis. The pro-survival proteins show a specific interaction pattern with BH3 domain of BH3 only proteins, determining the cellular fate during apoptotic stress. This interaction specificity is pivotal in designing BH3 mimetics, a class of anticancer drug molecules based on the BH3 domain of BH3 only proteins showing promising results in clinical trials. The role of the mitochondrial outer membrane in exhibiting Bcl2 complex interactome is extensively studied recently. Overall most studies addressed so far on the interactions of BH3 peptides and the truncated Bcl-2 proteins are reported in the solution / cytosolic environment while the quantitative interactions in membranes are still missing. To tackle this, we systematically quantified the library of BH3 peptides using two-color fluorescence correlation spectroscopy in solution and in the model membrane. We further extended our investigations to isolated yeast mitochondria using ensemble FRET and in mammalian cancer cell lines using a high throughput screening called BH3 profiling. We show that BH3 peptides derived from Hrk and Bim are the most effective in disrupting cBid/Bcl-xL complexes, which correlates with their response in mitochondria and in cells.

Moreover, to understand the activation process of pro-apoptotic effector protein Bax on membranes, we designed an *in-vitro* system to investigate its autoactivation by the recruitment of inactive cytosolic Bax molecules by active membrane-bound Bax. Furthermore, *in vitro* studies also showed active membrane-bound Bax recruits Bcl-xL to the membrane, which retrotranslocates active Bax back into the cytosol, thereby maintaining membrane integrity. Quantitative analysis showed that Bax retrotranslocation activity potentiates Bcl-xL antiapoptotic activity by at least 10 fold.

Overall, these findings highlights the importance of the membrane in Bcl-2 family interactions and thereby screening peptides that can disrupt specific interactions of these proteins in the membrane and can improve cancer therapies.

Zusammenfassung

Der mitochondriale Apoptosesignalweg wird durch die anti- und pro-apoptotischen Vertreter der Bcl-2 Proteinfamilie kontrolliert. Die anti-apoptotischen Proteine spielen eine zentrale Rolle, in dem sie durch die selektive Interaktion mit der BH3 Domäne der BH3-only Proteinen den apoptotischen Prozess regulieren. Basierend auf dieser Interaktion und der BH3 Domäne werden BH3-Mimetika, eine Gruppe von anti-Krebs Medikamenten, entworfen. BH3-Mimetika zeigen in klinischen Studien eine signifikante Aktivierung von Apoptose, indem sie diese Interaktion stören. Der Einfluss der äußeren Mitochondrienmembran auf die Interaktion der Bcl-2 Proteinen wird zur Zeit detailliert untersucht. Bisher wurde ausschließlich die Interaktion der BH3 Peptiden mit den verkürzten Formen der Bcl-2 Proteinen nur in Lösung und im Zytoplasma untersucht, während quantitative Interaktionen in Membranen komplett außer Acht gelassen wurden. Um diese Fragestellung anzugehen, haben wir systematisch die Interaktion bestehender BH3 Peptiden mit Hilfe der zwei Farben Fluoreszenz-Korrelations- Spektroskopie, sowohl in Lösung als auch in Modell Membranen, quantifiziert. Wir erweiterten unsere Untersuchungen auf isolierte Hefe Mitochondrien mit Hilfe der FRET Analyse und auf Säugetier Krebszelllinien mit Hilfe des Hochdurchsatz-Screenings BH3 Profiling. Wir zeigen, dass die BH3 Peptide, die von Hrk und Bim abgeleitet wurden, die effektivsten in der Störung des cBid / Bcl-xL Komplexes seien. Diese Daten spiegeln die Antwort in Mitochondrien und in Zellen wieder.

Um den Aktivierungsprozess des pro-apoptotischen Effektorproteins Bax an Membranen zu verstehen, haben wir ein *in-vitro* Assay entwickelt, das erlaubt, die Autoaktivierung von Bax zu untersuchen. Das aktive, membrangebundene Bax rekrutiert dabei das inaktive, zytoplasmatische Bax zu der Membran. Des Weiteren haben *in-vitro* Analysen gezeigt, dass membrangebundenes Bax, Bcl-xL zu der Membran rekrutiert. Bcl-xL retrotransloziert aktives, nicht oligomerisiertes Bax zurück in das Zytoplasma, um die Membranintegrität aufrecht zu erhalten. Quantitative Analysen zeigen, dass die Bax-retrotranslokationsaktivität die anti-apoptotische Bcl-xL-Aktivität um mindestens das 10fache verstärkt.

Unsere Ergebnisse zeigen die Wichtigkeit der Membran für die Interaktion der Bcl-2 Proteinen auf, deshalb ist das Screening von Peptiden, die die Interaktion dieser Proteine an der Membran stört von großer Bedeutung für die Krebstherapie.

Acknowledgements

My deep gratitude goes first to my supervisor, Prof. Dr. Ana J. Garcia Saez. Her support throughout these four years kept me going. She has been a perfect mentor to give freedom to think outside the box. Her suggestions both in PhD and in future career choices were invaluable.

I thank all my lab colleagues for creating an amazing working and chill environment in the lab and outside. As such, I would like to thank Dr. John Danial for every scientific and non-scientific discussions in lab and outside lab when I was down. I would like to extend my gratitude to Dr. Katia Cosentino, Dr. Begona Ugarte and Dr. Uris Ros for always being there for help anytime whenever needed and also being very kind in everything. I also thank Dr. Joseph Unsay for helping me with FCS and other technical microscopy stuff. I would deeply express my thanks to Fabronia Murad for everything from A to Z. She has been really a great working colleague sitting behind me and having non-scientific discussions in a scientific way. I also thank Aida for being a super nice helping colleague since the time we joined the IMPRS program together. Caro has been really supportive with all the technical and administrative help since my arrival to Tuebingen. I thank Vanessa and Raed for all their help and support. I extend my thanks to Rodrigo and Rafael for all their help. My journey to a PhD would not have been possible without amigos in Tuebingen and around the globe. I extend my thanks to all my drinking partners to sit and share happy and sad things. A lot happened during my PhD tenure and now it will all be a memory for lifetime. I thank Julien, Prateek, Francesco, Gosia, Aaron, Praful and many other fellas for wonderful time outside the lab. I extend my thanks to Diana for being there always during my good and bad days and motivating me to be better. Last but never the least, I thank my parents and family members for all their blessings and support throughout this journey.

Contents

Contents	1
List of Figures	3
List of Abbreviations	4
Part 1	5
Introduction	5
1.1 Apoptosis	6
1.2 Bcl-2 Family	6
1.2.1 Members of Bcl-2 family	7
1.2.2 Bcl-xL	8
1.2.3 BID	10
1.2.4 Bax	11
1.3 BH3 mimetics	12
1.4 BH3 profiling	13
1.5 Fluorescence Correlation Spectroscopy (FCS)	14
Part 2	16
Objectives	16
Part 3	18
Results	18
Chapter 1: Comparing the activity of BH3 peptides and BH3 mimetics with pro-survival Bcl-xL in solution and in the membrane environment, and its role on Bax activation to promote apoptosis.	19
Chapter 2: (Manuscript under Preparation) Optimization of BH3 peptides for increased activity in the membrane compartment.	20
Chapter 3: Understanding a minimal Bcl-2 interaction network (cBid, Bax, and Bcl-xL) in solution and in membranes using fluorescence cross-correlation spectroscopy and confocal imaging.	25
Chapter 4: How the shuttling of Bcl-2 family species between membrane and cytosol (solution) regulates MOMP sensitivity, and how BH3 peptides synergizes the activator BH3 only proteins for MOMP.	26
Chapter 5: Studying the interaction network of a new pro-apoptotic member of Bcl-2 family Bok with cBid and Bcl-xL. Further, characterizing the BH3 only activator Bim and its binding	

interactions in solution and on the membrane in the presence or absence of dynein light chain 1 (DLC-1).	27
Part 4	28
Discussion and Outlook	28
BIBLIOGRAPHY	34
PUBLICATIONS	42

List of Figures

1.1	Classification of Bcl-2 family proteins based on the Bcl-2 homology domains	7
1.2	Models of Bcl-2 family activation	9
1.3	Schematic of Bcl-xL conformation in soluble and membrane-bound forms	10
1.4	Structure of Bax on membrane	12
1.5	Principle of FCS	14
1.6	Principle of Scanning FCS	15
3.1	Full length Bcl-xL and Bcl-xL Δ C interaction with activator cBid	20
3.2	The sequence of BH3 peptides of BH3 only proteins	21
3.3	Quantitative analysis of the inhibitory activity of mutant BH3 peptides in solution	21
3.4	Quantitative analysis of the inhibitory activity of mutant BH3 peptides on membranes	22
3.5	Quantitative analysis of the inhibitory activity of mutant BH3 peptides in isolated mitochondria from yeast	23
3.6	BH3 profiling of mutant peptides in HCT116 WT cells	24
3.7	BH3 profiling of mutant peptides with and w/o His Tag in HCT116 WT cells	25

List of Abbreviations

2D	two dimensional
3D	three dimensional
Bak	Bcl-2 homologous antagonist killer
Bax	Bcl-2 associated protein X
Bcl-2	B-cell lymphoma 2
Bcl-xL	B-cell lymphoma extra large
BH	Bcl-2 homology domain
Bid	BH3 interacting domain death agonist
cBid	Cleaved Bid
cyt c	Cytochrome c
DISC	Death inducing silencing complex
DLC-1	Dynein light chain 1
FCS	Fluorescence Correlation Spectroscopy
FCCS	Fluorescence Cross Correlation Spectroscopy
FRET	Föster Resonance Energy Transfer
GUV	Giant Unilamellar Vesicles
LUV	Large Unilamellar Vesicles
MOM	Mitochondrial outer membrane
MOMP	Mitochondrial outer membrane permeabilization
PIE	Pulsed Interleaved Excitation
SFCS	Scanning Fluorescence Correlation Spectroscopy
tBid	truncated Bid
TNF	Tumor necrosis factor

Part 1

Introduction

1.1 Apoptosis

Apoptosis is a programmed form of cellular death that plays a central role in various biological processes from development to immunity and tissue homeostasis. Alterations in the apoptotic pathway lead to many diseases such as cancer (Lowe & Lin, 2000; Wyllie et al., 1999) and neurodegeneration (Mattson, 2000). Apoptotic cell death is characterized by DNA fragmentation, blebbing of the plasma membrane, formation of apoptotic bodies and plasma membrane lipid rearrangements with phosphatidyl serine exposure to the outer leaflet (Edinger & Thompson, 2004; Taylor, Cullen, & Martin, 2008). The major executioners of apoptosis are the caspases (cysteine-aspartic acid specific proteases) (Edinger & Thompson, 2004; Taylor et al., 2008)), further divided into initiator caspases (caspase 8 and 9) and executioner caspases (caspase 3, 6 and 7).

There are two major pathways of apoptosis. The extrinsic pathway and the intrinsic pathway of apoptosis. Briefly, the extrinsic pathway of apoptosis receives external signals upon binding of FasL or TNF α to death receptors to promote apoptosis, which is followed by the oligomerization of the death receptors in the plasma membrane forming a death-inducing signaling complex (DISC) that further activates caspase 8 and downstream executioner caspases.

The intrinsic or the mitochondrial pathway of apoptosis responds to internal cellular stress or damage. The Bcl-2 family of proteins form a complex interaction network that regulates the intrinsic apoptotic pathway leading to the release of apoptotic factors like cytochrome c, Smac etc. from mitochondria, which further triggers the downstream cascade of apoptosis.

1.2 Bcl-2 Family

Bcl-2 (B-cell lymphoma 2) was first characterized in follicular lymphoma as a proto-oncogene marked by chromosomal translocation t (14;18) (Tsujiimoto, Finger, Yunis, Nowell, & Croce, 1984). The Bcl-2 gene produces the Bcl-2 protein, which promotes cellular survival rather than proliferation (Cory, Huang, & Adams, 2003). Homologous proteins were later discovered and comprise the Bcl-2 family of proteins. Presently, there are more than 20 members of the Bcl-2 family of proteins, which have opposing functions and decide the fate of the cells to live or die.

1.2.1 Members of Bcl-2 family

The proteins of this family are divided into three groups based on the functions and the Bcl-2 homology domains (BH domains) they possess (Cory et al., 2003), (Adams, 1998; Gross, McDonnell, & Korsmeyer, 1999) .

1. The pro-survival or anti-apoptotic proteins like Bcl-xL, Bcl-2, Mcl-1, A-1 inhibit the process of apoptosis by sequestering pro-apoptotic effectors or BH3 only proteins, thus promoting survival.
2. The pro-apoptotic effectors like Bax, Bak, and recently Bok, are believed to form pores on the mitochondrial outer membrane (MOM) releasing apoptotic factors thereby activating the downstream cascade of caspases leading to apoptosis.
3. The pro-apoptotic Bh3 only proteins include the sensitizers (Hrk, Bad, Bik, etc.) that inhibit the anti-apoptotic members and the activators (Bim, Bid, etc.), which also directly activate the effectors.

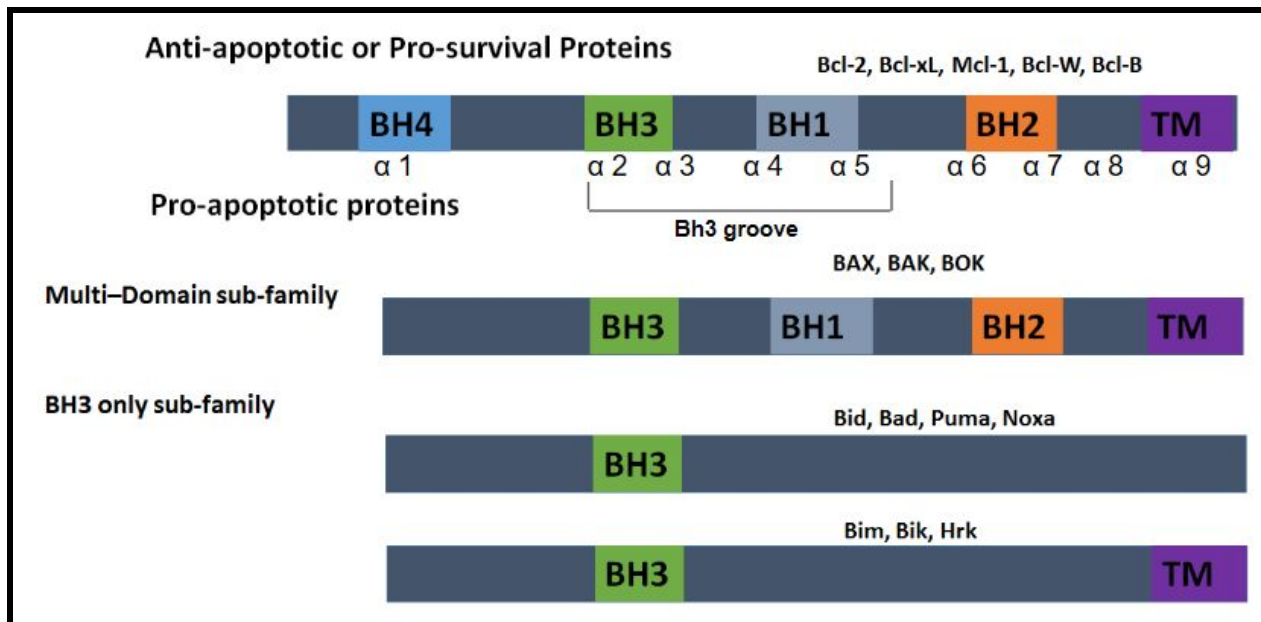


Fig.1.1: Classification of Bcl-2 family based on the Bcl-2 homology domains (BH domains). Anti-apoptotic members are composed of multiple BH domains and inhibit the process of apoptosis. Pro-apoptotic members are divided into multidomain effectors responsible for forming mitochondrial outer membrane pores and the BH3 only proteins as activators/ sensitizers either activating the effectors directly and/or binding to the anti-apoptotic proteins and liberating effectors. Adapted from (Das, Unsay, & Garcia-Saez, 2015) with permission from Elsevier.

The interactions among this Bcl-2 family network are intricate and several models have been proposed to explain the event of mitochondrial outer membrane permeabilization (MOMP) (Chipuk & Green, 2008; Czabotar, Lessene, Strasser, & Adams, 2013).

1. The direct activation model activates effector Bax/Bak by direct activator BH3-only proteins in order to promote MOMP (Kuwana et al., 2002; Wei et al., 2000).
2. The indirect “displacement model” the Bh3 only proteins sequester the anti-apoptotic proteins thereby liberating constitutively active Bax/Bak and inducing MOMP (Willis, 2005; Willis et al., 2007).
3. The embedded together model combines the direct and indirect activation model in presence of the membrane. This model introduces the role of membrane induced conformational changes in Bcl-2 family proteins (Leber, Lin, & Andrews, 2007; Lovell et al., 2008). This model is one of the most widely accepted models presently as shown in the figure below.
4. The unified model is an extension of the embedded together model and distinguishes the preference of interaction of anti-apoptotic members either with activator BH3 only or effector proteins (Llambi et al., 2011).

1.2.2 Bcl-xL

Bcl-xL is a prosurvival protein that promotes cellular survival by sequestering the proapoptotic proteins. Its overexpression has been reported to be linked with various forms of carcinomas, like breast cancers (España et al., 2004), colorectal cancers (Scherr et al., 2016), hepatocellular (Watanabe et al., 2002), renal (Gobé, Rubin, Williams, Sawczuk, & Buttyan, 2002), pancreatic cancers (Ghaneh, Kawesha, Evans, & Neoptolemos, 2002) and many others. Bcl-xL is believed to shuttle between soluble and membrane-bound conformations between the cytosol and the mitochondrial outer membrane, thus existing in dynamic equilibrium in healthy cells (Edlich et al., 2011). The soluble structure of Bcl-xL has eight alpha helices and a transmembrane helix (Petros, Olejniczak, & Fesik, 2004). Most of the X-ray crystal and NMR structure of Bcl-xL included the inactive form of the protein lacking its C-terminal transmembrane region. The water-soluble structure of full-length Bcl-xL is predicted to have the putative transmembrane helix residing in the BH3 binding groove formed by helices α -2, α -3 and α -4. During its shuttling to the membrane either induced by stress or cBid, Bcl-xL undergoes a conformational change in which the transmembrane helix is believed to be displaced from the BH3 binding pocket and finally insert to the membrane. Recent studies by Yao and colleagues (Yao et al., 2015) (Yao et al., 2016) using NMR and ITC on detergent-free lipid nanodiscs showed the conformational states of Bcl-xL protein differing in their C-terminus.

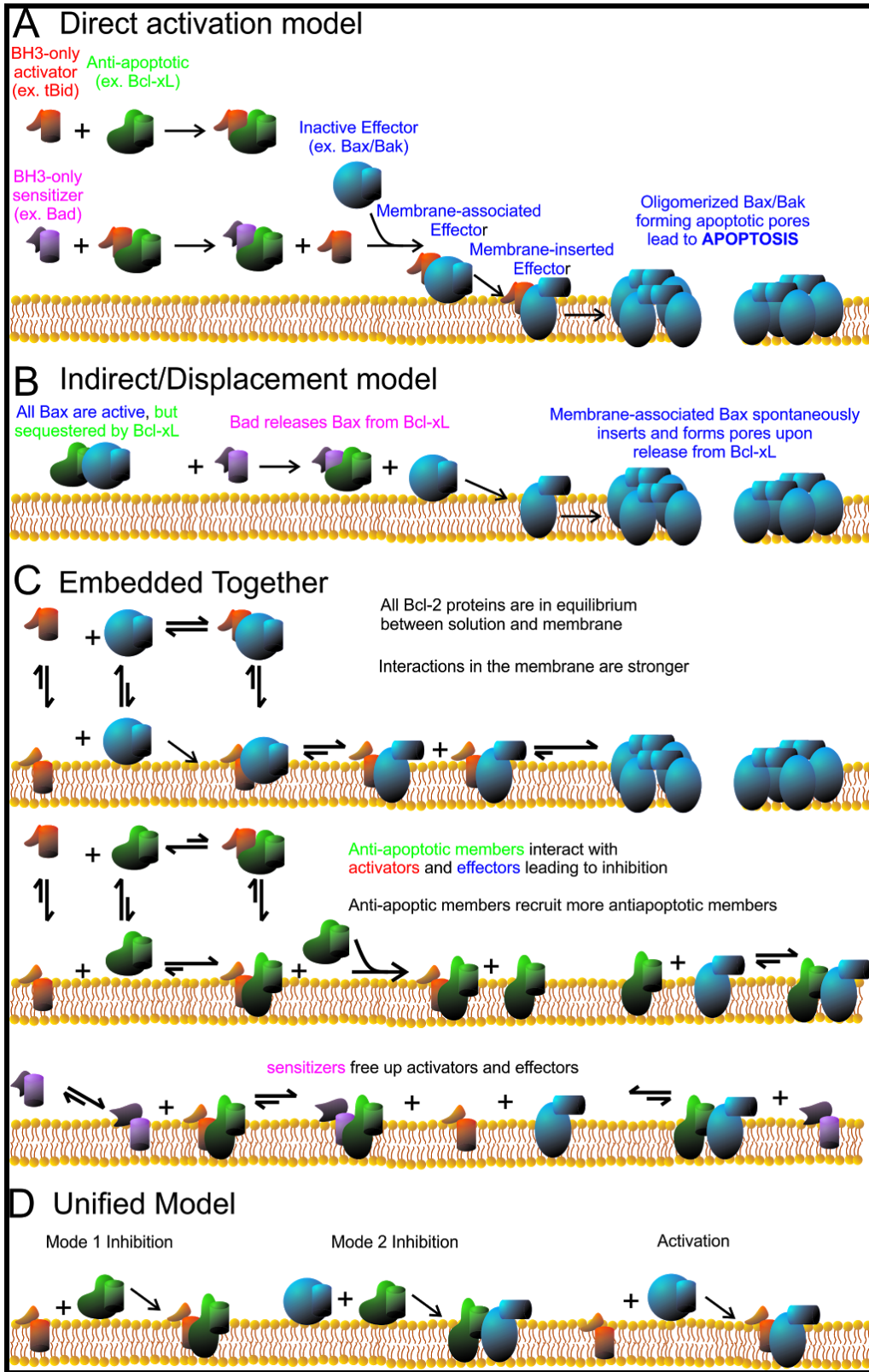


Fig.1.2 Models of Bcl-2 family activation. A) In the direct activation model, the effector proteins Bax/Bak are activated directly with tBid, which then oligomerize and cause MOMP. B) The Bh3 only

proteins sensitizers displace the sequestered active Bax/Bak from the anti-apoptotic proteins and causes MOMP. C) The embedded together model combines the direct and indirect activation models and presents the role of membrane in the conformational change of Bcl-2 proteins. D) The unified model distinguishes the preference of interaction of anti-apoptotic proteins with activators (Mode 1) and effectors (Mode 2). Reproduced from (Das et al. 2015) with permission from Elsevier.

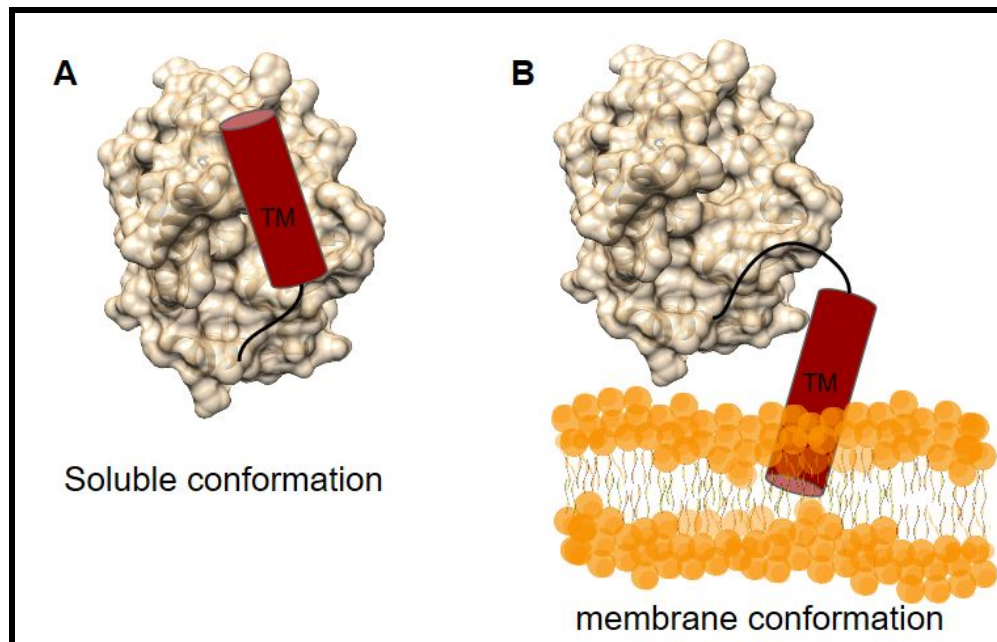


Fig.1.3 Schematic of Bcl-xL structure in soluble and membrane bound forms. A) The transmembrane helix is located in the BH3 binding groove. B) In membrane environment the transmembrane helix inserts into the membrane and thereby the protein becomes membrane bound.

Recent studies have also shown that the conformation of the soluble domain of Bcl-xL doesn't change significantly upon integration with lipid nanodiscs (Hill, Blake Hill, MacKenzie, & Harwig, 2015). Until now the most valid explanation for Bcl-xL membrane localization was the displacement of the transmembrane helix by the BH3 only activators and sensitizers, thus shifting the equilibrium from a soluble to a membrane-bound state.

1.2.3 Bid

Full-length inactive Bid (22 kDa) is activated by caspase 8 cleavage into a p7 fragment and a p15 fragment (truncated Bid, tBid) (Shamas-Din et al., 2013) (Leber, Geng, Kale, & Andrews, 2010). The p7 fragment together with the p15 fragment forms a stable complex in solution known as cBid (cleaved Bid 22 kDa) (Bleicken, García-Sáez, Conte, & Bordignon, 2012). In presence of membranes, the p7 fragment dissociates and the

active membrane-binding p15 fragment tBid is bound to the membrane and in turn activates effectors Bax/Bak to promote mitochondrial outer membrane permeabilization (Kuwana et al., 2002).

Recent kinetic studies have shown tBid as a potent activator of Bax without a lag phase compared to cBid, which causes membrane permeabilization in presence of Bax with a lag phase (Shamas-Din et al., 2013). The translocation of cytosolic Bcl-xL and Bax to the membrane also requires cBid/tBid (García-Sáez, Ries, Orzáez, Pérez-Payà, & Schwille, 2009). Quantitative interaction studies have shown their interactions to be weaker in solution compared to those on the membrane (García-Sáez et al., 2009) (Shamas-Din et al., 2013). Work by (Shamas-Din et al., 2013) showed that tBid undergoes multiple conformational changes upon insertion into the membrane, exposing its BH3 domain for interaction with pro- or anti-apoptotic proteins.

1.2.4 Bax

Cytosolic inactive Bax is a monomeric protein of 21 kDa and has a globular conformation with nine alpha helices. In its cytosolic inactive state the $\alpha 9$ C-terminal rests in the hydrophobic groove and, following its activation under stress or BH3 only proteins, cytosolic Bax undergoes a major conformational change from globular to extended membrane inserted conformation (Leber et al., 2007; Lovell et al., 2008), (Gavathiotis, Reyna, Davis, Bird, & Walensky, 2010), (Kim et al., 2009) (Cosentino & García-Sáez, 2017). The helices $\alpha 5$, $\alpha 6$, and $\alpha 9$ interact with the outer mitochondrial membrane during its active form (Bleicken et al., 2010; García-Sáez, Mingarro, Pérez-Payá, & Salgado, 2004). The assembly of Bax into the membrane is under debate and opposing views of symmetric dimers (Bleicken et al., 2014) (Kim et al., 2009) (Bleicken et al., 2014) and asymmetric dimers exist (Gavathiotis et al., 2010). Due to its resemblance to cytolytic toxins, (Annis et al., 2005) proposed the "Umbrella model" for Bax membrane insertion, where helices $\alpha 5$ and $\alpha 6$ form a transmembrane hairpin and other helices lie on the surface of the mitochondrial outer membrane in an umbrella-like configuration. Recently, the umbrella model was challenged by structural models of active Bax that showed the presence of a dimerization domain composed by helices $\alpha (2 - 5)$, whereas the helices $\alpha (6 - 9)$ form the piercing domain which destabilizes the membrane (Bleicken et al., 2014), (Annis et al., 2005; Czabotar, Westphal, et al., 2013). The resulting "clamp-like conformational model" (Bleicken et al., 2014) includes a partially open conformation formed by helices $\alpha 5$ and $\alpha 6$. Single molecule studies on Bax using supported lipid bilayers provided evidence of Bax oligomerization, showing that Bax first inserts as a monomer and rapidly oligomerizes into different species like dimers, tetramers, and hexamers (Subburaj et al., 2015). Super-resolution single molecule localization microscopy (SMLM) on active Bax on mitochondria of apoptotic cells showed Bax to

assemble into various nonrandom architectures including rings, arcs, lines, aggregates and dots (Salvador-Gallego et al., 2016).

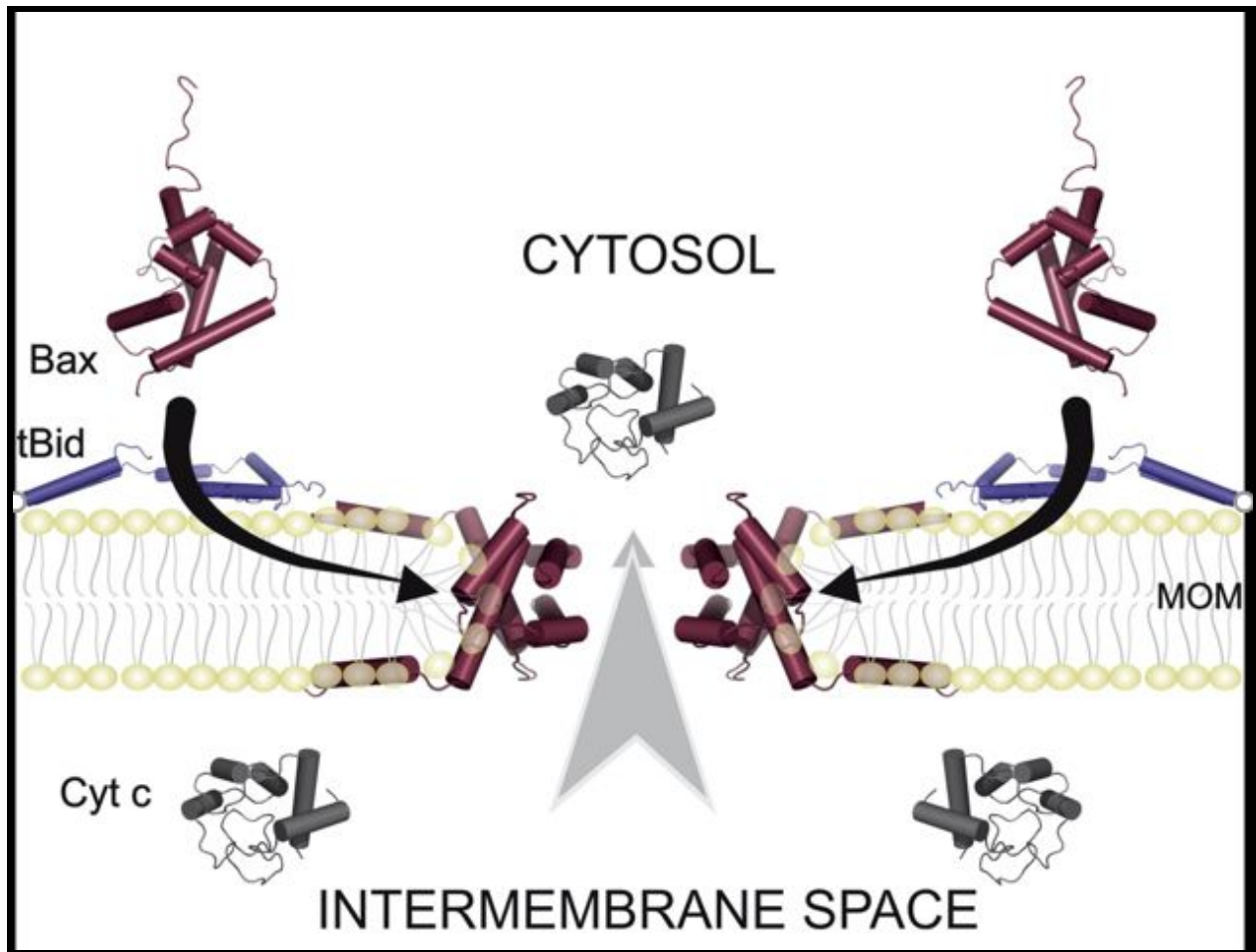


Fig.1.4 Structure of Bax on membrane. Bleicken et.al proposed the membrane embedded clamp like model of Bax dimers using DEER (double electron-electron spectroscopy). Reproduced from (Bleicken et al. 2014) with permission from Elsevier.

1.3 BH3 mimetics

BH3 mimetic compounds and BH3 peptides are derived from the BH3 domain of the BH3-only proteins, usually of 26 amino acids length, which is believed to antagonize the prosurvival proteins thereby inducing the process of apoptosis. The small molecule BH3 mimetics are modelled based on the BH3 domain of BH3 only proteins binding to the hydrophobic pocket of prosurvival proteins, thereby inhibiting their anti-apoptotic activity

(Baell & Huang, 2002; Lessene, Czabotar, & Colman, 2008; Ni Chonghaile & Letai, 2008). (Baell & Huang, 2002; Lessene et al., 2008), the proposed general rule of thumb for authentic BH3 mimetics: "high-affinity binding to targets (nM range) and induction of Bax/ Bak-dependent apoptosis". Work by the group of Letai et al showed that BH3 domain peptides of Bid and Bim are capable of inducing Bax/Bak oligomerization directly to induce cell death, whereas peptides derived from Bad and Bik could only displaced Bid from the hydrophobic cleft of anti-apoptotic proteins thereby activating Bax/Bak (Certo et al., 2006; Chen et al., 2005; Letai et al., 2002). Various quantitative studies of BH3 peptides in solution have been reported (Certo et al., 2006; Letai et al., 2002), (Certo et al., 2006; Chen et al., 2005; Letai et al., 2002)(Certo et al., 2006; Letai et al., 2002). Peptides derived from Bim and Puma have strong affinity (low nM) for all pro-survival proteins, while Hrk was specific to Bcl-xL, Noxa interacted with Mcl-1 and A1, and Bad bound to Bcl-2, Bcl-xL and Bcl-w but not A-1 nor Mcl-1. Work from Walensky et al. showed the use of hydrocarbon stapled BID BH3 domain peptides, which significantly improves the α -helical propensity of the molecules, as well as cellular penetrance and cellular stability from proteases, thereby improving drastically their biological activity (Walensky et al., 2006; Walensky & Bird, 2014). Bad like BH3 mimetics like ABT 737 and its orally available form ABT 263 (navitoclax) binds to Bcl-2, Bcl-xL and Bcl-w have shown promising results in clinical trials (Tse et al., 2008). Recently, a small molecule inhibitor targeting the Bcl-xL groove, WEHI 539, is under clinical trials for its high specificity and potency to Bcl-xL (Lessene et al., 2013). Inhibitors of Mcl-1 and A-1 are less explored compared to other pro-survival proteins. Recent work on a Mcl-1 inhibitor, BH3 mimetic S63845, showed promising results in diverse cancer models in preclinical studies (Kotschy et al., 2016).

1.4 BH3 profiling

BH3 profiling is a high throughput functional assay of MOMP that uses the peptides derived from the BH3 domain of Bcl-2 family proteins to induce cell death. The Letai laboratory developed this profiling assay which involves three basic steps: Generating the plate with different peptides, adding the cells of interest to expose them to the peptides and finally measuring MOMP by quantifying mitochondrial depolarization (Certo et al., 2006; Ryan & Letai, 2013). For the profiling assay, JC-1 dye is used as mitochondrial membrane potential indicator. When the mitochondria are polarised, JC-1 aggregates in the matrix of the mitochondria and emits red fluorescence. Once the polarization of mitochondria is lost due to MOMP, the change or decay in red fluorescence works as an indicator of cell death. This assay allows quick screening of various drugs in a matter of hours, which makes this method highly versatile.

1.5 Fluorescence Correlation Spectroscopy (FCS)

Fluorescence correlation spectroscopy (FCS) is a technique with single molecule sensitivity that, measures the fluorescence fluctuations arising from the diffusion of molecules passing through a confocal detection volume of sub-micrometer size. FCS provides quantitative information about the concentration of fluorophores, their diffusion properties, binding/unbinding processes and conformational changes (Ries & Schwille, 2012). It requires very low dye concentrations ($N < 100$) and low excitation laser power, to achieve 1-10 kHz (Counts per molecule). Meseth et al characterized the ability of FCS to resolve species based on their diffusion time in solution: the diffusion time of the larger molecule must be 1.6 times or greater than that of the smaller molecule (Meseth, Wohland, Rigler, & Vogel, 1999).

The basic setup and the principle of a confocal FCS microscope is shown in figure 1.5.

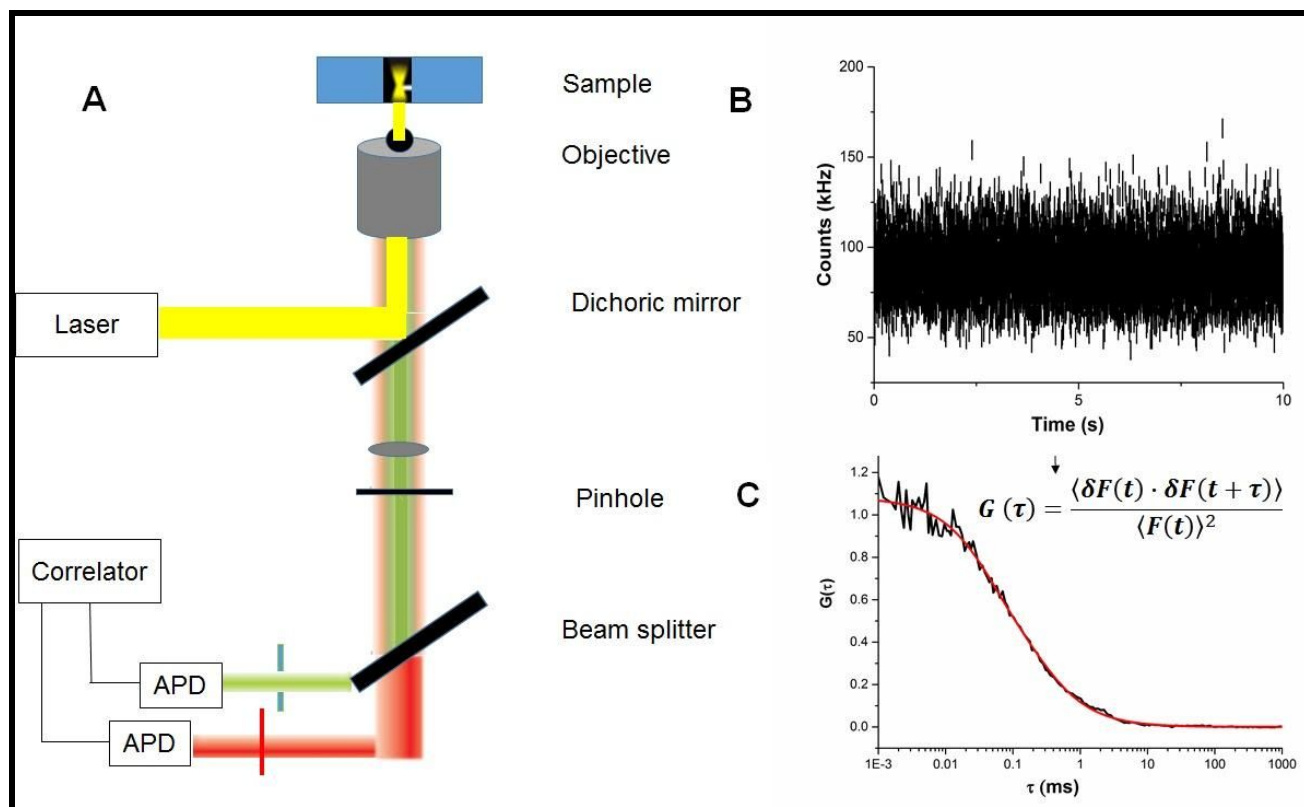


Fig.1.5 Principle of FCS. A) Schematic representation of a confocal FCS setup. B) Fluorescence fluctuation traces are recorded by avalanche photodiodes (APD) as photon counts and plotted vs time. C)

The fluctuations are temporally autocorrelated to measure self-similarity of the signal over time and then fitted with a model function. Here we used a 3D diffusion model for fitting FCS of fluorophores in solution. Adapted from (Das et al., 2015) with permission from Elsevier.

The derivation of FCS equations as well as different diffusion models are discussed in the Book chapter by (Das et al., 2015).

In two color FCS, also called FCCS, the fluorescence signals from two respective channels are collected and cross-correlated with respect to to each other to obtain the so called cross- correlation curve. If the particles do not interact, the cross-correlation amplitude is zero and if the two species are co-diffusing together as a complex, the cross-correlation amplitude increases.

In Scanning FCS or Scanning fluorescence correlation spectroscopy (SFCS) on membranes (2D) the detection volume is scanned perpendicular to the membrane, which can be used correct for membrane movements and decreases the illumination time on the membrane, minimizing bleaching. The principle of Scanning FCS is shown in fig 6.

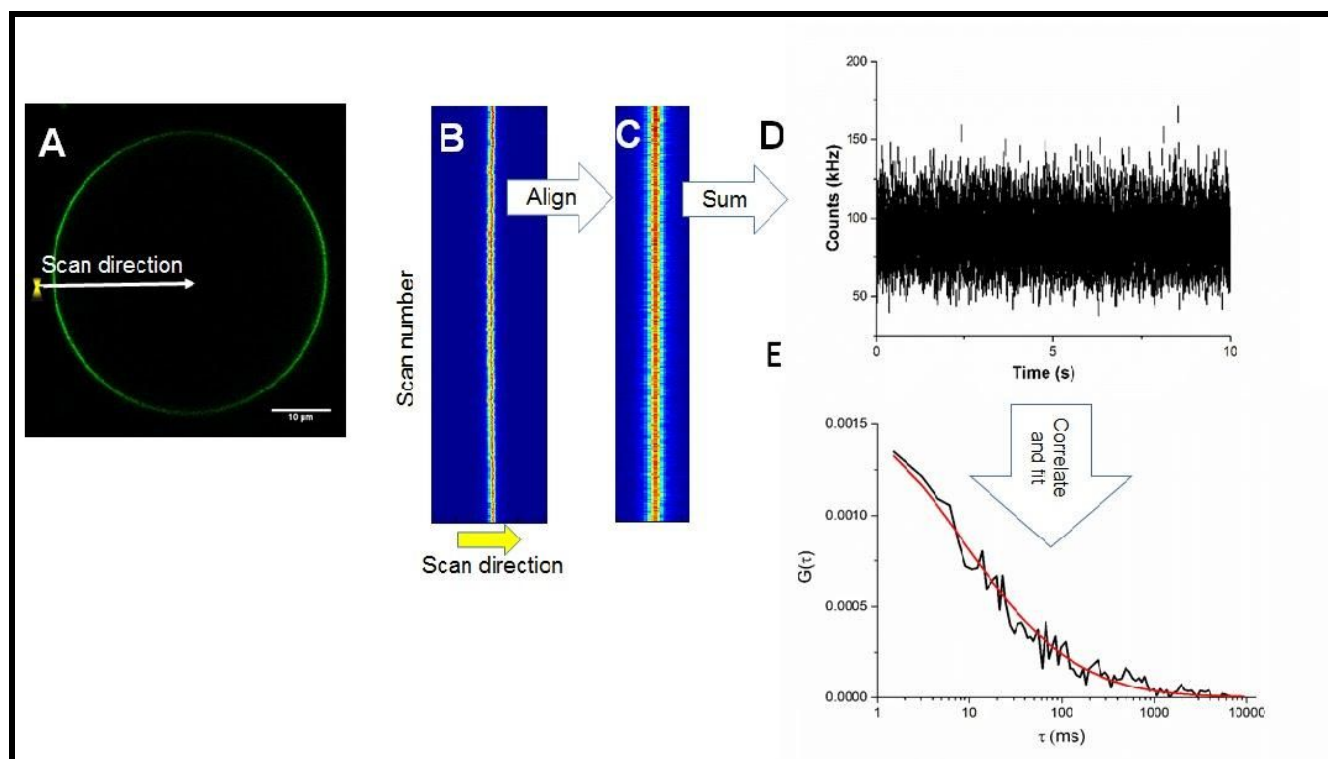


Fig.1.6 Principle of Scanning FCS. A) The detection volume is scanned perpendicular to the equatorial plane of the membrane. B) Contribution of the membrane to fluorescence fluctuations can be observed with the line signal plotted for all scans (scan direction/position vs scan number). C) Membrane movements are corrected by aligning the maxima for all scans. D) Fluctuation trace is generated, as summed up for the fluctuations of one scan as one time point. E) Fluctuations are temporally

autocorrelated and fitted with diffusion models. Here we used a 2D diffusion model for fitting the FCS data obtained in membranes. Adapted from (Das et al., 2015) with permission from Elsevier.

Some variations of FCS, like PIE-FCS (pulse interleaved excitation), can be applied in case that avoiding spectral crosstalk is an issue, for example in case of 1 focus two color measurements between mCherry and GFP tagged proteins.

2 focus two color SFCS is applied to GUVs with two parallel lines perpendicular to the equator of the GUV with two excitation laser lines. The spatial cross-correlation of the signal in the two lines allows calibration free measurements in case the distance between the two lines is known

Part 2

Objectives

Objective 1

The proteins of the Bcl-2 family are key regulators of cell death and decide the cellular fate. The interaction network between the members of this family is tightly regulated. The BH3 only proteins act as sensors of apoptotic stimuli and initiate the process of apoptosis either by direct or indirect interactions with other proteins of the Bcl-2 family. Despite the fact that the interactions of Bcl-2 members with BH3 only proteins takes place at the mitochondrial outer membrane, almost all studies available in the literature have quantified the interactions of BH3 domain peptides with pro-survival Bcl-2 proteins in the solution environment. These raise a question about the role of the membrane in the conformational change of Bcl-2 family proteins, and in the affinity of interactions in membrane environment compared to that in solution. The quantification of interactions in membrane environment has remained a technical challenge.

In order to gain insight into this question the first aim of my thesis is:

Aim 1: To characterize the interactions of BH3 peptides derived from the BH3 only proteins and the BH3 mimetics in solution and on model membrane using Solution FCCS and Membrane Scanning FCCS.

Aim 2: To decipher the sequence code that defines the pattern of binding affinities between BH3 peptides with the pro-survival members in the membrane, using BH3 peptides derived from the BH3 only proteins and mutant BH3 peptides which can be useful for drug development for selective targeted BH3 mimetics.

Objective 2

The role of Bax auto-activation and retrotranslocation have been under investigation since few years. Bcl-xL retrotranslocates mitochondrial Bax to the cytosol of healthy cells and maintains a steady state that prevents Bax accumulation and activation in the MOM via a yet obscure mechanism. The process of auto-activation of Bax i.e, recruitment of inactive soluble cytosolic Bax from the cytosol by membrane activated Bax is not clearly understood either.

To understand this two key processes in the Bcl-2 interaction network, the next aims of the thesis are:

Aim 3: In-vitro reconstitution of Bax auto-activation and retrotranslocation by Bcl-xL in a cell-free membrane model system.

Aim 4: Does Bax retrotranslocation potentiate Bcl-xL anti-apoptotic activity and do BH3 peptides synergize the effect of activator BH3 only proteins like Bid for Bax activation.

Objective 3

A minor objective was to contribute to generating and understanding a comprehensive Bcl-2 interactome, by studying the interactions of Bok and Bim with other Bcl-2 family

members.

Part 3

Results

Chapter 1: Comparing the activity of BH3 peptides and BH3 mimetics to inhibit Bcl-xL/cBid interaction in solution and in membranes.

Attached manuscript: Determinants of BH3 sequence specificity for the disruption of Bcl-xL/cBid complexes in membranes.

Contribution: I performed all the experiments and the data analysis in this manuscript except figure 1 panel C and figure 7 (performed by Raed shalaby).

Summary: In this manuscript, we systematically quantified the interaction pattern of BH3 peptides derived from the BH3 domain of BH3 only proteins and BH3 mimetics ABT 263 and ABT 737 in solution and in membrane model systems (GUVs). We validated these interactions in physiological membrane environment using mitochondria isolated from yeast. We performed both competitive and non-competitive assays for the interaction of cBid (activator) with Bcl-xL (pro-survival) and analyzed the ability of the respective peptides and mimetics to disrupt these complexes. Furthermore, our findings suggested that the available drugs in the market, ABT 263 and ABT 737 cannot disrupt cBid/Bcl-xL complexes preformed in membrane non competitively, but can disrupt these complexes competitively. The BH3 peptides derived from Hrk, Bid, Bim, and Bad were the most efficient in disrupting the complexes in the membrane.

Additional unpublished results

For our experiments, we expressed full-length human Bcl-xL and human cBid. To test the role of the C-terminal tail of Bcl-xL, we also produced a truncated form of it, Bcl-xL Δ C, and quantified its interaction with cBid using solution FCCS. The proteins Bcl-xL Δ C and Bcl-xL full length were labeled with Alexa-488, cBid labeled with Alexa-647 and used at 1:1 concentration of 50nM each. Figure 3.1 shows the solution FCCS of cBid 647 with full length Bcl-xL and Bcl-xL Δ C. We observed that the cross-correlation amplitude for Bcl-xL Δ C/cBid was higher compared to that of Bcl-xL full length, which suggests that the C-terminal transmembrane tail of full-length Bcl-xL occupies the BH3 binding groove in solution hindering its interaction with activator cBid, compared to its truncated form.

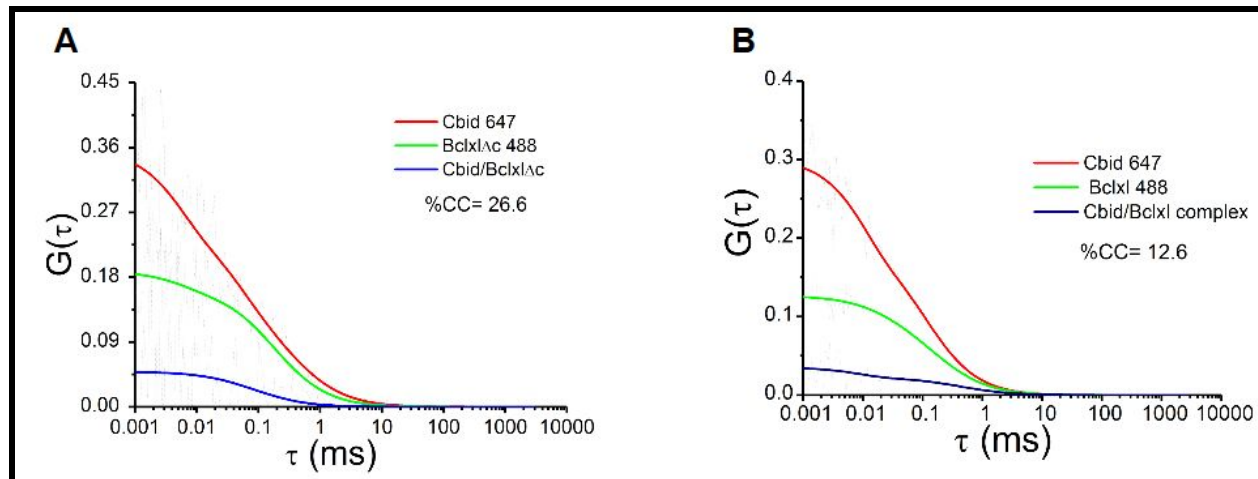


Fig.3.1 Full length Bcl-xL and Bcl-xL Δ C interaction with activator cBid . A) Solution interaction of Bcl-xL Δ C 488 with cBid 647 B) Solution interaction of full length Bcl-xL 488 with cBid 647.

In order to mimic the physiological conditions, we decided to use the full-length Bcl-xL for our studies with BH3 peptides and mimetics.

Chapter 2: Optimization of BH3 peptides for the inhibition of Bcl-xL/cBid complexes in membranes.

Summary: Based on our previous findings of chapter 1, Hrk and Bim BH3 peptides were the most efficient in disrupting cBid/Bcl-xL complexes in the membrane, thereby liberating cBid which can then activate pro-apoptotic Bax to promote apoptosis. Using the peptide sequence of Hrk and Bim, we generated mutant peptides at specific positions in order to generate molecules with a higher activity for disrupting the membrane-bound complexes compared to the native peptide sequence. For a rational design, we docked a number of mutant peptides with Rosetta Flexpepdock software using the backbone of Bcl-xL and evaluated the docking score of the Bcl-xL/mutant peptide complexes. This score defines the stability of the complexes formed. Based on this, we selected 5 mutant peptides with 6 His tag residues at the end and validated their activity in solution and on membrane environment using solution and membrane FCCS. Further, to validate the ability of these peptides to induce apoptosis in mammalian cells we used the BH3 profiling assays discussed above. Concretely, we quantified the effectiveness of these peptides to promote mitochondrial depolarization in HCT116 WT colon cancer cell line . The outlook of this work will be reduce the length of the BH3 peptides and to generate stapled versions with higher affinity, stability and penetrance in cells that disrupt the membrane complexes and can be used in the generation of novel cancer therapeutics targeting membrane Bcl-2 interactions.

	2d	2e	2f	2g	3a	3b	3c	3d	3e	3f	3g	4a	4b
Hrk	T	A	A	R	L	K	A	L	G	D	E	L	H
Bim	I	A	Q	E	L	R	R	I	G	D	E	F	N
Bid	I	A	R	H	L	A	Q	V	G	D	S	M	D
Bad	Y	G	R	E	L	R	R	M	S	D	E	F	V
Bik	L	A	L	R	L	A	C	I	G	D	E	M	D
Bmf	I	A	R	K	L	Q	C	I	A	D	Q	F	H
Puma	I	G	A	Q	L	R	R	M	A	D	D	L	N
	I	G	Q	E	L	R	R	I	S	D	S	F	N
	Y		R	H	L	A	Q	V	A	D	Q	M	D
	L		L	K	L	Q	C	M		D	D		V
				Q									

HM1	I	A	A	R	L	K	A	L	G	D	E	L	H	H	H	H	H	H
HM2	I	A	Q	R	L	K	A	L	G	D	E	L	H	H	H	H	H	H
HM3	I	A	Q	R	L	K	A	I	G	D	E	L	H	H	H	H	H	H
HM4	I	A	Q	E	L	K	A	I	G	D	E	L	H	H	H	H	H	H
HB2	I	A	Q	E	L	K	A	I	G	D	E	F	N	H	H	H	H	H

Fig.3.2 Sequence of BH3 peptides of BH3 only proteins. The red highlighted box shows the sequence of the peptides used as a basis to generate mutant peptides. The right panel shows the list of mutant peptides selected for our study.

Firstly, to study the ability of the mutant peptides to disrupt cBid/Bcl-xL complexes, we first tested their activity in solution using solution FCCS. We labeled cBid647 and Bcl-xL488 and incubated them for at least 30 minutes to allow them to form complexes (from our previous study we followed the same conditions as mentioned in the material and methods section of the publication). We then examined the disruption of these interactions non-competitively using the mutant peptides. Figure 3.3 shows the quantitative plot of solution FCS at different concentrations of the BH3 peptides. Most of the mutant peptides were able to disrupt the cBid/Bcl-xL interactions non-competitively compared to the negative control Noxa BH3 peptide.

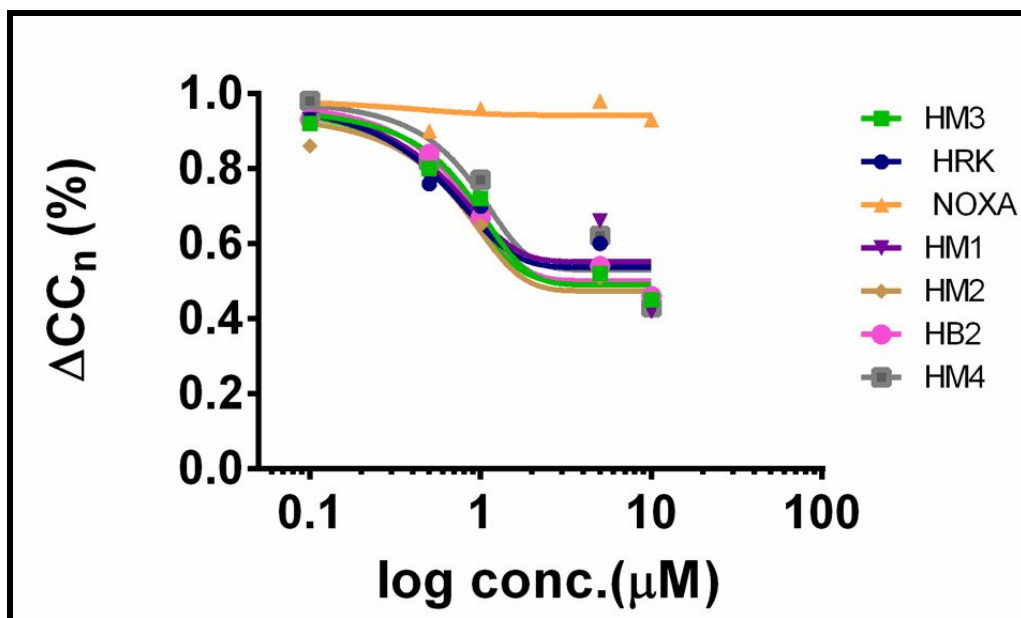


Fig.3.3 Quantitative analysis of the inhibitory activity of mutant BH3 peptides in solution. The normalized change in %CC of cBid/Bcl-xL in solution at different concentrations of BH3 peptides.

Next, we performed the competition assay with the mutant peptides to inhibit complex formation between cBid647 and Bcl-xL488 in model membrane systems using GUVs. We used peptides containing a 6-His tag to induce membrane binding, a strategy used successfully in our earlier paper. The working procedure was the same as discussed in the material and methods section of the paper. As before, the membrane complexes could not be disrupted non competitively. Competitive inhibition in the membrane inhibited the formation of the complexes compared to our control without any peptide treatment. Interestingly, HM3, HM4, and HB2 mutants were more effective in inhibiting complex formation compared to HM1 and HM2 as shown in figure 3.4.

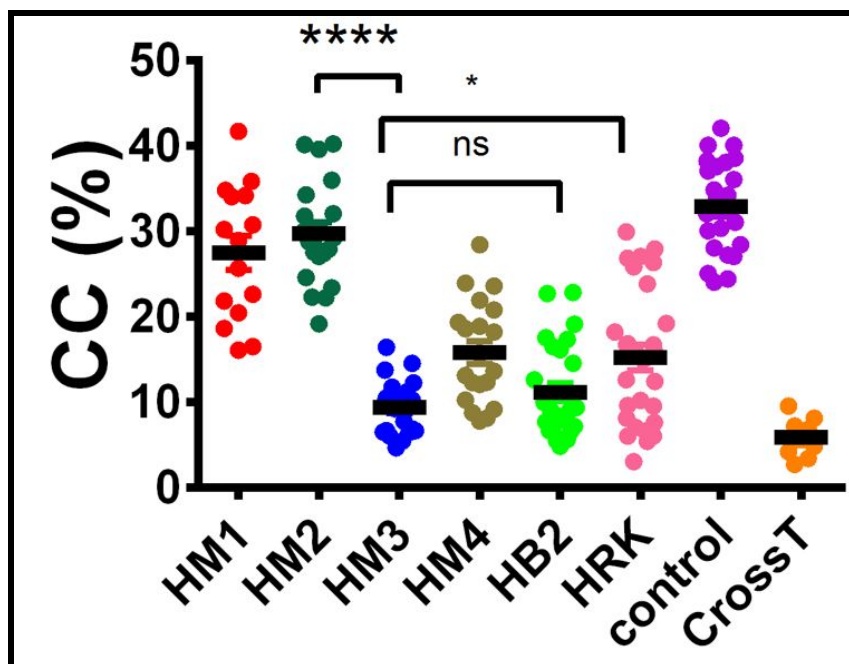


Fig.3.4 Quantitative analysis of the inhibitory activity of mutant BH3 peptides on membranes. %CC of cBid/Bcl-xL complexes in presence of the respective BH3 peptides. The crosstalk between channels of red and green is represented in orange. The black line represents the mean of %CC of each peptide. Significance test (Anova Turkey's multiple comparison test) are indicated **** $P < 0.0001$.

To validate the activity of the mutant peptides in physiological membranes, we isolated mitochondria from wild-type yeast cells and performed ensemble FRET measurements. The proteins were labeled with donor and acceptor fluorophores Atto488 and Atto565. The experimental procedure is described in the material and methods section of the previous paper and we followed the same working protocol. The physiological conditions of isolated mitochondrial membranes correlated best with the results obtained with the GUVs. We found that HM3 and HB2 peptides were the most effective in disrupting cBid/Bcl-xL complexes, as shown by the maximum change in the %FRET efficiency in

figure 3.5.

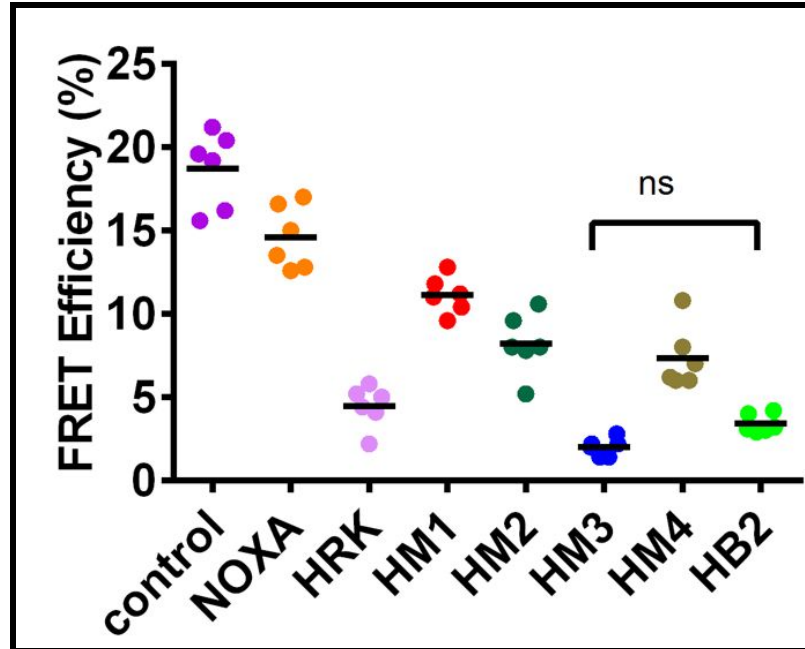


Fig.3.5 Quantitative analysis of the inhibitory activity of mutant BH3 peptides in isolated mitochondria from yeast. Quantitative analysis of the changes in FRET efficiency of Bcl-xL565/cBid488 complexes using mutant BH3 peptides. The black line represents the mean of % FRET efficiency change for each peptide.

To validate our findings in a cellular context, we screened the activity of the peptides using the BH3 profiling assay on mammalian colon cancer HCT116 WT cells. We used the loss in mitochondrial potential as indicator for the effectiveness of the peptides to induce cell death as shown in figure 3.6.

Material and Methods, BH3 profiling assay

The protocol from Ryan et al. was adapted. At the start of the assay, a peptide treatment plate was prepared in a 96-well black plate. Peptides were mixed with DTEB buffer (300mM Trehalose, 10 mM HEPES-KOH pH 7.7, 80 mM KCl, 1mM EGTA, 1mM EDTA, 0.1% BSA, 5mM Na succinate) to 2X of the final peptide concentration and 50 μ l was pipetted into each well. A positive control of FCCP (20 μ M) and a negative solvent control of DMSO (1 μ l in 49 μ l DTEB) were used. The final peptide concentration used was 500 μ M. Each well contained 25000 cells. 4X times cell suspension was mixed with 4X times dye solution (digitonin 0.1%, 20 μ l JC1 dye, 40 μ g/ml oligomycin and 10 mM 2-mercaptoethanol) and finally was added to the 96 well plates containing the peptides. We followed the kinetics of the loss of JC-1 fluorescence as indicator of mitochondrial membrane potential loss. Measurements were performed in a plate reader with Ex 545

nm and Em 590 nm for 3 hours at 37°C every 5 minutes.

The loss in mitochondrial potential was calculated as:

$$\% \text{ membrane potential loss} = 1 - \left[\frac{\text{Sample} - \text{FCCP}}{\text{DMSO} - \text{FCCP}} \right]$$

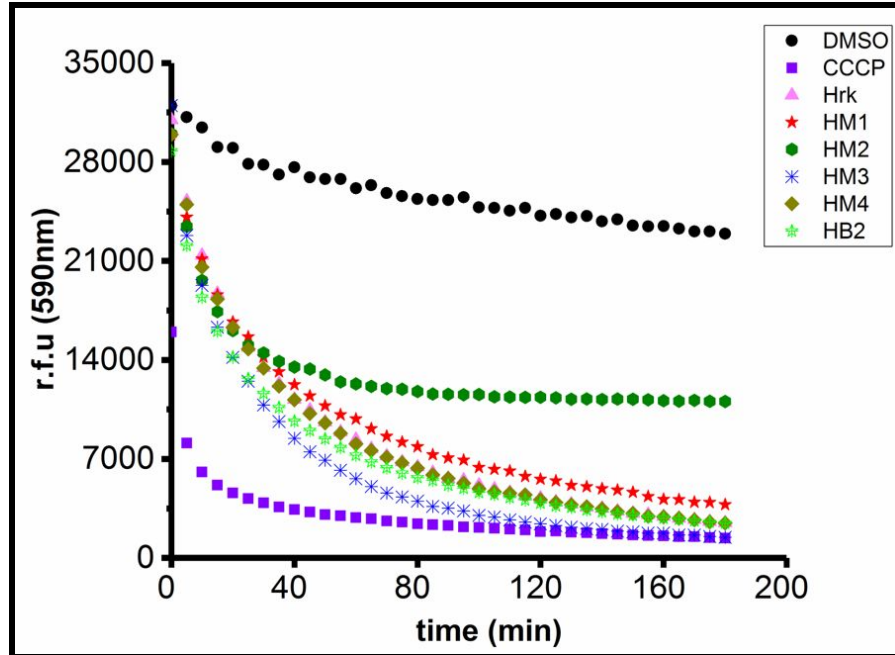


Fig. 3.6 BH3 profiling of mutant peptides in HCT116 WT cells. Kinetics of loss of mitochondrial polarization induced by mutant peptides using JC-1. DMSO and CCCP are the negative and positive control respectively. Hrk BH3 peptide was included as a reference.

As shown in Figure 3.6, HM3 exhibited slightly higher activity than Hrk BH3, while HB2 and HM4 had a similar effect compared to the reference peptide. These results are in very good agreement with the *in vitro* data in GUVs and isolated mitochondria.

Since all the peptides used so far contained a 6XHis tag, we compared the activity of the most effective peptides (i.e. HM3 and HB2) in the absence and presence of the His-Tag as shown in Fig 3.7. We found that the HB2 peptide without the His-Tag was now most effective in causing mitochondrial depolarisation, which was comparable to the original Hrk BH3 peptide with His-tag. Our results suggest that these peptides could be used as a leads to develop new, potent BH3 mimetics that efficiently promote cell death specifically targeting Bcl-xL.

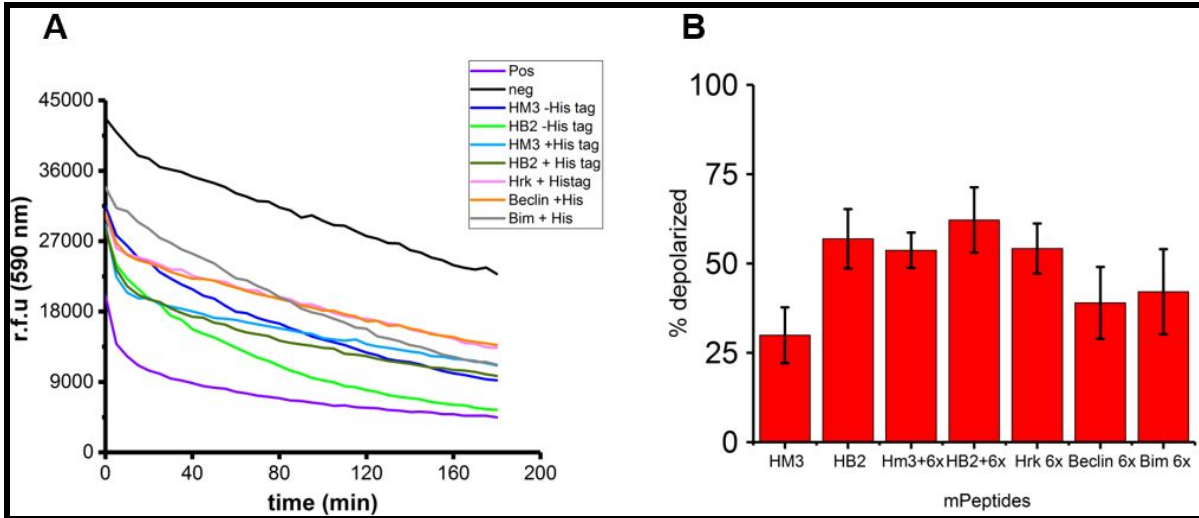


Fig. 3.7 BH3 profiling of mutant peptides with and w/o His Tag in HCT116 WT cells. A) Kinetics of loss of mitochondrial polarization monitored at Em 590 nm induced by mutant peptides using JC-1 . B) Percentage of mitochondrial depolarization of mutant peptides in presence and absence of His tag.

Chapter 3: Quantification of a minimal Bcl-2 interaction network (cBid, Bax, and Bcl-xL) in solution and in membranes using FCCS and confocal imaging.

Attached manuscript: Quantitative interactome of a membrane Bcl-2 network identifies a hierarchy of complexes for apoptosis regulation.

Contribution: I performed all experiments in figure 7 to characterize the auto-activation and retro-translocation of Bax in model membrane systems and the corresponding data analysis.

Summary: In this manuscript, we quantified the interactions of a minimal Bcl-2 network, comprising cBid, Bax, and Bcl-xL, in solution and in membranes. We also showed Bax auto-activation at physiological temperature and how active membrane-bound Bax molecules recruit inactive Bax molecules from solution. Surprisingly, we found that membrane active Bax also recruited Bcl-xL to membranes, which then retrotranslocated Bax molecules back to the solution. Finally, we generated an integrated model for Bcl-2 protein interaction network in solution and the MOM.

Activation of Bax is a target for cancer therapy and has been under investigation for

decades. In chapter 1 I studied the activity of BH3 peptides/mimetics to target anti-apoptotic proteins and liberate activator BH3 only proteins, which finally would lead to the activation of pro-apoptotic Bax to induce apoptosis. The structure of active, membrane-bound Bax has paved our understanding of Bax pore formation at the MOM. The role of the membrane has been the most crucial point in recent studies and findings associated with Bax activation. Bax is activated by interaction with activator BH3 only proteins like cBid, which translocates Bax from the cytosol to the outer mitochondrial membrane. Here we used model membrane systems to understand the process of Bax autoactivation and provide evidence for another efficient mechanism contributing to Bax activation based on the self-recruitment from solution to the membrane.. Understanding Bax autoactivation will pave the way to develop new drugs that target apoptosis for therapy. We also found that to keep the process of Bax activation under check, the soluble anti-apoptotic protein Bcl-xL was also recruited to the membrane by activated Bax and then, membrane-bound Bcl-xL further retrotranslocated Bax back to the cytosol thereby maintaining membrane integrity.

In general, understanding the key process of Bax autoactivation and retrotranslocation can help us in designing better BH3 mimetics and therapeutics against cancer.

Chapter 4: In this chapter we studied how the shuttling of Bcl-2 family species between MOM and cytosol (solution) regulates MOMP sensitivity, and how BH3 peptides synergize the activator BH3 only proteins for MOMP, using quantitative experimental and theoretical evidence.

Attached manuscript: Bax retrotranslocation potentiates Bcl-xL 's antiapoptotic activity and is essential for a switch-like transitions between MOMP competency and resistance.

Contribution: In this chapter, the theoretical mathematical modeling and analysis were done by Annika Hantusch, all the experimental part and data analysis were done by me.

Summary: Here we examined the interplay of tBid/cBid, Bax, and Bcl-xL using theoretical mathematical modeling and experimental validation of the modeling predictions. Interestingly, we found that both our experimental and theoretical results support a synergistic role of BH3-only sensitizer proteins in combination with the BH3 only activator proteins to induce MOMP. Quantitatively, we analyzed the role of Bax retrotranslocation in the overall anti-apoptotic activity of Bcl-xL. We propose that this retrotranslocation

activity acts as a switch between MOMP competency to MOMP resistance within a narrow range of Bcl-xL concentrations.

Our findings indicate that we should not neglect the role of BH3 only sensitizers in synergizing the process of MOMP in presence of activator BH3 only proteins. In our experimental assay, we used the BH3 peptides of Hrk and Bid to study their synergistic activity to promote the permeabilization of large unilamellar vesicles. In the future, these novel findings of the intricate Bcl-2 network should be kept in mind while designing BH3 mimetics for Bax activation and cell death.

Other collaboration Publications:

Chapter 5: In this chapter, we studied the interaction capabilities of Bok, a poorly understood pro-apoptotic member of the Bcl-2 family, with cBid and Bcl-xL. In addition, we characterized the association of the BH3 only activator Bim with itself in solution and in the membrane in presence or absence of dynein light chain 1 (DLC-1).

Attached manuscripts: Proapoptotic member Bok forms toroidal pores and is promoted by cBid.

Investigating Bim oligomerization in solution and on the membrane using FCCS and confocal imaging.

Contribution: In the article characterizing novel pro-apoptotic Bok, I contributed Figure 3 Panel A, B, and C and in the manuscript of Bim I contributed Figure 1 E, F, G.

Summary: We successfully purified Bok truncated at the C-terminal helix, Bok Δ C, and investigated its membrane activity using calcein permeabilization assays with LUVs, as well as its effect of cBid and Bcl-xL on this activity. We found Bok to be a highly active pro-apoptotic protein with an IC₅₀ of 7.5 nM. Furthermore activator cBid modulated its permeabilizing activity. We titrated Bcl-xL at fixed Bok concentration and we did not detect significant inhibition of Bok activity. To study the auto-interaction of Bim in solution and in the membrane in the presence or absence of DLC-1, we used solution and membrane scanning FCCS. Taken together, these findings add new light to the understanding of the Bcl-2 family that could contribute to targeting novel interaction partners using BH3 mimetics.

Part 4

Discussion and Outlook

The BH3 only proteins of the Bcl-2 family are activated or upregulated in response to apoptotic stimuli. These proteins induce apoptosis by either directly activating the pro-apoptotic members of the Bcl-2 family or binding to prosurvival members of the Bcl-2 family, thereby indirectly promoting the process of apoptosis. Furthermore, the interaction between BH3 only and antiapoptotic Bcl-xL occurs on the mitochondrial outer membrane. We know that interactions between Bcl-2 family members on the membrane is associated with major conformational changes. Thus previous studies on soluble conformations of the Bcl-2 family do not provide us an optimal basis for developing cancer therapeutics. (Leber et al., 2010) mentioned the importance of screening novel BH3 molecules that can disrupt interactions of these molecules in membranes, which might in future lead to specific and potent therapies to target cancer.

Quantitative information about the binding of BH3 molecules with full length prosurvival Bcl-2 proteins in the membrane environment had remained a technical challenge. Most of these interactions have been quantified either exclusively in solution or using ensemble FRET measurements, which provide information both from the solution and on the membrane. To exclusively study the interaction on the membrane environment, we studied the interaction of BH3 peptides with Bcl-xL using model membrane systems such as GUVs mimicking the mitochondrial outer membrane composition. In recent studies, (Hockings et al., 2015) investigated these interactions in mitochondria using Bid chimeras. They replaced the BH3 domain of respective BH3 only proteins while keeping the Bid backbone intact. Their findings showed an increased interaction of BH3 chimeras with Bcl-2 proteins and most BH3 chimeras activated Bax and Bak. The pitfall with these results is that the influence of the Bid backbone on its overall interactions cannot be neglected, as well as its influence on the helicity content of the BH3 domain. In our studies, we approached all these questions using BH3 peptides derived from the BH3 domain of BH3 only proteins, which have the potential to be further optimized into novel BH3 small molecules for cancer therapeutics. There has been a strong interest in the development of selective BH3 mimetics, with recent examples for Mcl1 specific mimetics (Kotschy et al., 2016) and Bcl-xL specific mimetics (Lessene et al., 2013). These specific BH3 mimetics would increase the specificity of these drug in therapy.

To investigate the interactions in solution/cytosolic environment for cBid/Bcl-xL, we tested the BH3 peptides and BH3 mimetics ABTs (ABT 263 and ABT 737) using a noncompetitive assay to disrupt the complexes. We found that most of these BH3 peptides and ABTs were able to disrupt the interactions after complex formation except Noxa and Bmf. These findings correlated with previous findings in solution by (Letai et al 2002), showing Noxa BH3 peptide having no effect in disrupting cBid/Bcl-xL complexes. This can be further explained because the Lys 11 residue of the Noxa BH3 peptide sequence orients towards the positively charged residues of Bcl-xL making it electrostatically unfavorable in the binding groove of Bcl-xL. To validate these findings in the membrane environment, we performed both competitive and non-competitive assays. As expected, in the competitive assay the BH3 peptides and ABTs were able to disrupt /modulate the interaction of cBid/Bcl-xL complexes, in contrast to the

non-competitive assay, where the complexes were allowed to form before the addition of the peptides/ABTs. This can be explained as a result of competition between the activators and the peptides for the binding groove of Bcl-xL which lowers the complex formation of cBid/Bcl-xL, liberating cBid free for Bax activation and cellular death. Peptides having higher affinity and specificity can displace the activator cBid and occupy the binding pocket of Bcl-xL. Interestingly, we hypothesize from our findings that ABTs (ABT 263 and ABT 737), which were approved in clinical trials for inducing cell death, bind to the newly synthesized pro-survival Bcl-2 proteins or compete with the activators for the common binding groove of pro-survival proteins before complexes are formed, to induce Bax activation and the downstream cascade of apoptosis. We found Hrk and Bim BH3 peptides to be the most effective in competitively disrupting the cBid/Bcl-xL complexes in membranes. Interestingly, Hrk has the higher specificity towards Bcl-xL compared with other prosurvival Bcl-2 proteins, which was previously reported by (Letai et.al 2002) in solution. This study underestimated its effectiveness in the membrane environment. When we compared these findings to ABT 263 and ABT 737, Hrk BH3 peptide was as effective in inhibiting the complex formation in the membrane thus becoming a promising candidate for specifically targeting Bcl-xL. ABT 263 and ABT 737 target the Bcl-xL, Bcl-2 and Bcl-W with slightly lower or higher affinity towards each other. In the future, disrupting or targeting membrane interactions with specifically targeted inhibitors can reduce the side effects of chemotherapy and can lead to better-targeted drug candidates to treat disease.

Also, to validate these findings under physiological membrane conditions we isolated mitochondria from yeast cells and used ensemble FRET with donor and acceptor labeled proteins incubated with the respective BH3 peptides and mimetics. BH3 peptides from Hrk, Bim, and Bad were more effective in decreasing the FRET efficiency of the complexes compared to other BH3 peptides. Interestingly, the results from isolated mitochondria correlate best with the data on GUV membranes. The lower activity of some peptides like Puma or Bik observed by FRET compared to lack of activity in GUVs can be due to the inhibitory effect of peptides in solution as in FRET it's a bulk measurement in solution and membrane, unlike GUVs which exclusively measure the membrane interactions. Overall, these findings suggested that the membrane interaction is the most relevant and reproduces best the situation in cells.

Furthermore, to understand how the amino acid sequences codify the binding affinity, and with an aim to design specific Bcl-xL inhibitors which can target membrane interactions more effectively, we designed mutant BH3 peptides based on the amino acid sequence of Hrk and Bim, as these were the two most effective BH3 peptides in disrupting membrane interactions. We generated peptides with one, two, three and four point mutations based on combinatorial approach.

We validated the efficiency of mutant peptides firstly in the solution environment, and in line with the previous findings of BH3 peptides in solution, the non-competitive disruption assay showed that most of the mutant peptides were able to disrupt the complexes formed by cBid/Bcl-xL. These findings suggested us that the weaker interactions in solution can be easily disrupted by the point variants of Hrk and Bim without any specific

preference for the amino acid sequence in its binding affinity. To study the inhibition on the membrane, we observed that mutant peptides HM3 and HB2 showed better inhibition activity than HM1 and HM2. The heterogeneity in the disruption of membrane complexes competitively can be explained due to the specific preferences of certain amino acids at certain positions of the BH3 peptide sequence. The replacement of a threonine with isoleucine and leucine to isoleucine in HM3 likely causes an increase in the hydrophobic interactions within the membrane-bound complex, making it more effective. When we compare the sequence of HM4 with HB2, we hypothesized that the presence of phenylalanine at its end position could make HB2 a potential candidate for disrupting membrane complexes. We found that the disruption of membrane interactions can be altered using specific amino acid mutations which in turn modifies the strength and binding affinity with the complexes.

Further, to validate our findings in physiological membranes we used isolated yeast mitochondria and found that the HM3 and HB2 peptides best reproduced the results obtained in model membranes. The experiment with isolated yeast mitochondria recapitulated best the findings in model membranes providing us evidence that the role of Bcl-2 family interactions on the membrane cannot be neglected while designing novel BH3 mimetics. In order to validate the effectiveness of these mutant peptides to induce apoptosis in cells, we took advantage of the BH3 profiling assay using a HCT116 WT colon cancer cell line. This cell line has been reported to have overexpression of antiapoptotic Bcl-xL making it ideal for studying specific Bcl-xL inhibitors. The HM2 peptide clearly showed lower ability to cause mitochondrial depolarization compared to HM3 and HB2, which were the most effective. We also observed some effectiveness of the peptide HM4, which was also observed in our FRET and membrane FCS experiments. Overall, these findings in cells provided us with evidence that the experiments using a model membrane and isolated mitochondria are valid in a more physiological context..

The peptides used in the assay have a 6XHis tagged a strategy to target them to model membranes with a low percentage of Ni-NTA nickel. To test the effect of the 6XHis tag on the affinity, we decided to examine the activity of HM3 and HB2 without the 6XHis tag by analyzing the mitochondrial depolarization using JC1. Removal of the His Tag reduced the activity of both HM3 and HB2 which may be due to the presence of positive charged 6 histidine residues and to lower helicity of the peptides. Surprisingly the HB2 peptide without the His tag was as much effective as the HM3 peptide without the His tag.

To sum up our findings with mutant peptides, we observed that HB2 BH3 peptide was the most effective in disrupting interactions of cBid/Bcl-xL in solution, model membranes, isolated mitochondria and finally in HCT116 WT colon cancer cells. In the future, one could staple the peptide with a hydrocarbon moiety to improve its helical propensity, cellular penetrance, and cellular stability, which could provide lead for drug development for targeted therapy in cancers with overexpression of Bcl-xL.

Until now, we saw how membrane plays an important role in altering cBid/Bcl-xL

complex formation and how BH3 peptides and mimetics differ in disrupting the complexes in membranes compared to solution. We also observed that results on isolated mitochondria and cells best correlate with the trends observed in model membrane systems.

To better understand the role of the membrane in Bax activation and in the hierarchy of Bcl-2 complexes, we reconstituted the process in-vitro using GUVs as our model membrane system and by labeling Bax molecules into two different colors. We could detect Bax autoactivation i.e.; recruitment of inactive cytosolic Bax by membrane active Bax molecules. This mode of Bax activation has been in discussion for a few years. Here Our recent findings shed light on the activation of Bax from the cytosol to the membrane activated form induced by previously activated Bax molecules residing on the membrane. The conventional way of Bax activation is based on BH3 activators like Bid or Bim, which induce the translocation of Bax molecules in the cytosol to the MOM. We hypothesize that Bax activation is based on lowering the energy barrier for Bax activation, which can also be promoted by using heat, change in pH or detergents . Once recruited to the membrane, membrane-bound active Bax molecules can recruit more soluble Bax in a feedback. How the recruitment of soluble Bax by membrane active Bax energetically compares to its activation by activator BH3 only proteins is a question that remains to be answered. If Bax autoactivation is the favored mode of Bax activation, then the number of pores at the MOM will be lower but their sizes or the oligomerization state of Bax in those pores will be larger when compared to the situation where Bax activation is more efficient with BH3 activators. This latter scenario would lead to more pores of lower size for an equal number of Bax molecules. In summary, these findings give us a better understanding of Bax activation, Bax pore formation and in the future could be translated to develop better therapies to maintain cellular homeostasis.

On the other hand, the recruitment of soluble Bax to MOM is counteracted by its retrotranslocation promoted by the antiapoptotic protein Bcl-xL. We found the recruitment of Bcl-xL from solution by membrane active Bax and how this Bcl-xL was sufficient to retrotranslocate Bax from the membrane back into solution, thereby controlling Bax oligomerization and pore formation.

Thus, despite various models for Bax activation in the literature, our findings using quantitative FCS showed that Bax/Bcl-xL interactions are weaker compared to cBid/Bcl-xL, which we studied earlier using BH3 mimetics/peptides. Finally, we proposed an integrated model for the Bcl-2 network in both solution and on the membrane that summarizes how multiple parallel interactions of Bcl-2 proteins are orchestrated to regulate apoptosis. Understanding the network on the membrane for Bax activation can help in the future to design BH3 mimetics to promote cell death in cancer therapy.

To quantify how Bax retrotranslocation contributes to the overall anti-apoptotic activity of Bcl-xL, we used mathematical modeling and experimental validation. Strikingly, when we examined retrotranslocation as part of Bcl-xL activity, mathematical modeling best reproduced the findings of the experiments when retrotranslocation was taken into consideration. We quantified that retrotranslocation enhanced the prosurvival potential of

Bcl-xL from 300 nM to 30 nM, almost by 10 fold. These findings were the first of this kind in modeling Bcl-2 family proteins. The retrotranslocation activity of Bcl-xL can further be extended to other antiapoptotic proteins like Mcl-1 and Bcl-2. Bak is retrotranslocated at a slower rate compared to Bax as studied recently (Todt et al., 2015). In addition, we showed for the first time the synergistic effect of sensitizers with BH3 only activators in promoting MOMP. These findings explain the effectiveness of BH3 sensitizers in activation of apoptosis in cells. Recently, this synergism of sensitizers and activators have been exploited in various combination treatments in tumors (Inoue-Yamauchi et al., 2017).

Overall we found that the retrotranslocation process is crucial for a switch separating MOMP competence and resistance. Thus understanding the shuttling rate and dynamics of Bcl-2 proteins on the membrane will help in a better prognosis of cancer.

To extend our understanding of other Bcl-2 family proteins, other proapoptotic and BH3 only activators were investigated in collaborations with other groups. We studied the proapoptotic activity of purified Bok Δ C and characterized its interaction with cBid and Bcl-xL. Bok is the most recent and widely debated proapoptotic protein, due to its localization in cells and its poorly understood function. Surprisingly we found that Bok itself is active in vitro by using LUV permeabilization assays as mitochondrial outer membrane mimics, and that addition of cBid modulates the activity of Bok positively. We also checked the antiapoptotic effect of Bcl-xL on Bok but didn't observe any inhibitory effect on pore formation as reported earlier (Hsu, Kaipia, McGee, Lomeli, & Hsueh, 1997). This suggests that there must be an alternative mechanism to regulate Bok activity, as recently reported with the involvement of the ERAD pathway (Llambi et al., 2016). The finding that Bcl-xL does not inhibit pore formation in presence of cBid was counterintuitive, as we already know from own previous studies that Bcl-xL has a high affinity for cBid and would be expected to sequester cBid thus preventing the synergistic effect of Bok pore formation.

Lastly, we studied the self-interaction of the BH3 only activator Bim and found that Bim oligomerizes in solution and that the interaction is significantly increased in presence of Dynein light chain 1 (DLC1). We concluded that Bim binding to DLC-1 leads to the formation of larger complexes. Thus, the interactome of Bcl-2 family members is not just limited to the pro-apoptotic and anti-apoptotic members of this family, but also involves other proteins. Understanding these interaction partners and targeting them can be an emerging strategy for developing novel therapeutics.

BIBLIOGRAPHY

- Adams, J. M. (1998). The Bcl-2 Protein Family: Arbiters of Cell Survival. *Science*, 281(5381), 1322–1326.
- Annis, M. G., Soucie, E. L., Dlugosz, P. J., Cruz-Aguado, J. A., Penn, L. Z., Leber, B., & Andrews, D. W. (2005). Bax forms multispinning monomers that oligomerize to permeabilize membranes during apoptosis. *The EMBO Journal*, 24(12), 2096–2103.
- Baell, J. B., & Huang, D. C. S. (2002). Prospects for targeting the Bcl-2 family of proteins to develop novel cytotoxic drugs. *Biochemical Pharmacology*, 64(5-6), 851–863.
- Bleicken, S., Classen, M., Padmavathi, P. V. L., Ishikawa, T., Zeth, K., Steinhoff, H.-J., & Bordignon, E. (2010). Molecular details of Bax activation, oligomerization, and membrane insertion. *The Journal of Biological Chemistry*, 285(9), 6636–6647.
- Bleicken, S., García-Sáez, A. J., Conte, E., & Bordignon, E. (2012). Dynamic Interaction of cBid with Detergents, Liposomes and Mitochondria. *PloS One*, 7(4), e35910.
- Bleicken, S., Jeschke, G., Stegmüller, C., Salvador-Gallego, R., García-Sáez, A. J., & Bordignon, E. (2014). Structural model of active Bax at the membrane. *Molecular Cell*, 56(4), 496–505.
- Certo, M., Del Gaizo Moore, V., Nishino, M., Wei, G., Korsmeyer, S., Armstrong, S. A., & Letai, A. (2006). Mitochondria primed by death signals determine cellular addiction to antiapoptotic BCL-2 family members. *Cancer Cell*, 9(5), 351–365.
- Chen, L., Willis, S. N., Wei, A., Smith, B. J., Fletcher, J. I., Hinds, M. G., ... Huang, D. C. S. (2005). Differential Targeting of Prosurvival Bcl-2 Proteins by Their BH3-Only Ligands Allows Complementary Apoptotic Function. *Molecular Cell*, 17(3), 393–403.

- Chipuk, J. E., & Green, D. R. (2008). How do BCL-2 proteins induce mitochondrial outer membrane permeabilization? *Trends in Cell Biology*, 18(4), 157–164.
- Cory, S., Huang, D. C. S., & Adams, J. M. (2003). The Bcl-2 family: roles in cell survival and oncogenesis. *Oncogene*, 22(53), 8590–8607.
- Cosentino, K., & García-Sáez, A. J. (2017). Bax and Bak Pores: Are We Closing the Circle? *Trends in Cell Biology*, 27(4), 266–275.
- Czabotar, P. E., Lessene, G., Strasser, A., & Adams, J. M. (2013). Control of apoptosis by the BCL-2 protein family: implications for physiology and therapy. *Nature Reviews. Molecular Cell Biology*, 15(1), 49–63.
- Czabotar, P. E., Westphal, D., Dewson, G., Ma, S., Hockings, C., Fairlie, W. D., ... Colman, P. M. (2013). Bax crystal structures reveal how BH3 domains activate Bax and nucleate its oligomerization to induce apoptosis. *Cell*, 152(3), 519–531.
- Das, K. K., Unsay, J. D., & Garcia-Saez, A. J. (2015). Microscopy of Model Membranes. In *Advances in Planar Lipid Bilayers and Liposomes* (pp. 63–97).
- Edinger, A. L., & Thompson, C. B. (2004). Death by design: apoptosis, necrosis and autophagy. *Current Opinion in Cell Biology*, 16(6), 663–669.
- Edlich, F., Banerjee, S., Suzuki, M., Cleland, M. M., Arnoult, D., Wang, C., ... Youle, R. J. (2011). Bcl-x(L) retrotranslocates Bax from the mitochondria into the cytosol. *Cell*, 145(1), 104–116.
- España, L., Fernández, Y., Rubio, N., Torregrosa, A., Blanco, J., & Sierra, A. (2004). Overexpression of Bcl-xL in human breast cancer cells enhances organ-selective lymph node metastasis. *Breast Cancer Research and Treatment*, 87(1), 33–44.

García-Sáez, A. J., Mingarro, I., Pérez-Payá, E., & Salgado, J. (2004).

Membrane-insertion fragments of Bcl-xL, Bax, and Bid. *Biochemistry*, *43*(34), 10930–10943.

García-Sáez, A. J., Ries, J., Orzáez, M., Pérez-Payà, E., & Schwille, P. (2009).

Membrane promotes tBID interaction with BCL(XL). *Nature Structural & Molecular Biology*, *16*(11), 1178–1185.

Gavathiotis, E., Reyna, D. E., Davis, M. L., Bird, G. H., & Walensky, L. D. (2010).

BH3-triggered structural reorganization drives the activation of proapoptotic BAX. *Molecular Cell*, *40*(3), 481–492.

Ghaneh, P., Kawesha, A., Evans, J. D., & Neoptolemos, J. P. (2002). Molecular

prognostic markers in pancreatic cancer. *Journal of Hepato-Biliary-Pancreatic Surgery*, *9*(1), 1–11.

Gobé, G., Rubin, M., Williams, G., Sawczuk, I., & Buttyan, R. (2002). Apoptosis and

expression of Bcl-2, Bcl-XL, and Bax in renal cell carcinomas. *Cancer Investigation*, *20*(3), 324–332.

Gross, A., McDonnell, J. M., & Korsmeyer, S. J. (1999). BCL-2 family members and the

mitochondria in apoptosis. *Genes & Development*, *13*(15), 1899–1911.

Hill, R. B., Blake Hill, R., MacKenzie, K. R., & Harwig, M. C. (2015). The Tail-End Is Only

the Beginning: NMR Study Reveals a Membrane-Bound State of BCL-XL. *Journal of Molecular Biology*, *427*(13), 2257–2261.

Hockings, C., Anwari, K., Ninnis, R. L., Brouwer, J., O’Hely, M., Evangelista, M., ...

Kluck, R. M. (2015). Bid chimeras indicate that most BH3-only proteins can directly

activate Bak and Bax, and show no preference for Bak versus Bax. *Cell Death & Disease*, 6, e1735.

Hsu, S. Y., Kaipia, A., McGee, E., Lomeli, M., & Hsueh, A. J. W. (1997). Bok is a pro-apoptotic Bcl-2 protein with restricted expression in reproductive tissues and heterodimerizes with selective anti-apoptotic Bcl-2 family members. *Proceedings of the National Academy of Sciences*, 94(23), 12401–12406.

Inoue-Yamauchi, A., Jeng, P. S., Kim, K., Chen, H.-C., Han, S., Ganesan, Y. T., ... Cheng, E. H. (2017). Targeting the differential addiction to anti-apoptotic BCL-2 family for cancer therapy. *Nature Communications*, 8, 16078.

Kim, H., Tu, H.-C., Ren, D., Takeuchi, O., Jeffers, J. R., Zambetti, G. P., ... Cheng, E. H.-Y. (2009). Stepwise activation of BAX and BAK by tBID, BIM, and PUMA initiates mitochondrial apoptosis. *Molecular Cell*, 36(3), 487–499.

Kotschy, A., Szlavik, Z., Murray, J., Davidson, J., Maragno, A. L., Le Toumelin-Braizat, G., ... Geneste, O. (2016). The MCL1 inhibitor S63845 is tolerable and effective in diverse cancer models. *Nature*, 538(7626), 477–482.

Kuwana, T., Mackey, M. R., Perkins, G., Ellisman, M. H., Latterich, M., Schneider, R., ... Newmeyer, D. D. (2002). Bid, Bax, and Lipids Cooperate to Form Supramolecular Openings in the Outer Mitochondrial Membrane. *Cell*, 111(3), 331–342.

Leber, B., Geng, F., Kale, J., & Andrews, D. W. (2010). Drugs targeting Bcl-2 family members as an emerging strategy in cancer. *Expert Reviews in Molecular Medicine*, 12. <https://doi.org/10.1017/s1462399410001572>

Leber, B., Lin, J., & Andrews, D. W. (2007). Embedded together: The life and death

- consequences of interaction of the Bcl-2 family with membranes. *Apoptosis: An International Journal on Programmed Cell Death*, 12(5), 897–911.
- Lessene, G., Czabotar, P. E., & Colman, P. M. (2008). BCL-2 family antagonists for cancer therapy. *Nature Reviews. Drug Discovery*, 7(12), 989–1000.
- Lessene, G., Czabotar, P. E., Sleebs, B. E., Zobel, K., Lowes, K. N., Adams, J. M., ... Watson, K. G. (2013). Structure-guided design of a selective BCL-X(L) inhibitor. *Nature Chemical Biology*, 9(6), 390–397.
- Letai, A., Bassik, M. C., Walensky, L. D., Sorcinelli, M. D., Weiler, S., & Korsmeyer, S. J. (2002). Distinct BH3 domains either sensitize or activate mitochondrial apoptosis, serving as prototype cancer therapeutics. *Cancer Cell*, 2(3), 183–192.
- Llambi, F., Moldoveanu, T., Tait, S. W. G., Bouchier-Hayes, L., Temirov, J., McCormick, L. L., ... Green, D. R. (2011). A Unified Model of Mammalian BCL-2 Protein Family Interactions at the Mitochondria. *Molecular Cell*, 44(4), 517–531.
- Llambi, F., Wang, Y.-M., Victor, B., Yang, M., Schneider, D. M., Gingras, S., ... Green, D. R. (2016). BOK Is a Non-canonical BCL-2 Family Effector of Apoptosis Regulated by ER-Associated Degradation. *Cell*, 165(2), 421–433.
- Lovell, J. F., Billen, L. P., Bindner, S., Shamas-Din, A., Fradin, C., Leber, B., & Andrews, D. W. (2008). Membrane Binding by tBid Initiates an Ordered Series of Events Culminating in Membrane Permeabilization by Bax. *Cell*, 135(6), 1074–1084.
- Lowe, S. W., & Lin, A. W. (2000). Apoptosis in cancer. *Carcinogenesis*, 21(3), 485–495.
- Mattson, M. P. (2000). Apoptosis in neurodegenerative disorders. *Nature Reviews. Molecular Cell Biology*, 1(2), 120–129.

- Meseth, U., Wohland, T., Rigler, R., & Vogel, H. (1999). Resolution of fluorescence correlation measurements. *Biophysical Journal*, *76*(3), 1619–1631.
- Ni Chonghaile, T., & Letai, A. (2008). Mimicking the BH3 domain to kill cancer cells. *Oncogene*, *27 Suppl 1*, S149–57.
- Petros, A. M., Olejniczak, E. T., & Fesik, S. W. (2004). Structural biology of the Bcl-2 family of proteins. *Biochimica et Biophysica Acta*, *1644*(2-3), 83–94.
- Ries, J., & Schwille, P. (2012). Fluorescence correlation spectroscopy. *BioEssays: News and Reviews in Molecular, Cellular and Developmental Biology*, *34*(5), 361–368.
- Ryan, J., & Letai, A. (2013). BH3 profiling in whole cells by fluorimeter or FACS. *Methods*, *61*(2), 156–164.
- Salvador-Gallego, R., Mund, M., Cosentino, K., Schneider, J., Unsay, J., Schraermeyer, U., ... García-Sáez, A. J. (2016). Bax assembly into rings and arcs in apoptotic mitochondria is linked to membrane pores. *The EMBO Journal*, *35*(4), 389–401.
- Scherr, A.-L., Gdynia, G., Salou, M., Radhakrishnan, P., Duglova, K., Heller, A., ... Koehler, B. C. (2016). Bcl-xL is an oncogenic driver in colorectal cancer. *Cell Death & Disease*, *7*(8), e2342.
- Shamas-Din, A., Bindner, S., Zhu, W., Zaltsman, Y., Campbell, C., Gross, A., ... Fradin, C. (2013). tBid undergoes multiple conformational changes at the membrane required for Bax activation. *The Journal of Biological Chemistry*, *288*(30), 22111–22127.
- Subburaj, Y., Cosentino, K., Axmann, M., Pedrueza-Villalmanzo, E., Hermann, E., Bleicken, S., ... García-Sáez, A. J. (2015). Bax monomers form dimer units in the

- membrane that further self-assemble into multiple oligomeric species. *Nature Communications*, 6, 8042.
- Taylor, R. C., Cullen, S. P., & Martin, S. J. (2008). Apoptosis: controlled demolition at the cellular level. *Nature Reviews. Molecular Cell Biology*, 9(3), 231–241.
- Todt, F., Cakir, Z., Reichenbach, F., Emschermann, F., Lauterwasser, J., Kaiser, A., ... Edlich, F. (2015). Differential retrotranslocation of mitochondrial Bax and Bak. *The EMBO Journal*, 34(1), 67–80.
- Tse, C., Shoemaker, A. R., Adickes, J., Anderson, M. G., Chen, J., Jin, S., ... Elmore, S. W. (2008). ABT-263: a potent and orally bioavailable Bcl-2 family inhibitor. *Cancer Research*, 68(9), 3421–3428.
- Tsujimoto, Y., Finger, L., Yunis, J., Nowell, P., & Croce, C. (1984). Cloning of the chromosome breakpoint of neoplastic B cells with the t(14;18) chromosome translocation. *Science*, 226(4678), 1097–1099.
- Walensky, L. D., & Bird, G. H. (2014). Hydrocarbon-stapled peptides: principles, practice, and progress. *Journal of Medicinal Chemistry*, 57(15), 6275–6288.
- Walensky, L. D., Pitter, K., Morash, J., Oh, K. J., Barbuto, S., Fisher, J., ... Korsmeyer, S. J. (2006). A stapled BID BH3 helix directly binds and activates BAX. *Molecular Cell*, 24(2), 199–210.
- Watanabe, J., Kushihata, F., Honda, K., Mominoki, K., Matsuda, S., & Kobayashi, N. (2002). Bcl-xL overexpression in human hepatocellular carcinoma. *International Journal of Oncology*. <https://doi.org/10.3892/ijo.21.3.515>
- Wei, M. C., Lindsten, T., Mootha, V. K., Weiler, S., Gross, A., Ashiya, M., ... Korsmeyer, S. J. (2006). Bcl-2 is an essential component of the B cell lineage. *Cell*, 127(1), 123–134.

- S. J. (2000). tBID, a membrane-targeted death ligand, oligomerizes BAK to release cytochrome c. *Genes & Development*, *14*(16), 2060–2071.
- Willis, S. N. (2005). Proapoptotic Bak is sequestered by Mcl-1 and Bcl-xL, but not Bcl-2, until displaced by BH3-only proteins. *Genes & Development*, *19*(11), 1294–1305.
- Willis, S. N., Fletcher, J. I., Kaufmann, T., van Delft, M. F., Chen, L., Czabotar, P. E., ... Huang, D. C. S. (2007). Apoptosis Initiated When BH3 Ligands Engage Multiple Bcl-2 Homologs, Not Bax or Bak. *Science*, *315*(5813), 856–859.
- Wyllie, A. H., Bellamy, C. O., Bubb, V. J., Clarke, A. R., Corbet, S., Curtis, L., ... Bird, C. C. (1999). Apoptosis and carcinogenesis. *British Journal of Cancer*, *80 Suppl 1*, 34–37.
- Yao, Y., Fujimoto, L. M., Hirshman, N., Bobkov, A. A., Antignani, A., Youle, R. J., & Marassi, F. M. (2015). Conformation of BCL-XL upon Membrane Integration. *Journal of Molecular Biology*, *427*(13), 2262–2270.
- Yao, Y., Nisan, D., Fujimoto, L. M., Antignani, A., Barnes, A., Tjandra, N., ... Marassi, F. M. (2016). Characterization of the membrane-inserted C-terminus of cytoprotective BCL-XL. *Protein Expression and Purification*, *122*, 56–63.

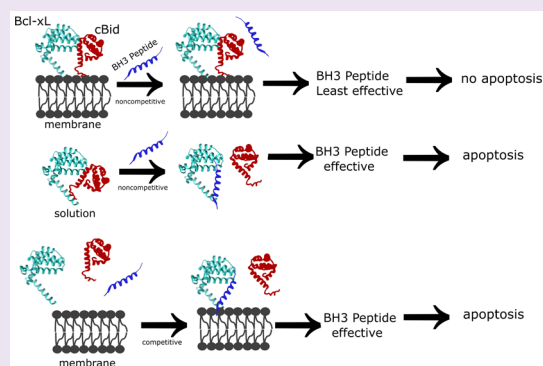
PUBLICATIONS

Determinants of BH3 Sequence Specificity for the Disruption of Bcl-xL/cBid Complexes in Membranes

Kushal Kumar Das,[†] Raed Shalaby,[†] and Ana J. García-Sáez^{*,†,‡,§}[†]Interfaculty Institute of Biochemistry, Eberhard Karls University Tübingen, Hoppe-Seyler-Str. 4, 72076 Tübingen, Germany[‡]Max Planck Institute for Intelligent Systems, Heisenbergstr. 3, 70569 Stuttgart, Germany

Supporting Information

ABSTRACT: The prosurvival Bcl-2 proteins exhibit a specific pattern of interactions with BH3-only proteins that determines the cellular dependence on apoptotic stress. This specificity is crucial for the development of BH3 mimetics, a class of anticancer molecules based on the BH3 domain with promising activity in clinical trials. Although complex formation mainly takes place in the mitochondrial outer membrane, most studies so far addressed the interaction between BH3 peptides and truncated Bcl-2 proteins in solution. As a consequence, quantitative understanding of the sequence specificity determinants of BH3 peptides in the membrane environment is missing. Here, we tackle this issue by systematically quantifying the ability of BH3 peptides to compete for the complexes between cBid and Bcl-xL in giant unilamellar vesicles and compare it with solution and mitochondria. We show that the BH3 peptides derived from Hrk, Bim, Bid, and Bad are the most efficient in disrupting cBid/Bcl-xL complexes in the membrane, which correlates with their activity in mitochondria. Our findings support the targeting to the membrane of small molecules that bind Bcl-2 proteins as a strategy to improve their efficiency.



The proteins of the Bcl-2 family are key regulators of the mitochondrial pathway of apoptosis.^{1,2} They control the permeabilization of the mitochondrial outer membrane (MOM) that leads to cytochrome c and Smac release into the cytosol, to caspase activation, and to cell death. Depending on their function and the number of Bcl-2 Homology (BH) domains they contain, Bcl-2 proteins are further classified into three subgroups: (i) executioners Bax and Bak are proapoptotic members that directly participate in MOM permeabilization; (ii) their action is counterbalanced by prosurvival Bcl-2 proteins, like Bcl-2, Bcl-xL, Mcl-1, or A1, which inhibit apoptosis by binding to Bax/Bak, and (iii) the so-called BH3-only proteins, which are also proapoptotic.

Apoptotic stimuli promote the upregulation and/or activation of the BH3-only proteins, including Bid, Bim, Puma, Noxa, Bad, Bik, Bmf, and Hrk.³ These proteins induce apoptosis by direct interaction with other Bcl-2 members *via* their BH3 domain. On the one hand, BH3-only proteins associate with prosurvival Bcl-2 proteins into inhibitory complexes. As a result, they effectively decrease the amount of prosurvival Bcl-2s available for Bax/Bak inhibition. On the other hand, a subset of BH3-only proteins called “direct activators” are also able to interact with Bax and Bak and to promote their activation, which includes accumulation at the MOM, oligomerization, and formation of the pores responsible for MOM permeabilization. In contrast to the direct activators, those BH3-only proteins that only bind to prosurvival Bcl-2 are known as “sensitizers.” Although the boundaries between both

subtypes are not completely clear, Bid, Bim, and Puma are classically considered direct activators.^{4,5} However, a recent study suggested that only Bad and Noxa were not activators.⁶

This ability to activate or not activate Bax and Bak reflects a key feature of BH3-only proteins, which is their different binding affinities for other Bcl-2 family members.^{7,8} This extends also to the prosurvival Bcl-2 homologues and results in a pattern of interactions whose specificity is mainly determined by the sequence of the BH3 domain. This specificity has clinical relevance because it is critical for the development of BH3 mimetics, a set of antitumor compounds derived from the BH3 domain of proapoptotic proteins that have promising activity in clinical trials.^{9–12} BH3 mimetics bind with high affinity to the hydrophobic groove of prosurvival Bcl-2 proteins and induce apoptosis *via* Bax/Bak. So far, the quantification of the affinities between prosurvival Bcl-2s and BH3 peptides has been performed in solution using C-terminal truncated proteins^{7,8} or overall in cells using a split-luciferase assay.¹³ However, in recent years it has become clear that the main interactions between pro- and antiapoptotic Bcl-2 proteins take place in the membrane environment.^{14–16} Moreover, the interaction of a BH3 peptide derived from Bid with Bcl-xL was 1.6 fold higher in the membrane environment compared to solution.¹⁷ This highlights the need to quantitatively analyze the interactions

Received: December 7, 2016

Accepted: February 7, 2017

Published: February 7, 2017

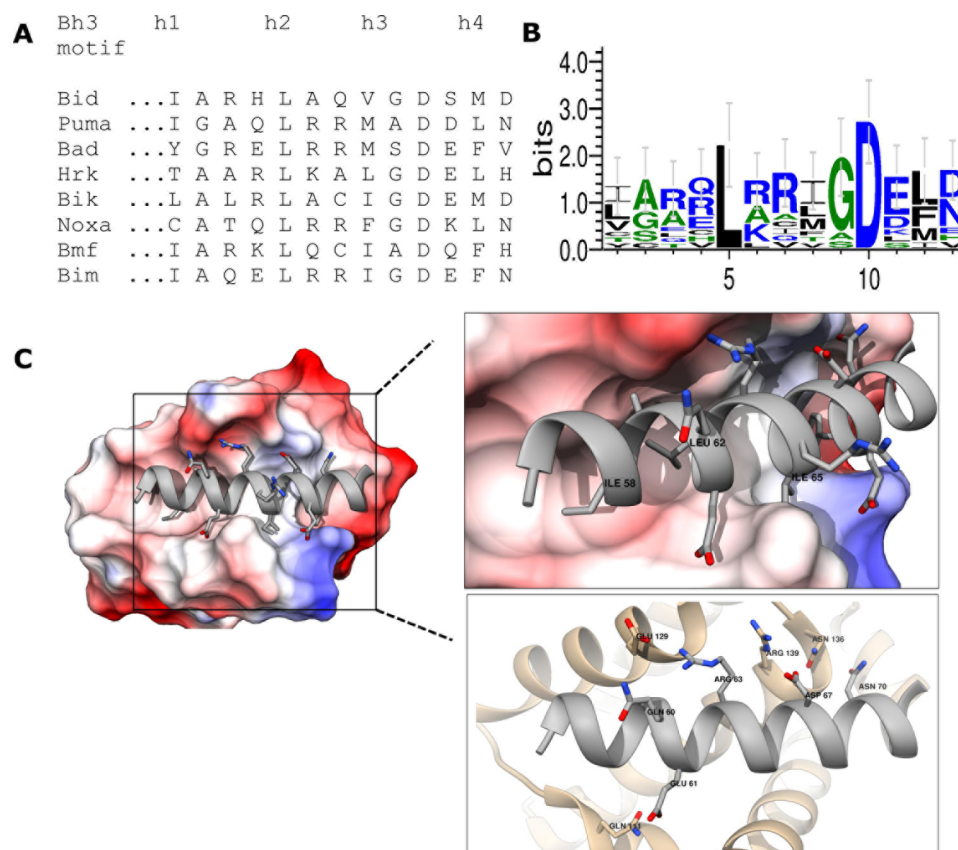


Figure 1. Sequence of BH3 peptides and structural insight of the interacting amino acid residues with the groove of Bcl-xL. (A) Peptides derived from the BH3 domains of Bid and seven other canonical human BH3-only proteins (Puma, Bad, Hrk, Bik, Noxa, Bmf, Bim). Sequence alignment shows the hydrophobic residues (h1–h4) important for the hydrophobic interaction with the groove of prosurvival proteins. For the measurements in membranes, we purchase the corresponding peptides containing additionally 6X His residues at the C-terminal end, for effective membrane targeting. (B) Sequence map showing the conserved amino acids relevant for determining the binding specificity to pro-survival Bcl-2 proteins (blue, green, and black represent hydrophilic, neutral, and hydrophobic amino acids, respectively). Error bars represent the Bayesian 95% confidence interval. (C) Structure of BH3Bim (26 amino acid) interacting with the Bcl-xL hydrophobic groove (PDB id 4QVF). The gray side chains of the amino acids pointing inside the hydrophobic groove (hydrophobic interactions); the red and blue (charged amino acids) pointing outside the groove (electrostatic interactions) are shown in the zoom-in.

between BH3 peptides and prosurvival Bcl-2 in the membrane environment for the improvement of BH3-based tools.

In a recent study using Bid chimeras substituted with the BH3 domains of the different BH3-only proteins, Kluck and colleagues elegantly showed that the BH3 domain determined binding specificity to Bcl-xL in the presence of mitochondria.⁶ Overall, the interactions with other Bcl-2 proteins were increased in this system, as most BH3 chimeras activated Bax and Bak. However, this study cannot exclude the role of the Bid backbone on the interaction with Bcl-2 proteins, which (1) could contribute with additional interaction interfaces, (2) could increase the helicity of the BH3 region, which plays a role in binding affinity,¹⁸ and (3) could promote the association by presenting the BH3 sequences in the optimal orientation. All of these factors would be missing in the context of BH3 mimetics. As a result, quantitative information about the affinity and specificity of the interactions between small BH3 molecules and full-length, prosurvival Bcl-2 proteins exclusively in the membrane environment is still lacking.

Here, we addressed this question by quantifying the ability of BH3-only peptides to compete for the membrane interaction between full-length cBid and Bcl-xL using fluorescence cross-correlation spectroscopy (FCCS) and giant unilamellar vesicles (GUVs).¹⁴ We also compared the efficiency of the peptides to

disrupt the cBid/Bcl-xL interaction in solution and in isolated mitochondria. We found that, while in solution all peptides had comparable inhibitory activity (except for Bmf and Noxa, which could not compete for the interaction), the most potent inhibitors of membrane complexes were Hrk, Bim, Bid, and Bad. Interestingly, the ability of the BH3 peptides to disrupt cBid/Bcl-xL complexes in mitochondria correlated best with their efficiency in the membrane. Our findings suggest that developing inhibitors of prosurvival Bcl-2s that target membrane complexes may improve drug design.

RESULTS AND DISCUSSION

Implementation of an Assay to Quantify cBid/BclxL Interactions in Membranes. The sequence of BH3 peptides used in the assay is shown in Figure 1A. The peptides were designed based on the sequence and structural data available in the literature.^{6,8,19–21} We designed BH3 peptides including the 13 core amino acids from the BH3 domain of the corresponding BH3-only protein and 6X His-tag residues at the C terminus. This ensured effective targeting to the membrane thanks to the incorporation of NTA lipids in the GUVs.¹⁴ The sequences map in Figure 1B highlights the conserved and the critical amino acid residues of the BH3 domain of BH3 only proteins. Both hydrophobic and

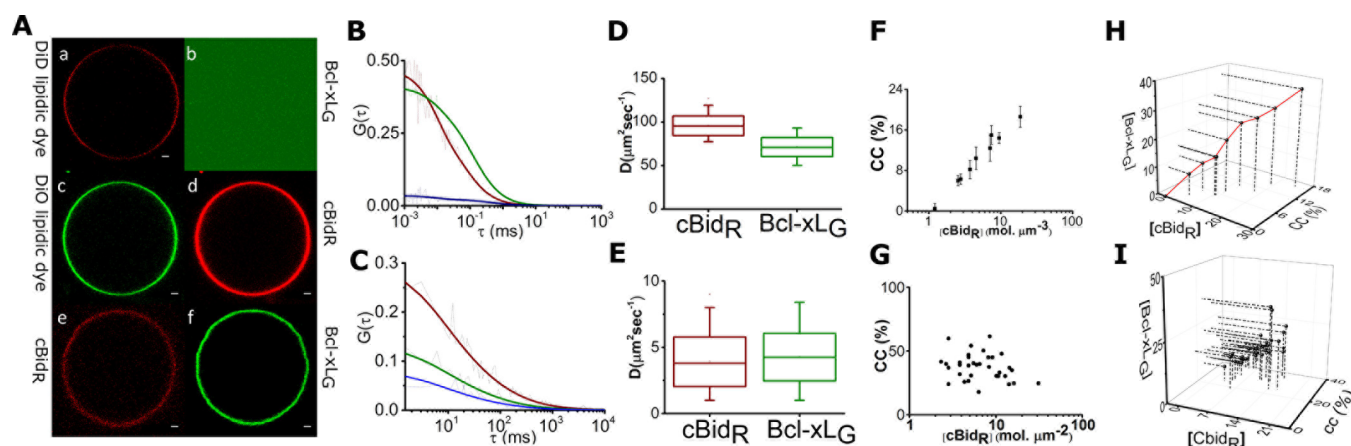


Figure 2. Binding of human cBidR and Bcl-xLG to giant unilamellar vesicles and quantification of the interaction of human cBidR and Bcl-xLG by fluorescence cross-correlation spectroscopy (FCCS) in solution and in the membrane environment. (A) Confocal images of cBidR and Bcl-xLG binding to GUVs. (a) GUVs PC/CL (8:2) labeled with 0.05% DiD in red. (b) Bcl-xLG binding to the same GUVs, no binding observed. (c) GUVs labeled with 0.05% DiO in green. (d) cBidR binding to the GUVs in c. (e) cBidR binding to GUVs (PC/CL, 8:2). (f) cBidR-induced binding of Bcl-xLG to the GUVs in e. Scale bar indicates 5 μm . (B) FCS analysis of the interactions in solution. Fitted AC curves of cBidR and Bcl-xLG are shown in red and green, respectively. CC curve is shown in blue. (C) FCS analysis of the interactions in the membrane of GUVs. The red, green, and blue lines correspond to cBidR, Bcl-xLG AC, and CC, respectively. (D) Diffusion coefficient of cBidR and Bcl-xLG in solution. (E) Diffusion coefficient of cBidR and Bcl-xLG in the membrane. (F) Quantification of cBidR/Bcl-xLG complexes in solution, expressed as %CC at varying cBidR concentrations ($\text{molecules}/\mu\text{m}^3$). (G) Quantification of cBidR/Bcl-xLG complexes in membrane, expressed as %CC at varying cBidR concentrations ($\text{molecules}/\mu\text{m}^2$). (H) %CC in solution represented in a three-dimensional plot as a function of individual protein concentrations. (I) %CC in the membrane represented in a three-dimensional plot as a function of individual protein concentrations. The error bars represent the SD.

electrostatic interactions are involved in the stabilization of the complexes between Bcl-xL and BH3 peptides, as shown by the structure of Bcl-xL in complex with the BH3 domain of Bim (encompassing 26 amino acids; PDB id 4QVF;²² Figure 1C). Residues Ile (58), Leu (62), Ile (65), and Phe (69) are facing the interior of the hydrophobic groove of Bcl-xL, while charged residues Glu (61), Arg (63), and Asp (67) project outward to interact electrostatically.

In order to estimate the affinity of BH3 peptides for Bcl-xL in solution and in the membrane, we developed a competition assay based on the quantification of the extent of complex formation between cBid and Bcl-xL in buffer solution and in GUVs by point FCCS and scanning, two-focus, two-color FCCS, respectively.^{14,23,24} FCCS is a technique with single molecule sensitivity that detects in two different channels the fluorescence fluctuations of individual particles labeled with spectrally different dyes, as they diffuse through the focal volume of the microscope.²⁵ The resulting fluorescence intensity traces are auto- and cross-correlated temporally to generate the FCS curves (Figure 2B,C). The autocorrelation (AC) curves (red and green lines) provide information about the total concentration of the fluorophores (inversely proportional to the amplitude of the AC curve) and their diffusion properties (decay of the AC curves). If the two molecules of interest form part of the same complex, they codiffuse, and the corresponding cross-correlation (CC) curve (blue line) shows positive amplitude, which is directly proportional to the fraction of molecules forming complexes. By referring the amount of complex to the total concentration of protein, the percentage of complex formation can be calculated and from here the binding affinity. The % CC was calculated with respect to the green channel as the focal volume is wavelength dependent and thereby the green channel has a smaller size compared to the red one.²⁶ For membrane experiments, a unique feature of scanning FCCS is that it specifically measures the interactions in membranes (also as cross-correlation of the fluorescence

fluctuations). This is possible because the FCCS signal is acquired by linear scanning across the GUV membrane, so that only the contributions of the membrane-bound proteins to the fluorescence signal are considered in the data analysis. Here, the FCCS analysis builds on previous work¹⁴ but incorporates the use of full-length Bcl-xL and cleaved Bid (including the p7 and p15 fragments) instead of tBid (only the p15). To this aim, we characterized the interaction of purified full-length, human cBid labeled with Alexa 647 (cBid_R) and full-length, human Bcl-xL labeled with Alexa 488 (Bcl-xL_G).

As a test for protein quality, we validated the membrane binding properties of labeled human cBid_R and labeled Bcl-xL_G in GUVs made of phosphatidyl choline (PC) and cardiolipin (CL) in an 8:2 ratio using confocal microscopy. Bcl-xL_G alone did not bind to the vesicles (Figure 2Aa,b; GUVs labeled with red lipid dye DiD), while cBid_R efficiently associated with GUVs as long as they contained cardiolipin (Figure 2Ac,d; GUVs labeled with green DiO lipid dye). When both proteins were incubated together, cBid_R induced the binding of the Bcl-xL_G to the vesicles as shown in Figure 2Ae,f. These results were in good agreement with previous work reporting that cBid recruits Bcl-xL to the membrane.^{14,16,27,28}

To determine the incubation time required to achieve equilibrium in the binding reaction, we monitored the kinetics of cBid_R/Bcl-xL_G complex formation in solution and in the membrane as shown in Supporting Information Figure 1. The reaction of complex formation in solution was characterized by an increase in the cross-correlation (CC) amplitude over time, which reached saturation after 30 min. In the case of membrane interactions, maximum CC was achieved after 1 h incubation.

The FCCS data in Figure 2B shows a representative experiment of the interaction between cBid_R and Bcl-xL_G in solution. The AC curves (red and green lines) comprise total protein including the free and bound fraction. The CC curves (blue line) provide a quantitative estimation of the interaction between the two proteins diffusing together as a complex. Thus,

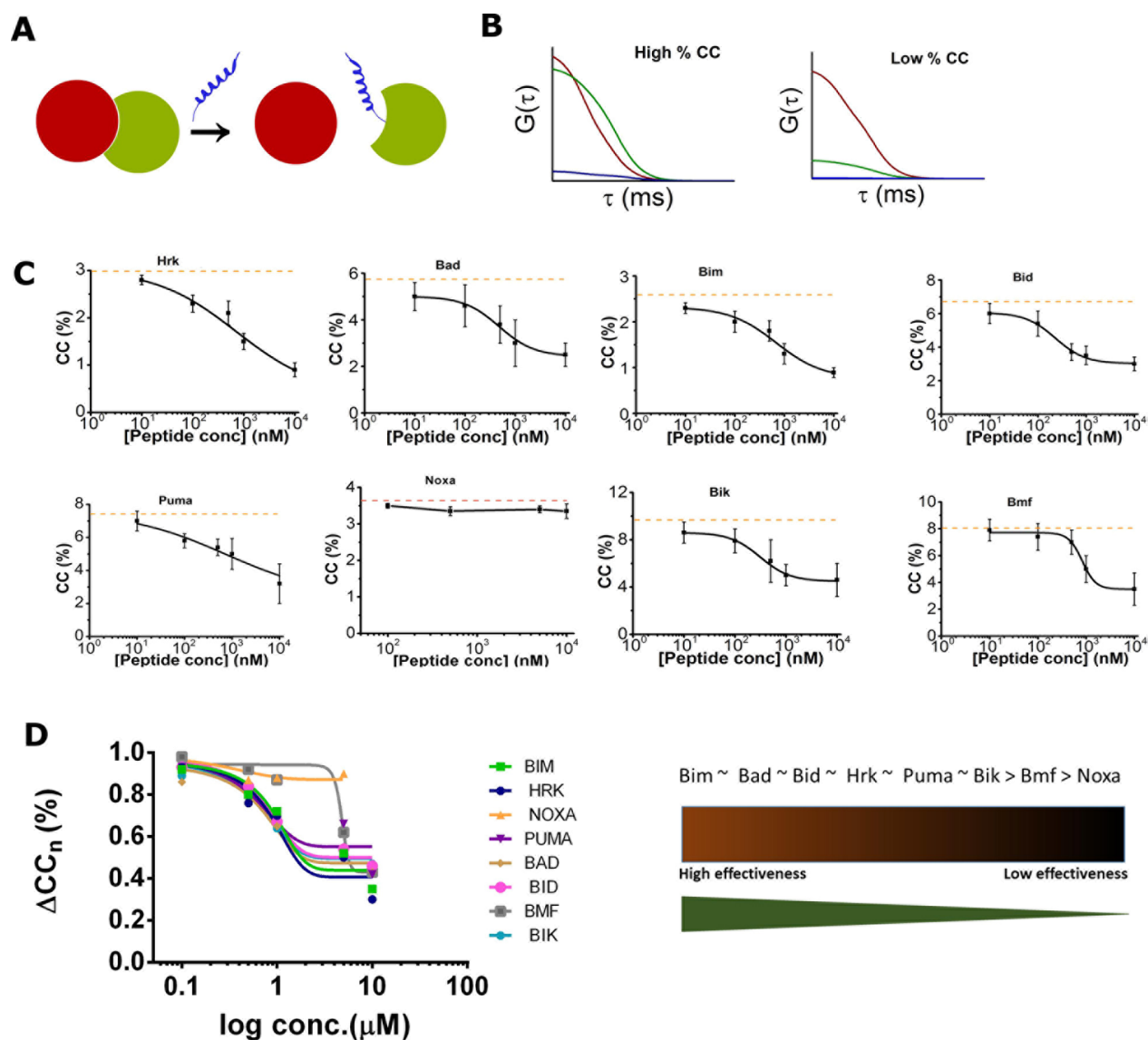


Figure 3. Quantitative analysis of the inhibitory activity of BH3 peptides in solution using FCCS. (A) Schematic representation of the displacement assay. BH3 peptides (blue) disrupt the cBidR/Bcl-xLG complexes by binding to the hydrophobic groove of Bcl-xLG. (B) Auto and CC analysis of interactions in solution. The blue curve shows the change in %CC before (high CC) and after the disruption of the complexes (low CC) in solution. (C) Quantitative analysis of the disruption of the cBidR/Bcl-xLG complexes in solution by the respective BH3 peptides (noncompetitive). The change in the %CC is shown at the different peptide concentrations. The red line represents the maximum CC observed in solution between cBidR and Bcl-xLG when no peptides were present. The error bars represent the standard deviation. (D) The normalized change in %CC of the cBidR/Bcl-xLG complexes in solution at different concentrations of the BH3 peptides. The comparative efficiency of the peptides in solution is depicted on the basis of the two-tailed student's *t* test.

a larger CC amplitude indicates a higher concentration of the cBid_R/Bcl-xL_G complexes in the sample. In Figure 2C, a representative scanning FCCS experiment of the interaction of the proteins within the membrane of GUVs (PC/CL, 8:2) after incubation at RT for 1 h is shown. The diffusion coefficients of cBid_R and Bcl-xL_G in solution were $96 \pm 11 \mu\text{m}^2 \text{s}^{-1}$ and $71 \pm 11 \mu\text{m}^2 \text{s}^{-1}$, respectively (Figure 2D), which is in agreement with their respective molecular weight. In the membrane, cBid_R and Bcl-xL_G were diffusing slower and in comparable range to each other, as expected by their restricted mobility in two dimensions (Figure 2E).

To compare the interactions between cBid and Bcl-xL in solution and in membranes, we quantified the CC amplitude in both environments at several concentrations (Figure 2F,G). The CC in solution was concentration dependent, and at 50

nM cBid_R and 100 nM Bcl-xL_G, a maximum CC amplitude of 18% was yielded. In contrast, in the membrane, we measured a CC amplitude close to 40% (with reaching saturation) already after adding 20 nM of cBid_R and 40 nM Bcl-xL_G to our samples (calculated concentration in solution). This analysis set the basis for our further experiments. In line with previous work,¹⁴ the CC amplitude in the membrane stayed around the saturation value at all concentrations of cBid_R and Bcl-xL_G in the membrane, indicating very tight complex formation. A 3D plot of the CC as a function of the concentration is shown in Figure 2H, I.

In summary, the quantitative analysis of the interaction between the full-length forms of cBid and Bcl-xL in solution and in membranes confirmed our previous findings that the lipid environment strongly enhances complex formation

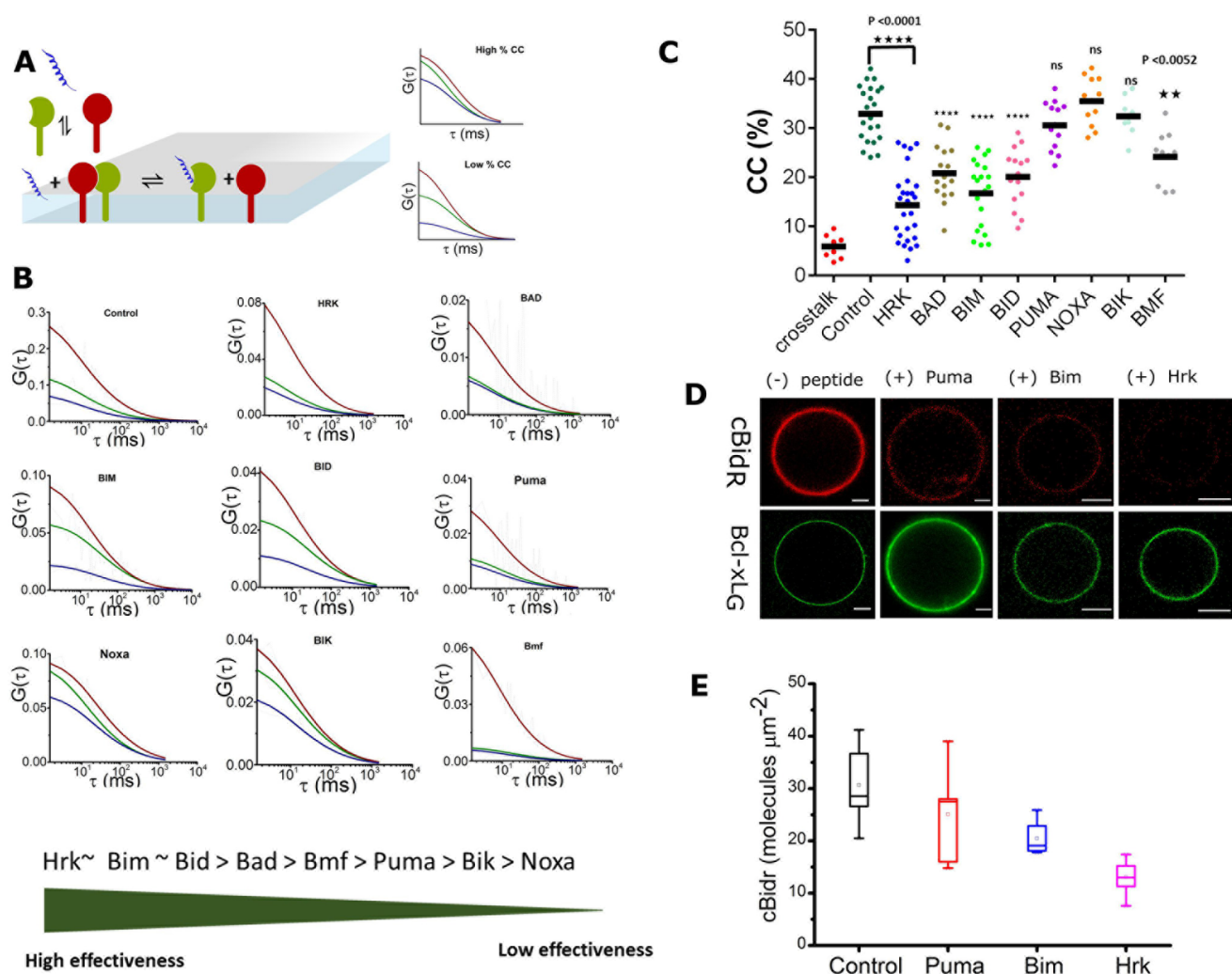


Figure 4. Quantitative analysis of the inhibitory activity of BH3 peptides in membranes using Scanning FCCS. **A**) Schematic representation of the displacement assay. cBidR and BH3 peptides (blue) compete for the binding groove in membrane-associated Bcl-xLG. The blue curve shows the change in the %CC before and after the adding the BH3 peptides. **B**) Representative FCCS graphs of different BH3 peptides. Fitted AC curves of cBidR and Bcl-xLG shown in red and green respectively, CC curve is shown in blue. The line shows the average CC (%) computed after scanning ≥ 20 GUVs. A comparative scheme of the peptides efficiency in membrane environment is also shown, based on the statistical analysis of all peptides (two-tailed students *t* test) with respect to Hrk. **C**) % CC between cBidR and Bcl-xLG in the presence of the respective BH3 Peptides. The background crosstalk between two channels red and green is represented in red. The black line represents the mean %CC, and the significance of each peptide with respect to the control (without peptides, representing the maximum possible cross-correlation between cBidR and Bcl-xLG in membranes). Statistically significant differences (Anova Turkey's multiple comparison test) are indicated. **** $P < 0.0001$, *** $P < 0.0052$ and ns (nonsignificant). **D**) GUV images of cBidR and Bcl-xLG before and after adding the BH3 peptides (Control, Puma, Bim, and Hrk). Scale bar indicates $5 \mu\text{m}$. The lack of fluorescence intensity at the rim shows the ability of the peptides in displacing cBidR. **E**) Quantification of the membrane density of cBidR bound to GUVs before and after the addition of BH3 Peptides calculated using scanning FCCS.

between both proteins.¹⁴ These results also indicate that this membrane effect is therefore independent of the C-terminal anchor. However, from this analysis we cannot discard that the presence of the C-terminal domain may affect the preference of the interactions of Bcl-xL with other Bcl-2 proteins, as suggested by other groups^{6,17,29} and our own unpublished observations.

Disruption of the cBid/BclxL Complexes in Solution by BH3 Peptides. Disruption of the heterodimerization of cBid_R/Bcl-xL_G complexes in solution is achieved by targeting BH3 peptides that bind to the hydrophobic pocket of Bcl-xL formed by its BH1, BH2, and BH3 domains and displace cBid from this groove (schematic representation of the assay in Figure 3A).

To optimize the conditions of the assay, we initially tested the ability of the BH3 peptides to disrupt the complexes of cBid_R/Bcl-xL_G in solution and in the membrane both competitively (proteins and peptides all incubated together) and noncompetitively (proteins were allowed to form complexes and peptides were added later) as shown in Supporting Information Figure 2. We found that while the BH3 peptides in solution were able to disrupt preformed cBid_R/Bcl-xL_G complexes in solution, they did not show any significant disruption when the complexes were preformed in the membrane.

These observations are in agreement with our previous work¹⁴ and confirm the different interaction patterns in solution and in the membrane. This also suggests that the nature of the interactions between Bcl-xL and cBid is different

in solution and in membranes. Since complex formation in the membrane is a reversible process,¹⁴ it is tempting to speculate that the BH3 peptides cannot disrupt efficiently membrane complexes due to the higher affinity between cBid and Bcl-xL in the membrane compared to solution. The question remains whether it will be possible to develop small molecules that surpass the membrane affinity between cBid and Bcl-xL, or perhaps molecules that bind irreversibly to Bcl-xL and slowly displace cBid. This would allow targeting preformed prosurvival Bcl-2/BH3-only complexes and direct induction of cell death, which could be of interest for example in the case of cells primed for death.

Moreover, our analysis is based on a competition assay of the corresponding BH3 peptide and cBid for binding to Bcl-xL. This is different from previous studies focused on the estimation of the binding affinity of BH3 peptides or cBid chimeras to Bcl-xL in the absence of BH3-only proteins.^{6–8} In this sense, the assay designed here compares better to the therapeutic situation in which BH3 mimetics compete with the BH3-only proteins present in the cell for binding to the prosurvival Bcl-2s.

On the basis of these results, we designed an assay to test the effectiveness of individual BH3 peptides in solution in which cBid_R and BclxL_G were allowed to form complexes and reach equilibrium before peptide addition (Figure 3A). Figure 3B shows a representative example of the FCCS data in an inhibition assay, where the high initial CC amplitude (blue line) turns into a CC amplitude close to zero after the cBid_R/BclxL_G has been disrupted due to the addition of the BH3 peptide. We performed similar displacement assays with concentrations varying from 0 to 10 μ M of each of the BH3 peptides. The changes in %CC measured for the individual BH3 peptides as a function of concentration are shown in Figure 3C. The red line indicates the maximum %CC amplitude in the control without peptide after taking into account the crosstalk between the red and the green channels.

We found that the BH3 peptides derived from Bim, Bad, Bid, Hrk, Puma, and Bik were able to disrupt the complexes between cBid/BclxL in solution, but not those derived from Bmf and Noxa. The BH3Bmf peptide was moderately effective. The normalized change in %CC shown in Figure 3D revealed that most of the BH3 peptides were similarly effective in disrupting the interaction between cBid_R/Bcl-xL_G in solution with slightly higher or lower preferences, except that of Bmf and Noxa. Based on this, we classified the BH3 peptides from Bim, Bad, Bid, Hrk, Puma, and Bik as high effective peptides, BH3Bmf as moderately active and NoxaBH3 as completely ineffective in the solution environment. Due to the relatively small working range of our assay in solution (change in %CC), we cannot reliably distinguish small differences in the binding affinity. Nevertheless, our results are in good agreement with previous quantifications of the affinity between Bcl-xL truncated in the C-terminus and BH3 peptides^{7,8} and demonstrate that the C-terminal transmembrane domain of Bcl-xL does not play an important role in the interaction with cBid or with the BH3 peptides in the aqueous environment. However, Yao et al. showed that the C-terminal domain of Bcl-xL modulates the conformation and BH3 ligand affinity of soluble Bcl-xL.¹⁷

BH3 Peptides Derived from Hrk, Bim, Bid, and Bad Are the Most Potent Inhibitors of cBid/Bcl-xL Complexes in Membrane. We performed the competition assay in the membrane by adding the proteins and the peptides to a

suspension of GUVs with a lipid composition of PC:CL: NTA-lipid (75:20:5). The 6XHis residues in the peptides ensured effective targeting to the membranes containing NTA-lipid (see Methods), a strategy that we and others successfully used previously.^{14,30} A simple scheme of the assay is represented in Figure 4A. By adding proteins and peptides simultaneously, the peptides compete with cBid for binding to the groove of Bcl-xL. Since membrane binding is faster than complex formation for both proteins and peptides, the competitive reaction takes place in the membrane. The inhibitory activity of the peptides can be quantified by measuring the extent of complex formation (CC amplitude) between labeled cBid_R and Bcl-xL_G within the GUVs by scanning FCCS.

We then compared the ability of each peptide to compete with cBid_R for binding to Bcl-xL_G exclusively in the membrane environment by quantifying %CC between cBid_R and Bcl-xL_G in GUVs using scanning FCCS (Figure 4B,C). We found that the BH3Hrk peptide was the most effective inhibitor, followed by Bim, Bid and Bad BH3 peptides. The differences between the %CC of the BH3 peptides Hrk, Bim, Bid and Bad and the control sample in absence of peptide were significant. In contrast, the peptides derived from Bmf, Puma, Bik and Noxa was less or not effective in inhibiting the membrane interactions of cBid_R and Bcl-xL_G. On the basis of this, we classified the peptides as highly effective (BH3 from Hrk, Bim, Bid and Bad) and less effective BH3 peptides (from Bmf, Puma, Bik, and Noxa).

To the best of our knowledge, the comparative, quantitative analysis of the interactions in the membrane environment described here is the first of its kind, as it focuses exclusively on the effect of the peptides on the membrane complexes (previous studies including membranes were performed in bulk and cannot discard interactions in solution⁶). We found that four BH3 peptides were most potent in competing for the cBid/Bcl-xL interactions, namely those derived from Hrk, Bim, Bid, and Bax. In contrast, for Noxa, Bmf, Bik, and Puma, no or very little inhibitory activity could be detected. It is interesting to note that the high affinity of Hrk for Bcl-xL had been underestimated in previous studies. We found that BH3Hrk, which has been reported to bind specifically to Bcl-xL and not to other prosurvival Bcl-2s,^{7,13} was also the most potent inhibitor of the cBid_R/Bcl-xL_G complexes in the membrane.

In parallel, we measured the binding of cBid_R and Bcl-xL_G to the membrane of the GUVs in control samples and in the presence of the BH3 peptides. As shown in Figure 4D, in the absence of peptides, both proteins were clearly detected at the vesicle rim. Strikingly, addition of BH3 peptides like those of Puma, Bim, and Hrk at a concentration of 5 μ M showed significant reduction in the binding intensity of cBid_R compared to the controls, while that of Bcl-xL_G remained constant. We quantified this effect using scanning FCCS, which provides the number of cBid_R molecules per square micrometer in each individual vesicle (Figure 4E). In good agreement with their ability to interfere with Bcl-xL/cBid complexes, the BH3 peptide derived from Hrk was the most potent to block the association of cBid with the membrane. This indicates that the BH3 peptides not only interfere with the cBid_R/Bcl-xL_G complexes but also displace cBid_R from the membrane. These results suggest that although cBid can bind to the GUV membranes in the presence of CL, it is stabilized there by complex formation with Bcl-xL *via* the hydrophobic groove. If this is not possible, a lesser amount of cBid associates with the membrane and stays in solution (thanks to the presence of the

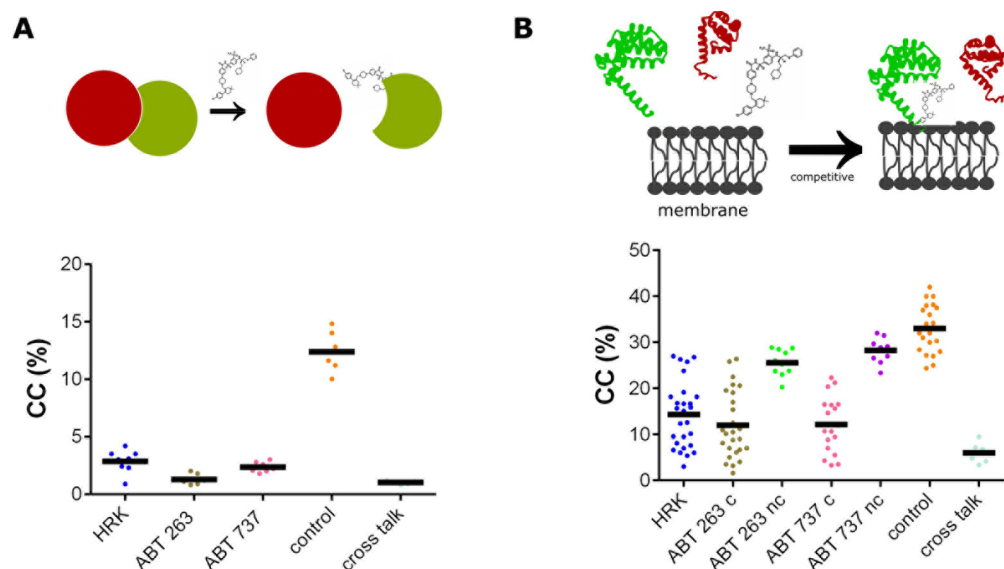


Figure 5. Potency of ABT 263 and ABT 737 to disrupt the complexes between Bcl-xL and cBid in solution and in membranes. (A) Top: Schematic representation of the assay in solution. Interaction of cBidR and Bcl-xLG in solution. Bottom: %CC in solution in the absence and presence of ABTs. (B) Top: Schematic representation of the assay in membranes. cBidR and ABTs (BH3 mimetics) compete for the binding groove in membrane-associated Bcl-xLG. Bottom: % CC between cBidR and Bcl-xLG in the presence of the respective BH3 mimetics (ABTs) in GUVs, where c represents competitive and nc represents noncompetitive assays, respectively. The results obtained with BH3Hrk are included for comparison. The black lines represent the mean %CC. The background crosstalk in solution and in membranes between the two channels is shown.

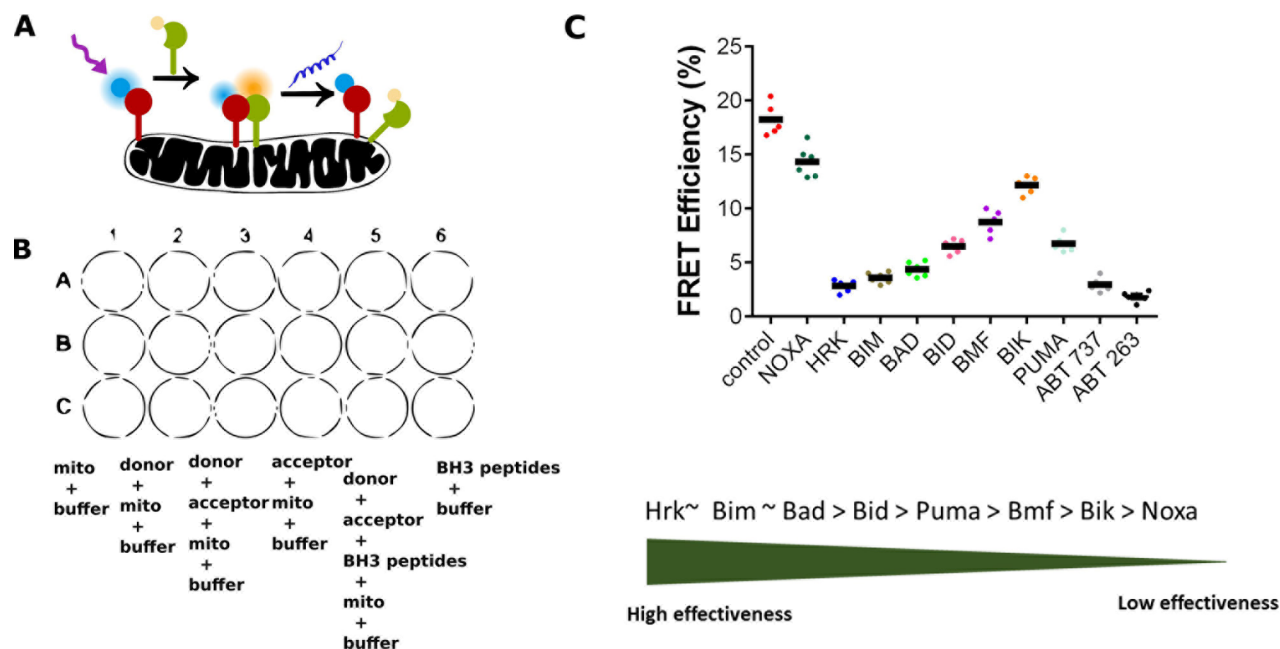


Figure 6. Quantitative analysis of the inhibitory activity of BH3 peptides in isolated mitochondria from yeast using FRET. (A) Schematic representation of the displacement assay. The Atto 488-labeled cBid is shown in green and Bcl-xL-Atto 565 in red. The peptides in blue disrupt the possible interaction between the proteins. (B) Schematic of the 96 well plate showing the sample controls and tests used for the measurements in the plate reader. (C) Quantitative analysis of the change in the FRET efficiencies of cBid-Atto488/Bcl-xL-Atto565 complexes using BH3 peptides and ABTs on isolated mitochondria. The black line represents the mean. A comparative scheme of the peptides efficiency in mitochondria is also shown, based on the statistical analysis of all peptides (two-tailed students *t* test).

p7 fragment of cBid, which contributes to solubility). As a result, the association of cBid with membranes not only depends on the lipid composition but also on direct binding to Bcl-2 proteins.

BH3 Mimetics Disrupt the Interactions between Bcl-xL and cBid Both in Solution and in the Membrane Environment. One of the most important implications of our

study is to provide information for the optimization of small molecule BH3 mimetics. To compare the potency of the peptides analyzed here with current BH3 mimetics, we quantified the ability of ABT263 and ABT737 to disrupt Bcl-xL/cBid complexes with our FCS-based assays both in solution and in the membrane of GUVs. As shown in Figure 5, both molecules were efficient in disrupting the complexes in solution

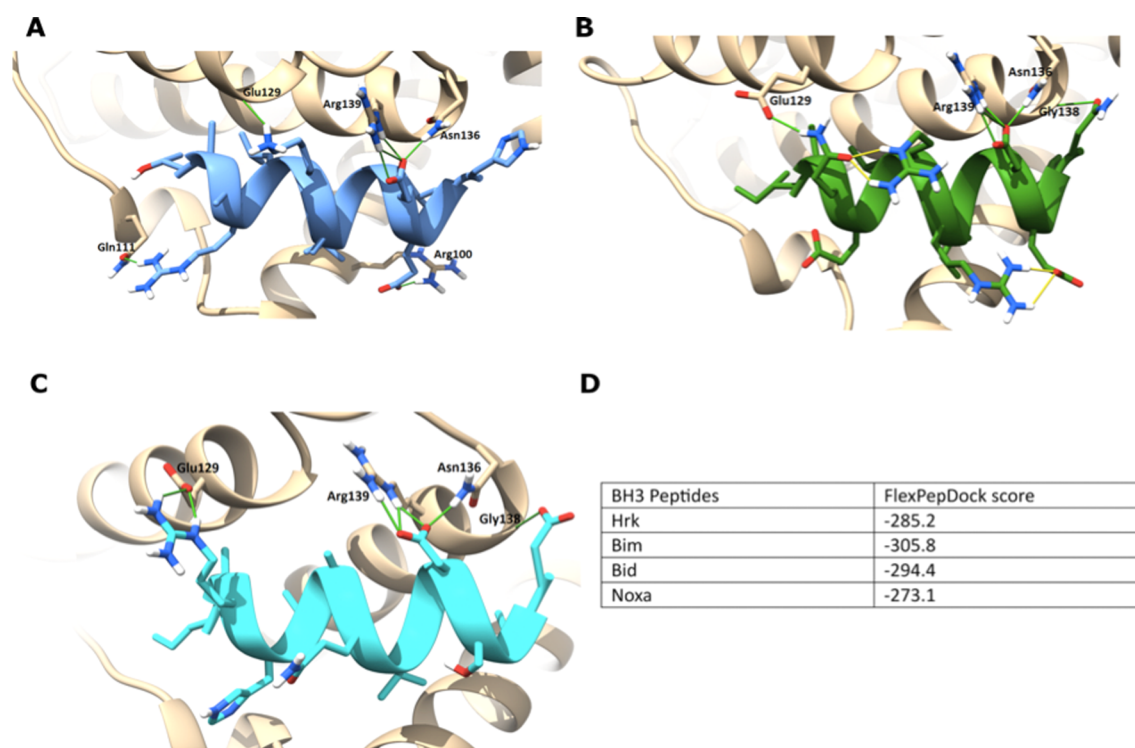


Figure 7. Snapshots of docked BH3 peptides inside the binding groove of Bcl-xL. Bcl-xL and peptides here are shown in ribbon representation; all peptide residues and interacting residues of Bcl-xL are shown in stick representation. (A) Hrk BH3 peptide (13 a.a. length) docked (blue). (B) Docked Bim BH3 peptide (13 a.a. length) shown in green. (C) Docked Bid BH3 peptide (13 a.a. length) shown in cyan. (D) Summary of the docking scores. The Bcl-xL binding pocket is shown in pale yellow; hydrogen bonds are represented by green lines. Intramolecular hydrogen bonds of the Bim BH3 peptide are represented by yellow lines.

and in membranes. Their potency in both environments was in the same range as the Hrk peptide (also included in Figure 5 for comparison). And similarly to the effect of BH3 peptides, both ABT263 and ABT737 were only effective in the membrane environment when added simultaneously to the proteins in a competitive assay. These results indicate that the BH3 mimetics are not efficient either in disrupting already formed complexes between Bcl-xL and cBid in the membrane. Moreover, the comparable activity of BH3Hrk suggests that this peptide could also be an interesting molecule to develop potent, specific Bcl-xL inhibitors.

The Inhibition of BH3 Peptides in Mitochondria Correlates Best with Their Efficiency in the Membrane.

To investigate the efficiency of BH3 peptides to displace cBid_R/Bcl-xL_G complexes in a more physiological environment, we used isolated mitochondria from yeast, which resemble the complex protein and lipid composition found in cells but are devoid of other Bcl-2 proteins. As so far it is not possible to measure FCCS to quantify interactions within mitochondria, we implemented a FRET-based assay.^{15,31,32} A scheme of the experiment is shown in Figure 6A. We selectively labeled cBid with a donor fluorophore Atto 488 and Bcl-xL with an acceptor fluorophore Atto 565, which are a good FRET pair with high quantum yields. To ensure that the system mimics faithfully the natural process, we incubated six samples in parallel: (1) the isolated yeast mitochondria alone to control for background and light scattering effects, (2) the donor fluorophore cBid-488 at 20 nM concentration with the isolated mitochondria, (3) the control for maximum FRET with the donor and acceptor cBid-488:Bcl-xL-Atto565 (20 nM:100 nM) with isolated mitochondria, (4) the acceptor Bcl-xL-Atto565 alone, (5) the BH3

peptides alone as a control for background fluorescence, and finally (6) the donor and acceptor at 20/100 nM in the presence of 5 μM BH3 peptides, as shown in Figure 6B. We recorded the FRET signal upon excitation at 500 nm wavelength for 90 min in a plate reader at 1 min intervals for 90 min. To calculate the FRET efficiency, we averaged the values for the last 10–15 min of the assay, which exhibited a stable signal (Supporting Information Table 2). We then compared the change in the FRET efficiency in the presence and absence of the peptides. Although FRET data do not provide an absolute measurement of complex formation, the relative change in the extent of binding between cBid and Bcl-xL in the presence of the BH3 peptides could be estimated by monitoring the change in the FRET efficiency.

A comparison of the change in the FRET efficiency measured for the different BH3 peptides is shown in Figure 6C. Those from Hrk, Bim, and Bid were more effective in disrupting the cBid_R/Bcl-xL_G interactions in isolated mitochondria, when compared to the ones from Bid, Puma, Bmf, Bik, and Noxa, which were moderately effective (BH3Bid, BH3Puma, BH3Bmf) to relatively ineffective peptides (BH3Bik, BH3Noxa). Interestingly, the ABT compounds also showed an effective disruption of the complex formation in the same order of magnitude as BH3Hrk, in agreement with the data in solution and in GUVs.

In the case of the disruption of cBid/Bcl-xL complexes in mitochondria by BH3 peptides, the closest work is that by Kluck and colleagues using cBid chimeras.⁶ Our data are generally in good agreement with their result that BH3Noxa does not interact readily with Bcl-xL; however, the quantitative nature of our analysis additionally allows disentangling the

inhibitory activities of the different peptides. While in our case only the BH3 sequences of Hrk, Bim, and Bad are most able to displace cBid from the complex with Bcl-xL, in their case all chimeras except for that with the BH3 sequence of Noxa are able to bind Bcl-xL.

If now we compare the data obtained for the different compartments (solution, membrane and mitochondria), the results in isolated mitochondria correlate best with the activity pattern found in the experiments with GUVs. Only in the case of BH3Bid, the peptide seems less potent in mitochondria than in GUVs. Overall, this suggests that the membrane interaction is the most relevant and the one that recapitulates best the situation in the cell. Moreover, there is a clear increase in the specificity of the interactions between Bcl-xL and the BH3 peptides in the membrane environment. The lower activity in mitochondria of the BH3 peptides from Puma, Bik, and Noxa compared to the lack of activity in the GUV assay could be due to the inhibitory effect of these peptides in solution. Since the binding affinity of BH3 peptides depends on their length, we cannot discard either that the length,³³ the sequence (i.e., human versus mouse), or the presence of tags may be underlying reasons for the differences among the different studies.³⁴ Nevertheless, in light of our findings, the consideration of Bcl-xL as a prosurvival Bcl-2 with poor BH3-only selectively mainly concluded from previous studies based on solution experiments^{7,8} should be re-evaluated.

Molecular Docking of BH3Hrk, BH3Bim, and BH3Bid As Efficient Inhibitor BH3 Peptides. We found that the BH3 derived from Hrk was the most potent inhibitor of Bcl-xL/cBid interactions both in the membrane and in mitochondria. Although Hrk has already been acknowledged as a BH3-only protein that specifically inhibits Bcl-xL,⁷ the higher strength of the interaction compared to only BH3-only's had been underestimated. Hrk plays a role in apoptosis regulation *via* selective interaction with its BH3 domain mainly in the context of hematopoietic tissues and cultured neurons.³⁵ Unfortunately, there is no structure available for Bcl-xL in complex with the BH3 domain of Hrk.

To understand the basis for the different inhibitory activities of the BH3 peptides, we performed molecular docking analysis. Although little is known about the structure of Bcl-xL in the membrane, Marassi and co-workers recently reported that Bcl-xL inserts the C-terminal domain in the lipid bilayer, which anchors to the membrane the rest of the protein in a globular conformation similar to its soluble structure.¹⁷ In this membrane bound conformation, the hydrophobic groove remained accessible to bind a BH3 peptide from Bid, supporting the use of the soluble structure of Bcl-xL for the docking experiments. Previous docking studies included additional amino acids in the BH3 peptides and cannot be faithfully compared with our experimental data. We then selected BH3Hrk, BH3Bim, BH3Bid (as highly active peptides), and BH3Noxa (as ineffective peptide) for docking with the hydrophobic groove of Bcl-xL. We numbered the BH3 peptide residues consecutively from 1 to 13 starting from the N-terminus.

Snapshots of the docking for the BH3 peptides of Hrk, Bim, and Bid with the hydrophobic groove of Bcl-xL are shown in Figure 7. The visual inspection of the top 10 images of each peptide showed that they converged to a consensus solution. The conserved residue Asp10 in all peptides was salt-bridged to Arg139 and formed an additional hydrogen bond with Asn136. As it was flanked between the two residues, it was critical for

the binding to the groove. The side chain of Glu129 of Bcl-xL accepted a proton from Gln3 of BH3Bim and Arg3 of BH3Bid, while its backbone oxygen accepted a proton from Lys6 of Hrk. The backbone nitrogen of Gly138 of Bcl-xL donated a proton to Asn13 of BH3Bim and Asp13 of BH3Bid. Additionally, BH3Hrk Arg4 and Glu11 residues showed the formation of two additional H bonds with the side chains of Gln111 and Arg100 respectively. In contrast, the Lys11 residue in BH3Noxa was electrostatically unfavorable in the groove, because of its orientation toward the positive charge residues of Bcl-xL (shown in Supporting Information Figure 3). This electrostatic repulsion could be the reason for the poor performance of this peptide in the complex disruption experiments. In agreement with this, mutant versions of BH3Noxa substituting that Lys showed increased binding to truncated Bcl-xL in solution.⁸ In all docked poses, the hydrophobic residues of peptides were directed to the "bottom" of the Bcl-xL groove while other polar residues formed hydrogen bonds with different shallow residues of Bcl-xL. The most important of them was the conserved Asp that formed hydrogen bonds with two residues in Bcl-xL, and its position seems to be very critical for binding. In addition, the Bim peptide was further stabilized by intramolecular hydrogen bonds that could contribute by fixing the structure in the helical conformation required for binding.

The energy scores of the BH3 peptides were best consistent with our experimental findings in solution, where Bim was the most potent and Noxa was the least able to disrupt Bcl-xL/cBid interactions. These scores are however not consistent with our results in the membrane environment, where we observed the trend that Hrk was more active than Bim. This is likely due to hydrophobic effects that cannot be accounted for using the docking study presented here.

Altogether, our findings suggest that the special features of Hrk should be taken into account in the directed design of small inhibitors of specific prosurvival Bcl-2 homologues. Unfortunately, the crucial role of Bcl-xL in platelet survival limits the use of specific Bcl-xL inhibitors in anticancer therapy.^{36,37} Nevertheless, specific Bcl-xL inhibitors have proved valuable tools for research in mitochondrial apoptosis and in the characterization of specific Bcl-2 addition of tumors.^{34,38} Moreover, the findings reported here could be considered when designing small molecules that specifically do not bind to Bcl-xL^{10,39} and therefore expand the therapeutic window for treatment.

In summary, we report here a comparative study of the ability of BH3 peptides derived from Bid, Bim, Bik, Noxa, Puma, Hrk, Bmf, and Bad to disrupt complexes between cBid and Bcl-xL in solution, in the membrane and in isolated mitochondria. We find that, while all peptides except those of Noxa and Bmf have a comparable activity in solution, only those of the BH3 peptides from Hrk, Bim, Bid, and Bad are effective inhibitors of the membrane complexes. Moreover, the inhibitory activity in mitochondria correlates best with that of the membrane environment, which underscores the physiological relevance of the interactions between Bcl-2s in membranes and supports the interest of Bcl-2 complexes in membranes as a target for improved therapeutic treatment.

METHODS

Protein Production and Labeling and Peptide Preparation. Full-length, human, mutant Bid (Bid C15S, C28S, and S64C) and full-length, human, mutant Bcl-xL (Bcl-xL S4C and C151A) were expressed in *E. coli* and purified as described in refs 40 and 41.

From Bid, cBid was cleaved using caspase 8⁴² and purified as described in ref 40. All protein mutants contained only one accessible cysteine that was labeled with Alexa 488-maleimide and Alexa 647-maleimide in the case of the Bcl-xL and cBid, respectively. The labeling efficiency of Bcl-xL was $\geq 90\%$, and the cBid labeling efficiency was $\geq 65\%$ labeled. Peptides 13 amino acid long from the BH3 domain of BH3-only proteins and containing a 6His tag at the C-terminal end were purchased from Proteogenix (France), with a purity of $\geq 90\%$. The sequence map of the peptides was generated using webLogo 3.

Composition of the Lipid Mixtures. A lipid mixture composed of 75% PC and 20% CL and 5% NTA-Ni-lipid (1,2-dioleoyl-*sn*-glycero-3-[(N-(5-amino-1-carboxypentyl)iminodiacetic acid) succinyl], nickel salt) (mol/mol) was used as described earlier in ref 43. All lipids were purchased from Avanti polar lipids (Alabaster, Alabama).

GUV Formation and Sample Preparation. GUVs were produced by electro-formation, and the experiments were done as described in refs 41 and 44. Briefly, 5 μg of lipid mixture dissolved in chloroform were spread on each platinum electrode of the electro-formation chamber and allowed to dry, before immersion in 300 mM sucrose. Electro-formation proceeded for 2 h at 10 Hz, followed by 30 min at 2 Hz. A total of 75 to 100 μL of the GUVs suspension was added to a solution of PBS buffer mixed with the proteins of interest in Lab-Tek eight-well chamber slides (NUNC) to a final volume of 300 μL .

Solution FCS Measurements. For solution FCS measurements, the proteins of interest were mixed with PBS buffer, at pH 7.4, in a total volume of 200 μL and incubated at least 30 min before measurements. Incubation and measurements were done in a Lab-Tek eight-well chamber slides (NUNC) that were blocked with BSA (10 mg mL^{-1}) before use. To disrupt the interaction of cBid Bcl-xL BH3, peptides were added after 30 min of incubation. For the assay, we used cBid_R, Bcl-xL_G 50 nM and 100 nM (approx.), respectively, in solution and BH3 peptides varying from 0 to 10 μM , and a fixed concentration of ABTs 1 μM was added. The experiments were performed using a LSM710 confocal microscope equipped with a Confocor3, a C-Apochromat 40 \times N.A. 1.2 water immersion objective, and a laser to excite at 488 and 633 nm. Each acquisition lasted at least 10 000 times longer than the diffusion time of the labeled proteins to ensure sufficient data points to generate the autocorrelation curves. To calculate the diffusion time (τ_D), diffusion coefficients (D), the protein concentration, and the cross-correlation, we assumed a three-dimensional diffusion and used the equations introduced in Supporting Information Table 1.

Membrane FCS Measurements. For (competitive) membrane FCS measurements, the proteins cBid_R, Bcl-xL_G, and peptides were mixed with PBS buffer, at pH 7.4, to 80 μL of GUVs containing Ni lipid, in a total volume of 300 μL and incubated at least 1 h before the measurements. For the assay, we used cBid_R, Bcl-xL_G 20 nM, and 40 nM, respectively, in the membrane, and 5 μM BH3 peptides and ABTs were added.

We performed two-focus scanning FCCS measurements at 22 $^\circ\text{C}$ using a Confocor 3 module. Photon arrival times were recorded with a hardware correlator Flex 02-01D/C (<http://correlator.com>). We repeatedly scanned the detection volume with two perpendicular lines across a GUV equator (the distance between the two bleached lines d was measured on a film of dried fluorophores). Data analysis was performed with home-built software (see ref 43). We binned the photon stream in 2 μs , and arranged it as a matrix such that every row corresponded to a one-line scan. We corrected for membrane movements by calculating the maximum of a running average over several hundred line scans and shifting it to the same column. We fitted an average over all rows with a Gaussian, and we added only the elements of each row between -2.5 and $+2.5$ s to construct the intensity trace. We computed the auto-, spectral, and spatial cross-correlation curves from the intensity traces and excluded irregular curves resulting from instabilities and distortions. We fitted the auto- and cross-correlation functions with a nonlinear least-squares global fitting algorithm as previously.¹⁴ The used equations are shown in Supporting Information Table 1.

Isolated Yeast Mitochondria and FRET Experiment. Mitochondria were isolated from WT303a yeast cells grown in YPG media as described.⁴⁵ The FRET measurements were performed as described in Pogmore *et al.*³² Mitochondria at a concentration of 1 mg mL^{-1} were incubated with 20 nM cBid-Atto 488 and 100 nM Bcl-xL-Atto 565. The Atto488 and Atto565 signals were recorded using a Tecan Infinite M200 plate reader. We acquired data using excitation at 500 nm, a 5 nm slit width and emission at 590 nm, and 10 nm slit width for 90 min at 37 $^\circ\text{C}$. BH3 peptides at a 5 μM concentration were added to the corresponding samples. FRET efficiency was calculated as $\% E = 1 - (F_{DA}/F_D)100$, where E is % fret efficiency, F_{DA} is the donor in the presence of labeled acceptor, and F_D is the unlabeled acceptor.³¹

Molecular Docking. The crystal structure of Bcl-xL in complex with Bim (26 residues) was retrieved from the PDB (id: 4QVF) and prepared by removing Bim and water molecules followed by adding hydrogen atoms and partial charges. The peptides 13 amino acids long were docked into the binding site of Bcl-xL using the Rosetta FlexPepDock application,⁴⁶ which utilizes Monte Carlo simulation to optimize the peptide backbone and its rigid-body orientation relative to Bcl-xL. In addition, all of the peptide's side chains and the receptor's interface side chains were considered flexible and were subject to optimization. A total of 200 independent models were generated and sorted according to Flexpepdock reweighted score, which gives interface residues double weight and peptide residues triple weight. The final score was the average of the top 10 models. The top-scoring models of each peptide were inspected and visualized using UCSF Chimera software.⁴⁷

■ ASSOCIATED CONTENT

📄 Supporting Information

The Supporting Information is available free of charge on the ACS Publications website at DOI: 10.1021/acscchembio.6b01084.

Supporting Table 1 and Figures 1–4 (PDF)

■ AUTHOR INFORMATION

Corresponding Author

*Tel.: +49 7071 29 73318. E-mail: ana.garcia@uni.tuebingen.de.

ORCID

Ana J. García-Sáez: 0000-0002-3894-5945

Notes

The authors declare no competing financial interest.

■ ACKNOWLEDGMENTS

We thank J. C. Martinou for kindly providing caspase 8 for the preparation of cBid. We also thank C. Stegmüller for technical assistance and S. Bleicken, J. Unsay, and J. Danial for helpful discussions. This work was funded by the DFG (FOR 2036) and the University of Tübingen (scholarship to K.K.D. within the IMPRS program).

■ REFERENCES

- (1) Garcia-Saez, A. J. (2012) The secrets of the Bcl-2 family. *Cell Death Differ.* 19, 1733–1740.
- (2) Westphal, D., Kluck, R. M., and Dewson, G. (2014) Building blocks of the apoptotic pore: how Bax and Bak are activated and oligomerize during apoptosis. *Cell Death Differ.* 21, 196–205.
- (3) Happon, L., Strasser, A., and Cory, S. (2012) BH3-only proteins in apoptosis at a glance. *J. Cell Sci.* 125, 1081–1087.
- (4) Ren, D., Tu, H. C., Kim, H., Wang, G. X., Bean, G. R., Takeuchi, O., Jeffers, J. R., Zambetti, G. P., Hsieh, J. J., and Cheng, E. H. (2010) BID, BIM, and PUMA are essential for activation of the BAX- and BAK-dependent cell death program. *Science* 330, 1390–1393.

- (5) Kim, H., Tu, H. C., Ren, D., Takeuchi, O., Jeffers, J. R., Zambetti, G. P., Hsieh, J. J., and Cheng, E. H. (2009) Stepwise activation of BAX and BAK by tBID, BIM, and PUMA initiates mitochondrial apoptosis. *Mol. Cell* 36, 487–499.
- (6) Hockings, C., Anwar, K., Ninnis, R. L., Brouwer, J., O'Hely, M., Evangelista, M., Hinds, M. G., Czabotar, P. E., Lee, E. F., Fairlie, W. D., Dewson, G., and Kluck, R. M. (2015) Bid chimeras indicate that most BH3-only proteins can directly activate Bak and Bax, and show no preference for Bak versus Bax. *Cell Death Dis.* 6, e1735.
- (7) Certo, M., Moore, V. D., Nishino, M., Wei, G., Korsmeyer, S., Armstrong, S. A., and Letai, A. (2006) Mitochondria primed by death signals determine cellular addiction to antiapoptotic BCL-2 family members. *Cancer Cell* 9, 351–365.
- (8) Chen, L., Willis, S. N., Wei, A., Smith, B. J., Fletcher, J. I., Hinds, M. G., Colman, P. M., Day, C. L., Adams, J. M., and Huang, D. C. S. (2005) Differential Targeting of Prosurvival Bcl-2 Proteins by Their BH3-Only Ligands Allows Complementary Apoptotic Function. *Mol. Cell* 17, 393–403.
- (9) Tse, C., Shoemaker, A. R., Adickes, J., Anderson, M. G., Chen, J., Jin, S., Johnson, E. F., Marsh, K. C., Mitten, M. J., Nimmer, P., Roberts, L., Tahir, S. K., Xiao, Y., Yang, X., Zhang, H., Fesik, S., Rosenberg, S. H., and Elmore, S. W. (2008) ABT-263: a potent and orally bioavailable Bcl-2 family inhibitor. *Cancer Res.* 68, 3421–3428.
- (10) Souers, A. J., Levenson, J. D., Boghaert, E. R., Ackler, S. L., Catron, N. D., Chen, J., Dayton, B. D., Ding, H., Enschede, S. H., Fairbrother, W. J., Huang, D. C., Hymowitz, S. G., Jin, S., Khaw, S. L., Kovar, P. J., Lam, L. T., Lee, J., Maecker, H. L., Marsh, K. C., Mason, K. D., Mitten, M. J., Nimmer, P. M., Oleksijew, A., Park, C. H., Park, C. M., Phillips, D. C., Roberts, A. W., Sampath, D., Seymour, J. F., Smith, M. L., Sullivan, G. M., Tahir, S. K., Tse, C., Wendt, M. D., Xiao, Y., Xue, J. C., Zhang, H., Humerickhouse, R. A., Rosenberg, S. H., and Elmore, S. W. (2013) ABT-199, a potent and selective BCL-2 inhibitor, achieves antitumor activity while sparing platelets. *Nat. Med.* 19, 202–208.
- (11) Delbridge, A. R., and Strasser, A. (2015) The BCL-2 protein family, BH3-mimetics and cancer therapy. *Cell Death Differ.* 22, 1071–1080.
- (12) Billard, C. (2013) BH3 mimetics: status of the field and new developments. *Mol. Cancer Ther.* 12, 1691–1700.
- (13) Campbell, S. T., Carlson, K. J., Buchholz, C. J., Helmers, M. R., and Ghosh, I. (2015) Mapping the BH3 Binding Interface of Bcl-xL, Bcl-2, and Mcl-1 Using Split-Luciferase Reassembly. *Biochemistry* 54, 2632–2643.
- (14) Garcia-Saez, A. J., Ries, J., Orzaez, M., Perez-Paya, E., and Schwill, P. (2009) Membrane promotes tBID interaction with BCLXL. *Nat. Struct. Mol. Biol.* 16, 1178–1185.
- (15) Lovell, J. F., Billen, L. P., Bindner, S., Shamas-Din, A., Fradin, C., Leber, B., and Andrews, D. W. (2008) Membrane Binding by tBid Initiates an Ordered Series of Events Culminating in Membrane Permeabilization by Bax. *Cell* 135, 1074–1084.
- (16) Leber, B., Lin, J., and Andrews, D. W. (2010) Still embedded together binding to membranes regulates Bcl-2 protein interactions. *Oncogene* 29, 5221–5230.
- (17) Yao, Y., Fujimoto, L. M., Hirshman, N., Bobkov, A. A., Antignani, A., Youle, R. J., and Marassi, F. M. (2015) Conformation of BCL-XL upon Membrane Integration. *J. Mol. Biol.* 427, 2262–2270.
- (18) Walensky, L. D., Pitter, K., Morash, J., Oh, K. J., Barbuto, S., Fisher, J., Smith, E., Verdine, G. L., and Korsmeyer, S. J. (2006) A stapled BID BH3 helix directly binds and activates BAX. *Mol. Cell* 24, 199–210.
- (19) Lomonosova, E., and Chinnadurai, G. (2008) BH3-only proteins in apoptosis and beyond: an overview. *Oncogene* 27, S2–19.
- (20) Letai, A., Bassik, M. C., Walensky, L. D., Sorcinelli, M. D., Weiler, S., and Korsmeyer, S. J. (2002) Distinct BH3 domains either sensitize or activate mitochondrial apoptosis, serving as prototype cancer therapeutics. *Cancer Cell* 2, 183–192.
- (21) Czabotar, P. E., Lessene, G., Strasser, A., and Adams, J. M. (2014) Control of apoptosis by the BCL-2 protein family: implications for physiology and therapy. *Nat. Rev. Mol. Cell Biol.* 15, 49–63.
- (22) Rajan, S., Choi, M., Baek, K., and Yoon, H. S. (2015) Bh3 induced conformational changes in Bcl-XL revealed by crystal structure and comparative analysis. *Proteins: Struct., Funct., Genet.* 83, 1262–1272.
- (23) Ries, J., and Schwill, P. (2006) Studying Slow Membrane Dynamics with Continuous Wave Scanning Fluorescence Correlation Spectroscopy. *Biophys. J.* 91, 1915–1924.
- (24) Schwill, P., Meyer-Almes, F. J., and Rigler, R. (1997) Dual-color fluorescence cross-correlation spectroscopy for multicomponent diffusional analysis in solution. *Biophys. J.* 72, 1878–1886.
- (25) Garcia-Saez, A. J., and Schwill, P. (2008) Fluorescence correlation spectroscopy for the study of membrane dynamics and protein/lipid interactions. *Methods* 46, 116–122.
- (26) Weidemann, T., Wachsmuth, M., Tewes, M., Rippe, K., and Langowski, J. (2002) Analysis of Ligand Binding by Two-Colour Fluorescence Cross-Correlation Spectroscopy. *Single Mol.* 3, 49–61.
- (27) Billen, L. P., Kokoski, C. L., Lovell, J. F., Leber, B., and Andrews, D. W. (2008) Bcl-XL Inhibits Membrane Permeabilization by Competing with Bax. *PLoS Biol.* 6, e147.
- (28) Shamas-Din, A., Kale, J., Leber, B., and Andrews, D. W. (2013) Mechanisms of Action of Bcl-2 Family Proteins. *Cold Spring Harbor Perspect. Biol.* 5, a008714.
- (29) Ding, J., Mooers, B. H., Zhang, Z., Kale, J., Falcone, D., McNichol, J., Huang, B., Zhang, X. C., Xing, C., Andrews, D. W., and Lin, J. (2014) After embedding in membranes antiapoptotic Bcl-XL protein binds both Bcl-2 homology region 3 and helix 1 of proapoptotic Bax protein to inhibit apoptotic mitochondrial permeabilization. *J. Biol. Chem.* 289, 11873–11896.
- (30) Oh, K. J., Barbuto, S., Pitter, K., Morash, J., Walensky, L. D., and Korsmeyer, S. J. (2006) A membrane-targeted BID BCL-2 homology 3 peptide is sufficient for high potency activation of BAX in vitro. *J. Biol. Chem.* 281, 36999–37008.
- (31) Kale, J., Chi, X., Leber, B., and Andrews, D. (2014) Chapter One - Examining the Molecular Mechanism of Bcl-2 Family Proteins at Membranes by Fluorescence Spectroscopy, In *Methods in Enzymology* (Avi Ashkenazi, J. Y., and James, A. W., Eds.), pp 1–23, Academic Press.
- (32) Pogmore, J. P., Pemberton, J. M., Chi, X., and Andrews, D. W. (2016) Using Forster-Resonance Energy Transfer to Measure Protein Interactions Between Bcl-2 Family Proteins on Mitochondrial Membranes. *Methods Mol. Biol. (N. Y., NY, U. S.)* 1419, 197–212.
- (33) Boersma, M. D., Sadowsky, J. D., Tomita, Y. A., and Gellman, S. H. (2008) Hydrophile scanning as a complement to alanine scanning for exploring and manipulating protein-protein recognition: application to the Bim BH3 domain. *Protein Sci.* 17, 1232–1240.
- (34) Dutta, S., Ryan, J., Chen, T. S., Kougentakis, C., Letai, A., and Keating, A. E. (2015) Potent and specific peptide inhibitors of human pro-survival protein Bcl-xL. *J. Mol. Biol.* 427, 1241–1253.
- (35) Nakamura, M., Shimada, K., and Konishi, N. (2008) The role of HRK gene in human cancer. *Oncogene* 27, S105–S113.
- (36) Roberts, A. W., Seymour, J. F., Brown, J. R., Wierda, W. G., Kipps, T. J., Khaw, S. L., Carney, D. A., He, S. Z., Huang, D. C., Xiong, H., Cui, Y., Busman, T. A., McKeegan, E. M., Krivoshik, A. P., Enschede, S. H., and Humerickhouse, R. (2012) Substantial susceptibility of chronic lymphocytic leukemia to BCL2 inhibition: results of a phase I study of navitoclax in patients with relapsed or refractory disease. *J. Clin. Oncol.* 30, 488–496.
- (37) Rudin, C. M., Hann, C. L., Garon, E. B., Ribeiro de Oliveira, M., Bonomi, P. D., Camidge, D. R., Chu, Q., Giaccone, G., Khaira, D., Ramalingam, S. S., Ranson, M. R., Dive, C., McKeegan, E. M., Chyla, B. J., Dowell, B. L., Chakravarty, A., Nolan, C. E., Rudersdorf, N., Busman, T. A., Mabry, M. H., Krivoshik, A. P., Humerickhouse, R. A., Shapiro, G. I., and Gandhi, L. (2012) Phase II study of single-agent navitoclax (ABT-263) and biomarker correlates in patients with relapsed small cell lung cancer. *Clin. Cancer Res.* 18, 3163–3169.
- (38) Lessene, G., Czabotar, P. E., Sleeb, B. E., Zobel, K., Lowes, K. N., Adams, J. M., Baell, J. B., Colman, P. M., Deshayes, K., Fairbrother, W. J., Flygare, J. A., Gibbons, P., Kersten, W. J., Kulasegaram, S., Moss, R. M., Parisot, J. P., Smith, B. J., Street, I. P., Yang, H., Huang, D. C.,

and Watson, K. G. (2013) Structure-guided design of a selective BCL-X(L) inhibitor. *Nat. Chem. Biol.* 9, 390–397.

(39) Foight, G. W., Ryan, J. A., Gulla, S. V., Letai, A., and Keating, A. E. (2014) Designed BH3 peptides with high affinity and specificity for targeting Mcl-1 in cells. *ACS Chem. Biol.* 9, 1962–1968.

(40) Bleicken, S., Classen, M., Padmavathi, P. V., Ishikawa, T., Zeth, K., Steinhoff, H. J., and Bordignon, E. (2010) Molecular details of Bax activation, oligomerization, and membrane insertion. *J. Biol. Chem.* 285, 6636–6647.

(41) Bleicken, S., Wagner, C., and García-Sáez, A. J. (2013) Mechanistic Differences in the Membrane Activity of Bax and Bcl-xL Correlate with Their Opposing Roles in Apoptosis. *Biophys. J.* 104, 421–431.

(42) Li, H., Zhu, H., Xu, C.-j., and Yuan, J. (1998) Cleavage of BID by Caspase 8 Mediates the Mitochondrial Damage in the Fas Pathway of Apoptosis. *Cell* 94, 491–501.

(43) Garcia-Saez, A. J., Ries, J., Orzaez, M., Perez-Paya, E., and Schwille, P. (2009) Membrane promotes tBID interaction with BCL(XL). *Nat. Struct. Mol. Biol.* 16, 1178–1185.

(44) Bleicken, S., and Garcia-Saez, A. J. (2014) New biophysical methods to study the membrane activity of bcl-2 proteins. *Methods Mol. Biol. (N. Y., NY, U. S.)* 1176, 191–207.

(45) Meisinger, C., Pfanner, N., and Truscott, K. N. (2006) Isolation of yeast mitochondria. *Methods in molecular biology (Clifton, N.J.)* 313, 33–39.

(46) Raveh, B., London, N., and Schueler-Furman, O. (2010) Sub-angstrom modeling of complexes between flexible peptides and globular proteins. *Proteins: Struct., Funct., Genet.* 78, 2029–2040.

(47) Pettersen, E. F., Goddard, T. D., Huang, C. C., Couch, G. S., Greenblatt, D. M., Meng, E. C., and Ferrin, T. E. (2004) UCSF Chimera—A visualization system for exploratory research and analysis. *J. Comput. Chem.* 25, 1605–1612.

ARTICLE

DOI: 10.1038/s41467-017-00086-6

OPEN

Quantitative interactome of a membrane Bcl-2 network identifies a hierarchy of complexes for apoptosis regulation

Stephanie Bleicken^{1,2,3,5}, Annika Hantusch⁴, Kushal Kumar Das³, Tancred Frickey⁴ & Ana J. Garcia-Saez ^{1,2,3}

The Bcl-2 proteins form a complex interaction network that controls mitochondrial permeabilization and apoptosis. The relative importance of different Bcl-2 complexes and their spatio-temporal regulation is debated. Using fluorescence cross-correlation spectroscopy to quantify the interactions within a minimal Bcl-2 network, comprised by cBid, Bax, and Bcl-xL, we show that membrane insertion drastically alters the pattern of Bcl-2 complexes, and that the C-terminal helix of Bcl-xL determines its binding preferences. At physiological temperature, Bax can spontaneously activate in a self-amplifying process. Strikingly, Bax also recruits Bcl-xL to membranes, which is sufficient to retrotranslocate Bax back into solution to secure membrane integrity. Our study disentangles the hierarchy of Bcl-2 complex formation in relation to their environment: Bcl-xL association with cBid occurs in solution and in membranes, where the complex is stabilized, whereas Bcl-xL binding to Bax occurs only in membranes and with lower affinity than to cBid, leading instead to Bax retrotranslocation.

¹Max Planck Institute for Intelligent Systems, Heisenbergstr. 3, 70569 Stuttgart, Germany. ²German Cancer Research Center, Im Neuenheimer Feld 280, 69120 Heidelberg, Germany. ³Interfaculty Institute of Biochemistry, Eberhard Karls University Tübingen, Hoppe-Seyler-Str. 4, 72076 Tübingen, Germany. ⁴University of Konstanz, Applied Bioinformatics, Universitaetsstr. 10, 78457 Konstanz, Germany. ⁵Present address: ZEMOS, Ruhr-University Bochum, Universitaetsstr. 150, 44801 Bochum, Germany. Correspondence and requests for materials should be addressed to A.J.G-S. (email: ana.garcia@uni-tuebingen.de)

The proteins of the Bcl-2 family are key regulators of several cellular functions including mitochondrial dynamics and apoptosis^{1–3}. They form a complex network with multiple, parallel interactions that regulates the permeabilization of the mitochondrial outer membrane (MOM). Once the membrane is perforated, cytochrome *c* is released, which is considered the point of no return in the cell commitment to death. Because the Bcl-2 network lies at the heart of apoptosis regulation and is linked to diseases like cancer, Bcl-2 proteins are attractive targets in drug development^{3, 4}.

The Bcl-2 family is classified into three sub-groups: Bax and Bak are proapoptotic and directly mediate MOM permeabilization by opening pores at the MOM. Prosurvival proteins like Bcl-2, Bcl-xL, and Mcl-1 promote cell survival by inhibiting their proapoptotic counterparts. The BH3-only proteins have evolved to sense stress stimuli and to promote apoptosis either directly by activating Bax and Bak or indirectly by inhibiting the prosurvival Bcl-2 proteins^{1, 2}.

In healthy cells, Bax is monomeric and shuttles continuously between the cytosol and the MOM^{5, 6}. During apoptosis, it accumulates at the MOM and undergoes a conformational change that leads to membrane-insertion, oligomerization, and MOM permeabilization^{7–12}, which is accompanied by Bax assembly into a mixture of lines, rings, and arc-like structures^{13, 14}. The active membrane-embedded conformation is suggested to form a clamp-like structure that remodels the membrane and stabilizes pores of tunable size^{10, 15, 16}. Bax activity is regulated by other Bcl-2 members, including cBid and Bcl-xL. Bid is inactive in the cytosol until it is cleaved by caspase 8 into the active form cBid, which consists of two fragments: p7 and tBid^{17, 18}. cBid translocates to the MOM and promotes Bax activation⁸, as well as the insertion of Bcl-xL into the membrane^{19–21}. Bcl-xL inhibits apoptosis via three incompletely understood modes (Fig. 1a). Mode 0 proposes that Bcl-xL shifts the equilibrium between membrane-bound and soluble Bax towards the soluble form^{5, 6}. In Mode 1, Bcl-xL sequesters activator-type BH3 only proteins like cBid, and thereby prevents Bax activation^{21, 22}. Mode 2 proposes inhibition by direct interaction of Bax and Bcl-xL. However, this is based on indirect evidence like co-immunoprecipitation, the use of chimeric proteins, or interaction-defective protein mutants^{22–24}. In addition, Bcl-xL alters the way cBid and Bax remodel membranes¹⁶.

Several models aim to explain how the Bcl-2 network controls MOM permeabilization. The indirect activation or de-repression model²⁵ implies that Bax is spontaneously active, unless it is bound to and inhibited by prosurvival Bcl-2 homologs. BH3 only proteins can compete with this interaction by binding to the prosurvival Bcl-2 family members, which releases Bax to induce MOM permeabilization. In contrast, the direct activation model^{26, 27} proposes that Bax is inactive until it interacts with an activator-type BH3-only protein, like cBid, which triggers membrane insertion and the conformational change. The unified²², the embedded together²⁸, and the hierarchical models²⁹ integrate the de-repression and the direct activation idea into one model.

To understand how the association between Bcl-2 members is orchestrated to regulate MOM permeabilization, a systems approach that provides detailed, quantitative understanding of the relative affinities between full-length Bcl-2 proteins, especially of their active, membrane-embedded forms, is necessary. Performing detailed interaction experiments in living cells is extremely difficult or impossible, due to at least four reasons: (i) the many interactions competing simultaneously, (ii) the difficulties to calculate protein concentrations in organelles of living cells, (iii) the presence of a mixture of different regulatory post-translational modifications, (iv) and the use of fusions to green fluorescent protein (GFP) or similar fluorescent proteins,

which due to their size could affect the function and interactions of the proteins of interest. To solve these limitations, we used here a bottom up approach based on a minimal interaction network composed of full-length cBid, Bax, and Bcl-xL that reproduces the functionality of the Bcl-2 family in vitro. Although the extrapolation to the physiological context needs to be done with extreme care, reconstituted systems allowed great advances in understanding the detailed molecular mechanisms of Bcl-2 function^{26, 30, 31}. The main advantage of our approach is that it is chemically controlled so that the individual interactions between Bcl-2 members can be studied, whereas additional factors, as well as post-translational modifications are absent, or can be added separately when necessary.

Scanning fluorescence cross correlation spectroscopy (FCCS) allows to selectively detect interactions within membranes by removing signals from solution, which was not possible in earlier studies^{22, 30, 32}. This is a critical advantage as cBid, Bax, and Bcl-xL constantly shuttle between soluble and membrane-bound conformations^{5, 6, 18} and both environments should be considered separately. By applying FCCS on soluble and membrane-embedded proteins, we show that the interactions within the Bcl-2 family are spatially regulated. Soluble Bax is monomeric, while upon membrane insertion, it associates into homo-oligomers and hetero-oligomers with cBid and Bcl-xL. In contrast, cBid/Bcl-xL hetero-dimers are detected in solution and membranes. Bcl-xL also forms homo-dimers in solution and its C-terminal transmembrane region modulates the preference for interaction partners. Moreover, we show that membrane-associated Bax recruits soluble Bax and Bcl-xL to the membrane. Bax self-recruitment is a feed-forward mechanism to enhance Bax activity, whereas Bcl-xL recruitment is inhibitory by reducing the size of Bax oligomers via direct interaction and by translocating Bax back into solution. Our findings demonstrate that no additional components are necessary for Bcl-xL-mediated retro-translocation of Bax, which, based on our data, might be driven by Bcl-xL homo-dimerization in solution. This work has implications for the understanding of the Bcl-2 signaling network in its natural context and supports a new model for the integration of Bcl-2 interactions during apoptosis regulation.

Results

The majority of Bcl-xL molecules are dimers in solution. Here we used solution and scanning FCCS to quantify the concentrations, diffusion coefficients (*D*), and the interaction of cBid, Bax, and Bcl-xL (coupled to individual fluorophores) in solution and membranes. FCCS measures intensity fluctuations of fluorophores over time using the detection volume of a confocal microscope. On the basis of the intensity fluctuations over time auto-correlation (AC) and cross-correlation (CC) curves are calculated. The detection volumes of the two detection channels do not overlap perfectly, which affects the maximum CC detectable and as a result our CC values are slightly underestimated. The effect of channel cross talk and noise were calculated with free versions of the used dyes. In solution, the CC was below 2% (μ : 1.4, σ : 0.7; see Supplementary Fig. 1) and values above 2.8% ($\mu \pm 2\sigma$, or 95% confidence) indicate protein interactions. More detailed information is given in Supplementary Methods and in ref. ³³.

We quantified the homo-interactions and hetero-interactions between cBid, Bax, and Bcl-xL in solution (Fig. 1b, c). Bax showed no interactions with itself, cBid or Bcl-xL, indicating that it was present as a monomeric protein. In contrast, the small but significant positive CC of Bcl-xL labeled with red and green dyes indicated the formation of Bcl-xL homo-complexes, most likely

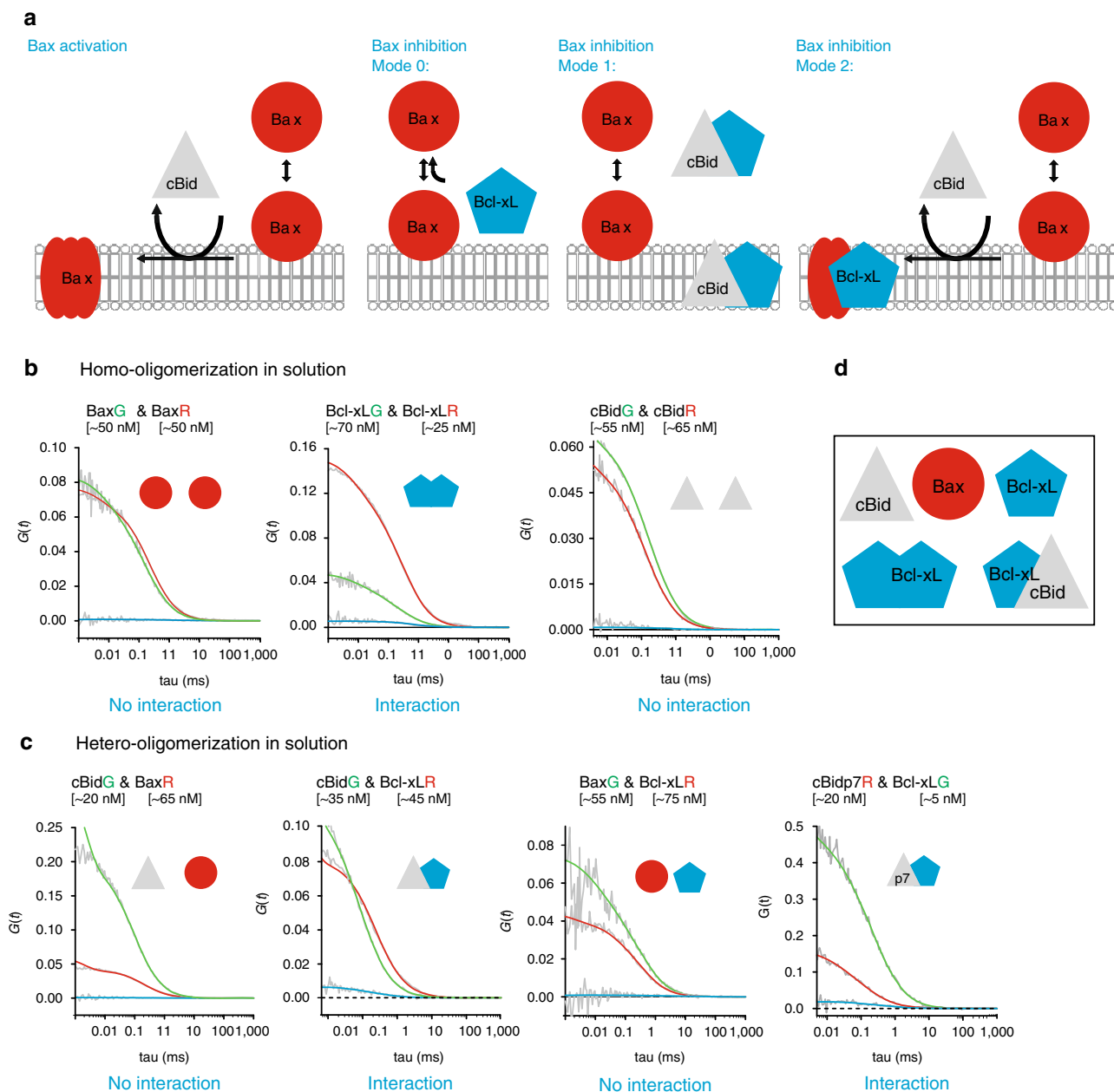


Fig. 1 Analysis of interactions between cBid, Bax, and Bcl-xL in solution. **a** Representation of current models on Bax activation and inhibition by cBid and Bcl-xL. **b, c** Representative FCCS graphs of cBid, Bax, and Bcl-xL homo-hetero-oligomerization (B) and hetero-oligomerization in solution. For visual guidance: The amplitude of the AC curves is inversely proportional to the number of fluorophores, whereas the amplitude of the CC curves is proportional to the number of dual-color complexes. The decay of the AC and CC curves provides quantitative information on the diffusion properties of the particles and therefore of their size. All particle concentrations calculated from FCCS measurements refer to fluorescent particles that diffuse as a unit. Only Bcl-xL_G/Bcl-xL_R and cBid_G/Bcl-xL_R present positive CC amplitude (blue curve) indicative of interaction. The unfitted AC and CC curves are shown in grey ($n \geq 3$ independent experiments), and the fitted AC curves corresponding to the species labeled with green and red fluorophores and shown in green and red, respectively. We studied interactions at different protein concentrations up to 200 nM. **d** Scheme of the five different monomeric and dimeric species that can be detected in solution. FCCS fluorescence cross correlation spectroscopy

dimers, in line with ref. ³⁴. In addition, Bcl-xL interacted with cBid, as shown before^{21, 32}. By using two cBid variants labeled at the N- (cBid_{-p7R}) or C-terminal fragment (cBid_R or cBid_G), we found that the cBid/Bcl-xL complex contained both cBid fragments. In addition, no homo-oligomerization of cBid molecules was detected. Our results show that in solution three different complexes are formed: p7/tBid, Bcl-xL/Bcl-xL, and p7/tBid/Bcl-xL (Fig. 1d). Those complexes are potentially competing in the cytosolic environment and based on our data only Mode 1 of Bcl-xL inhibition takes place in solution.

Contradictory results concerning the oligomeric state (monomeric vs. dimeric) of soluble Bcl-xL exist³⁴⁻³⁹. This is likely due to the use of C terminally truncated protein versions, which cannot dimerize³⁴. Thus, the extent of Bcl-xL dimerization and its relevance remains obscure. The CC curves of Bcl-xL self-association showed low amplitudes, typical of weak interactions and supporting the existence of a major monomeric population (Fig. 1b, and Supplementary Fig. 2, $K_D \sim 600$ nM). Intriguingly, the D of Bcl-xL (Fig. 2a) was smaller than that of cBid and Bax, and varied strongly with protein concentration (Fig. 2a, b),

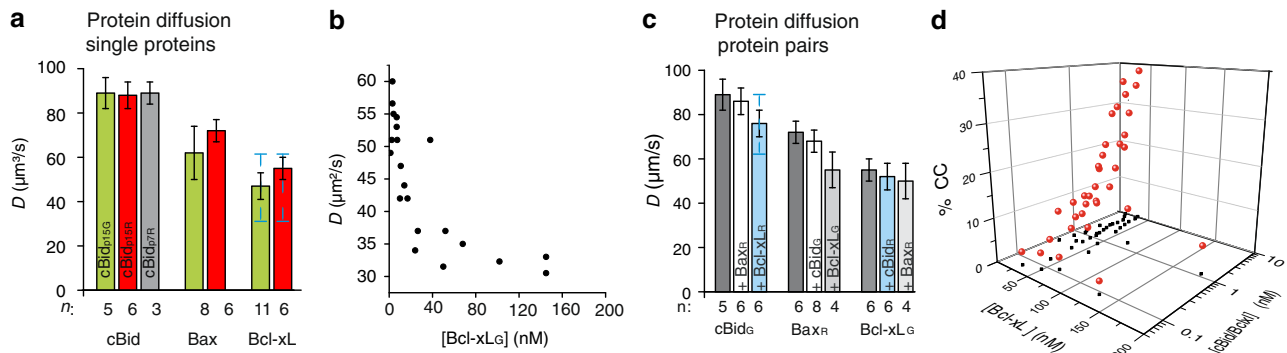


Fig. 2 Quantitative analysis of the interactions between cBid and Bcl-xL in solution. **a** D of cBid, Bax, and Bcl-xL labeled with Alexa488 or Atto488 (green columns), or Alexa633 or Atto655 (red columns). The grey column corresponds to cBid_{p7R}. Mean and error bars as s.d. are shown in black; the additional blue error bars for Bcl-xL indicate scattering of D values depending on concentration, n is indicated in the figure. **b** The D of Bcl-xL_G in dependence of the protein concentration ($n = 4$). **c** Effect of protein co-incubation on the D of cBid, Bax, and Bcl-xL. Addition of Bcl-xL_R, induced a decrease in cBid_G diffusion as expected from direct interaction ($n = 3$, mean and error bars as s.d. are shown in black); the additional blue error bar for cBid in presence of Bcl-xL indicates scattering of D values depending on the Bcl-xL/cBid ratio. **d** The CC between cBid_G and Bcl-xL_R increased with protein concentration (data as red dots with black shadows in xy , $n = 6$)

suggesting a particle size in line with high dimer content. The structures of the inactive, soluble conformations of cBid, Bax, and Bcl-xL^{17, 36, 40} show protein radii in the range of 1.7–2.5 nm, transferring into a D of roughly 70–110 $\mu\text{m}^2\text{s}^{-1}$. The D of cBid, Bax, and Bcl-xL Δ CT fall in this range (Fig. 2a and $D_{\text{Bcl-xL}\Delta\text{CT}}$: 78 $\mu\text{m}^2\text{s}^{-1}$ see²¹), whereas the full length Bcl-xL had a smaller D ($\sim 50 \mu\text{m}^2\text{s}^{-1}$), as would be expected for Bcl-xL dimers. These results indicated that, full length Bcl-xL was mainly dimeric in solution, whereas the C-terminal truncated version was monomeric (in agreement with refs. 21, 34).

To test whether we could detect full-length Bcl-xL monomers in solution, we diluted the protein (Fig. 2b). Interestingly, the D of Bcl-xL grew at concentrations below 20 nM indicating an increase in the monomer population at lower concentrations in line with a high binding affinity between Bcl-xL monomers (low nano-molar K_D). In human cells, the concentration of Bcl-xL (10–1000 nM) and Bax (50–500 nM) was recently estimated⁴¹, suggesting that at physiological concentrations Bcl-xL is mainly dimeric.

To further correlate particle mobility and interactions within the minimal Bcl-2 network, we tested how the presence of a second Bcl-2 protein affects the D of cBid, Bax, and Bcl-xL (Fig. 2c). As expected from the CC data, Bax diffusion was not affected by the presence of cBid or Bcl-xL and vice versa, whereas the mean D of cBid decreased in the presence of Bcl-xL, as expected for hetero-dimerization (p -value: 0.0089, unpaired two tailed t -test). In contrast, the D of Bcl-xL was barely affected by the presence of cBid (Fig. 2c), in line with Bcl-xL being homo- or hetero-dimeric in solution.

cBid can dissociate Bcl-xL homo-dimers. Next, we probed the competition between Bcl-xL homo-complexes and the hetero-complexes by adding increasing amounts of cBid_G to Bcl-xL_R and measuring the CC after 1 h incubation. As expected for hetero-dimer formation, the amount of two colored complexes increased with the cBid concentration (up to 40% CC, Fig. 2d). Hetero-dimerization of this pair in solution was reported before^{21, 22, 25, 32, 42–46}, and in some cases quantified (with K_D s: between 12 nM⁴² and 350 nM⁴⁶). However, this can only be an effective value, as it does not take into account the presence of Bcl-xL_R homo-dimers.

To understand the interaction between cBid and Bcl-xL quantitatively, we needed to determine the exact reactions taking place. In Fig. 3a, three possible scenarios are suggested. In the

simplest scenario 1, cBid can only interact with Bcl-xL monomers and the formation of cBid/Bcl-xL and Bcl-xL/Bcl-xL complexes are competing. Scenario 2 differs from scenario 1 by an additional reaction, in which cBid is able to interact with Bcl-xL dimers, leading to the formation of a cBid/Bcl-xL hetero-dimer and one released Bcl-xL monomer. Scenario 3 considers instead that the interaction of cBid with a Bcl-xL dimer forms, a hetero-trimer, that can disassemble into two hetero-dimers after the addition of a second cBid molecule.

On the basis of these three scenarios, we designed an experiment that together with mathematical modeling allowed us to falsify one of the suggested scenarios. Bcl-xL_R and Bcl-xL_G were mixed and incubated for 120 min at room temperature (RT). Afterwards, the initial CC was measured (time –20 min) and the sample was divided into two equal parts. To one, we added unlabeled cBid in ~ 10 -fold excess (time 0 min) to shift the equilibrium towards cBid/Bcl-xL complexes. To the second one, we added buffer as negative control. In both samples, the CC was followed over time (Fig. 3b). To our surprise, addition of cBid led to a clear increase in the CC between Bcl-xL_R and Bcl-xL_G, whereas the CC remained unchanged in the negative control. Thus, cBid provoked not only hetero-dimer formation (Fig. 2d), but additionally boosted the amount to two-colored Bcl-xL homo-dimers (Fig. 3b). This can be explained by the existence of stable Bcl-xL homo-dimers with very slow exchange rates, so that in absence of cBid monomer exchange hardly takes place. cBid addition provokes hetero-complex formation and the release of Bcl-xL monomers, which in turn form new Bcl-xL homo-dimers increasing the number of two-colored Bcl-xL homo-dimers. Thereby, the total number of Bcl-xL homo-dimers did not increase and homo-dimer and hetero-dimer formation is in equilibrium.

Modeling cBid and Bcl-xL interactions in solution. To discriminate between the three reaction scenarios (Fig. 3a), we built mathematical models based on ordinary differential equations (ODEs), and analyzed the kinetics of association and dissociation of Bcl-xL molecules with themselves and with cBid. For scenario 1, a simple ODE system describing the two reversible interactions based on the law of mass action was fitted to the experimental data shown in Fig. 3b. The increase in two-colored Bcl-xL homo-dimers after cBid addition could not be reproduced by the model even when searching a large parameter space with a

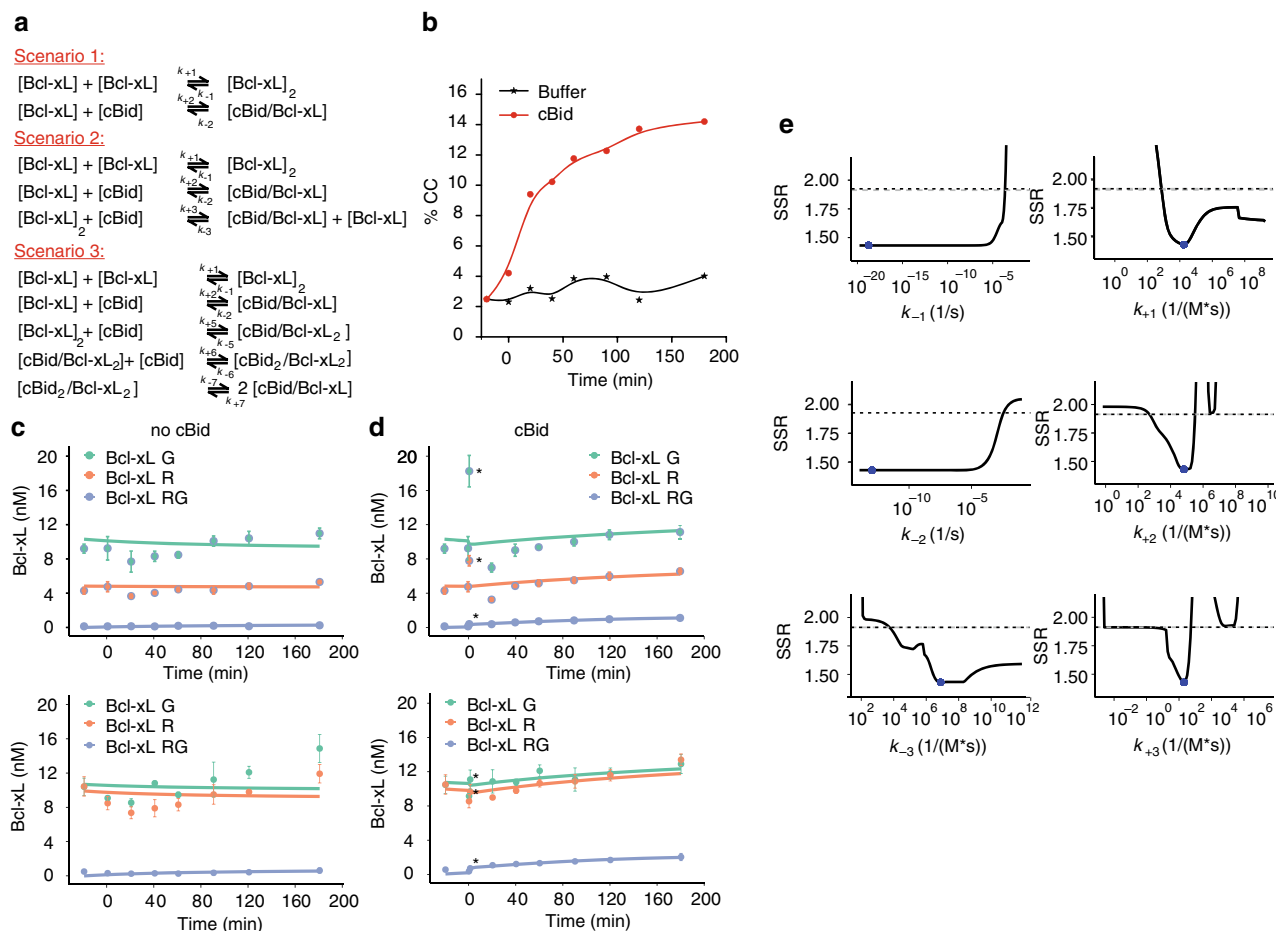


Fig. 3 Bcl-xL forms stable dimers in solution that exchange in presence of cBid. **a** Possible reaction scenarios between cBid and Bcl-xL in solution tested by modeling. **b** FCCS kinetic experiment on Bcl-xL_R/Bcl-xL_G dimerization in absence and presence of cBid (exemplary experiment out of $n = 3$). **c, d** Best fit of ODE model considering scenario 2 to the evolution of fluorescent Bcl-xL species based on the data shown in **b**. The upper and the lower panels show two independent experiments (mean and error bars as s.d. of three technical repetitions) with the Y-axis corresponding to the concentration of Bcl-xL particles. The first data point in presence of cBid is introduced as $t = 1$ min and highlighted in the figure by asterisk. This is applicable as each data point had a total FCS measurement time of 2 min. **e** Likelihood profiles of model parameters that define rate constants. The fitted parameter is shown as a blue dot, the reoptimized SSR is shown as black line and the dashed grey line indicates the confidence limit. FCCS fluorescence cross correlation spectroscopy

global optimization method (Supplementary Fig. 3). Thus, scenario 1 could be excluded.

In contrast, ODE modeling suggested that both scenarios 2 and 3 could quantitatively reproduce the experimental data (Fig. 3a–d and Supplementary Fig. 4). Thus, ODE modeling supports the idea that cBid can interact with Bcl-xL monomers and dimers.

To test whether scenario 2 or 3 are more likely, we used the difference in Akaike's information criterion (AIC), which considers the difference between the experimental data and the fit of the model as well as the number of parameters (model complexity). The differences in AIC values and the Akaike weights can then be used to select which scenario approximates the data best⁴⁷. In our case, the values support scenario 2 over scenario 3 (Supplementary Table 2).

Finally, we performed a parameter identifiability analysis to examine and compare the velocity of all modeled association and dissociation reactions⁴⁸ (Fig. 3e and Supplementary Figs. 5 and 6). For scenario 2, two of the parameters were identified with 95% confidence within the tested parameter range, and the other could be constrained in at least one direction based on the 95% confidence limit and a reoptimized sum of squared residuals (SSR, with a minimum SSR value for each parameter). On the basis of the likelihood profiles of the model corresponding to

scenario 2 (Fig. 3e), we could conclude that conversion of Bcl-xL homo-dimers to cBid/Bcl-xL hetero-dimers via cBid addition is a slow process (k_{+3} 10–700 1/(M*s)). The slow association rate constant indicates that conformational changes are involved in the reaction leading to hetero-dimer formation⁴⁹. A comparison of the likelihood profiles for k_{-3} (exchange of cBid with Bcl-xL in a hetero-dimer to form a Bcl-xL homo-dimer) and k_{+1} (association of two Bcl-xL) further suggested that cBid binding to Bcl-xL may speed up Bcl-xL dimerization. The calculated weak K_D (~600 nM) for Bcl-xL homo-dimers (Supplementary Fig. 2) could then be explained by a very slow dissociation of Bcl-xL homo-dimers, causing the experimental system to reach an equilibrium much later than experimentally accessible. Thus the real K_D for Bcl-xL homo-dimerization would be much smaller (in the order of 10 nM), as suggested before (Fig. 2b). In summary, our modeling data excluded scenario 1, whereas scenario 2 and 3 were both plausible with scenario 2 being more likely.

In the membrane only Bax and Bcl-xL can self-associate. The active conformations of the Bcl-2 proteins are membrane-embedded. Thus, it is crucial to understand the protein

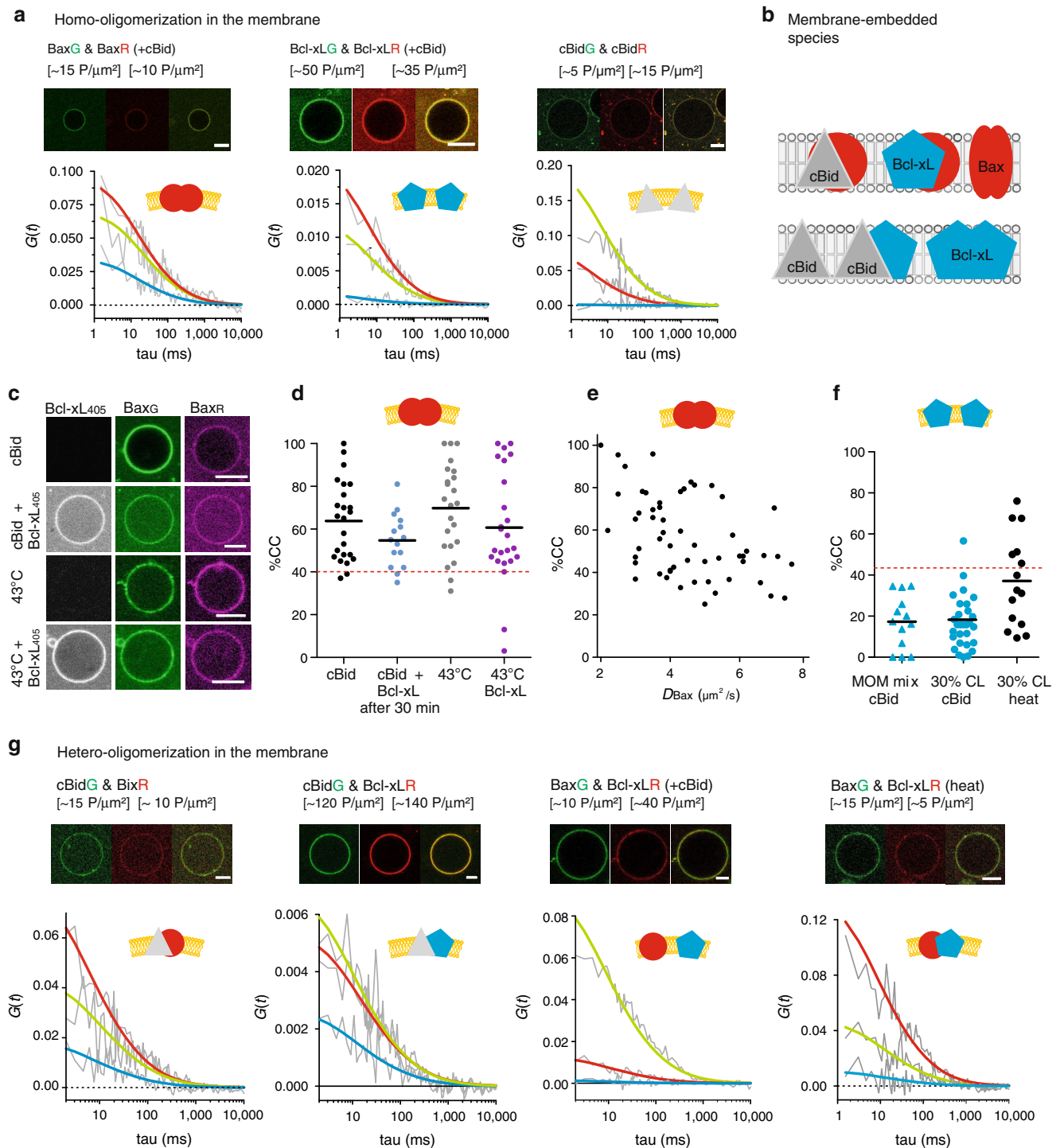


Fig. 4 Analysis of the interactions between cBid, Bax and Bcl-xL within membranes. **a** Representative FCCS graphs and corresponding GUV images of cBid, Bax, and Bcl-xL homo-oligomerization in membranes (30% CL, Scale bar: 10 μm). Only the Bax_G/Bax_R pair presents positive CC amplitude indicative of interaction. The AC and CC curves are shown in *grey*, whereas the fitted curves are shown in *green* (green protein), *red* (red protein), or *blue* (complex). **b** Scheme of the different species that can be detected in the membrane. **c** Representative images of Bax_R, Bax_G, and Bcl-xL₄₀₅ binding to GUVs (30% CL, Scale bar: 10 μm) in presence of unlabeled cBid or after incubation at 43 °C. **d** Comparison of the oligomerization expressed as %CC between Bax_G and Bax_R in individual GUVs after activation by cBid or 43 °C and in presence or absence of Bcl-xL₄₀₅ (30% CL; $n = 4$). All data are from one batch of labeled Bax to ensure that the degree of labeling is the same under all conditions. The maximal possible %CC for dimer formation considering the degree of labeling and a Mendel-based distribution of *red-red*, *red-green*, and *green-green* complexes is indicated by the *dotted red line*. **e** Relationship between CC and D of Bax_G and Bax_R activated by cBid in individual GUVs (30% CL; $n = 5$ independent experiments using three independent Bax batches; degree of labeling 80–100%). The CC values of three experiments were already published in ref. ¹⁹ (see also Supplemental Fig. 8A–C). **f** Comparison of the CC between Bcl-xL_G and Bcl-xL_R in GUVs composed of the both lipid mixtures. Membrane insertion was induced by cBid or 43 °C. The dotted red line indicates the maximal %CC possible considering dimer formation ($n = 3$). Only one protein batch was used due to the same reasons as in **d**. Data from independent Bcl-xL batches are shown in Supplemental Fig. 8A, B. **g** Representative FCCS graphs and corresponding GUV images of cBid, Bax, and Bcl-xL hetero-oligomerization in GUVs (30% CL; Scale bar: 10 μm ; color code as in **a**). FCCS fluorescence cross correlation spectroscopy

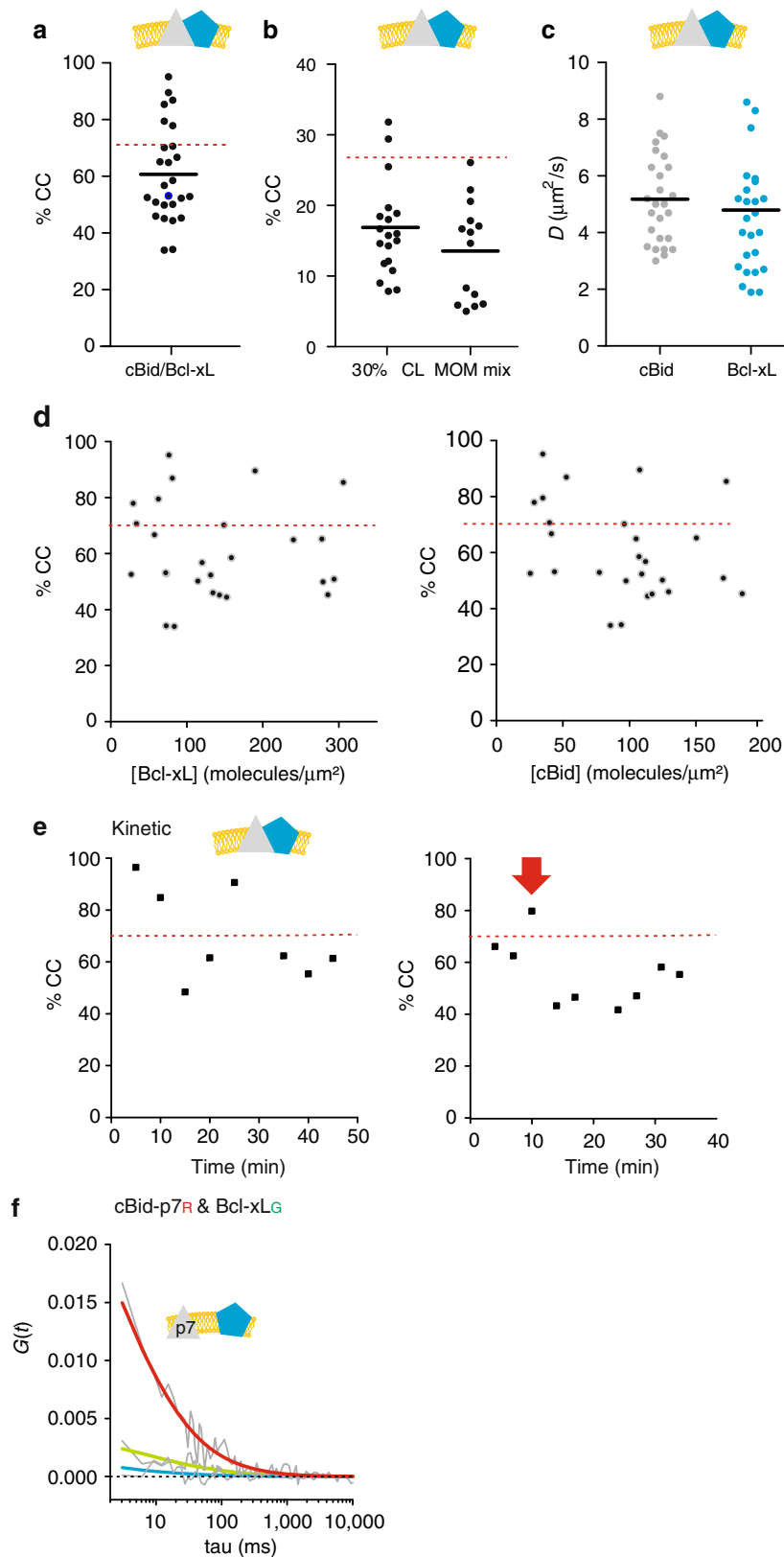


Fig. 5 Quantitative analysis of cBid-Bcl-xL association in membranes. **a** %CC between cBid_G and Bcl-xL_R in membranes (30% CL; $n = 5$). **b** %CC between cBid_G and Bcl-xL_R in GUV membranes comparing both lipid mixtures ($n = 3$). **c** D of cBid_G and Bcl-xL_R in individual 30% CL GUVs ($n = 5$). **d** %CC vs. the cBid_G or Bcl-xL_R protein concentration in GUVs (30% CL; $n = 5$). **e** Evolution of %CC between cBid_G and Bcl-xL_R in two individual GUVs as a function of time. The red arrow marks the time point at which the GUV was permeabilized (see also Supplemental Fig. 9). **f** Representative FCCS graph of cBid_{p7R} and Bcl-xL_G interaction. The absence of positive CC indicates that the labeled proteins do not interact in the membrane (color code as in 4 A). In **a**, **d**, and **e**, the dotted red line indicates the maximal CC considering dimer formation and degree of labeling. FCCS fluorescence cross correlation spectroscopy

interactions within the membrane. For this purpose, we measured scanning FCCS in giant unilamellar vesicles (GUVs) of two different lipid compositions (Methods and refs. 10, 15, 19, 30): one is mimicking the MOM (MOM mix, ~5% cardiolipin (CL)), whereas the other has a high CL content (30% CL) to enhance protein membrane binding and therefore the contrast (Supplementary Fig. 7A). Both lipid mixtures have been studied before and Bax-induced membrane pores had similar properties in both¹⁵, whereas permeabilization was more efficient with the higher CL concentration¹⁵.

As a control for false-positive CC in the membrane, we measured the CC between Bcl-xL and a lipidic dye, two molecules that should not interact (Supplementary Fig. 7B). Based on this, we assumed that mean CC values above 20% (for 30% CL $\mu \pm 2\sigma = 19\%$ CC) indicated protein interactions in membranes. Some vesicles containing cBid and/or Bax exhibited bright spots, which we interpreted as membrane buds¹⁶. Those vesicles were excluded from analysis as artificial CC can be detected (Supplementary Fig. 7C). Finally, to induce Bax and Bcl-xL membrane insertion, we used two methods: we added cBid¹⁹, or we applied a mild heat treatment^{11, 50, 51} to avoid effects of unlabeled cBid on the interactions measured.

After membrane insertion, the interaction network between cBid, Bax, and Bcl-xL strongly changed. Once inserted into the membrane, Bax formed homo-oligomers (in agreement with refs. 10, 12, 19, 30, 52, 53) irrespectively of the activation method (Fig. 4a, c, d and ref. 11). In line with oligomer formation, the mean D of membrane-embedded Bax was clearly smaller than the D of cBid or Bcl-xL, whereas the CC between Bax molecules was much higher than the CC between cBid or Bcl-xL molecules (Fig. 4a and Supplementary Fig. 8A, B). Moreover, the mean CC between Bax molecules was higher and more disperse than expected for pure dimers (reaching 100% in some GUVs, Fig. 4c). This is in agreement with higher order oligomer formation and a broad distribution of oligomers sizes (Fig. 4e and Supplementary Fig. 8C).

We did not detect Bcl-xL homo-dimers in presence of cBid (Fig. 4a, f and ref. 19), but when Bcl-xL membrane-insertion was induced by heat, we observed a significant amount of CC in line with homo-complex formation. This demonstrates for the first time that the membrane-inserted Bcl-xL can self-associate when no other interaction partners are present (Fig. 4f). However, cBid and Bax were preferred interaction partners over the self-interaction. Finally, we could not detect cBid homo-dimers in the membrane (Fig. 4a). This is at odds with studies reporting cBid homo-oligomerization in membranes⁵⁴. One reason could be cBid ability to reorganize membranes¹⁶, which can lead to artificial oligomer detection (Supplemental Fig. 7c).

Of note, we published CC data on Bax and Bcl-xL homo-interactions in membranes before¹⁹. Here, we included those data together with two new independent experimental repetitions, to compare the CC and D values with other complexes, as well as measurements under different conditions, e.g., absence of cBid (data used already in ref. 19) are included in Fig. 4e, f and Supplemental Fig. 8a, c). In summary, membrane-embedded Bax and Bcl-xL could be detected in homo-complexes and hetero-complexes, whereas cBid was present as a part of hetero-complexes or as a monomer.

In the membrane cBid–Bcl-xL complexes are stable and exclude p7. The only complex detected in solution and membranes was the cBid/Bcl-xL hetero-dimer. Upon membrane insertion, hetero-complex formation dominated over Bcl-xL homo-dimerization (Figs. 4a, f, g and 5a), which indicates a stronger interaction between cBid and Bcl-xL in membranes

compared to solution. The mean CC between cBid/Bcl-xL in membranes was close to the maximum expected considering hetero-dimer formation (Fig. 5a), and it did not change significantly with lipid composition (Fig. 5b) or protein concentration (Fig. 5d). The mean D for cBid and Bcl-xL was $\sim 5 \mu\text{m}^2 \text{s}^{-1}$ (Fig. 5c), in line with previous work^{19, 21}.

We also followed the kinetics of complex formation in individual GUVs (Fig. 5e and Supplementary Fig. 9) and found that the extent of association was high, stable over time, and independent of membrane permeabilization. This indicates again a very high binding affinity between cBid and Bcl-xL, and suggests that they insert into the membrane as a complex or, if there is recruitment, that it happens very fast. Thus, Mode 1 inhibition of MOMP will mainly happen in the membrane-bound state.

The soluble cBid/Bcl-xL complex contained tBid and the p7 fragment (Fig. 1c). To test if the same was true for the membrane-embedded complex, we used cBid_{p7R}. The CC between labeled p7 and Bcl-xL was as low as in the negative controls (Fig. 5f) indicating that the membrane-embedded complex does not contain p7.

cBid–Bax interaction decreases upon Bax oligomerization. cBid has been proposed to interact transiently with Bax to catalyze its activation and membrane insertion^{12, 30, 31, 52, 55}. A transient interaction seems necessary as the binding site of Bid to the Bax BH-groove is overlapping with one interaction interface between Bax monomers in the homo-oligomer¹². Detecting the cBid/Bax complex in membranes has remained challenging and could only be validated once³⁰. Here, we could identify cBid/Bax complexes as well (Fig. 6a), but the level of CC was much lower than for cBid/Bcl-xL complexes (<40% CC compared to >60% CC), indicating a low affinity or a short lifetime of the cBid/Bax complex.

We wondered if the dispersed CC data (Fig. 6a) could be the result of two populations of GUVs: one with high and one with low cBid and Bax interaction. On average, Bax clearly diffused slower than cBid (Fig. 6b), supporting this hypothesis. However, in GUVs with a high CC between cBid and Bax, cBid diffused similar to Bax (Fig. 6c), suggesting that Bax-oligomer assembly happened faster than cBid release. In addition, kinetic experiments revealed a decrease in the CC between cBid and Bax over time, in line with a transient interaction (Fig. 6d and Supplementary Fig. 10). Thus, the cBid–Bax complex in membranes is likely transient, and cBid is released after Bax homo-oligomerization.

In membranes Bcl-xL hetero-dimerizes with Bax, but prefers cBid. Although the inhibitory role of Bcl-xL via direct interaction with Bax (Mode 2) was first proposed more than two decades ago⁵⁶, the interaction between these two proteins has escaped detailed characterization. Here, despite the lack of association in solution (Fig. 1c), membrane-embedded Bax and Bcl-xL formed complexes (Fig. 6e). They were mainly detectable when membrane insertion was induced by mild heat treatment. In the presence of cBid, we could hardly detect Bax/Bcl-xL complexes (Fig. 6e–g and Supplementary Fig. 8D), likely due to the formation of competing cBid/Bcl-xL complexes (Fig. 5a). Performing these experiments was complicated as Bcl-xL excludes Bax from membranes^{5, 6, 19}. To overcome this difficulty, we incubated cBid, Bax_G, and GUVs for 30 min prior to Bcl-xL_R addition, which allowed Bax to insert into the membrane before Bcl-xL was added. This experiment revealed two important facts. First, a direct interaction between Bax and Bcl-xL is possible, but takes place only in the membrane-bound state.

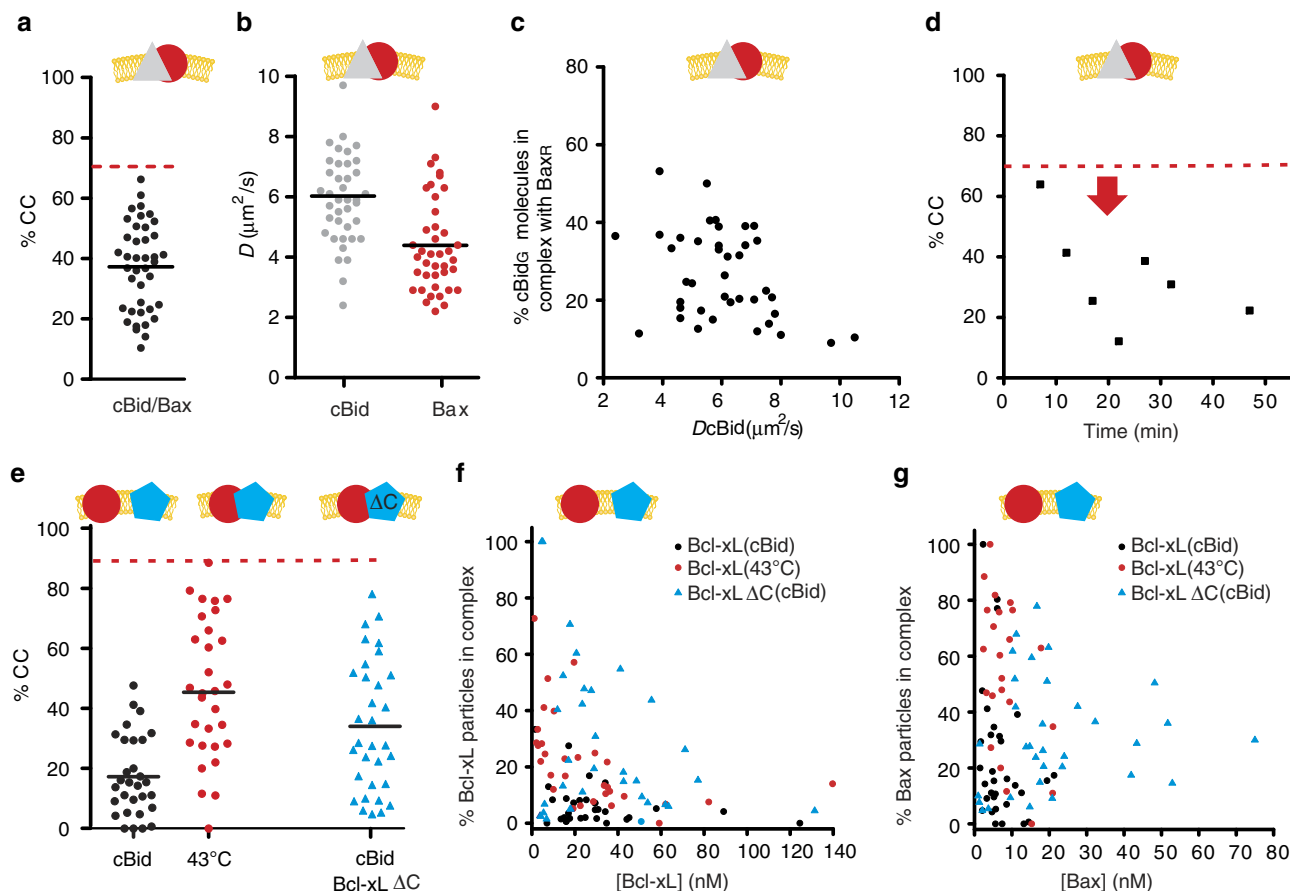


Fig. 6 Quantitative analysis of the interaction of Bax with cBid and Bcl-xL in membranes. **a, b** %CC (**a**) and D (**b**) of membrane-embedded cBid_G and Bax_R in individual GUVs (30% CL; $n = 8$). **c** Percentage of cBid_G molecules in complex with Bax_R vs. the D of cBid_G in individual GUVs (30% CL; $n = 8$). **d** Temporal evolution of %CC between cBid_G and Bax_R in a single GUV. The red arrow marks the time point at which the GUV was permeabilized (see also Supplemental Fig. 9). **e** Comparison of %CC between membrane-embedded Bax_R (90% labeled) and Bcl-xL_G (100% labeled) or Bcl-xL Δ C_G (90% labeled) in individual GUVs (30% CL). Protein insertion into the membrane was activated by cBid or heat, as indicated ($n = 3$). **f** Percentage of membrane-embedded Bcl-xL or Bcl-xL Δ C molecules in complex with Bax in relation to the absolute concentration of Bcl-xL (after activation by cBid (black dots) or heat (red dots)) or Bcl-xL Δ C (blue triangles) ($n = 3$). **g** Percentage of membrane-embedded Bax molecules in complex with Bcl-xL (after activation by cBid (black dots) or heat (red dots)) or Bcl-xL Δ C (blue triangles) in relation to the absolute concentration of Bax ($n = 3$). The dotted red line in **a, d**, and **e** indicates the maximal possible CC considering the degree of labeling and dimer formation ($n = 3$). **e-g** Experiments done with one protein batch so that the results can be directly compared

Second, Bcl-xL interacts more strongly with cBid, when both partners are present, which indicates that Bcl-xL has a higher affinity for cBid than for Bax.

The presence of Bcl-xL reduces the size of Bax oligomers. These results raised the question of the functional impact of Bcl-xL on Bax oligomerization in membranes, which we addressed by comparing the CC between membrane-embedded Bax_G and Bax_R in presence and absence of Bcl-xL (Fig. 4c, d). To visualize Bcl-xL binding to GUVs, we used Bcl-xL₄₀₅ (labeled with Alexa 405), which was imaged in a third detection channel. The experiment was done after inducing Bax and Bcl-xL membrane insertion either with heat or cBid. When heat was used, Bax_R, Bax_G, and Bcl-xL₄₀₅ were added simultaneously to the GUVs, whereas when cBid was used, Bcl-xL₄₀₅ was added after Bax oligomer formation. In both cases, Bcl-xL₄₀₅ decreased the average CC between Bax molecules, indicating that Bcl-xL inhibited Bax oligomerization or reduced the oligomer size (Fig. 4d and ref. ¹¹). This suggests that Bcl-xL is able to bind to the membrane-embedded, active conformation of Bax.

FCFS is an equilibrium method that cannot establish the order of events for single molecules or the stoichiometry within complexes. Thus, we cannot distinguish whether Bcl-xL binds to and disassembles large Bax oligomers or whether it preferentially binds to monomers or dimers, preventing them from forming larger oligomers. However, we observed that membrane-embedded Bcl-xL diffused slightly faster in presence of cBid than in presence of Bax (Supplementary Fig. 8E), which suggests that Bax/Bcl-xL hetero-complexes are bigger as cBid/Bcl-xL dimers. This supports the idea that Bcl-xL is able to bind Bax oligomers, and suggests that one Bcl-xL molecule is able to inhibit more than one Bax molecule. However, we cannot discard the possibility that Bcl-xL preferentially binds Bax monomers.

Bcl-xL C-terminus regulates the preference of interactions.

Until recently, most of the work done with recombinant Bcl-2 proteins used truncated proteins without the C-terminal membrane-anchoring helix. We tested the implications of this truncation on Bcl-2 interactions, because this helix has been related to homo-complex and hetero-complex formation,^{10, 34, 57, 58} and

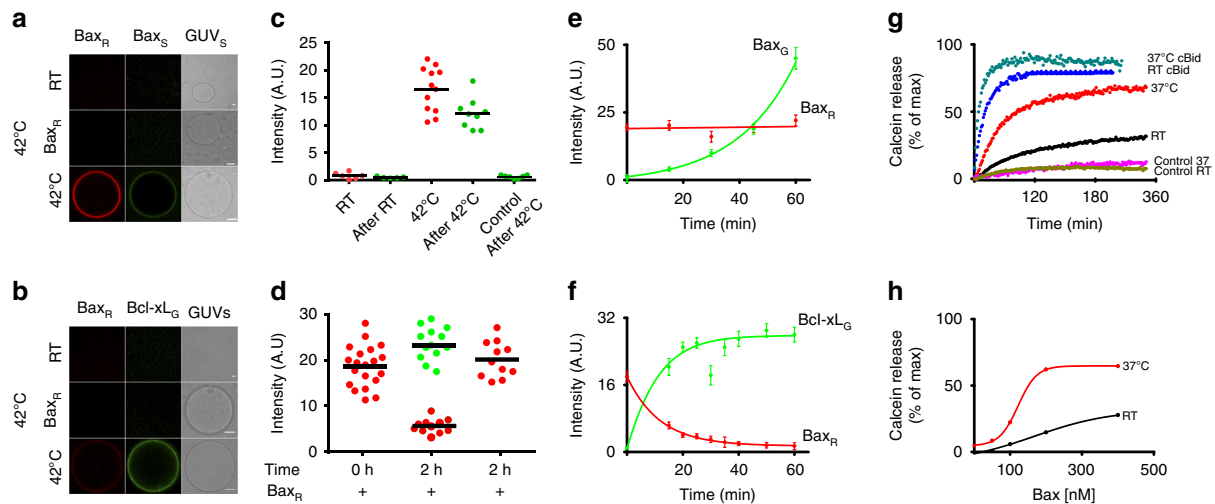


Fig. 7 Bax auto-activation and retrotranslocation in model membranes. **a** Bax_G binding to GUVs (30% CL) with or without membrane-embedded Bax_R at room temperature (RT) and after incubation at 42 °C for 30 min. (Scale bar: 10 μm). **b** Binding of Bcl-xL_G to 30% CL GUVs containing or not Bax_R at RT and 42 °C for 30 min. **c** Quantification of Bax_R (red dots) and Bax_G (green dots) binding to individual GUVs before and after incubation at RT or 42 °C. The control corresponds to samples treated at 42 °C but in the absence of Bax_R. (Black line represents mean of the distribution). **d** Quantification of Bax_R (red dots) and Bcl-xL_G (green dots) binding to individual GUVs after heat activation (0 h after Bcl-xL addition) and after 2 h incubation at RT in presence and absence of Bcl-xL. (Black line represents mean of the distribution). **e** Temporal evolution of Bax_R (previously bound by incubation at 42 °C) and Bax_G intensity on GUVs at RT. (Error bars represent s.d. of $n = 3$ experiments). **f** Temporal evolution of Bax_R (previously bound by incubation at 42 °C) and Bcl-xL_G intensity on GUVs at RT. (Error bars represent s.d. of the average intensity of all GUVs in three experiments). **g** Kinetics of calcein release from LUVs, comparing 200 nM Bax activity at ~37 °C and RT in the presence and absence of 20 nM cBid. **h** Dose response curve of % calcein release at varying Bax concentration at ~37 °C as compared to RT. For all experiments $n = 3$

removal of the helix interfered with homo-dimerization³⁴ as well as with Bax retro-translocation^{59, 60}. To do so, we compared the interaction of Bax_R with full length Bcl-xL_G and Bcl-xLΔCT_G (Fig. 6e–g). Similar to the full-length version, Bcl-xLΔCT_G did not interact with Bax_R in solution (data not shown). However, in contrast to full-length Bcl-xL, the truncated protein failed to inhibit Bax membrane insertion, and once in the membrane, it interacted with Bax_R even in the presence cBid (Fig. 6e–g). This demonstrates that the C-terminal helix of Bcl-xL tunes the hierarchy of interactions with other Bcl-2 family members.

Membrane-bound Bax can recruit soluble Bax and Bcl-xL.

After analyzing the interactions between Bax, cBid, and Bcl-xL in solution and in membranes, we examined the translocation between both environments. We took advantage of direct visualization of protein binding to GUV membranes and investigated protein recruitment and retro-translocation. The presence of all three proteins leads to cBid and Bcl-xL translocation to the membrane, whereas Bax stays largely in solution¹⁹. Recently, it was suggested that membrane-bound Bax recruits soluble Bax via an auto-activation mechanism⁵⁷. To test this hypothesis, we incubated 30% CL GUVs with Bax_R at 42 °C, inducing Bax_R association to the membrane (Fig. 7a, c). After cooling down, we added Bax_G molecules, incubated for 1 h at RT and imaged the vesicles. Bax_G bound to GUVs, confirming that membrane-bound Bax can recruit soluble Bax molecules (Fig. 7a, c, e). Binding did not happen when Bax_R was absent or not treated with heat. To our surprise, membrane-associated Bax_R recruited not only soluble Bax_G but also soluble Bcl-xL_G to the membrane (Figs. 7b, d). The accumulation of Bcl-xL_G on the membrane was accompanied by a decrease in the mean fluorescence intensity of membrane-bound Bax_R (Fig. 7b, d), indicating that Bcl-xL_G promoted the release of Bax molecules

from the membrane into solution. The kinetics of this association/dissociation processes are shown in Fig. 7e, f. Interestingly, Bax recruitment to the membrane increased with the amount of Bax associated to the membrane, supporting a positive feedback mechanism. In contrast, the association of Bcl-xL to the membrane was faster initially, when most Bax molecules were membrane-bound, and decreased with time as the concentration of Bax in the membrane decreased (Fig. 7e, f). Thus, membrane-bound Bax recruits Bcl-xL to the membrane without positive feedback or additional recruitment of Bcl-xL by Bcl-xL. Most importantly, our data show that Bcl-xL promotes the dissociation of Bax from the membrane in the absence of any additional component. To our knowledge, this is the first measurement of Bax retro-translocation in recombinant systems.

These findings suggest that the energy barrier for Bax binding to the membrane, which is the limiting step in activation, is low. Indeed, in absence of all other Bcl-2 proteins, low expression of Bax in cells leads to its spontaneous activation, characterized by accumulation at the MOM and cell death⁶¹. To determine the role of temperature in Bax activation, we performed vesicle content release assays at RT or 37 °C (Fig. 7g, h). Spontaneous activation of Bax was negligible at RT, whereas incubation at 37 °C induced significant permeabilization of the membrane even in absence of cBid. As expected, at both temperatures, addition of cBid led to full and faster membrane permeabilization. Altogether, these findings demonstrate that Bax can spontaneously activate at physiological temperature, which is amplified by a positive feedback mechanism.

Discussion

Here we report quantitative analysis of the interactions within a minimal Bcl-2 network that takes into account the spatial regulation of complexes in solution and membranes. One important finding is that the association of Bcl-2 proteins changes

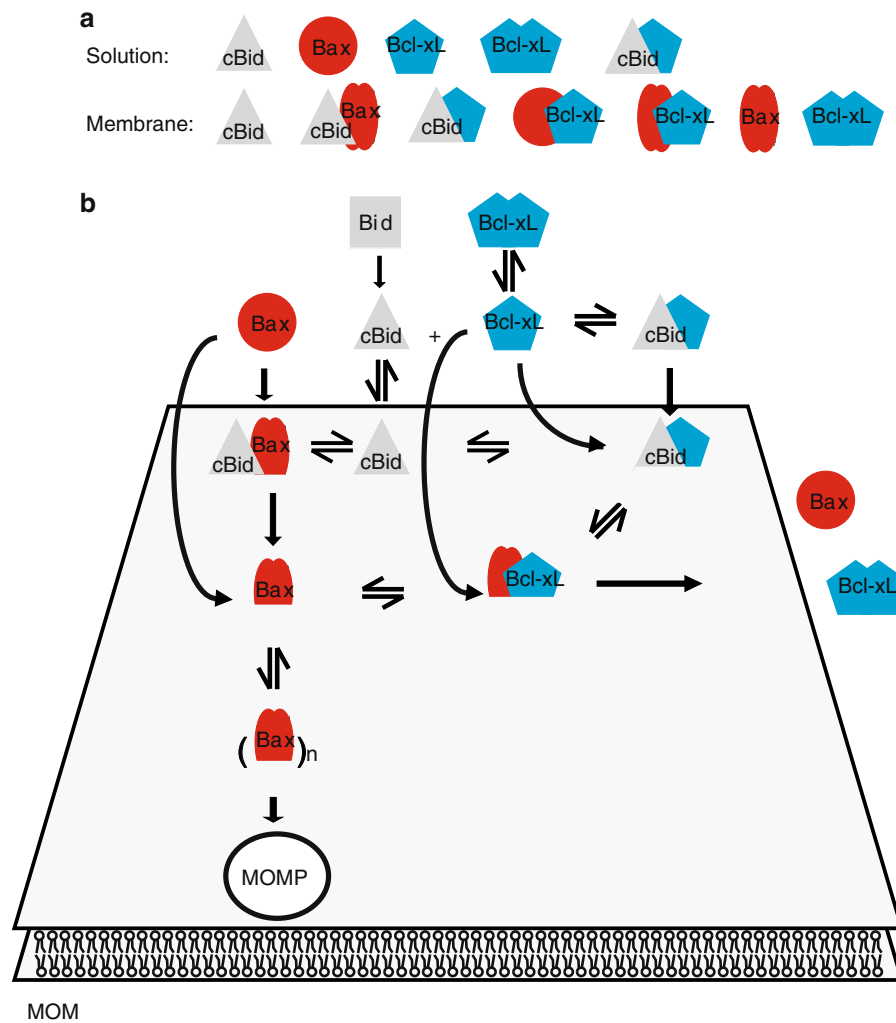


Fig. 8 Integrated model for the multiple interactions between Bcl-2 proteins in solution and in membranes to regulate MOM permeabilization. **a** Species detected in solution and membranes. Bax is schematically shown in two conformations corresponding to monomeric as filled red circles and the membrane-embedded as two red, filled ovals. For the Bax/Bcl-xL complex, we showed that a complex containing oligomeric Bax exists, whereas we suggest the existence of the complex containing monomeric Bax. **b** Schematic representation of an integrated model of Bcl-2 protein interaction network in solution and at the MOM. MOM mitochondrial outer membrane

markedly upon membrane insertion, which is most likely due to the conformational changes associated with the process^{10, 62}. In solution, Bax was monomeric, whereas cBid was present as a complex between its two fragments or associated with Bcl-xL. Bcl-xL itself hardly existed as a monomer, but formed homo-dimers and hetero-dimers with cBid (Fig. 8).

The existence of soluble Bcl-xL and Bax homo-dimers is strongly debated. Bcl-xL homo-dimers were detected in cells³⁴, but structural data are controversial^{35, 37, 38}. Jeong et al.³⁴ showed that the C-terminal helix of Bcl-xL is critical for homo-dimerization and suggested that the helix of one monomer would bind to the hydrophobic groove of the second one, enabling dimerization. We found this hypothesis intriguing, as the C-terminal helix would be shielded in the dimer (Supplementary Fig. 10), which could explain why a fraction of Bcl-xL is cytosolic in cells despite the membrane anchor. Our data support this model, as we detected stable Bcl-xL dimers that dissociated by the addition of cBid. In this scenario, the C-terminal helix and the BH3 domain of cBid compete for the same binding site (the BH groove)¹², which provides a molecular basis for how cBid facilitates Bcl-xL membrane insertion by displacing the membrane anchor (Supplementary Fig. 10B).

In contrast to our results, the existence of soluble Bax homo-dimers and oligomers was recently reported^{63, 64}. Garner et al.⁶³ detected autoinhibited Bax homo-dimers in the cytosol of the cell extracts of a number of cell lines, whereas in other cell lines, no Bax homo-dimers were found, suggesting that a very specific regulation might be necessary. Thus, the fact that we did not detect these dimers suggests that dimerization in solution requires additional factors (e.g., chaperones) or modifications absent in our system. Sung et al.⁶⁴ reported the oligomerization of soluble Bax upon incubation with BH3-only peptides at millimolar Bax concentrations. We never detected similar oligomers upon addition of cBid in the nanomolar (analyzed here) to micromolar⁵² range. However, incubation of Bax Δ C and BH3 peptides produced non-physiological swapped-dimers¹² and we cannot discard that the soluble Bax oligomers in ref.⁶⁴ are multimers of swapped-dimers formed at very high protein concentrations.

Upon membrane insertion, the Bcl-2 interaction network strongly changed. Bax was always part of complexes with itself, with cBid, or with Bcl-xL, whereas Bcl-xL existed in complex with cBid or with Bax, or in the absence of both, as a mixture of monomers and homo-complexes (Fig. 8). This indicates that the

affinity of Bcl-xL to itself is lower than the affinity to cBid or Bax molecules. A transient interaction between cBid and Bax has been proposed as part of the “hit-and-run” model. Here, we provide additional evidence for the cBid/Bax complex and for its dissociation upon Bax homo-oligomerization. This is in line with the fact that one Bax oligomerization interface overlaps with the binding site for cBid¹².

Despite the many models proposed for the regulation of Bax activation by the other Bcl-2 proteins, the lack of direct detection of Bax/Bcl-xL complexes in membranes and the lack of a quantitative characterization of the different interactions had left a key question open. When all proteins are present, does Bcl-xL inhibit apoptosis mainly by blocking the activators, like cBid, or the executioners, like Bax? Our results point to the first, as the affinity between Bcl-xL and cBid is larger than between Bcl-xL and Bax. This also explains why BH3 mimetics are efficient inducing apoptosis. Most likely they would not be as effective if Bcl-xL/Bax interactions were the stronger ones. Remarkably, our data showed that deletion of the C-terminal anchor of Bcl-xL altered its interaction preferences. This is likely due to the participation of the C-terminal helix in interaction surfaces^{10, 57, 58}. Our data are at odds with the claim that Mode 2 inhibition is more efficient than Mode 1 inhibition in the unified model, but these studies were performed using C terminally truncated prosurvival Bcl-2 homologs²². Thus, caution should be exercised when interpreting experiments performed with truncated Bcl-2 members.

Our findings shed new light on Bax activation and inhibition. Recent work showed that in cells lacking all Bcl-2 proteins, Rb, and p53, reintroduction of Bax led to its spontaneous activation and cell death even at low Bax expression levels⁶¹, in favor of the indirect activation model. However, the direct activation model is supported by the fact that Bax can be produced in vitro in an inactive form that can be activated by BH3-only activators to form membrane pores^{15, 30}, as well as by the structural data of BH3 peptides bound to Bax¹². To reconcile both views, it is important to consider that activating Bax in absence of BH3 activators is also relatively easy: it can be achieved in vitro by exposure to mild heat^{11, 51}, acidic pH⁶⁵, detergents²⁶, or proteins like Drp1⁶⁶. This all argues for a low energy barrier for Bax activation, in the order of thermal energy at physiological temperature. Here, we show that without activator molecules Bax remains inactive at RT, but presents a significant membrane permeabilizing activity at 37 °C. Once in the membrane, Bax promotes recruitment of soluble Bax. In the context of the cell, a small fraction of Bax molecules could spontaneously become active, which could be kept in place by complex formation with prosurvival Bcl-2 homologs. In agreement with this, we show that membrane-bound, active Bax-recruited Bcl-xL to the membrane and formed complexes with it, which led to a release of Bax from the membrane back into solution and to a reduction in Bax oligomer size. The protein retro-translocation into solution also supports a low energy barrier for dissociation of Bax/Bcl-xL complexes from the membrane. This barrier could be overcome by the high affinity between Bcl-xL monomers in solution, providing the necessary driving force for Bax retro-translocation. Moreover, the fact that membrane-bound Bax can recruit Bax and Bcl-xL supports a common molecular mechanism for both processes that was so far unanticipated, and it demonstrates that Bcl-xL is sufficient to retro-translocate Bax from the membrane back into solution.

Our observations link so-far unconnected observations: the low fraction of Bax/Bcl-xL complexes naturally found in mitochondria²⁹; the finding that in cells lacking direct activators, Bax and Bak can still be activated and their activation depends on the absence of prosurvival Bcl-2 proteins^{29, 61}; and the spontaneous

minority MOM permeabilization observed when prosurvival Bcl-2 proteins are inhibited with ABT-737⁶⁷. It is important to consider that in cells, the Bcl-2 regulation network is much more complex and includes additional factors and post-translational modifications that add a layer of complexity to the observations reported here. Moreover, beyond their function in MOMP, Bcl-2 proteins have been associated with regulatory functions in mitochondrial dynamics and Ca²⁺ homeostasis^{1, 68–70}. The underlying mechanisms are not completely understood, but several Bcl-2 proteins are proposed to interact with MOM or ER membrane proteins without inducing MOM permeabilization^{1, 68–70}. Therefore, the regulation of Bcl-2 protein function is more complex than considered so far, which could potentially also be examined with the system developed here.

On the basis of our findings, we propose a new, “integrated” model that explains how the multiple, parallel interactions between the Bcl-2 proteins are orchestrated to regulate apoptosis (Fig. 8). In absence of proapoptotic stimuli, Bax activation could proceed spontaneously. The membrane-bound Bax molecules could behave as seeding points for further Bax recruitment from solution in a positive feedback loop (here and refs. ^{11, 29, 61}). Direct interaction with prosurvival Bcl-2 homologs in the membrane would inhibit MOM permeabilization by relocation of loosely bound Bax molecules from the membrane to the cytosol, and it would additionally block the oligomerization of membrane-embedded Bax. In the presence of proapoptotic stimuli, the activation of BH3-only proteins would be first inhibited by direct association with the prosurvival Bcl-2s proteins, for which they have a higher affinity. In this scenario, a low level of Bax activation would still be counterbalanced by excess prosurvival Bcl-2s, but would prime the cells to die^{27, 42}. On the basis of literature data, continued stress would further increase the levels of BH3-only proteins. Above a certain threshold in the relative concentration of proapoptotic vs. prosurvival Bcl-2 proteins, the prosurvival Bcl-2 homologs would be engaged mostly with BH3-only proteins and would not be able to sustain the steady state of Bax activation/inactivation, which would turn the balance and switch towards Bax activation and MOM permeabilization. In situations with intense cellular stress, any additional excess of BH3-only proteins would create a pool of free direct activators that would promote a rapid and efficient activation of Bax and Bak, full MOM permeabilization, and cell death.

In summary, the minimal network reported here explains the spatial regulation of Bcl-2 complexes in solution and membranes. We disentangle the hierarchy of competing reactions, as well as the modulatory role of the membrane and the C-terminal anchor, which has implications for the prevalence of the different inhibition modes depending on the environment and proteins present. At physiological temperatures, a fraction of Bax molecules spontaneously activates. These molecules can recruit to the membrane additional soluble Bax to promote MOM permeabilization, as well as soluble Bcl-xL, which inhibits Bax homo-oligomerization and releases Bax back into solution, thereby inhibiting MOM permeabilization. Altogether, these findings support an integrated model for Bcl-2 proteins that reconciles previously opposing experimental observations.

Methods

Protein production and labeling. Full length mouse Bid (wild type, Bid C30S, or Bid C126S), full length human Bax (wild type and Bax S4C, C62S, C126S), and full length human Bcl-xL (wild type and Bcl-xL S4C, C151A) were expressed in *E. coli* BL21/RILP cells (Stratagene, now Agilent, Santa Clara, CA). Bacterial cultures were started at 37 °C at OD₆₀₀ ~ 0.03. Protein expression was induced with 1 mM IPTG at OD₆₀₀ ~ 0.5 followed by 4 h incubation at 20 °C. Cells were harvested by centrifugation at 6000 ×g for 20 min. The cell pellets were shock-frozen in liquid nitrogen and stored at –80 °C. Before purification, the cells were thawed on ice,

resolved in buffer, and broken on ice by five passages through an Emulsiflex C5 (Avestin, Mannheim, Germany). Afterwards, ~1–200 U DNase I were added per liter bacterial culture (Merck, Darmstadt, Germany) and the mixture was incubated 30 min on ice. Then unbroken cells and membranes were removed by centrifugation at 25,000 rpm (60 min at 4 °C; using a JA25.50 rotor in a Beckmann Avanti centrifuge (Beckman Coulter, Brea, CA). Bid variants were purified using Nickel-NTA beads (Qiagen, Hilden, Germany) as the protein has an N-terminal His tag (plasmid pET23-His-Bid). Purification was done using 5 ml Nickel-NTA beads loaded into an empty gravity flow column. Buffers and purification steps were done following the manufacturer instructions, and protein elution was done by step a gradient adding 10, 25, and 250 nM Imidazol (in buffer). Protein purity was tested by SDS-PAGE showing about 95% purity. Afterwards to buffer was replaced by the caspase 8 cleavage buffer (50 mM NaCl, 5 mM DTT, 0.5 mM EDTA, 25 mM HEPES, 5% Sucrose; pH 7.4) using dialysis. Bid was cleaved to cBid by 4 h incubation with caspase 8 (at RT, Bid/Caspase 8 ratio ~1000:1; Caspase 8 was a gift J.-C. Martinou). Afterwards, a second purification (again based on Nickel-NTA) was done to remove Caspase 8, followed by an SDS PAGE performed to control protein purity (>95% see Supplemental Fig. 1E). Bax and Bcl-xL variants were expressed as intein-fusion proteins using the IMPACT-system from NEB (NEB, Ipswich, MA; plasmids pTYB1-BaxWT, pTYB1-Bax S4C, C62S, C126S, pTYB1-Bcl-xLWT, or pTYB1-Bcl-XL S4C, C151A). Buffers and purification were done following the manufacturer instructions. Samples were always kept on ice or at 4 °C and the cleavage reaction was done ~16 h at 4 °C. After elution protein purity was tested based on SDS-PAGE showing about ~90% purity. To remove residual impurities the sample was further purified using an anion exchange column (using a HiTrap Q column from GE healthcare on an AKTA purifier FPLC system from GE healthcare). First, the buffer was exchanged to 20 mM TRIS, pH 8 by dialysis to afterwards load the protein onto the column. The bound protein was washed with >20 column volumes (CV) of the buffer and then eluted with a gradient (8 CV) of high salt buffer (1 M NaCl, 20 mM TRIS, pH 8). The elution fractions were analyzed by SDS-PAGE (purity >95%, see Supplemental Fig. 1E) and finally, the buffer was exchanged using dialysis (to 150 mM NaCl, 20 mM TRIS, pH 7.5 or 150 mM NaCl, 20 mM HEPES, pH 7.5). The wild type proteins were aliquoted in 10 µl portions and shock-frozen in liquid nitrogen. Protein mutants were labeled before freezing (with Alexa 488-maleimide and Alexa 633-maleimide in the case of the cBid and ATTO 488-maleimide or ATTO 655-maleimide in the case of Bax and Bcl-xL). For labeling, the protein was incubated with threefold excess TCEP for 30 min on ice. Afterwards, a tenfold excess of the label was added and the sample incubated 2 h at 4 °C, before another fivefold excess of label was added and the sample incubated overnight at 4 °C. Free label and protein were separated using desalting columns, and the degree of labeling was calculated using a combination of UV-VIS spectroscopy, Bradford assays, and ESI-LC-MS.

Composition of the lipid mixtures. The lipid mixture mimicking the MOM had a composition of 49% egg 1- α -phosphatidyl choline (PC), 27% egg 1- α -phosphatidyl ethanolamine (PE), 10% bovine liver 1- α -phosphatidyl inositol (PI), 10% 18:1 phosphatidyl serine (PS) and 4% CL (all percentages mol/mol). Moreover lipid mixtures composed of 30% CL and 70% PC or 20% CL and 70% PC (mol/mol) were used. All lipids were purchased from Avanti polar lipids (Alabaster, AL) and mixed in chloroform. Afterwards the chloroform was evaporated overnight under vacuum and then flushed with nitrogen or argon gas and stored at -28 °C.

GUV formation and sample preparation. GUVs were produced by electro-formation and the experiments were done as described in ref. ¹⁹. Briefly, 5 µg lipid mixture dissolved in chloroform were spread on each platinum electrode of the electro-formation chamber and allowed to dry, before immersion in 300 mM sucrose. Electro-formation proceeded for 2 h at 10 Hz, followed by 30 min at 2 Hz. Overall, 75 to 100 µl of the GUVs suspension was added to a solution of buffer mixed with the proteins of interest in Lab-Tek 8-well chamber slides (NUNC) to a final volume of 300 µl.

For experiments of Bax and Bcl-xL binding to GUVs, the sample mixtures were prepared in 8-well Lab-Tek chamber slides (NUNC) in buffer (150 mM NaCl, 20 mM Tris, pH 7.5) and 80 µl of GUV suspension, in total volume of 300 µl. The working concentration of Bax_R, Bax_G, and Bcl-xL_G were 0.5–200 nM, respectively. To monitor Bax auto-activation, Bax_R was incubated at 42 °C for 30 min, allowed to cool down to RT for 1 h, followed by subsequent addition of Bax_G at RT and incubation for 1 h. The binding of the proteins to GUVs was imaged using a LSM710 confocal microscope. For Bax retro-translocation in model membranes, Bax_R was heat activated at 42 °C for 30 min, cooled down to RT for 1 h, followed by the addition of Bcl-xL_G and incubation for 1 h at room temperature. To quantify the binding intensity of Bax_R, Bax_G, and Bcl-xL_G, the radial profile plugin of Image J was used with an integration angle of 60°. The background intensity was always taken into account for the intensity measurements. The curves were fitted using a nonlinear curve fitting function with sigmoidal dose response fit in Origin Lab.

Calcein permeabilization assay. LUVs composed of 80% PC and 20% CL were prepared by solving dried lipid mixtures in buffer (20 nM HEPES, pH 7.4 and 80 mM Calcein [fluorescein-bis-methyl-iminodiacetic acid at pH 7.5] with 4 mg mg⁻¹

lipid) using intensive vortexing paused by five cycles of freezing and thawing. The multilamellar vesicles were passed 31 times through an extruder (Avestin) using membranes with 400 nm pore size (Avestin). Calcein was entrapped in the vesicles at a self-quenching concentration, so that its release in external medium was accompanied by an increase of the intensity of fluorescence. LUVs were incubated with different concentrations of Bax, varying from 0 to 400 nM at ~37 °C in buffer (140 mM NaCl, 20 mM HEPES, 1 mM EDTA, pH 7.4) at room temperature with a lipid to protein concentration of >1:500 at the highest Bax concentration. The kinetics of calcein release were measured using a Tecan Infinite M200 microplate reader (Tecan, Männedorf, Switzerland).

The percentage of release R was calculated from the expression:

$$R = ((FS - F_0) \div (F_{max} - F_0)) \times 100$$

where, F₀ is the initial fluorescence of LUVs, F_{max} is the maximum fluorescence after addition of 5% TritonX-100, and FS is the equilibrium fluorescence in the sample of interest.

FCCS measurements. All FCCS experiments were performed using a LSM710 confocal microscope equipped with a Confocor3, a C-Apochromat 40 × N.A. 1.2 water immersion objective and laser to excite at 488 and 633 nm. Photons emitted from different fluorophores were separated by dichroic mirrors and detected by Avalanche photo diodes placed after suitable filters (for Atto/Alexa488, 505–540 nm band pass filter; for the far red dyes a >655 nm long pass filter). Each sample was measured at least 10,000× longer as their diffusion time to assure sufficient data points to generate the autocorrelation curves. To calculate the diffusion time (t_D), diffusion coefficients (D), protein concentration, and the cross-correlation, we assumed 3D Brownian diffusion and used the equations in Supplementary Table 1.

For solution FCS measurements, the proteins of interest were mixed with buffer (150 mM NaCl, 20 mM Tris, pH 7.5) in a total volume of 100–200 µl and incubated at least 30 min before measurements. Incubation and measurements were done in Lab-Tek 8-well chamber slides (NUNC) that were blocked with Casein (saturated solution in 150 mM NaCl, 20 mM TRIS, pH 7.5) before use. For all solution, FCCS measurements we did three technical repetitions and removed traces that contained large fluorescent particles disturbing the measurement. However, all *n* in the figure legends refer to experimental repetitions.

For scanning FCCS, we performed two-focus scanning FCCS measurements at 22 °C using a Confocor 3 module. Photon arrival times were recorded with a hardware correlator Flex 02-01D/C (<http://correlator.com>). We repeatedly scanned the detection volume with two perpendicular lines across a GUV equator (the distance between the two bleached lines *d* was measured on a film of dried fluorophores). Data analysis was performed with home-build software²¹. We binned the photon stream in 2 µs and arranged it as a matrix such that every row corresponded to one line scan. We corrected for membrane movements by calculating the maximum of a running average over several hundred line scans and shifting it to the same column. We fitted an average over all rows with a Gaussian and we added only the elements of each row between -2.5σ and 2.5σ to calculate the fluorescence intensity trace. We computed the auto-cross-correlation, spectral cross-correlation, and spatial cross-correlation curves from the intensity traces and excluded irregular curves resulting from instabilities and distortions. We fitted the auto-correlation and cross-correlation functions with a nonlinear least-squares global fitting algorithm as in ref. ²¹. The equations used are shown in Supplementary Table 1.

In scanning FCCS, each value measured refers to one GUV. In total, we did *n* ≥ 3 independent experiments for each condition and interaction pair. In each experiment, we measured several GUVs that are shown as individual data points. Overall, 25–50% of measured GUVs were not included in the analysis for three reasons: (1) The GUV moved out of the focal volume during the measurement time (300 s). (2) Identification of large aggregates/buds on the surface of the GUV (see Supplemental Fig. 7) that strongly affected the measurement. (3) Large changes in protein concentration in the membrane during the measurement. The experiments were set up as a way that GUVs were added with a lipid to protein ratio of ~500:1 or higher.

Mathematical modeling. For each possible interaction scenario, an ODE-based model based on mass action kinetics was set up in COPASI (4.15, build 95)⁷¹. Differently labeled Bcl-xL proteins were included as separate species in the reactions.

Model parameters were fitted against four time courses of three different particle concentrations (Bcl-xL_G, Bcl-xL_R, and Bcl-xL_G/Bcl-xL_R) measured by FCS, with and without cBid addition. Bcl-xL_G particles denote Bcl-xL_G monomers and all possible multimers including at least one Bcl-xL_G (same for Bcl-xL_R particles). Bcl-xL_G/Bcl-xL_R particles denote any particles including at least one Bcl-xL_G and one Bcl-xL_R. Initial concentrations of monomeric and homo-dimeric Bcl-xL_G and Bcl-xL_R were included into parameter estimation (constrained between 0 and 10 nM).

For parameter fitting, first a global optimization method was applied by using the Evolutionary Programming algorithm in COPASI, where the population size was 10 times the number of parameters, and the maximum number of generations was 10 times the population size. To further improve the best parameter set found

by the global optimization method, the local method “Hooke and Jeeves” from within COPASI was used with default parameter settings. This procedure was described in ref. ⁷².

The following objective function was used for parameter fitting (weighted SSR, sum of squared residuals):

$$SSR = \sum_{ij} \omega_j \cdot (x_{ij} - y_{ij}(P))^2$$

with weight $\omega_j = \frac{1}{x_j^2}$; j = time course of one particle type; i = measurement at one time point; x_{ij} = measurement of one particle type at one time point; $y_{ij}(P)$ = simulated value of one particle type at one time point given the parameter set P .

Bcl-xL_R and Bcl-xL_G were mixed and incubated 2 h at RT, before the first data point was taken at $t = -20$. Afterwards, the sample was split into two parts: to one buffer was added at $t = 0$, to the other 400 nM cBid was added at $t = 0$, thereby the sample was diluted 1:1. The dilution was accounted for by assuming half particle concentrations in measurements at $t = -20$ min. To improve fit performance, measurement of buffer control sample at 0 min was added to the time course including cBid addition, which was possible because the time courses of buffer control and cBid addition were derived from the same reaction sample and only separated at $t = 0$ min. The value of cBid addition was set from $t = 0$ to 1 min, which is justifiable by relatively long measurement times of FCS for every time point (2 min per time point).

The experiments were corrected for unlabeled Bcl-xL proteins by adding an unlabeled Bcl-xL species to the ODE systems. Initial concentrations of unlabeled monomers, and (partially) unlabeled Bcl-xL dimers were calculated the following way, assuming that the label has no influence on association and dissociation behavior:

DOL \bullet -labeling efficiency of Bcl-xL_G ($B\bullet$); DOL \circ -labeling efficiency of Bcl-xL_R ($B\circ$)
unlabeled BclxL monomer:

$$[B] = (1 - \text{DOL}_{B\circ}) \cdot \frac{[B\circ]}{\text{DOL}_{B\circ}} + (1 - \text{DOL}_{B\bullet}) \cdot \frac{[B\bullet]}{\text{DOL}_{B\bullet}}$$

unlabeled Bcl-xL homo-dimer:

$$[B - B] = (1 - \text{DOL}_{B\circ})^2 \cdot \frac{[B\circ - B\circ]}{\text{DOL}_{B\circ}^2} + (1 - \text{DOL}_{B\bullet})^2 \cdot \frac{[B\bullet - B\bullet]}{\text{DOL}_{B\bullet}^2}$$

Bcl-xL homo-dimer including one labeled Bcl-xL (correspondingly for $B\bullet - B$):

$$[B\circ - B] = \text{DOL}_{B\circ} (1 - \text{DOL}_{B\circ}) \cdot 2 \cdot \frac{[B\circ - B\circ]}{\text{DOL}_{B\circ}^2}$$

The standard deviation shown in the particle time courses of Bcl-xL_G-Bcl-xL_R particles was calculated the following way: 10,000 numbers were sampled from the cross-correlation (CC) value of Bcl-xL_G with Bcl-xL_R with a gaussian distribution around the measured mean with the measured standard deviation. The same procedure was applied vice versa (CC of Bcl-xL_R with Bcl-xL_G). From these 20,000 values the mean and standard deviation were calculated. All ODE equations used are listed in Supplementary Table 3.

Differences in AIC_c (AIC corrected for small sample size) values and the Akaike weight w_i were calculated as following and as described elsewhere⁷³:

k = number of parameters; n = number of data points; R = number of tested models

$$\text{AIC}_c = 2k + n \cdot \ln(\text{SSR}) + 2k \cdot \left(\frac{n}{n - k - 1} \right)$$

$$\Delta_i = \text{AIC}_{c,i} - \text{AIC}_{c,\min}$$

$$w_i = \frac{\exp(-\Delta_i/2)}{\sum_{j=1}^R \exp(-\Delta_j/2)}$$

Parameter identifiability analysis. Parameter identifiability analysis was performed and the 95% confidence regions of each parameter were determined as described in ref. ⁴⁸. Briefly, the objective function was reoptimized for each parameter on discrete logarithmic steps surrounding the optimized parameter value \hat{p} with respect to all other parameters using the Hooke and Jeeves algorithm in COPASI. The confidence region was determined as described in ref. ⁴⁸:

$P_{CR} = \left\{ p : \text{SSR}(p) \leq \text{SSR}(\hat{p}) \left(1 + \frac{k}{n-k} F_{k,n-k}^\alpha \right) \right\}$, where, $F_{k,n-k}^\alpha$ is the upper α -critical value of the $F_{k,n-k}$ distribution.

Received: 29 June 2016 Accepted: 31 May 2017

Published online: 13 July 2017

References

1. Youle, R. J. & Strasser, A. The BCL-2 protein family: opposing activities that mediate cell death. *Nat. Rev. Mol. Cell Biol.* **9**, 47–59 (2008).
2. Garcia-Saez, A. J. The secrets of the Bcl-2 family. *Cell Death. Differ.* **19**, 1733–1740 (2012).
3. Czabotar, P. E., Lessene, G., Strasser, A. & Adams, J. M. Control of apoptosis by the BCL-2 protein family: implications for physiology and therapy. *Nat. Rev. Mol. Cell Biol.* **15**, 49–63 (2014).
4. Delbridge, A. R. & Strasser, A. The BCL-2 protein family, BH3-mimetics and cancer therapy. *Cell. Death. Differ.* **22**, 1071–1080 (2015).
5. Schellenberg, B. et al. Bax exists in a dynamic equilibrium between the cytosol and mitochondria to control apoptotic priming. *Mol. Cell* **49**, 959–971 (2013).
6. Edlich, F. et al. Bcl-x(L) retrotranslocates bax from the mitochondria into the cytosol. *Cell* **145**, 104–116 (2011).
7. Wolter, K. G. et al. Movement of bax from the cytosol to mitochondria during apoptosis. *J. Cell Biol.* **139**, 1281–1292 (1997).
8. Eskes, R., Desagher, S., Antonsson, B. & Martinou, J. C. Bid induces the oligomerization and insertion of Bax into the outer mitochondrial membrane. *Mol. Cell Biol.* **20**, 929–935 (2000).
9. Antonsson, B., Montessuit, S., Lauper, S., Eskes, R. & Martinou, J. C. Bax oligomerization is required for channel-forming activity in liposomes and to trigger cytochrome c release from mitochondria. *Biochem. J.* **345**, 271–278 (2000).
10. Bleicken, S. et al. Structural model of active bax at the membrane. *Mol. Cell* **56**, 496–505 (2014).
11. Subburaj, Y. et al. Bax monomers form dimer units in the membrane that further self-assemble into multiple oligomeric species. *Nat. Commun.* **6**, 8042 (2015).
12. Czabotar Peter, E. et al. Bax crystal structures reveal how BH3 domains activate bax and nucleate its oligomerization to induce apoptosis. *Cell* **152**, 519–531 (2013).
13. Salvador-Gallego, R. et al. Bax assembly into rings and arcs in apoptotic mitochondria is linked to membrane pores. *EMBO J.* **35**, 389–401 (2016).
14. Große, L. et al. Bax assembles into large ring-like structures remodeling the mitochondrial outer membrane in apoptosis. *EMBO J.* **35**, 402–413 (2016).
15. Bleicken, S., Landeta, O., Landajuela, A., Basanez, G. & Garcia-Saez, A. J. Proapoptotic bax and Bak form stable protein-permeable pores of tunable size. *J. Biol. Chem.* **288**, 33241–33252 (2013).
16. Bleicken, S., Hofhaus, G., Ugarte-Urbe, B., Schroder, R. & Garcia-Saez, A. J. cBid, bax and Bcl-xL exhibit opposite membrane remodeling activities. *Cell Death. Dis.* **7**, e2121 (2016).
17. Chou, J. J., Li, H., Salvesen, G. S., Yuan, J. & Wagner, G. Solution structure of BID, an intracellular amplifier of apoptotic signaling. *Cell* **96**, 615–624 (1999).
18. Bleicken, S., Garcia-Saez, A. J., Conte, E. & Bordignon, E. Dynamic interaction of cBid with detergents, liposomes and mitochondria. *PLoS ONE* **7**, e35910 (2012).
19. Bleicken, S., Wagner, C. & García-Saez Ana, J. Mechanistic differences in the membrane activity of bax and Bcl-xL correlate with their opposing roles in apoptosis. *Biophys. J.* **104**, 421–431 (2013).
20. Billen, L. P., Kokoski, C. L., Lovell, J. F., Leber, B. & Andrews, D. W. Bcl-xL inhibits membrane permeabilization by competing with Bax. *PLoS Biol.* **6**, e147 (2008).
21. Garcia-Saez, A. J., Ries, J., Orzaez, M., Perez-Paya, E. & Schulle, P. Membrane promotes tBid interaction with BCL(XL). *Nat. Struct. Mol. Biol.* **16**, 1178–1185 (2009).
22. Llambi, F. et al. A unified model of mammalian Bcl-2 protein family interactions at the mitochondria. *Mol. Cell* **44**, 1–15 (2011).
23. Cheng, E. H., Levine, B., Boise, L. H., Thompson, C. B. & Hardwick, J. M. Bax-independent inhibition of apoptosis by Bcl-xL. *Nature* **379**, 554–556 (1996).
24. Hsu, Y. T. & Youle, R. J. Nonionic detergents induce dimerization among members of the Bcl-2 family. *J. Biol. Chem.* **272**, 13829–13834 (1997).
25. Willis, S. N. et al. Apoptosis initiated when BH3 ligands engage multiple Bcl-2 homologs, not Bax or Bak. *Science* **315**, 856–859 (2007).
26. Kuwana, T. et al. Bid, bax, and lipids cooperate to form supramolecular openings in the outer mitochondrial membrane. *Cell* **111**, 331–342 (2002).
27. Letai, A. et al. Distinct BH3 domains either sensitize or activate mitochondrial apoptosis, serving as prototype cancer therapeutics. *Cancer Cell* **2**, 183–192 (2002).
28. Leber, B., Lin, J. & Andrews, D. W. Still embedded together binding to membranes regulates Bcl-2 protein interactions. *Oncogene* **29**, 5221–5230 (2010).
29. Chen, H. C. et al. An interconnected hierarchical model of cell death regulation by the BCL-2 family. *Nat. Cell Biol.* **17**, 1270–1281 (2015).

30. Lovell, J. F. et al. Membrane binding by tBid initiates an ordered series of events culminating in membrane permeabilization by Bax. *Cell* **135**, 1074–1084 (2008).
31. Gavathiotis, E. et al. BAX activation is initiated at a novel interaction site. *Nature* **455**, 1076–1081 (2008).
32. Aranovich, A. et al. Differences in the mechanisms of proapoptotic BH3 proteins binding to Bcl-XL and Bcl-2 quantified in live MCF-7 cells. *Mol. Cell* **45**, 754–763 (2012).
33. Ries J., Petrasek Z., Garcia-Saez A. J. & Schwille P. A comprehensive framework for fluorescence cross-correlation spectroscopy. *N. J. Phys.* **12**, 113009 (2010).
34. Jeong, S. Y. et al. Bcl-x(L) sequesters its C-terminal membrane anchor in soluble, cytosolic homodimers. *EMBO J.* **23**, 2146–2155 (2004).
35. Yao, Y. et al. Conformation of BCL-XL upon membrane integration. *J. Mol. Biol.* **427**, 2262–2270 (2015).
36. Muchmore, S. W. et al. X-ray and NMR structure of human Bcl-xL, an inhibitor of programmed cell death. *Nature* **381**, 335–341 (1996).
37. O'Neill, J. W., Manion, M. K., Maguire, B. & Hockenbery, D. M. BCL-XL dimerization by three-dimensional domain swapping. *J. Mol. Biol.* **356**, 367–381 (2006).
38. Denisov, A. Y., Sprules, T., Fraser, J., Kozlov, G. & Gehring, K. Heat-induced dimerization of BCL-xL through alpha-helix swapping. *Biochemistry* **46**, 734–740 (2007).
39. Rajan, S. et al. Structural transition in Bcl-xL and its potential association with mitochondrial calcium ion transport. *Sci. Rep.* **5**, 10609 (2015).
40. Suzuki, M., Youle, R. J. & Tjandra, N. Structure of Bax: coregulation of dimer formation and intracellular localization. *Cell* **103**, 645–654 (2000).
41. Lindner, A. U. et al. Systems analysis of BCL2 protein family interactions establishes a model to predict responses to chemotherapy. *Cancer Res.* **73**, 519–528 (2013).
42. Certo, M. et al. Mitochondria primed by death signals determine cellular addiction to antiapoptotic BCL-2 family members. *Cancer Cell* **9**, 351–365 (2006).
43. Kim, H. et al. Hierarchical regulation of mitochondrion-dependent apoptosis by BCL-2 subfamilies. *Nat. Cell Biol.* **8**, 1348–1358 (2006).
44. Chen, L. et al. Differential targeting of prosurvival Bcl-2 proteins by their BH3-only ligands allows complementary apoptotic function. *Mol. Cell* **17**, 393–403 (2005).
45. Hockings, C. et al. Bid chimeras indicate that most BH3-only proteins can directly activate Bak and Bax, and show no preference for Bak versus Bax. *Cell Death Dis.* **6**, e1735 (2015).
46. Kuwana, T. et al. BH3 domains of BH3-only proteins differentially regulate Bax-mediated mitochondrial membrane permeabilization both directly and indirectly. *Mol. Cell* **17**, 525–535 (2005).
47. Burnham, K. P. & Anderson, D. R. *Model Selection and Multimodel Inference: A Practical Information-Theoretic Approach* (Springer, 2002).
48. Schaber, J. Easy parameter identifiability analysis with COPASI. *Biosystems* **110**, 183–185 (2012).
49. Schreiber, G., Haran, G. & Zhou, H. X. Fundamental aspects of protein–protein association kinetics. *Chem. Rev.* **109**, 839–860 (2009).
50. Hermann, E., Bleicken, S., Subburaj, Y. & Garcia-Saez, A. J. Automated analysis of giant unilamellar vesicles using circular Hough transformation. *Bioinformatics* **30**, 1747–1754 (2014).
51. Pagliari, L. J. et al. The multidomain proapoptotic molecules Bax and Bak are directly activated by heat. *Proc. Natl Acad. Sci. USA* **102**, 17975–17980 (2005).
52. Bleicken, S. et al. Molecular details of Bax activation, oligomerization, and membrane insertion. *J. Biol. Chem.* **285**, 6636–6647 (2010).
53. Antonsson, B., Montessuit, S., Sanchez, B. & Martinou, J. C. Bax is present as a high molecular weight oligomer/complex in the mitochondrial membrane of apoptotic cells. *J. Biol. Chem.* **276**, 11615–11623 (2001).
54. Shivakumar, S. et al. The proapoptotic protein tBid forms both superficially bound and membrane-inserted oligomers. *Biophys. J.* **106**, 2085–2095 (2014).
55. Gavathiotis, E., Reyna, D. E., Davis, M. L., Bird, G. H. & Walensky, L. D. BH3-triggered structural reorganization drives the activation of proapoptotic BAX. *Mol. Cell* **40**, 481–492 (2010).
56. Korsmeyer, S. J. Regulators of cell death. *Trends Genet.* **11**, 101–105 (1995).
57. Zhang, Z. et al. BH3-in-groove dimerization initiates and helix 9 dimerization expands Bax pore assembly in membranes. *EMBO J.* **35**, 208–236 (2016).
58. Andreu-Fernandez, V. et al. Bax transmembrane domain interacts with prosurvival Bcl-2 proteins in biological membranes. *Proc. Natl Acad. Sci. USA* **114**, 310–315 (2017).
59. Todt, F., Cakir, Z., Reichenbach, F., Youle, R. J. & Edlich, F. The C-terminal helix of Bcl-xL mediates Bax retrotranslocation from the mitochondria. *Cell Death Differ.* **20**, 333–342 (2013).
60. Renault, T. T. et al. Bcl-xL stimulates Bax relocation to mitochondria and primes cells to ABT-737. *Int. J. Biochem. Cell Biol.* **64**, 136–146 (2015).
61. O'Neill, K. L., Huang, K., Zhang, J., Chen, Y. & Luo, X. Inactivation of prosurvival Bcl-2 proteins activates Bax/Bak through the outer mitochondrial membrane. *Genes Dev.* **30**, 973–988 (2016).
62. Wang, Y. & Tjandra, N. Structural insights of tBid, the caspase-8-activated Bid, and its BH3 domain. *J. Biol. Chem.* **288**, 35840–35851 (2013).
63. Garner, T. P. et al. An autoinhibited dimeric form of BAX regulates the BAX activation pathway. *Mol. Cell* **63**, 485–497 (2016).
64. Sung, T.-C. et al. Solution structure of apoptotic BAX oligomer: oligomerization likely precedes membrane insertion. *Structure* **23**, 1878–1888 (2015).
65. Cartron, P. F., Oliver, L., Mayat, E., Meflah, K. & Vallette, F. M. Impact of pH on Bax alpha conformation, oligomerisation and mitochondrial integration. *FEBS Lett.* **578**, 41–46 (2004).
66. Montessuit, S. et al. Membrane remodeling induced by the dynamin-related protein Drp1 stimulates Bax oligomerization. *Cell* **142**, 889–901 (2010).
67. Ichim, G. et al. Limited mitochondrial permeabilization causes DNA damage and genomic instability in the absence of cell death. *Mol. Cell* **57**, 860–872 (2015).
68. Youle, R. J. & Karbowski, M. Mitochondrial fission in apoptosis. *Nat. Rev. Mol. Cell Biol.* **6**, 657–663 (2005).
69. Karbowski, M., Norris, K. L., Cleland, M. M., Jeong, S. Y. & Youle, R. J. Role of bax and bak in mitochondrial morphogenesis. *Nature* **443**, 658–662 (2006).
70. Vervliet, T., Parys, J. B. & Bultynck, G. Bcl-2 proteins and calcium signaling: complexity beneath the surface. *Oncogene* **35**, 5079–5092 (2016).
71. Hoops, S. et al. COPASI—a COmplex pathway simulator. *Bioinformatics* **22**, 3067–3074 (2006).
72. Schaber, J., Baltanas, R., Bush, A., Klipp, E. & Colman-Lerner, A. Modelling reveals novel roles of two parallel signalling pathways and homeostatic feedbacks in yeast. *Mol. Syst. Biol.* **8**, 622 (2012).
73. Johnson, J. B. & Omland, K. S. Model selection in ecology and evolution. *Trends Ecol. Evol.* **19**, 101–108 (2004).

Acknowledgements

We thank C. Stegmüller for excellent technical assistance, J.C. Martinou for providing Caspase 8 and J. Suckale for critical reading of the manuscript. This work was supported by the Max Planck Society (S.B., K.K.D., and A.J.G.-S.), the German Cancer Research Center (S.B. and A.J.G.-S.), the German Ministry for Education and Research (BMBF, Grant No. 0312040; S.B. and A.J.G.-S.), the European Research Council (ERC-2012-StG 309966; S.B., K.K.D., and A.J.G.-S.) as well as the Forschergruppe 2036 (S.B., A.H., K.K.D., T.F., and A.J.G.-S.), Konstanz Research School Chemical Biology (AH), and the Cluster of Excellence RESOLV (EXC 1069; S.B.) funded by the Deutsche Forschungsgemeinschaft.

Author contributions

S.B. designed and performed experiments, analyzed data, and wrote the manuscript. K.K.D. performed experiments and analyzed data. A.H. and T.F. did the modeling and wrote the modeling part of the manuscript. A.J.G.-S. designed the study, planned experiments, and wrote the manuscript.


Additional information

Supplementary Information accompanies this paper at doi:10.1038/s41467-017-00086-6.

Competing interests: The authors declare no competing financial interests.

Reprints and permission information is available online at <http://npg.nature.com/reprintsandpermissions/>

Publisher's note: Springer Nature remains neutral with regard to jurisdictional claims in published maps and institutional affiliations.

 **Open Access** This article is licensed under a Creative Commons Attribution 4.0 International License, which permits use, sharing, adaptation, distribution and reproduction in any medium or format, as long as you give appropriate credit to the original author(s) and the source, provide a link to the Creative Commons license, and indicate if changes were made. The images or other third party material in this article are included in the article's Creative Commons license, unless indicated otherwise in a credit line to the material. If material is not included in the article's Creative Commons license and your intended use is not permitted by statutory regulation or exceeds the permitted use, you will need to obtain permission directly from the copyright holder. To view a copy of this license, visit <http://creativecommons.org/licenses/by/4.0/>.

© The Author(s) 2017

1 **Bax retrotranslocation potentiates Bcl-x_L's antiapoptotic activity and is essential for**
2 **switch-like transitions between MOMP competency and resistance**

3
4 Annika Hantusch^{1,2}, Kushal K. Das³, Ana J. García-Sáez³, Thomas Brunner^{1,2,#}, Markus
5 Rehm^{4,5,6,7,#*}

6 ¹Department of Biology, Chair of Biochemical Pharmacology, University of Konstanz, 78457
7 Konstanz, Germany

8 ²Konstanz Research School Chemical Biology, University of Konstanz, 78457 Konstanz,
9 Germany

10 ³ Interfaculty Institute of Biochemistry, Eberhard Karls University Tübingen, Hoppe-Seyler-Str.
11 4, 72076 Tübingen, Germany

12 ⁴Department of Physiology & Medical Physics, Royal College of Surgeons in Ireland, Dublin
13 2, Ireland

14 ⁵Centre for Systems Medicine, Royal College of Surgeons in Ireland, Dublin 2, Ireland

15 ⁶Institute of Cell Biology and Immunology, University of Stuttgart, 70569 Stuttgart, Germany

16 ⁷Stuttgart Research Center Systems Biology, University of Stuttgart, 70569 Stuttgart,
17 Germany

18 [#]joint senior authors

19
20 *To whom correspondence should be addressed:

21 Prof Dr Markus Rehm

22 Institute of Cell Biology and Immunology

23 University of Stuttgart

24 70569 Stuttgart, Germany

25 Phone: +49 711 68 56 6988

26 E-mail: markus.morrison@izi.uni-stuttgart.de

27

28 **Abstract**

29 The rapid, typically all-or-none process of mitochondrial outer membrane permeabilization
30 (MOMP) constitutes a primary cell death decision that is controlled by the dynamic interplay of
31 pro- and antiapoptotic Bcl-2 family proteins. Even though a wealth of quantitative biochemical
32 and biophysical data on Bcl-2 family interactions is available, our understanding of how
33 MOMP decisions are controlled by the Bcl-2 family interactome remains incomplete. Besides
34 the question if our knowledge on Bcl-2 protein interactions is sufficient to explain MOMP
35 decisions during cell death induction, it is unclear if and to which extent the recently described
36 shuttling of Bcl-2 family species between lipid and aqueous phases contributes to regulating
37 MOMP sensitivity. To address these questions, we studied the interplay of tBid, Bax and Bcl-
38 x_L , using a combined approach of deterministic mathematical modeling and retrospective as
39 well as prospective experimental testing of model predictions. We first developed a core
40 model of the tBid-Bax interplay that accurately reproduced quantitative experimental data on
41 tBid-triggered Bax activation and oligomerization measured in membranes. This model was
42 then extended by heterodimeric Bcl- x_L interactions, with the additional option to account for
43 Bcl- x_L -dependent retrotranslocation of Bax from the mitochondria into the cytosol. Strikingly,
44 only when retrotranslocation was taken into account, the model outputs accurately
45 reproduced and correctly predicted all quantitative experimental results. These included the
46 potency of Bcl- x_L in suppressing Bax oligomerization and its role in limiting Bax recruitment to
47 membranes. Likewise, the resistance to low concentrations of MOMP triggers as well as
48 synergistic responses to combinations of tBid and sensitizer BH3-only peptides were correctly
49 predicted. Importantly, retrotranslocation activity of Bcl- x_L seems essential to strictly separate
50 conditions of MOMP competency and resistance, thus establishing an all-or-none cell fate
51 decision. Our results therefore support indispensable and currently underappreciated roles of
52 Bcl- x_L -mediated Bax retrotranslocation in MOMP regulation.

53

54 **Key words:** Cell death, apoptosis, Bcl-2 family, mitochondrial outer membrane
55 permeabilisation (MOMP), mathematical modeling

56 **Introduction**

57 Pro- and antiapoptotic members of the Bcl-2 (B-cell lymphoma 2) protein family gather signals
58 from pathways sensing stresses, such as DNA damage or cytokine deprivation, and regulate
59 the mitochondrial pathway of apoptosis (1,2). The primary mediators of incoming stress
60 signals are Bcl-2 family members with a single Bcl-2 homology (BH) domain, the so-called
61 BH3-only proteins. The subgroup of activator BH3-only proteins, such as truncated Bid (tBid),
62 Bim or Puma, directly activate the effector Bcl-2 family proteins Bax and Bak (3,4). These in
63 turn oligomerize to form pores in the outer mitochondrial membrane, causing the release of
64 cytochrome *c* and other proapoptotic factors into the cytosol (5). This process of mitochondrial
65 outer membrane permeabilization (MOMP) typically is an all-or-none event, resulting in the
66 rapid and efficient activation of effector caspases and apoptosis execution (6,7). Prosurvival
67 family members, such as Bcl-x_L, Bcl-2 and Mcl-1, efficiently antagonize both activator and
68 sensitizer BH3-only proteins as well as Bax and Bak, thereby protecting cells from unwanted
69 MOMP. However, their increased expression might also completely prevent apoptosis and
70 thereby the elimination of excessively stressed and damaged cells (8,9). Imbalances in the
71 expression of Bcl-2 family members therefore interfere with normal cellular homeostasis in
72 multicellular organisms and can contribute to the complex etiologies of diverse degenerative
73 and proliferative diseases (3).

74 Importantly, the majority of critical interactions between Bcl-2 family members occur at or
75 within the outer mitochondrial membrane. Membrane association and integration significantly
76 affect protein conformations and binding affinities of Bcl-2 family members, so that authentic
77 interaction data cannot be obtained from studies carried out solely in aqueous environments
78 (10,11). For example, membrane environments dramatically promote the association of tBid
79 with Bcl-x_L (10). Furthermore, membrane bound proteins induce the recruitment of further
80 family members, and membrane insertion leads to altered interaction patterns (12). Similar

81 findings regarding the regulatory role of the membrane were made for various Bcl-2 family
82 members and interactions, using NMR structure elucidation in artificial micelles (13),
83 subcellular fractionation (14,15), or by studying GFP fusion proteins and their recruitment to
84 the outer mitochondrial membrane (16).

85 Recently, Bax activation was described at greater mechanistic detail. Binding of the tBid BH3
86 domain to Bax unlatches the Bax core domain, thereby exposing the Bax BH3 domain and
87 preparing Bax to form BH3-in-groove homodimers (17). Strikingly, the lipidic environment at
88 the mitochondrial outer membrane appears to facilitate the disengagement of core and latch
89 domains and provides a surface to preorientate Bax for homooligomerisation (17). Bak is
90 likely activated by a similar molecular mechanism in mitochondrial membranes (18). Even
91 though technologies such as scanning fluorescence cross correlation spectroscopy (sFCCS)
92 or FRET-based assays in lipid environments now begin to provide reliable data from well-
93 controlled experimental conditions (12,19,20), obtaining a quantitative and kinetic
94 understanding of the Bcl-2 interactome and MOMP regulation remains challenging (4,21).

95 A further layer of complexity in the regulation of MOMP sensitivity might be added by the
96 recently reported shuttling of Bcl-2 family members. Most prominently, it was demonstrated
97 that the cytosolic fraction of Bax and Bax bound to the mitochondrial outer membrane exist in
98 a dynamic equilibrium in healthy cells (22–24). Bcl-x_L, a predominantly membrane integrated
99 family member, promotes retrotranslocation of Bax from the mitochondria into the cytosol and
100 thereby limits Bax cytotoxicity (22,25). However, to which extent retrotranslocation contributes
101 to the antiapoptotic potential of Bcl-x_L remains so far undetermined.

102 Here, we studied the regulation of MOMP by the interplay of tBid, Bax and Bcl-x_L at and within
103 membranes, using a combined approach of deterministic mathematical modeling and
104 experimental validation of model predictions. We were able to quantify for the first time the
105 contribution of Bax retrotranslocation to the overall antiapoptotic potential of Bcl-x_L. Bax

106 retrotranslocation functionally appears to be essential to provide MOMP resistance to
107 residual, basal BH3-only protein stress while still allowing rapid and synergistic MOMP
108 induction in response to combinations of activator and sensitizer BH3-only protein inputs.
109 Furthermore, retrotranslocation activity is required to control switch-like transitions from
110 MOMP competency to MOMP resistance across a narrow Bcl-xL concentration range.

111 **Results**

112 **Quantitative kinetic modeling of the tBid-Bax interplay accurately simulates Bax** 113 **activation and oligomerization**

114 We initially developed a core mathematical model of the tBid-Bax interplay at and within
115 membranes to study if membrane recruitment, activation and oligomerization of Bax, leading
116 to MOMP, can be simulated authentically. This core model subsequently was used to analyze
117 the potency of Bcl-x_L in preventing MOMP and to determine the contribution of Bax
118 retrotranslocation to the antiapoptotic function of Bcl-x_L. All processes were modeled using
119 ordinary differential equations (see methods section and Supplementary Material 1 for
120 detailed information).

121 The activator BH3-only protein tBid was implemented to promote the insertion of monomeric
122 Bax into the outer mitochondrial membrane (26) (Figure 1a). In the model, this process
123 comprised serial reversible reactions, including tBid-mediated Bax membrane association and
124 subsequent membrane insertion to yield Bax in its fully active conformation (aBax). The two-
125 step activation process of Bax is in agreement with the recently proposed core/latch
126 disengagement mechanism, in which the BH3 domain of tBid first binds to Bax and thereby
127 induces the dissociation of Bax's core and latch domains (17). aBax subsequently can form
128 symmetric homodimers with other aBax molecules by BH3 domain/binding groove
129 interactions (17). In line with experimental evidence, aBax was assumed to recruit further Bax
130 molecules to the membrane, thereby driving a Bax autoactivation loop (27–29) (Figure 1a).
131 Since Bax autoactivation relies on the Bax BH3 domain (27), the reaction sequence was
132 implemented analogous to Bax activation by tBid (Figure 1a). Experimentally, mostly even-
133 numbered oligomers of aBax can be detected in membranes (30). We thus modeled aBax
134 oligomerization by assuming dimeric aBax species aggregating into tetramers (aBax₄) and
135 hexamers (aBax₆) (Figure 1b). Higher order oligomers were not explicitly modeled, since

136 aBax₄ and aBax₆ appear to be sufficient for pore formation and cytochrome *c* release into the
137 cytosol (31,32). The amounts of aBax₄ and aBax₆ were therefore regarded as a final output of
138 the model, indicative of the extent of membrane permeabilization (Figure 1b).

139 Bax multimers rapidly accumulate in membranes in response to tBid addition, as was
140 demonstrated by measuring oligomerization kinetics in lipid bilayers (30). However, the rate
141 and dissociation constants for the underlying reactions and interactions so far can only be
142 estimated within biologically plausible and justifiable parameter ranges. We therefore tested if
143 model parameterizations could be obtained from these ranges that allowed us to reproduce
144 experimental kinetics of Bax oligomerization. A detailed description of this procedure and the
145 definition of suitable parameter ranges are provided in the methods section and in
146 Supplementary Material 1. Results from ensemble simulations (n = 340) using optimized
147 parameter ranges demonstrate that oligomerization of membrane bound aBax proceeds
148 swiftly upon addition of tBid, with aBax₄ and aBax₆ species rapidly reaching equilibrium
149 concentrations within 1-2 min of triggering the reaction network (Figure 2a), thus closely
150 matching reported kinetics (30). The distribution of oligomeric Bax species indicated that
151 predominantly Bax tetramers and, albeit in lower amounts, Bax hexamers are formed. This
152 distribution agreed well with the distribution of Bax oligomers measured experimentally
153 (Figure 2b).

154 Next, we used this core model to study oligomerization of aBax resulting from autoactivation.
155 To this end, we ran simulations in absence of tBid and used small amounts of aBax as model
156 inputs. For inputs of up to 10-20% aBax, we noted roughly equimolar amounts of aBax₂ and
157 aBax₄ forming. To validate these predictions, we examined experimental data in which heat-
158 activated aBax was used to initiate Bax oligomerization and pore formation in absence of tBid
159 (30). Comparison of model predictions and experimentally observed distributions confirmed a
160 close match of the results, with aBax₂ and aBax₄ being the predominant species (Figure 2c).

161 For conditions with high amounts of aBax inputs (80%), it would be assumed that oligomer
162 distributions similar to those in presence of tBid would be obtained. Control simulations
163 indeed confirmed this assumption (not shown).

164 To conclude, our core model of the tBid-Bax interplay therefore reproduces experimental
165 findings on tBid-induced Bax oligomerization, kinetically and quantitatively, and, without
166 further modification of its structure or parameter values, accurately predicts Bax oligomer
167 distributions obtained by autoactivation.

168

169 **Bcl-x_L-mediated Bax retrotranslocation is critical for limiting Bax oligomerization**

170 We next integrated Bcl-x_L into the model to study the interplay of this classical triad of
171 activator, effector and prosurvival Bcl-2 family members, and to assess the potency of Bcl-x_L
172 in preventing Bax pore formation in this signaling context. Bcl-x_L mediates its prosurvival
173 function by at least two well-characterized mechanisms, i.e. (i) by binding to aBax and thereby
174 preventing oligomerization and pore formation (33,34), as well as (ii) by sequestering BH3-
175 only proteins such as tBid (26,35). We thus accounted for heterodimerization of Bcl-x_L with
176 tBid and aBax in the extended model (Figure 3a). Recent experimental studies interestingly
177 revealed that Bcl-x_L also retrotranslocates aBax from mitochondrial membranes into the
178 cytosol, a process that could add to the antiapoptotic potency of Bcl-x_L (22,24,25).
179 Retrotranslocation was therefore implemented as an optional model extension (Figure 3a,
180 black box).

181 Experimentally, the ability of Bcl-x_L to disassemble tBid-induced, pre-formed aBax oligomers
182 can be quantified in lipid bilayers isolated from large unilamellar vesicles (30) (Figure 3b).
183 Data on steady state distributions of aBax oligomers and heterodimers with Bcl-x_L indicate
184 that aBax hexamers cannot be observed upon addition of Bcl-x_L and that the majority of aBax
185 resides within aBax₂ and Bcl-x_L-aBax species (Figure 3c). Interestingly, simulations

186 conducted with our core model, extended by the tBid-Bcl-x_L and aBax-Bcl-x_L interplay, failed
187 to reproduce such data (Figure 3d). Instead, we found that the majority of aBax still formed
188 tetramers and hexamers (Figure 3d). Even when searching a large parameter space, we
189 failed to fit the model to the experimental data shown in Figure 3c. We next tested if the
190 model variant that included the possibility for Bcl-x_L to retrotranslocate membrane-bound Bax
191 into the cytosol was better suited to provide outputs that correspond to experimental findings.
192 Indeed, results obtained with this model variant agreed very well with experimentally
193 observed aBax oligomer distributions when assuming retrotranslocation rates of 5 to 10 s⁻¹
194 (Figure 3e).

195 In summary, these results demonstrate that the interplay of tBid, Bax and Bcl-x_L at and within
196 membranes can be quantitatively recapitulated by mathematical modeling, and that the ability
197 of Bcl-x_L to retrotranslocate aBax from membranes into the cytosol needs to be taken into
198 account to reproduce experimental data on Bax oligomerization.

199

200 **Mathematical modeling accurately predicts limited Bax membrane recruitment in** 201 **presence of Bcl-x_L.**

202 We next used our model to estimate the overall amount of Bax recruitment to membranes in
203 presence of Bcl-x_L. To this end, we studied conditions at which small amounts of tBid (20 nM)
204 activate higher concentrations of Bax (100 nM), in absence or presence of increasing
205 amounts of Bcl-x_L. To determine the overall recruitment of Bax, we took into account all Bax
206 containing species at or within membranes (ΣBax_M) (Figure 4a). Without inclusion of Bax
207 retrotranslocation, Bcl-x_L was not able to limit Bax membrane recruitment (Figure 4b), even
208 when assuming rapid association of Bcl-x_L with tBid and aBax, and high affinity of the
209 resulting complexes (k_{on} 10 nM⁻¹s⁻¹, K_D 0.1 nM). In contrast, ensemble simulations that took
210 Bax retrotranslocation into account predicted that Bax membrane recruitment would be

211 antagonized very potently already at concentrations of 20 nM Bcl-x_L (Figure 4c). In
212 comparison to previously reported experimental findings (36), these predictions seemed to be
213 highly accurate (Figure 4d). We next eliminated the binding of tBid to Bcl-x_L in the model to
214 study the contribution of this interaction to the potency of Bcl-x_L in limiting Bax membrane
215 recruitment. For these conditions, higher amounts of Bax were predicted to accumulate at
216 membranes, with high Bcl-x_L concentrations nevertheless efficiently limiting overall Bax
217 recruitment to approximately 15% (Figure 4e). Very similar trends were observed
218 experimentally using the tBid variant tBid-mt1 (36), albeit with our predictions slightly
219 overestimating the potency of Bcl-x_L at lower concentrations (Figure 4e,f).
220 Overall, these findings demonstrate that the capability of Bcl-x_L to retrotranslocate Bax from
221 membranes into the cytosol significantly contributes to its antiapoptotic potential and that
222 overall Bax membrane recruitment can be accurately predicted by mathematically modeling
223 the tBid-Bax-Bcl-x_L interplay.

224

225 **Activator/sensitizer BH3-only synergies can be predicted if retrotranslocation activity**
226 **of Bcl-x_L is taken into account.**

227 Sensitizer BH3-only proteins play major cell type- and tissue-specific roles in the regulation of
228 apoptosis susceptibility (37). We therefore studied how sensitizer BH3 peptides (38) co-
229 regulate Bax oligomerization together with activator BH3-only protein tBid, and how the
230 retrotranslocation activity of Bcl-x_L influences Bax oligomerization in this scenario. For
231 implementation into the mathematical model, we assumed that sensitizers and activators bind
232 to Bcl-x_L with identical affinity, but that sensitizers cannot interact with or activate Bax (Figure
233 5a). We first calculated if a sensitizer alone would be sufficient to trigger efficient Bax
234 oligomerization in presence of Bcl-x_L and limited amounts of aBax (10%). At these conditions,
235 even high amounts of sensitizer failed to induce Bax oligomerization (Figure 5b). In contrast,

236 low concentrations of >20 nM tBid were sufficient to oligomerize nearly the entire pool of Bax
237 (approx. 95%) (Figure 5b). We next tested if these predictions could be confirmed
238 experimentally by testing tBid and an Hrk-derived BH3 peptide (38). Indeed, Bax pores only
239 formed when activator BH3-only protein tBid was added to Bax and Bcl-x_L, as evidenced by
240 the release of calcein from large unilamellar vesicles (LUVs) (Figure 5c). Simulations for
241 various combinations of sensitizer and activator concentrations suggested that sensitizers
242 would be expected to potently enhance tBid-induced Bax oligomerization and pore formation,
243 with sensitizer in nM amounts sufficient for significantly decreasing the concentration of tBid
244 required for Bax pore formation (Figure 5d). In comparison to the theoretical additive isobole
245 for half-maximal Bax recruitment into pores (Figure 5d, blue line), the interaction between
246 activator and sensitizer reveals a highly synergistic behavior. Additional simulations predicted
247 that synergies can be expected as long as the retrotranslocation activity of Bcl-x_L is taken into
248 account, since otherwise the reaction system was hypersensitive to residual amounts of
249 activator BH3-only proteins (Figure 5e, Supplemental Figure 1). Subsequent experiments
250 confirmed these predictions, with combinations of suboptimal amounts of tBid and Hrk peptide
251 inducing efficient calcein release from liposomes (Figure 5f). Of note, we utilized the Hrk
252 peptide at micromolar concentrations, as it was shown previously that BH3 peptides are
253 orders of magnitude less potent than the full length proteins (39), most likely due to
254 decreased membrane binding affinity of the soluble peptides (40). Taken together, these
255 results therefore demonstrate that upon inclusion of retrotranslocation into the model,
256 experimentally observed synergies between activator and sensitizer BH3-only proteins can be
257 predicted.

258

259 **Bax retrotranslocation is essential to separate conditions of MOMP competency and**
260 **resistance.**

261 As reported previously (5,6), MOMP typically is a rapid, all-or-none cell fate decision to initiate
262 the apoptosis execution phase. The binary nature of death decisions (yes vs. no) implies that
263 conditions of MOMP competency and resistance must be strictly separated to avoid or
264 minimize the chance for an inefficient or submaximal induction of apoptosis execution (41).
265 We therefore studied if the signaling system would be capable of controlling Bax
266 oligomerization and pore formation competency in a switch-like manner, and to which extent
267 this decision switch relies on the capacity of Bcl-x_L to retrotranslocate Bax into the cytosol. In
268 these simulations, we steadily upregulated Bcl-x_L and calculated whether Bax oligomerization
269 was inhibited. The results from these analyses demonstrate that as long as Bcl-x_L is capable
270 of retrotranslocating Bax, conditions of complete Bax oligomerization and absence of Bax
271 oligomerization are separated by a very narrow concentration range of sub-stoichiometric
272 amounts of Bcl-x_L (Figure 6a,b). In contrast, loss of retrotranslocation activity resulted in an
273 approximately inversely proportional relationship between the amounts of oligomerized Bax
274 and the amounts of Bcl-x_L, with super-stoichiometric amounts of Bcl-x_L being required to
275 prevent Bax oligomerization and pore formation (Figure 6a,b). This threshold behavior was
276 observed regardless of whether sensitizer BH3-only contributions were taken into account or
277 not. Based on the conditions studied here, we can estimate that retrotranslocation activity
278 increases the antiapoptotic potency of Bcl-x_L at least 10-fold (30 nM vs. 300 nM to prevent
279 Bax oligomerization). These findings therefore demonstrate that Bax retrotranslocation is
280 essential to generate sharp decision thresholds that separate MOMP competency from
281 MOMP resistance, with near-binary characteristics.

282

283 **Discussion**

284 Here, we studied the interplay of activator BH3-only protein tBid, multi-domain effector Bax
285 and their antagonist Bcl-x_L, using a combined approach of mathematical systems modeling as

286 well as retrospective and prospective experimental validation of model predictions
287 (summarized in Figure 7). The results of our simulations demonstrate that inclusion of Bax
288 retrotranslocation by Bcl-x_L is indispensable for reproducing Bax membrane integration and
289 oligomerization quantitatively and kinetically. We furthermore determined that, under the
290 conditions studied here, retrotranslocation enhances the antiapoptotic potential of Bcl-x_L
291 approximately 10-fold, indicating a highly significant and currently still underestimated
292 contribution of Bax shuttling towards defining cellular apoptosis resistance. Furthermore, the
293 process of Bax retrotranslocation is essential for the MOMP decision to display near-binary,
294 switch-like characteristics, with the signaling system transitioning from high MOMP
295 competency to complete MOMP resistance across a narrow Bcl-x_L concentration range.
296 Even though Bax and Bcl-x_L have long been identified as key regulators of MOMP and
297 apoptosis susceptibility (42,43), evidence for continuous shuttling of Bax from mitochondrial
298 membranes back into the cytosol emerged only in recent years (22,23). While other
299 antiapoptotic Bcl-2 family members might likewise possess retrotranslocation activity, the
300 molecular mechanisms have been studied predominantly for Bcl-x_L (24,25,44). For
301 retrotranslocation to occur, Bax must interact with the hydrophobic groove of Bcl-x_L via its
302 BH3 domain and additionally with Bcl-x_L's COOH-terminal membrane anchor, since
303 preventing any of these interactions results in mitochondrial Bax accumulation (25).
304 Retrotranslocation can be observed in minimalistic, but well-controlled *in vitro* experimental
305 settings, as evidenced by a decrease in Bax binding to the membrane in giant unilamellar
306 vesicles upon Bcl-x_L membrane insertion (12). However, within the complexity of living cells
307 additional processes might undoubtedly play coregulatory roles. Indeed, some evidence in
308 this direction has been provided. Mitochondrial specificity and membrane affinity for Bax may
309 rely on additional cofactors such as VDAC2, which recently was reported to also contribute to
310 Bax retrotranslocation (45). Additionally, mitochondria-ER contact sites seem to be

311 preferential binding sites for Bcl-2 family proteins, probably through the local accumulation of
312 Ca^{2+} , which might foster the formation of membrane microdomains rich in negatively charged
313 cardiolipin (46–48). Cardiolipin indeed promotes tBid recruitment to membranes and efficient
314 Bax activation (49,50). Furthermore, posttranslational modifications of Bax, such as
315 phosphorylation of S184, were proposed to interfere with its membrane binding and apoptotic
316 activity (51,52).

317 Interestingly, in living cells engineered to be devoid of all known BH3-only activator proteins,
318 antagonizing antiapoptotic family members alone is sufficient to induce Bax translocation and
319 apoptotic cell death (53). *In vitro*, however, Bax does not spontaneously form pores (26,39).
320 These results therefore hint at additional processes contributing to Bax activation *in cellulo*, or
321 at environments more prone to induce basal rates of Bax membrane insertion. These
322 observations further support an important role of retrotranslocation activity in preventing
323 apoptosis hypersensitivity and unwanted cell death. Retrotranslocation activity is not
324 restricted to Bcl-x_L, since other antiapoptotic family members, such as Bcl-2 and Mcl-1,
325 retrotranslocate Bax at similar rates (22). Effector protein Bak, closely related to Bax, likewise
326 is retrotranslocated from mitochondria into the cytosol, albeit at far lower rates (24). Overall,
327 this indicates a continuous shuttling to and from mitochondrial membranes, including all major
328 multi-domain Bcl-2 family members. Based on our results on the relevance of
329 retrotranslocation, it is therefore likely that the continuous interplay of pro- and antiapoptotic
330 fluxes establishes a steady state that prevents MOMP in stress-free scenarios. Indeed,
331 replacing the C-terminal membrane anchor of Bax with that of Bak, not only targets Bax to
332 mitochondria, but also reduces Bax retrotranslocation and is sufficient to trigger spontaneous
333 MOMP and apoptosis execution (24).

334 Another notable finding of our study is that retrotranslocation generates a signaling system in
335 which conditions of MOMP competency and MOMP resistance are separated in a near

336 binary, switch-like manner by small changes in the amounts of Bcl-x_L. The binary nature of
337 the MOMP decision is well known from studies on mitochondrial permeabilization during
338 intrinsic and extrinsic apoptosis. Typically, all or no mitochondria in individual cells commit
339 complete MOMP (6,7). Conditions of submaximal or incomplete MOMP instead appear to be
340 exceptions (41). We furthermore show that sensitizer and activator BH3-only proteins can act
341 synergistically in overcoming the threshold for effective MOMP execution. By sequestering
342 Bcl-x_L and thereby blocking its prosurvival functions, sensitizers efficiently lower the amount
343 of tBid necessary for MOMP competence. This may explain the effectiveness of sensitizer
344 BH3-mimetics in promoting apoptosis induction in cells that are addicted to prosurvival Bcl-2
345 family proteins, where the latter hold in check subthreshold amounts of activator BH3-only
346 proteins (54). Synergies between sensitizer and activator BH3-only proteins were also
347 described for various combination treatments for which signal transduction pathways
348 culminate at the level of Bcl-2 family members, resulting in improved apoptosis responses of
349 otherwise resistant tumors (55,56).

350 The Bcl-2 family interplay and the control of the MOMP decision have been the subject of
351 previous systems biological studies (57,58). However, the detail at which the interactions
352 were modeled varied greatly, and model development served different purposes. Additionally,
353 quantitative and time-resolved data, especially for the oligomerization processes of full-length
354 proteins in membrane environments, only recently became available by the use of biophysical
355 methods in *in vitro* systems (30).

356 In an early theoretical study, a cellular automaton as well as an ODE-based modeling
357 approach were employed to study robustness properties of Bax-induced MOMP. The positive
358 feedback of activator BH3-only proteins that are freed by binding of aBax to Bcl-2 was
359 identified to contribute substantially to a swift accumulation of active Bax molecules (60). At
360 the time of the study, experimental information on membrane recruitment, insertion and

361 kinetics of oligomerization of active Bax molecules were not available, but the simulations
362 nevertheless emphasized that non-linear causation is very likely an important driver of Bax
363 pore formation. An expansion of this modeling strategy, using a combined experimental and
364 mathematical approach, demonstrated that the amounts of mitochondrial Bax measured at
365 the time of MOMP would indeed be sufficient to allow higher order oligomers to form by lateral
366 aBax diffusion and aggregation, linking for the first time mitochondrial Bax amounts to pore
367 formation propensity and MOMP competence (61). However, whether switching between full
368 MOMP competency and resistance can be achieved by small changes in antiapoptotic family
369 members was outside of the scope of the study. The so far most sophisticated and detailed
370 model of the Bcl-2 family interplay successfully linked chemotherapy responsiveness to
371 calculated resistances to BH3-only stress doses in colorectal cancer (62). These resistances
372 were determined from the antiapoptotic thresholds that emerge from the interplay of
373 prosurvival and effector Bcl-2 family protein concentrations. Interestingly, a calculated
374 resistance to high stress doses correlated with a higher risk for disease recurrence in stage III
375 colorectal cancer patients that received adjuvant chemotherapy, indicating the potential of
376 mathematical models of protein interaction networks as innovative systems-based biomarkers
377 (62,63). Since we demonstrated that retrotranslocation of Bax and, by extension, possibly Bak
378 is crucial to strictly separate conditions of MOMP competency and resistance, it is tempting to
379 speculate that including information on steady-state dynamics and shuttling rates of Bcl-2
380 family members might improve the prognostic power of translationally relevant systems
381 models.

382

383

384 **Materials and Methods**

385 **Model Implementation**

386 The model was implemented as an ordinary differential equations (ODE)-based model in R
387 (version 3.3.2). Supplementary Material 1 (Supplementary Figure 2 and Supplementary
388 Tables 1-3) provides detailed information on all species, interactions and rate constants.
389 ODEs were integrated numerically using R's routine lsoda (package deSolve, version 1.13),
390 which provides an interface to the lsoda FORTRAN ODE solver, which switches automatically
391 between stiff and nonstiff methods.

392 **Parameter estimates, sampling procedure and model training**

393 Biologically plausible parameter ranges were chosen as described in Supplementary Material
394 1. Ensemble simulations were performed as part of model training, using the following
395 procedure. Biologically plausible parameter ranges were transformed to be \log_{10} uniformly
396 distributed in $[0,1]$ and parameters were sampled from these distributions. We discretized the
397 parameter space into a 20-level grid. Two hundred trajectories were sampled in parameter
398 space following a previously described procedure (64): In brief, for each trajectory a random
399 grid point was selected. From this point one parameter was changed (in- or decreased) at a
400 time by a value of $d=20/[2*(20-1)]$ until each parameter was changed exactly once. This
401 provides a trajectory through parameter space with $(n+1)$ sampling points, where n is the
402 number of parameters in the respective model used for the simulation. The choice of d as
403 $20/[2*(20-1)]$ (for a 20-level grid) ensured that all levels have equal probability of being
404 selected in the sampling strategy (64). This resulted in an ensemble size of $200*(n+1)$ model
405 parameterizations. A function written in R generating trajectories in parameter space is
406 provided as Supplementary Material 2.

407 For each output of interest (e.g. aBax [%]), dot plots of ensemble simulations were generated,
408 where each dot corresponds to one simulation. This allowed us to assess the influence of

409 each parameter on model outputs. Regions of the parameter space not providing outputs in
410 agreement with experimental training data were excluded. Restriction of parameter ranges,
411 simulation and analysis of dot plots in an iterative procedure lead to the parameter ranges of
412 the trained model (see also section on parameter ranges of the trained core and complete
413 model in Supplementary Material 1, Supplementary Figures 3-25).

414 **Simulations and Model Predictions**

415 Ensemble predictions were generated by sampling from parameter ranges of the trained
416 models as defined in Supplementary Table 1 (Supplementary Material 1). 20 trajectories in
417 parameter space were generated for simulations shown in Figures 2a, 5 and 6; 200
418 trajectories were generated for all other simulations. Associated protein amounts used as
419 model inputs are listed in Supplementary Table 2 (Supplementary Material 1). All results were
420 reproducible by independent resampling in parameter space.

421 **Testing for Synergy**

422 Dose response curves for tBid and sensitizer addition alone or in combination were generated
423 by evaluating the amounts of aBax₄ and aBax₆ at 2 h of modeled reaction time. A hill curve
424 was fitted to these data using R's built-in function nls (package stats, version 3.3.2, algorithm
425 'port'):

$$E = \frac{E_{\max} \cdot A^h}{A^h + EC_{50}^h} + I$$

426 With E = effect (Bax recruitment into tetrameric and hexameric pores), h = hill coefficient, E_{max}
427 = maximal effect, E₅₀ = halfmaximal effect, A = BH3-only concentration, I = baseline effect.

428 As described previously (65), the theoretical additive isobole was calculated from the hill
429 curves for tBid and sensitizer inputs:

$$b = EC_{50,tBid} - \frac{EC_{50,tBid}}{\left[\frac{E_{max,tBid}}{E_{max,sensitizer}} \left(1 + \frac{A_c^{h_{sensitizer}}}{a^{h_{sensitizer}}} \right) - 1 \right]^{\frac{1}{h_{tBid}}}}$$

430 With b = sensitizer [nM], a = tBid [nM], $E_{max,tBid}$ and $E_{max,sensitizer}$ = maximal effects achieved
 431 with tBid alone or sensitizer alone (including baseline effect), $EC_{50,tBid}$ = concentration of tBid
 432 alone that induced half of $E_{max,tBid}$, A_c = concentration of sensitizer that induced half of
 433 $E_{max,sensitizer}$, h_{tBid} and $h_{sensitizer}$ = hill coefficient of single treatments.

434 **Peptides and Proteins**

435 Hrk peptide H-LRSSAAQLTAARLKALGDELH-OH was ordered with > 95% purity from
 436 AnaSpec Inc (Fremont, CA).

437 Purification of cleaved Bid, Bax and Bcl-x_L was described by us previously (12)

438 **LUV permeabilization assay / Calcein release assay**

439 LUVs of a size of approximately 100 nm were prepared, composed of 80% phosphatidyl
 440 choline and 20% cardiolipin. The dried lipid mixture was dissolved in buffer (20 nM HEPES,
 441 pH7.4) and 80 mM calcein (fluorescein-bis-methyl-iminodiacetic acid at pH7.5) was entrapped
 442 in lipid vesicles at a self-quenching concentration, so that its release into the external medium
 443 is accompanied by an increase in fluorescence intensity. To form the vesicles, the solution
 444 with lipids at a final concentration of 4 mg ml⁻¹ was vortexed and passed through 5 cycles of
 445 freezing and thawing. The generated multilamellar vesicles were extruded >30 times with a
 446 100 nm membrane filter (Avestin). LUVs were incubated with Bid, Bax, Bcl-x_L and Hrk peptide
 447 at room temperature. The kinetics of calcein release were studied using a Tecan Infinite M200
 448 microplate reader (Tecan, Switzerland).

449 The percentage of release R was calculated from:

$$450 \quad R = (FS - F0) \div (Fmax - F0) \times 100$$

451 Where F_0 is the initial fluorescence of LUVs; F_{max} is the maximum fluorescence after final
452 addition of 5% TritonX-100; F_S is the equilibrium fluorescence following addition of Bcl-2
453 family proteins.

454

455 Supplementary information is available at Cell Death and Differentiation's website.

456

457 **References**

- 458 1. Roos WP, Thomas AD, Kaina B. DNA damage and the balance between survival and
459 death in cancer biology. *Nat Rev Cancer*. 2015 Dec 18;16(1):20–33.
- 460 2. Cory S, Roberts AW, Colman PM, Adams JM. Targeting BCL-2-like Proteins to Kill Cancer
461 Cells. *Trends Cancer*. 2016 Aug;2(8):443–60.
- 462 3. Czabotar PE, Lessene G, Strasser A, Adams JM. Control of apoptosis by the BCL-2
463 protein family: implications for physiology and therapy. *Nat Rev Mol Cell Biol*. 2013 Dec
464 20;15(1):49–63.
- 465 4. Luna-Vargas MPA, Chipuk JE. The deadly landscape of pro-apoptotic BCL-2 proteins in
466 the outer mitochondrial membrane. *FEBS J*. 2016 Jul;283(14):2676–89.
- 467 5. Lopez J, Tait SWG. Mitochondrial apoptosis: killing cancer using the enemy within. *Br J*
468 *Cancer*. 2015 Mar 5;112(6):957–62.
- 469 6. Goldstein JC, Waterhouse NJ, Juin P, Evan GI, Green DR. The coordinate release of
470 cytochrome c during apoptosis is rapid, complete and kinetically invariant. *Nat Cell Biol*.
471 2000 Mar;2(3):156–62.
- 472 7. Rehm M, Huber HJ, Hellwig CT, Anguissola S, Dussmann H, Prehn JHM. Dynamics of
473 outer mitochondrial membrane permeabilization during apoptosis. *Cell Death Differ*. 2009
474 Apr;16(4):613–23.
- 475 8. Opferman JT. Attacking cancer’s Achilles heel: antagonism of anti-apoptotic BCL-2 family
476 members. *FEBS J*. 2016 Jul;283(14):2661–75.
- 477 9. Hata AN, Engelman JA, Faber AC. The BCL2 Family: Key Mediators of the Apoptotic
478 Response to Targeted Anticancer Therapeutics. *Cancer Discov*. 2015 May 1;5(5):475–87.
- 479 10. García-Sáez AJ, Ries J, Orzáez M, Pérez-Payà E, Schwille P. Membrane promotes
480 tBID interaction with BCLXL. *Nat Struct Mol Biol*. 2009 Nov;16(11):1178–85.
- 481 11. Chi X, Kale J, Leber B, Andrews DW. Regulating cell death at, on, and in membranes.
482 *Biochim Biophys Acta BBA - Mol Cell Res*. 2014 Sep;1843(9):2100–13.
- 483 12. Bleicken S, Hantusch A, Das KK, Frickey T, Garcia-Saez AJ. Quantitative interactome
484 of a membrane Bcl-2 network identifies a hierarchy of complexes for apoptosis regulation.
485 *Nat Commun*. 2017 Jul 13;8(1):73.
- 486 13. Wang Y, Tjandra N. Structural Insights of tBid, the Caspase-8-activated Bid, and Its
487 BH3 Domain. *J Biol Chem*. 2013 Dec 13;288(50):35840–51.
- 488 14. Jeong S-Y, Gaume B, Lee Y-J, Hsu Y-T, Ryu S-W, Yoon S-H, et al. Bcl-xL sequesters
489 its C-terminal membrane anchor in soluble, cytosolic homodimers. *EMBO J*. 2004 May
490 19;23(10):2146–55.

- 491 15. Wilson-Annan J, O'Reilly LA, Crawford SA, Hausmann G, Beaumont JG, Parma LP, et
492 al. Proapoptotic BH3-only proteins trigger membrane integration of prosurvival Bcl-w and
493 neutralize its activity. *J Cell Biol.* 2003 Sep 1;162(5):877–88.
- 494 16. Wilfling F, Weber A, Potthoff S, Vögtle F-N, Meisinger C, Paschen SA, et al. BH3-only
495 proteins are tail-anchored in the outer mitochondrial membrane and can initiate the
496 activation of Bax. *Cell Death Differ.* 2012 Aug;19(8):1328–36.
- 497 17. Czabotar PE, Westphal D, Dewson G, Ma S, Hockings C, Fairlie WD, et al. Bax Crystal
498 Structures Reveal How BH3 Domains Activate Bax and Nucleate Its Oligomerization to
499 Induce Apoptosis. *Cell.* 2013 Jan;152(3):519–31.
- 500 18. Brouwer JM, Westphal D, Dewson G, Robin AY, Uren RT, Bartolo R, et al. Bak Core
501 and Latch Domains Separate during Activation, and Freed Core Domains Form
502 Symmetric Homodimers. *Mol Cell.* 2014 Sep;55(6):938–46.
- 503 19. Bogner C, Leber B, Andrews DW. Apoptosis: embedded in membranes. *Curr Opin Cell
504 Biol.* 2010 Dec;22(6):845–51.
- 505 20. Shamas-Din A, Bindner S, Chi X, Leber B, Andrews DW, Fradin C. Distinct lipid effects
506 on tBid and Bim activation of membrane permeabilization by pro-apoptotic Bax. *Biochem
507 J.* 2015 May 1;467(3):495–505.
- 508 21. Volkman N, Marassi FM, Newmeyer DD, Hanein D. The rheostat in the membrane:
509 BCL-2 family proteins and apoptosis. *Cell Death Differ.* 2014 Feb;21(2):206–15.
- 510 22. Edlich F, Banerjee S, Suzuki M, Cleland MM, Arnoult D, Wang C, et al. Bcl-xL
511 Retrotranslocates Bax from the Mitochondria into the Cytosol. *Cell.* 2011 Apr;145(1):104–
512 16.
- 513 23. Schellenberg B, Wang P, Keeble JA, Rodriguez-Enriquez R, Walker S, Owens TW, et
514 al. Bax Exists in a Dynamic Equilibrium between the Cytosol and Mitochondria to Control
515 Apoptotic Priming. *Mol Cell.* 2013 Mar;49(5):959–71.
- 516 24. Todt F, Cakir Z, Reichenbach F, Emschermann F, Lauterwasser J, Kaiser A, et al.
517 Differential retrotranslocation of mitochondrial Bax and Bak. *EMBO J.* 2015 Jan
518 2;34(1):67–80.
- 519 25. Todt F, Cakir Z, Reichenbach F, Youle RJ, Edlich F. The C-terminal helix of Bcl-xL
520 mediates Bax retrotranslocation from the mitochondria. *Cell Death Differ.* 2013
521 Feb;20(2):333–42.
- 522 26. Lovell JF, Billen LP, Bindner S, Shamas-Din A, Fradin C, Leber B, et al. Membrane
523 Binding by tBid Initiates an Ordered Series of Events Culminating in Membrane
524 Permeabilization by Bax. *Cell.* 2008 Dec;135(6):1074–84.
- 525 27. Gavathiotis E, Reyna DE, Davis ML, Bird GH, Walensky LD. BH3-Triggered Structural
526 Reorganization Drives the Activation of Proapoptotic BAX. *Mol Cell.* 2010 Nov;40(3):481–
527 92.

- 528 28. Tan C, Dlugosz PJ, Peng J, Zhang Z, Lapolla SM, Plafker SM, et al. Auto-activation of
529 the Apoptosis Protein Bax Increases Mitochondrial Membrane Permeability and Is
530 Inhibited by Bcl-2. *J Biol Chem*. 2006 May 26;281(21):14764–75.
- 531 29. Valentijn AJ, Upton J-P, Bates N, Gilmore AP. Bax targeting to mitochondria occurs via
532 both tail anchor-dependent and -independent mechanisms. *Cell Death Differ*. 2008
533 Aug;15(8):1243–54.
- 534 30. Subburaj Y, Cosentino K, Axmann M, Pedrueza-Villalmanzo E, Hermann E, Bleicken
535 S, et al. Bax monomers form dimer units in the membrane that further self-assemble into
536 multiple oligomeric species. *Nat Commun*. 2015 Aug 14;6:8042.
- 537 31. Saito M, Korsmeyer SJ, Schlesinger PH. BAX-dependent transport of cytochrome c
538 reconstituted in pure liposomes. *Nat Cell Biol*. 2000 Aug;2(8):553–5.
- 539 32. Xu X-P, Zhai D, Kim E, Swift M, Reed JC, Volkman N, et al. Three-dimensional
540 structure of Bax-mediated pores in membrane bilayers. *Cell Death Dis*. 2013
541 Jun;4(6):e683.
- 542 33. Ding J, Mooers BHM, Zhang Z, Kale J, Falcone D, McNichol J, et al. After Embedding
543 in Membranes Antiapoptotic Bcl-XL Protein Binds Both Bcl-2 Homology Region 3 and
544 Helix 1 of Proapoptotic Bax Protein to Inhibit Apoptotic Mitochondrial Permeabilization. *J*
545 *Biol Chem*. 2014 Apr 25;289(17):11873–96.
- 546 34. Zhou H, Hou Q, Chai Y, Hsu Y. Distinct domains of Bcl-X are involved in Bax and Bad
547 antagonism and in apoptosis inhibition. *Exp Cell Res*. 2005 Oct 1;309(2):316–28.
- 548 35. Bleicken S, Wagner C, García-Sáez AJ. Mechanistic Differences in the Membrane
549 Activity of Bax and Bcl-xL Correlate with Their Opposing Roles in Apoptosis. *Biophys J*.
550 2013 Jan;104(2):421–31.
- 551 36. Billen LP, Kokoski CL, Lovell JF, Leber B, Andrews DW. Bcl-XL Inhibits Membrane
552 Permeabilization by Competing with Bax. Walter P, editor. *PLoS Biol*. 2008 Jun
553 10;6(6):e147.
- 554 37. Hoppo L, Strasser A, Cory S. BH3-only proteins in apoptosis at a glance. *J Cell Sci*.
555 2012 Mar 1;125(Pt 5):1081–7.
- 556 38. Das KK, Shalaby R, García-Sáez AJ. Determinants of BH3 Sequence Specificity for
557 the Disruption of Bcl-xL/cBid Complexes in Membranes. *ACS Chem Biol*. 2017 Apr
558 21;12(4):989–1000.
- 559 39. Kuwana T, Bouchier-Hayes L, Chipuk JE, Bonzon C, Sullivan BA, Green DR, et al.
560 BH3 domains of BH3-only proteins differentially regulate Bax-mediated mitochondrial
561 membrane permeabilization both directly and indirectly. *Mol Cell*. 2005 Feb 18;17(4):525–
562 35.
- 563 40. Oh KJ, Barbuto S, Pitter K, Morash J, Walensky LD, Korsmeyer SJ. A Membrane-
564 targeted BID BCL-2 Homology 3 Peptide Is Sufficient for High Potency Activation of BAX
565 *in Vitro*. *J Biol Chem*. 2006 Dec 1;281(48):36999–7008.

- 566 41. Ichim G, Lopez J, Ahmed SU, Muthalagu N, Giampazolias E, Delgado ME, et al.
567 Limited Mitochondrial Permeabilization Causes DNA Damage and Genomic Instability in
568 the Absence of Cell Death. *Mol Cell*. 2015 Mar;57(5):860–72.
- 569 42. Oltval ZN, Milliman CL, Korsmeyer SJ. Bcl-2 heterodimerizes in vivo with a conserved
570 homolog, Bax, that accelerates programmed cell death. *Cell*. 1993 Aug;74(4):609–19.
- 571 43. Boise LH, González-García M, Postema CE, Ding L, Lindsten T, Turka LA, et al. bcl-x,
572 a bcl-2-related gene that functions as a dominant regulator of apoptotic cell death. *Cell*.
573 1993 Aug;74(4):597–608.
- 574 44. Renault TT, Tejjido O, Missire F, Ganesan YT, Velours G, Arokium H, et al. Bcl-xL
575 stimulates Bax relocation to mitochondria and primes cells to ABT-737. *Int J Biochem Cell*
576 *Biol*. 2015 Jul;64:136–46.
- 577 45. Lauterwasser J, Todt F, Zerbes RM, Nguyen TN, Craigen W, Lazarou M, et al. The
578 porin VDAC2 is the mitochondrial platform for Bax retrotranslocation. *Sci Rep*. 2016 Sep
579 13;6:32994.
- 580 46. Grijalba MT, Vercesi AE, Schreier S. Ca²⁺-Induced Increased Lipid Packing and
581 Domain Formation in Submitochondrial Particles. A Possible Early Step in the Mechanism
582 of Ca²⁺-Stimulated Generation of Reactive Oxygen Species by the Respiratory Chain[†].
583 *Biochemistry (Mosc)*. 1999 Oct;38(40):13279–87.
- 584 47. Csordás G, Várnai P, Golenár T, Roy S, Purkins G, Schneider TG, et al. Imaging
585 Interorganelle Contacts and Local Calcium Dynamics at the ER-Mitochondrial Interface.
586 *Mol Cell*. 2010 Jul;39(1):121–32.
- 587 48. Cosentino K, García-Sáez AJ. Mitochondrial alterations in apoptosis. *Chem Phys*
588 *Lipids*. 2014 Jul;181:62–75.
- 589 49. Kuwana T, Mackey MR, Perkins G, Ellisman MH, Latterich M, Schneider R, et al. Bid,
590 Bax, and lipids cooperate to form supramolecular openings in the outer mitochondrial
591 membrane. *Cell*. 2002 Nov 1;111(3):331–42.
- 592 50. Gonzalez F, Pariselli F, Dupaigne P, Budihardjo I, Lutter M, Antonsson B, et al. tBid
593 interaction with cardiolipin primarily orchestrates mitochondrial dysfunctions and
594 subsequently activates Bax and Bak. *Cell Death Differ*. 2005 Jun;12(6):614–26.
- 595 51. Arokium H, Ouerfelli H, Velours G, Camougrand N, Vallette FM, Manon S.
596 Substitutions of Potentially Phosphorylatable Serine Residues of Bax Reveal How They
597 May Regulate Its Interaction with Mitochondria. *J Biol Chem*. 2007 Nov
598 30;282(48):35104–12.
- 599 52. Wang Q, Sun S-Y, Khuri F, Curran WJ, Deng X. Mono- or Double-Site Phosphorylation
600 Distinctly Regulates the Proapoptotic Function of Bax. Hooker B, editor. *PLoS ONE*. 2010
601 Oct 14;5(10):e13393.

- 602 53. O'Neill KL, Huang K, Zhang J, Chen Y, Luo X. Inactivation of prosurvival Bcl-2 proteins
603 activates Bax/Bak through the outer mitochondrial membrane. *Genes Dev.* 2016 Apr
604 15;30(8):973–88.
- 605 54. Sarosiek KA, Letai A. Directly targeting the mitochondrial pathway of apoptosis for
606 cancer therapy using BH3 mimetics - recent successes, current challenges and future
607 promise. *FEBS J.* 2016 Oct;283(19):3523–33.
- 608 55. Schneider-Jakob S, Corazza N, Badmann A, Sidler D, Stuber-Roos R, Keogh A, et al.
609 Synergistic induction of cell death in liver tumor cells by TRAIL and chemotherapeutic
610 drugs via the BH3-only proteins Bim and Bid. *Cell Death Dis.* 2010 Oct;1(10):e86.
- 611 56. Inoue-Yamauchi A, Jeng PS, Kim K, Chen H-C, Han S, Ganesan YT, et al. Targeting
612 the differential addiction to anti-apoptotic BCL-2 family for cancer therapy. *Nat Commun.*
613 2017 Jul 17;8:16078.
- 614 57. Würstle ML, Zink E, Prehn JHM, Rehm M. From computational modelling of the
615 intrinsic apoptosis pathway to a systems-based analysis of chemotherapy resistance:
616 achievements, perspectives and challenges in systems medicine. *Cell Death Dis.*
617 2014;5:e1258.
- 618 58. Huber HJ, Duesmann H, Wenus J, Kilbride SM, Prehn JHM. Mathematical modelling
619 of the mitochondrial apoptosis pathway. *Biochim Biophys Acta BBA - Mol Cell Res.* 2011
620 Apr;1813(4):608–15.
- 621 59. Kueh HY, Zhu Y, Shi J. A simplified Bcl-2 network model reveals quantitative
622 determinants of cell-to-cell variation in sensitivity to anti-mitotic chemotherapeutics. *Sci*
623 *Rep.* 2016 Nov 4;6:36585.
- 624 60. Chen C, Cui J, Lu H, Wang R, Zhang S, Shen P. Modeling of the Role of a Bax-
625 Activation Switch in the Mitochondrial Apoptosis Decision. *Biophys J.* 2007
626 Jun;92(12):4304–15.
- 627 61. Düssmann H, Rehm M, Concannon CG, Anguissola S, Würstle M, Kacmar S, et al.
628 Single-cell quantification of Bax activation and mathematical modelling suggest pore
629 formation on minimal mitochondrial Bax accumulation. *Cell Death Differ.* 2010
630 Feb;17(2):278–90.
- 631 62. Lindner AU, Concannon CG, Boukes GJ, Cannon MD, Llambi F, Ryan D, et al.
632 Systems analysis of BCL2 protein family interactions establishes a model to predict
633 responses to chemotherapy. *Cancer Res.* 2013 Jan 15;73(2):519–28.
- 634 63. Lindner AU, Salvucci M, Morgan C, Monsefi N, Resler AJ, Cremona M, et al. BCL-2
635 system analysis identifies high-risk colorectal cancer patients. *Gut.* 2016 Sep 23;
- 636 64. Saltelli A, editor. *Global sensitivity analysis: the primer.* Chichester, England ; Hoboken,
637 NJ: John Wiley; 2008. 292 p.
- 638 65. Grabovsky Y. Isobolographic Analysis for Combinations of a Full and Partial Agonist:
639 Curved Isoboles. *J Pharmacol Exp Ther.* 2004 May 6;310(3):981–6.

640

641 **Figure Legends**

642

643 **Figure 1. Molecular mechanisms of the tBid-Bax interplay and Bax pore formation**

644 **captured in the core mathematical model. a**, Signaling processes providing active Bax

645 species. Cytosolic Bax in its inactive conformation can be integrated into the membrane and

646 activated either by interaction with tBid or with active Bax molecules (aBax) that already

647 reside in the membrane. These processes were implemented as two-step reversible

648 mechanisms, taking into account intermediate Bax species that are attached to but not yet

649 fully integrated into the membrane. **b**, Bax oligomerization and pore formation. Dimers of

650 aBax were implemented to form higher order oligomers (tetramers, hexamers). Tetramers

651 and hexamers were considered as a minimum requirement for pore formation.

652

653 **Figure 2. Ensemble simulations accurately reproduce tBid-induced Bax**

654 **oligomerization kinetics and reliably predict Bax autoactivation. a**, Rapid oligomerization

655 of Bax. Oligomerization kinetics are shown for an ensemble of 340 individual simulations. The

656 mean kinetic is shown in blue. Input protein concentrations were 2.5 nM Bax and 5 nM tBid

657 (30). **b**, Distribution of tBid-induced Bax oligomeric species obtained from the trained model at

658 1 and 60 min. Data are shown as mean and SD of the ensemble simulations. Quantitative

659 experimental data were estimated from (30) and are shown for comparison. **c**, Distribution of

660 Bax oligomeric species obtained by autoactivation. Model predictions are shown for inputs of

661 10% and 20% aBax. Experimental data as estimated from (30) are shown for comparison and

662 validation of predictions. Experimentally valid observations were assumed to be within the

663 shown errorbars. Data are shown as means and SD.

664

665 **Figure 3. Retrotranslocation of Bax by Bcl-x_L is required to significantly impair Bax**
666 **oligomerization.** **a**, Model extension by Bcl-x_L. Bcl-x_L exerts its prosurvival function by
667 binding to tBid as well as to active Bax monomers. The extension of the model by Bcl-x_L was
668 implemented in two variants, including the retrotranslocation of mitochondrial Bax into the
669 cytosol (black box) or not. **b**, Experimental conditions for studying the influence of Bcl-x_L on
670 Bax oligomerization, as described in (30). This scenario served as the reference for *in silico*
671 studies. **c**, Experimentally measured Bax oligomer distribution in presence of Bcl-x_L, as
672 estimated from (30). Experimentally valid observations were assumed to be within the shown
673 errorbars. **d**, Bax oligomer distribution obtained from the model without Bcl-x_L
674 retrotranslocation activity. Model predictions and additional model fitting approaches failed to
675 replicate experimental data shown in c. Shown are simulation assuming rapid binding of Bcl-
676 x_L to aBax and high affinity of the resulting complex (k_{on} 10 nM⁻¹s⁻¹, K_D 0.1 nM). **e**, Bax
677 oligomer distribution obtained from the trained model with Bcl-x_L retrotranslocation activity.
678 Experimental data shown in c can be reproduced. Data are shown as means and SD of
679 ensemble simulations.

680

681 **Figure 4. Systems modeling can accurately predict Bax membrane recruitment when**
682 **taking Bax retrotranslocation activity of Bcl-x_L into account.** **a**, Definition of Bax
683 membrane recruitment. As readout for Bax membrane recruitment, all Bax containing species
684 residing at or in the membrane were considered (ΣBax_M). **b**, In the mathematical model
685 lacking retrotranslocation activity, Bax translocation to membranes cannot be prevented. **c,d**
686 The mathematical model including retrotranslocation activity of Bcl-x_L accurately predicts tBid-
687 induced ΣBax_M at different concentrations of Bcl-x_L (c) when compared to the experimental
688 data estimated from (36) (d). **e,f** Model predictions for conditions in which a tBid variant was

689 implemented that cannot bind to Bcl-x_L. Predictions (e) correspond to trends observed
690 experimentally as estimated from (36) (f). Data are shown as means and SD from ensemble
691 simulations or experimental data estimated from (36), where experimental valid observations
692 were assumed to be within the shown errorbars.

693

694 **Figure 5. Mathematical modeling reliably predicts activator/sensitizer BH3-only**

695 **synergies. a**, Model extension for inclusion of BH3-only sensitizer. The sensitizer was

696 implemented to reversibly bind Bcl-x_L, with kinetics identical to tBid. **b**, Bax oligomerization

697 predictions in response to sensitizer or tBid. Starting conditions were 45 nM Bax, 5 nM aBax

698 and 20 nM Bcl-x_L. Vertical grey dashed lines indicate EC₅₀ concentrations. **c**, Experimental

699 validation of model predictions. Dose response curves of calcein release from large

700 unilamellar vesicles after incubation with 50 nM Bax, 20 nM Bcl-x_L and varying amounts of

701 Hrk peptide or cBid (cleaved Bid, consisting of tBid and a p7 fragment). **d**, Isobologram of

702 simulations with combined tBid and sensitizer addition. Black dots correspond to EC₅₀ Bax

703 oligomerization. The additive isobole (blue) was calculated from data shown in b (see

704 methods for details). **e**, Prediction of Bax oligomerization for single or combined addition of

705 tBid and sensitizer, when added to a system of 20 nM Bcl-x_L, 45 nM Bax and 5 nM aBax. **f**

706 Experimental validation of model predictions. Bax pore formation was experimentally

707 determined by release of calcein from large unilamellar vesicles. LUVs were incubated with

708 20 nM Bcl-x_L, 50 nM Bax, and cBid and/or Hrk peptide as indicated. Data are shown as

709 means and SD of ensemble simulations or experimental data.

710

711 **Figure 6. Retrotranslocation activity of Bcl-x_L is essential to strictly separate**

712 **conditions of MOMP competency and resistance.** Simulations of Bax oligomerization into

713 pores (MOMP competency) in relation to increasing amounts of Bcl-x_L. Simulations are

714 performed for 50 nM bax and 10 nM tBid (**a**) or 10 nM tBid plus 50 nM sensitizer (**b**). The
715 negative hill curve was fitted to simulated data points to determine IC_{50} values (see methods
716 for details). Blue lines refer to results from the model variant including retrotranslocation
717 activity of Bcl-x_L. Data are shown as means and SD of ensemble simulations.

718

719 **Figure 7. Flow chart providing an overview of model training, successful predictions**
720 **and experimental validation.**

721

722 **Acknowledgements**

723 This work was funded by the Deutsche Forschungsgemeinschaft (DFG) within the FOR2036
724 initiative “New insights into Bcl-2 family interactions” (BR 3369/5-2 to TB, 1641/2-2 to AJGS,
725 MO 3226/1-1 to MR). AJGS was additionally supported by the European Research Council
726 (ERC grant n306699). KKD was supported by a scholarship from the IMPRS Program. AH
727 was supported by Konstanz Research School Chemical Biology. Work in the group of MR is
728 additionally supported by the EC Horizon 2020 program (GA 642295, GA 675448).

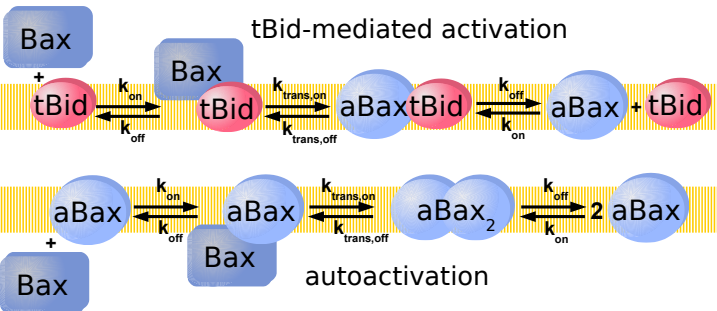
729

730 **Conflict of Interest**

731 The authors declare no conflict of interest.

Figure 1

a



b

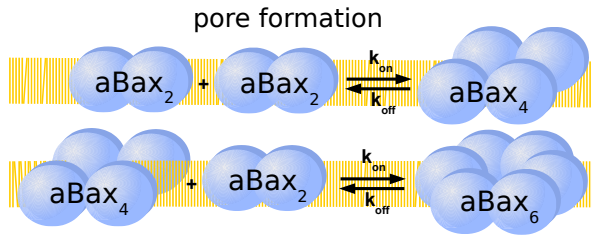


Figure 2

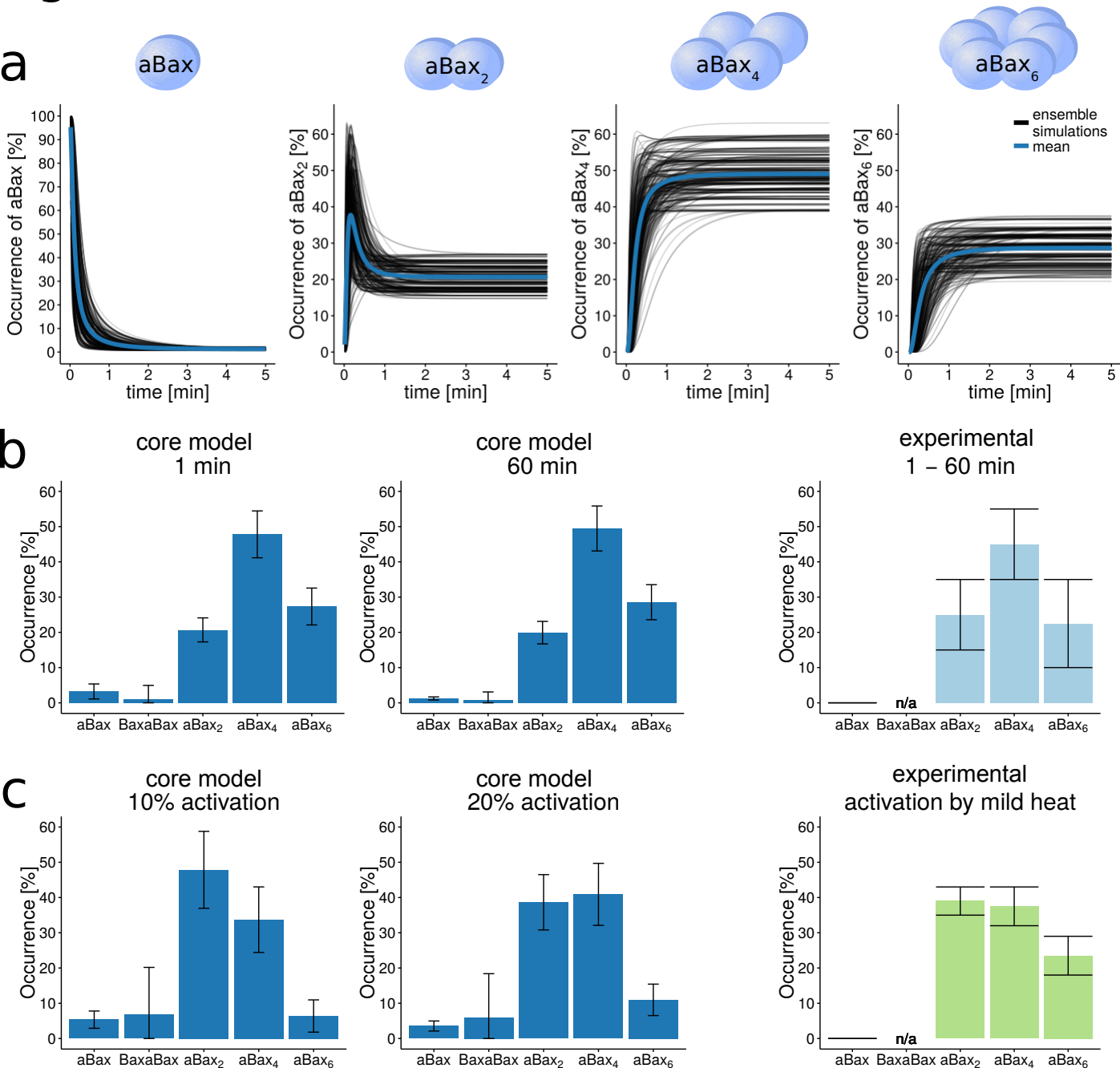


Figure 3

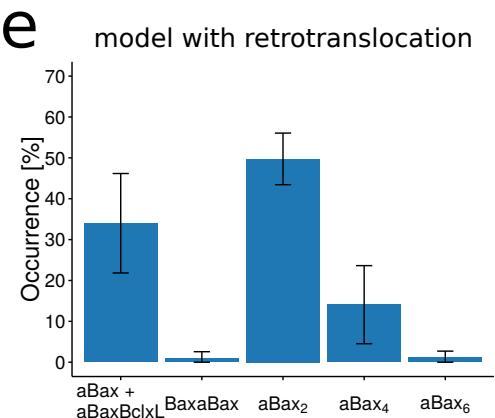
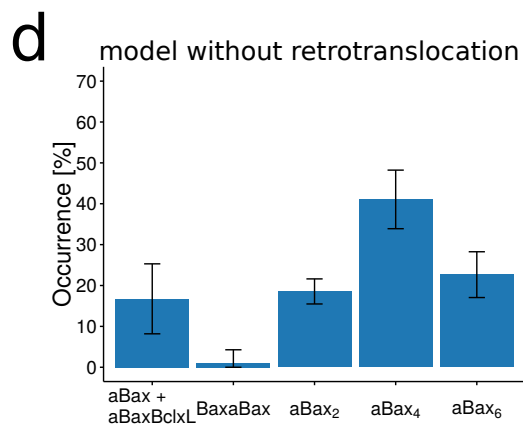
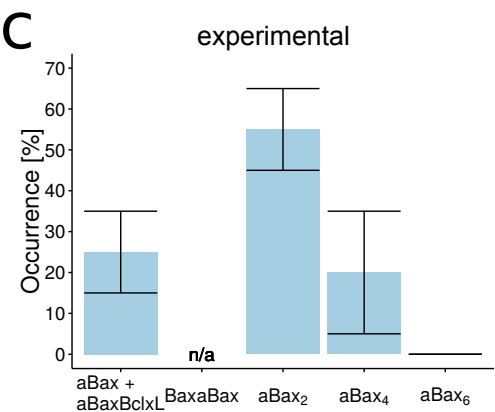
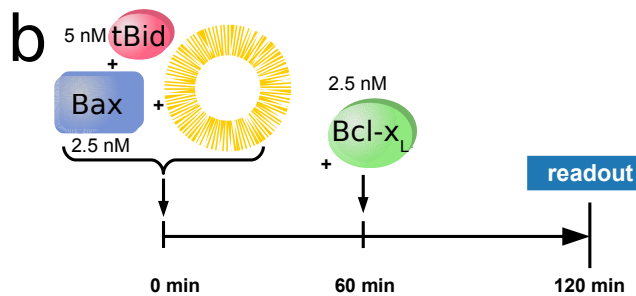
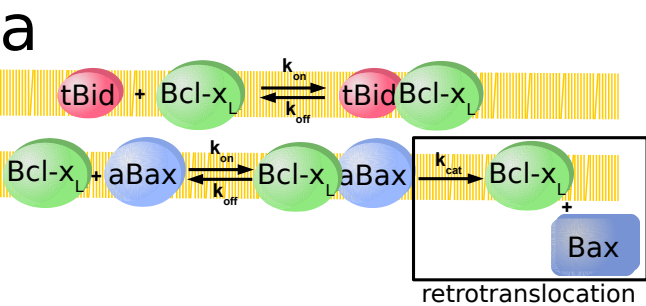
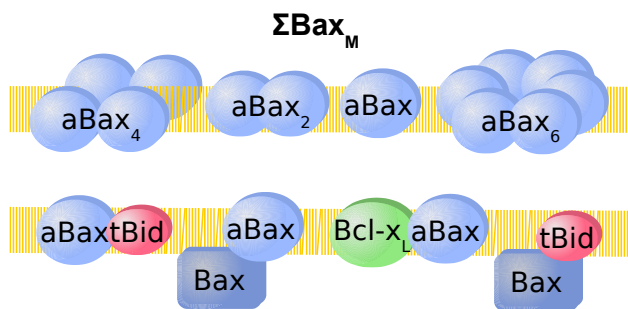


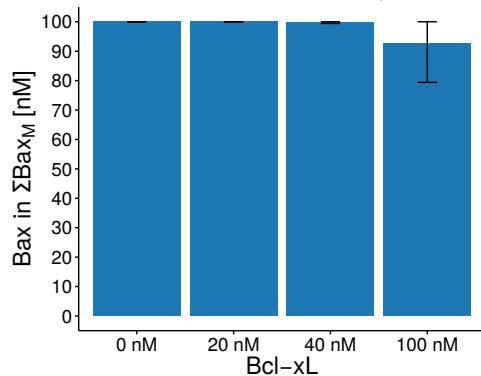
Figure 4

a



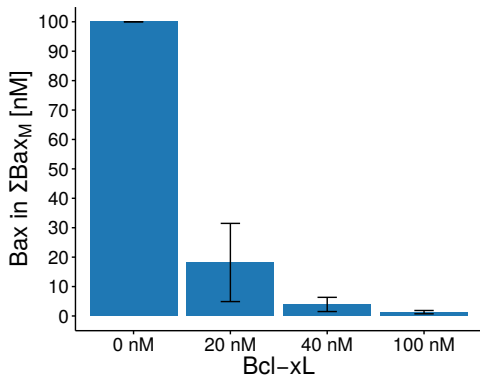
b

model without retrotranslocation
100 nM Bax + 20 nM tBid (120 min)



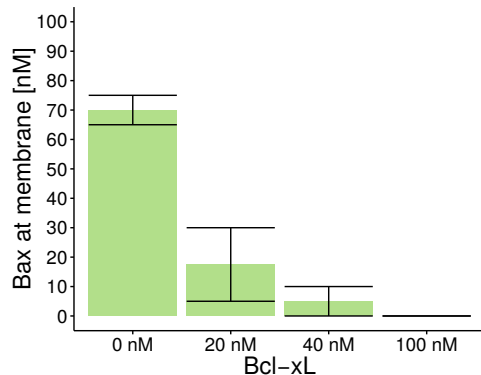
c

model with retrotranslocation
100 nM Bax + 20 nM tBid (120 min)



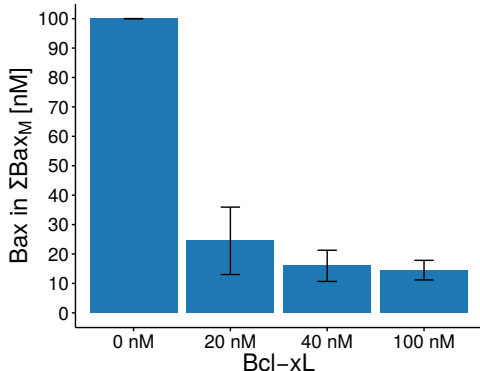
d

experimental



e

model with retrotranslocation
100 nM Bax + 20 nM tBid-*mt1* (120 min)



f

experimental

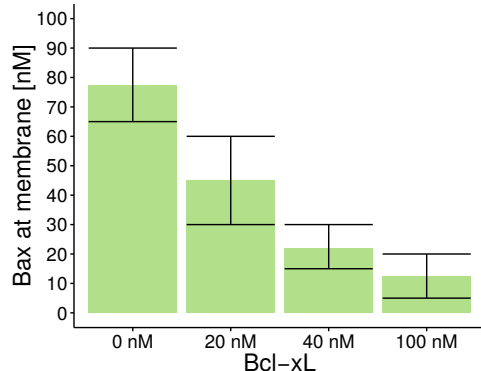
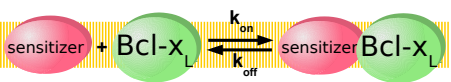
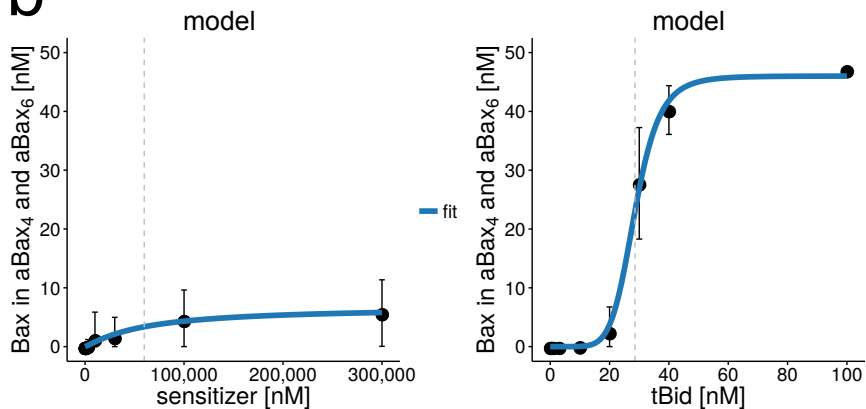


Figure 5

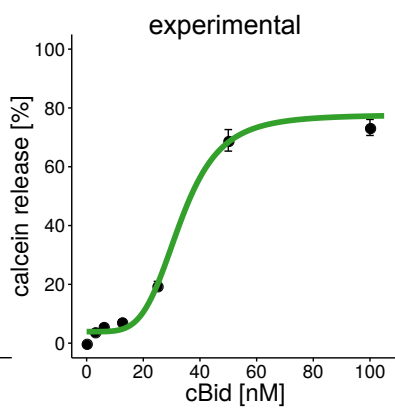
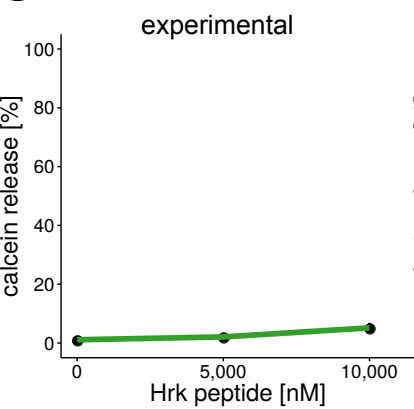
a



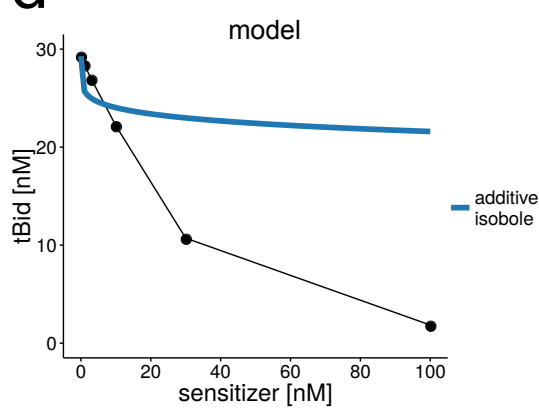
b



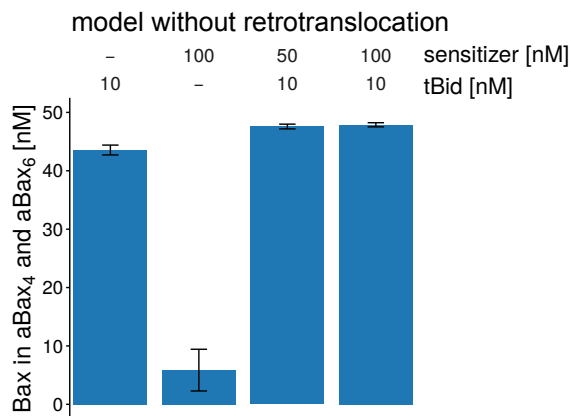
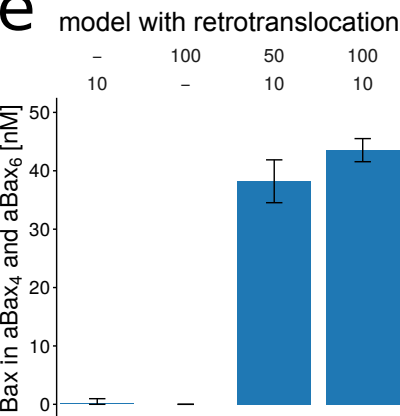
c



d



e



f

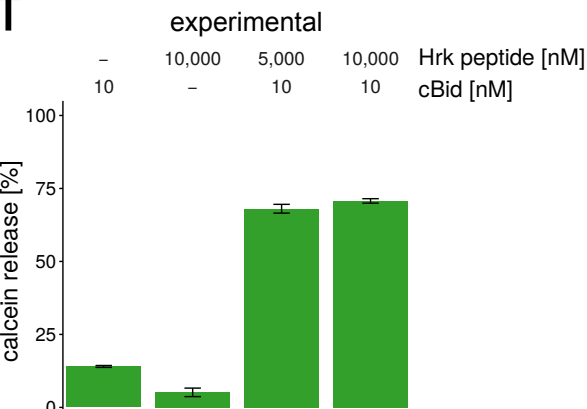
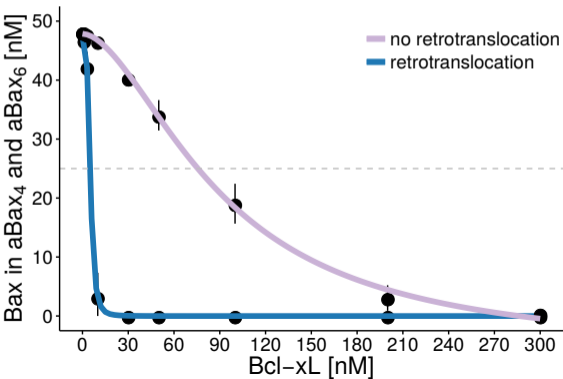


Figure 6

a

model with 10 nM tBid

**b**

model with 10 nM tBid + 50 nM sensitizer

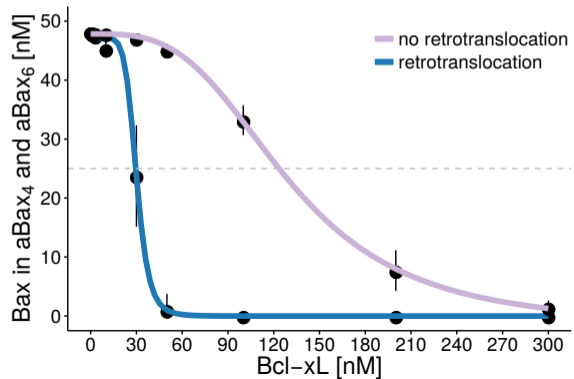
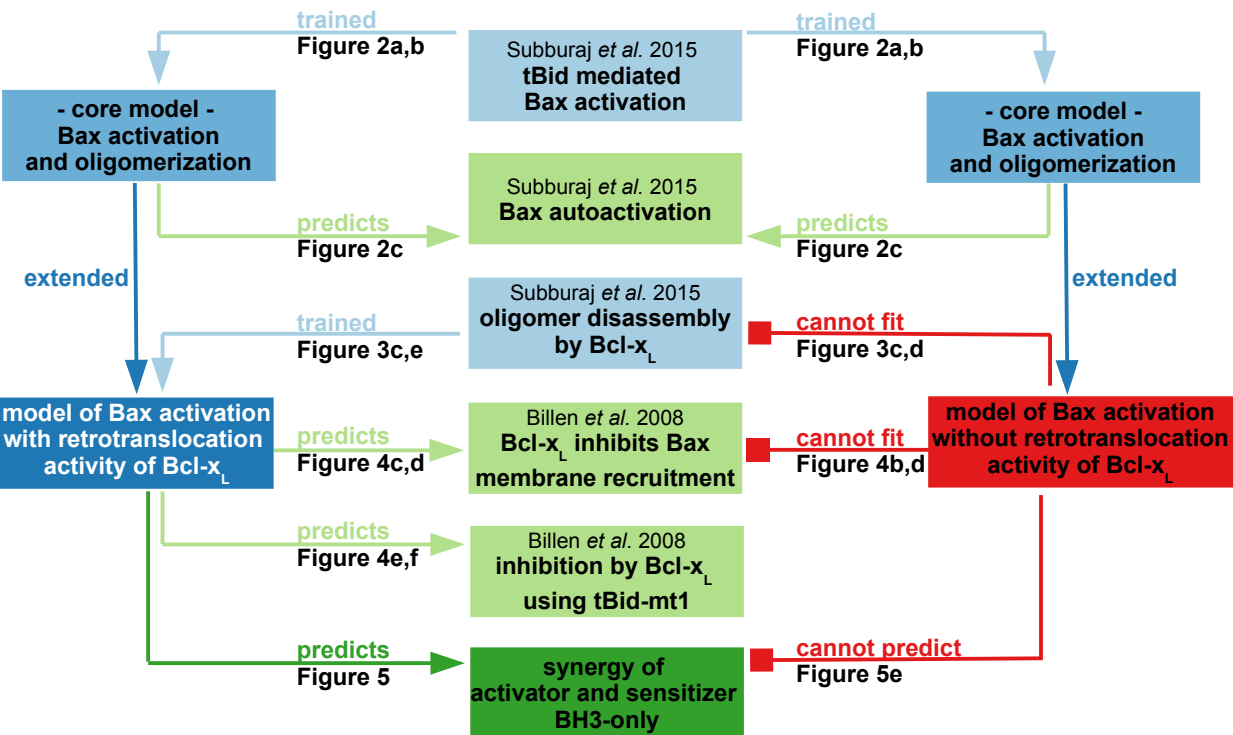


Figure 7



■ model of tBid and Bax
■ model of tBid, Bax and Bcl-x_L
■ model of tBid, Bax and Bcl-x_L
 without retrotranslocation

■ published experimental data
■ predicted published experimental data
■ predicted experimental data

The membrane activity of BOK involves formation of large, stable toroidal pores and is promoted by cBID

Yuniel Fernández-Marrero¹, Stephanie Bleicken^{2,†}, Kushal Kumar Das², Daniel Bachmann¹, Thomas Kaufmann^{1,‡}  and Ana J. Garcia-Saez^{2,‡}

¹ Institute of Pharmacology, University of Bern, Switzerland

² Interfaculty Institute of Biochemistry, University of Tübingen, Germany

Keywords

apoptosis; BOK; liposome; mitochondria; pore

Correspondence

A. J. Garcia-Saez, Interfaculty Institute of Biochemistry, University of Tübingen, 72076 Tübingen, Germany

Fax: +49 7071 29 5070

Tel: +49 7071 29 73318

E-mail: ana.garcia@uni-tuebingen.de and

T. Kaufmann, Institute of Pharmacology, University of Bern, Inselspital, INO-F, CH-3010 Bern, Switzerland

Fax: +41 31 632 49 92

Tel: +41 31 632 32 89

E-mail: thomas.kaufmann@pki.unibe.ch

†Present address

Zentrum für molekulare Spektroskopie und Simulation Solvensgesteuerter Prozesse, Ruhr-Universität Bochum, Bochum, Germany

‡Both authors contributed equally to this work

(Received 14 September 2016, revised 19 December 2016, accepted 6 January 2017)

doi:10.1111/febs.14008

The BCL-2 family members are key regulators of the intrinsic apoptotic pathway, which is defined by permeabilization of the mitochondrial outer membrane by members of the BAX-like subfamily. BOK is classified as a BAX-like protein; however, its (patho-)physiological role remains largely unclear. We therefore assessed the membrane permeabilization potential of C-terminally truncated recombinant BOK, BOK^{ΔC}. We show that BOK^{ΔC} can permeabilize liposomes mimicking the composition of mitochondrial outer membrane, but not of endoplasmic reticulum, forming large and stable pores over time. Importantly, pore formation was enhanced by the presence of cBID and refractory to the addition of antiapoptotic BCL-X_L. However, isolated mitochondria from *Bax*^{-/-}*Bak*^{-/-} cells were resistant to BOK-induced cytochrome *c* release, even in the presence of cBID. Taken together, we show that BOK^{ΔC} can permeabilize liposomes, and cooperate with cBID, but its role in directly mediating mitochondrial permeabilization is unclear and may underlie a yet to be determined negative regulation.

Abbreviations

AF488, AlexaFluor-488 dye; APC, allophycocyanin; Chol, cholesterol; CL, cardiolipin; cyt. *c*, cytochrome *c*; Dil, 1,1'-dioctadecyl-3,3,3',3'-tetramethylindocarbocyanine perchlorate; DPBS, Dulbecco's phosphate-buffered saline; ER, endoplasmic reticulum; GUV, giant unilamellar vesicles; LPC, lysophosphatidylcholine; LUV, large unilamellar vesicles; MEF, murine embryonic fibroblast; PA, phosphatidic acid; PC, phosphatidylcholine; PE, phosphatidylethanolamine; PG, phosphatidylglycerol; PI, L- α -phosphatidylinositol; PS, phosphatidylserine; Sph, sphingomyelin.

Introduction

The members of the BCL-2 family are critical regulators of the intrinsic apoptotic pathway, which is defined by mitochondrial outer membrane permeabilization (MOMP). The members of the family contain up to four short conserved BCL-2 homology domains (BH1-4) and are subdivided into the proapoptotic BH3-only proteins or the multi-BH domain members. The latter comprises the prosurvival BCL-2-like group (BCL-2, MCL-1, BCL-X_L, and BFL-1/A1) and the proapoptotic BAX-like group (BAX, BAK, and maybe BOK) [1].

Currently, it is accepted that in the absence of cellular stress these proteins coexist in a network of balanced interactions, neutralizing each other in their functions. Upon metabolic, pathogen- or damage-induced cellular stress, the network is altered resulting in apoptotic cell death or survival, depending on the magnitude of the insult. During apoptosis, MOMP is promoted by the oligomerization of BAX and/or BAK resulting in the release to the cytosol of apoptogenic proteins from the mitochondrial intermembrane space, including cytochrome *c* (cyt. *c*) and SMAC/DIABLO, with subsequent activation of caspases [2]. A prerequisite for MOMP is the disengagement of BAK from antiapoptotic MCL-1 and BCL-X_L, as well as recruitment of cytosolic BAX to the MOM [3]. A well-known factor aiding BAX translocation and mitochondrial pore formation is the p15 fragment of the BH3-only protein BID [4]. BID is proposed to interact transiently with BAX, promoting the conformational changes for BAX membrane insertion in a catalyst-like manner [4]. Importantly, the lipid composition of the membranes where these proteins exert their activities provides an extra layer of complexity [5,6]. Cardiolipin, a mitochondria-specific phospholipid, seems crucial for the concerted activity of cBID and BAX [7–10].

BCL-2-related ovarian killer (BOK, gene name *BOK* or *BCL2L9*) is a 23.4 kDa protein highly conserved in the animal kingdom, with sequence homology to BAK and BAX [11]. In contrast to BAX or BAK, BOK predominantly localizes to the membranes of the endoplasmic reticulum (ER) and the Golgi apparatus, and to a lesser extent to mitochondria [12]. BOK is widely expressed and readily detectable at protein level in mouse tissues, with high expression in reproductive tissues, brain, kidney, spleen, and gastrointestinal tract [12,13]. BOK function in cells is enigmatic. Although enforced expression of BOK induces apoptosis [11,12,14,15], genomic deletion of *Bok/Bak* or *Bok/Bax* did not produce an enhanced phenotype beyond that

accounted for *Bax* or *Bak* single knockout mice, with the exception of increased oocyte numbers in *Bok*^{-/-}*Bax*^{-/-} females [16]. Recent work from Ke *et al.* [17] on chimeric mice with a *Bok*^{-/-}*Bak*^{-/-}*Bax*^{-/-} triple knockout hematopoietic system provided evidence that BOK's redundancy with BAX and BAK exists but might be restricted to specific tissues. However, other studies suggest that depending on the tissue or the nature of the apoptotic stressor, BOK may have non-apoptotic functions, such as in trophoblast proliferation [18], or may even have a prosurvival function [12,19].

BOK has been shown to interact with IP3 receptors, protecting IP3Rs from caspase-mediated degradation and BOK from proteasomal degradation [20,21]. Degradation of BOK via the ubiquitin/proteasome was also shown by Llambi *et al.* [14] in the context of the ERAD pathway. This paper also describes a BAX-like apoptosis inducing function of BOK when the ERAD pathway is blocked [14].

In this work, we generated an untagged, C-terminally truncated version of recombinant BOK (BOK^{ΔC}), and characterized its pore-forming potential in liposomes and isolated mitochondria. BOK^{ΔC} provoked the permeabilization of artificial membranes by forming long-lived toroidal pores, large enough for passage of a 104 kDa protein. BOK^{ΔC}'s induced pore formation strongly depended on the lipid composition, with liposomes resembling MOM being much more efficiently permeabilized than those mimicking ER composition. Importantly, we provide solid evidence that cleaved BID (cBID) cooperates with BOK^{ΔC} in pore formation, while BCL-X_L was unable to inhibit BOK^{ΔC} activity. Strikingly, however, our studies on mitochondria isolated from *Bax*^{-/-}*Bak*^{-/-} cells indicated that BOK^{ΔC} is highly inefficient in promoting MOMP, even in the presence of cBID or after heat activation. Overall, these data suggest that despite its effects on artificial membranes, the role of BOK on biological membranes may be subject to yet to be described negative regulatory mechanisms.

Results

Purification of recombinant BOK^{ΔC}

BCL-2 proteins have been purified in the past by affinity-based methodologies using histidine or GST tag-based approaches. Tagged proteins come with the risk of introducing artifacts. One notable exception is the purification of full-length BAX and BCL-X_L in bacteria using an intein–chitin-binding domain fused to their C termini [22,23]. The intein domain can be

subsequently removed by addition of dithiothreitol, releasing the untagged protein with a high purity degree in one step. Based on these advantages, we decided to use the same approach to produce recombinant BOK and its C-terminally truncated form, BOK^{ΔC}. A major pitfall while establishing the purification workflow was the amount of contaminants present in the elution from the chitin-affinity step. One explanation would lie in the acidic nature of the *Escherichia coli* proteome [24,25] contrasting with the high isoelectric point (pI) of BOK, which seems unique among the multidomain members of the BCL-2 family (Fig. 1A), thus favoring the binding of unwanted proteins. To overcome this effect, we incorporated a cation-exchange step while working at high salt concentration and pH. This method has been reported to outperform those using Ni-NTA and GST for the purification of basic proteins [26]. The purified full-length BOK did not reach an acceptable purity and the total yield was extremely low, likely due to protein

aggregation because of its hydrophobic C-terminal tail. On the other hand, significantly higher amounts (300–700 μg protein from 5 L cultures) of pure (> 90%) BOK^{ΔC} could be purified, which is comparable to the purification of BAX (Fig. 1B–D). Therefore, we decided to work with BOK^{ΔC}. The identity of the purified protein was assessed using western blotting and mass spectrometry (Fig. 1C and data not shown).

BOK^{ΔC} induces membrane permeabilization of large unilamellar vesicles depending on the lipid composition

We hypothesized that BOK follows a similar mechanism of action as BAX and BAK when interacting with membranes. Thus, we explored the potential of recombinant BOK^{ΔC} to promote membrane permeabilization, by following content release of the fluorophore calcein (~ 1 kDa) from large unilamellar vesicles (LUVs). As BOK, under physiological

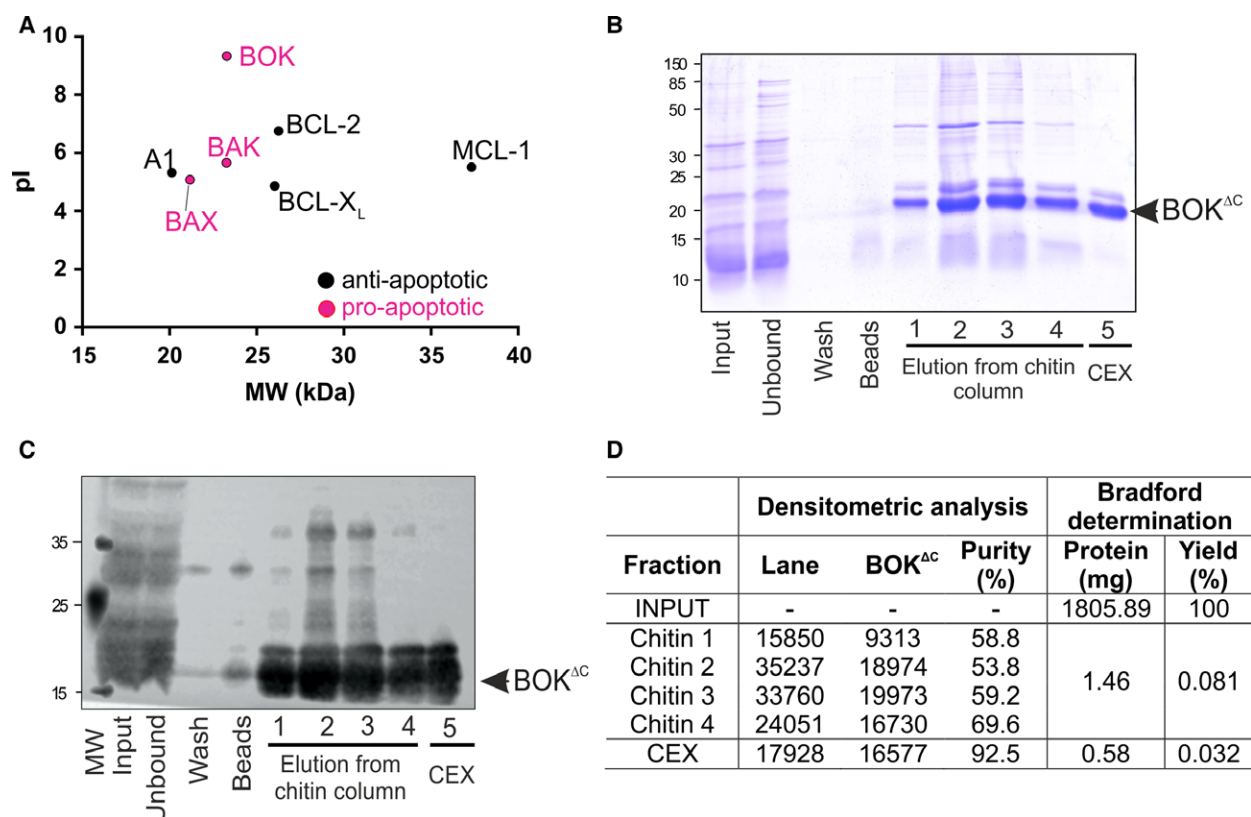


Fig. 1. Purification of recombinant BOK^{ΔC} using a two-step affinity-based strategy. (A) Predicted isoelectric point of multidomain BCL-2 family members (based on ExPASy Compute pI/Mw tool, http://web.expasy.org/compute_pi/). (B) Representative Coomassie-stained SDS/PAGE gel evaluating the purification process of recombinant BOK^{ΔC}. Beads: 10 μL of chitin beads after lysate input and before DTT-induced intein cleavage, CEX, cation affinity chromatography. (C) Immunoblot of the same samples from panel (B) using a rabbit monoclonal anti-BOK antibody. (D) Purification tables for a typical production of recombinant BOK^{ΔC}.

conditions, is largely localized to the membranes of the ER [12], we reasoned that BOK might differentially affect artificial membranes mimicking ER or MOM lipid composition. Indeed, LUVs made from a mitochondria-like lipid mixture (MITOmix) were readily permeabilized, in contrast to those resembling an ER lipid composition (ERmix), which required much higher protein concentrations to reach comparable permeabilization levels (Fig. 2A).

A major difference in those membrane model compositions was the presence of the mitochondria-specific lipid cardiolipin in MITOmix, while it was absent from ERmix. Hence, we decided to test the contribution of this lipid to the BOK^{ΔC}-induced calcein release. As shown in Fig. 2B, the CL content positively correlated with BOK^{ΔC}-induced calcein release from LUVs.

Cardiolipin is a negatively charged phospholipid inducing intrinsic monolayer curvature that has been suggested to play a specific role in BAX pore formation [8]. To find out whether this is also the case for BOK^{ΔC}, or whether it is a general charge effect, we substituted CL for phosphatidylglycerol (PG; Fig. 2B). When a similar proportion of PG was used in the assay, the dye release was similar, suggesting that the

overall negative charge of the membrane plays a role in the pore activity of BOK^{ΔC}.

The pores formed by BOK^{ΔC} show features of toroidal pores

Several lines of evidence suggest that BAX and BAK form toroidal pores, which involve the participation of lipids at the pore edge. Consequently, these pores would be affected by lipids modulating the intrinsic membrane curvature. The formation of nonlamellar structures, like toroidal pores, frequently requires the presence of lipids with opposite geometrical and intrinsic curvature properties to compensate the defective packaging in the pore rim [27]. To investigate the impact of the lipid geometry on BOK^{ΔC}-induced membrane permeabilization, we varied the concentrations of CL (cone, negative curvature inducer) and lysophosphatidylcholine (LPC; inverted cone, positive curvature inducer). Surprisingly, even small amounts of LPC enabled BOK^{ΔC}-mediated calcein release to a degree comparable to that obtained using 20% of CL (Fig. 2C). This effect was further enhanced when CL and LPC were combined in the same vesicles, in line

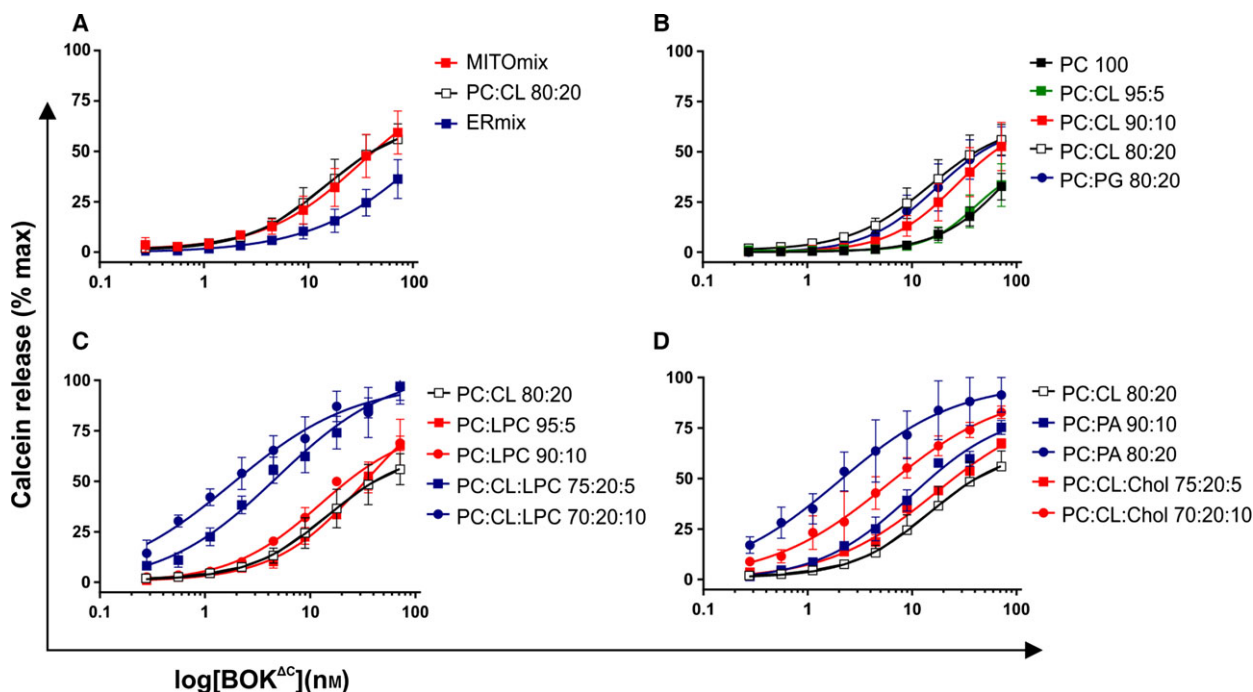


Fig. 2. The lipid composition modulates the permeabilization potential of BOK^{ΔC}. Several lipid mixtures were used to determine the influence on BOK^{ΔC}-mediated permeabilization of: (A) vesicles mimicking mitochondria (MITOmix) or endoplasmic reticulum (ERmix), (B) negatively charged lipids (CL), (C) positive curvature inducers (LPC) and (D) nonlamellar compatible lipids (PA) together with a neutral negative curvature inducer lipid (Chol). Lipid ratios are indicated for each composition as molar percentages. Calcein release was normalized to the maximum release induced by Triton-X100 on each sample. PC, phosphatidylcholine; CL, cardiolipin; PG, phosphatidylglycerol; LPC, lyso-phosphatidylcholine; PA, phosphatidic acid; Chol, cholesterol. Values correspond to mean \pm SEM; $N = 3$.

with the idea that BOK^{ΔC} could be involved in the formation of nonlamellar structures like toroidal pores. However, we could not discard the possibility that the role of CL was merely due to its negative curvature. To corroborate this, we included phosphatidic acid (PA) in our analysis, which is a lipid that combines negative charge and a very pronounced negative curvature. Indeed, from all the binary lipid mixtures tested, those containing PA exhibited the highest sensitivity to BOK^{ΔC} treatment (Fig. 2D). Additionally, we also used cholesterol, which is a neutral lipid with a high negative curvature; indeed, addition of cholesterol also increased BOK^{ΔC}-mediated dye release, although its impact was lower than that of LPC (Fig. 2D). These results demonstrate that BOK^{ΔC} membrane activity largely depends on the presence of negatively charged lipids and on their intrinsic curvature, suggesting that BOK^{ΔC} pores are of toroidal nature.

cBID cooperates with BOK^{ΔC} to form pores that allow the passage of the 104 kDa protein APC

Considering the concerted mechanism described for cBID to activate BAX to form pores in membranes [28], we tested if the membrane activity of BOK^{ΔC} would be modulated by cBID in a similar manner. As BOK^{ΔC} could permeabilize LUVs of several lipid compositions, we choose the MITOMix for these experiments due to its physiological relevance and positive, but still moderate, reactivity to BOK^{ΔC}.

We first determined the BOK^{ΔC} concentration that *per se* induced 50% of the maximum calcein release in the LUVs (7 nM, Fig. 3A), which was then used together with serial dilutions of cBID to test for synergy. Surprisingly, cBID, but not its BH3 peptide nor a BIM BH3 peptide, clearly exacerbated the calcein release activity of BOK^{ΔC} (Fig. 3B,C). Of note, cBID also clearly enhanced the calcein release activity of full-length BOK (Fig. 3B).

At this point, we hypothesized that, similar to BAX, BOK^{ΔC} could promote the trespassing of molecules bigger than calcein (> 1 kDa). To investigate the dimension of BOK^{ΔC}-mediated membrane pores, we used cell-sized vesicles known as giant unilamellar vesicles (GUV), composed of the MITOMix and a lipid dye to visualize the membrane. We incubated GUVs with two differently sized proteins: AlexaFluor-488-conjugated cytochrome *c* (cyt. *c*₄₈₈; 12 kDa) and allophycocyanin (APC; 104 kDa) and followed their passage through the membrane in the presence or absence of cBID, or cBID plus BCL-X_L. As positive and negative references, we used cBID and BAX in the presence or absence of BCL-X_L after incubation time of 60 min, as shown before [29,30].

Using the previous conditions in this membrane model, BOK^{ΔC} alone had negligible activity at 10 nM concentration, but the population of nonpermeabilized GUVs was significantly reduced in the samples treated with BOK^{ΔC} and cBID. This effect was comparable to the positive control, BAX plus cBID (Fig. 3D), and confirmed the cBID effect on BOK activity observed in the calcein assay. Interestingly, and contrasting with cBID/BAX, the permeabilization of GUVs by cBID/BOK^{ΔC} was not inhibited by BCL-X_L. Analysis of individual vesicles revealed that most were simultaneously filled with both dyes, indicating that the pores formed by BOK^{ΔC} plus cBID are permissive to molecules up to the size of 104 kDa (APC; Fig. 3E).

BOK^{ΔC}-induced membrane permeabilization can be accomplished by thermal activation

A simplistic but still efficient approach described by Pagliari *et al.* [31] used thermal activation of BAX and BAK to promote cyt. *c* release from isolated mitochondria. A similar strategy has also been used to induce BAX oligomerization and pore formation on GUVs [29] and LUVs [32]. After the robust permeabilization induced by BOK^{ΔC} alone, we investigated the energetic threshold of this effect.

We coincubated BOK^{ΔC} or BAX with MITOMix-derived GUVs for 45 min at 42 °C and evaluated the permeabilization to cyt. *c*₄₈₈ and APC. As shown in Fig. 4A, heat-activated BOK (as well as BAX) facilitated the passage of both permeabilization tracers into GUVs, indicating that cBID is not necessary for BOK^{ΔC} to form pores capable of accommodating a wide range of molecular sizes (Fig. 4A,B) and that also in this aspect BOK activity is similar to BAX.

BOK^{ΔC} forms long-lived pores

After establishing the GUV permeabilization potential by BOK^{ΔC}, we tested if BOK^{ΔC} pores were transient and unstable structures or if they remained stably open under equilibrium conditions. To address this question, we used an assay previously described [30,33] in which two additional dyes of different size are added to GUVs preincubated with BCL-2 proteins that have induced pores. If the dyes are still able to enter the vesicles, this indicates that the membrane permeabilized state is stable at least during the incubation time.

We incubated MITOMix-derived GUVs for 45 min with BOK^{ΔC} plus cBID in the presence of free AlexaFluor-555 (AF555) dye. Immediately after that we added cyt. *c*₄₈₈ and APC to the wells and

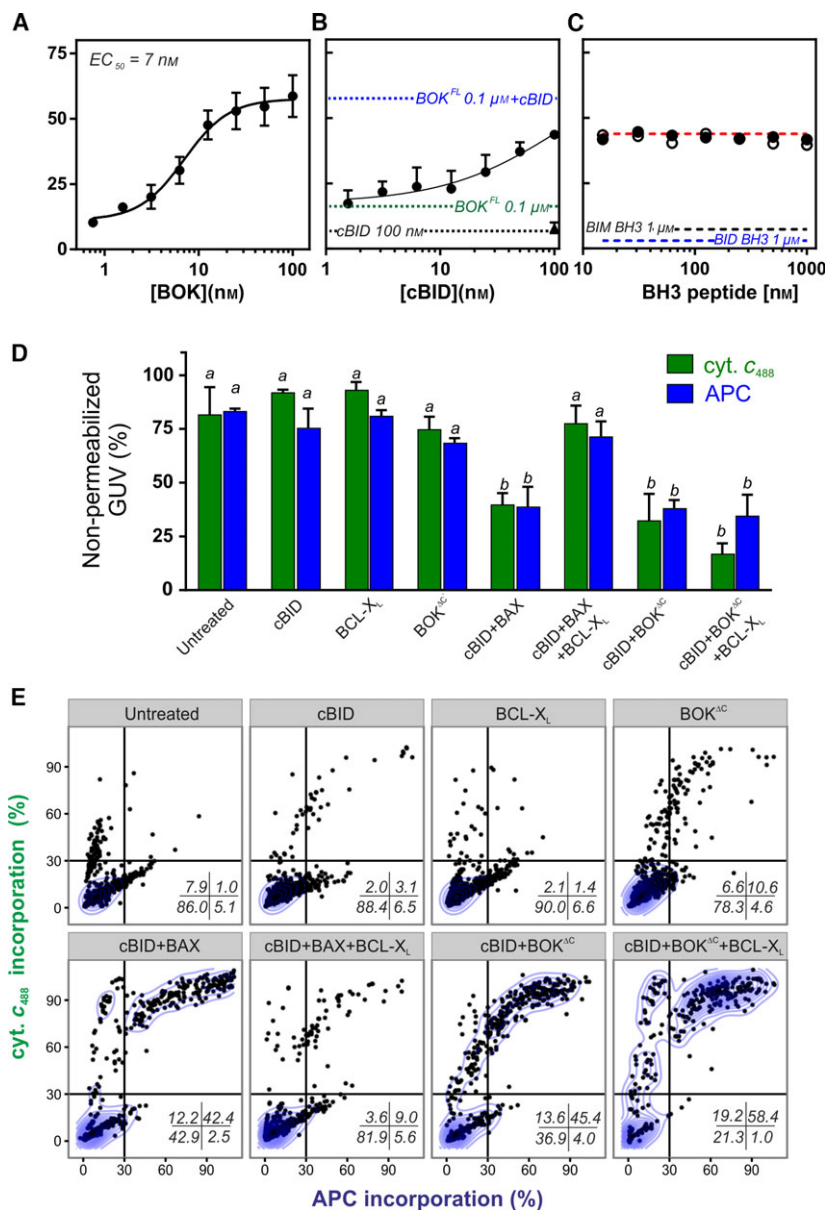


Fig. 3. BOK AC -mediated vesicle permeabilization is enhanced by cBID and allows the passage of molecules of up to 104 kDa. (A) Determination of EC_{50} value for BOK AC in PC : CL 80 : 20 vesicles. (B) Calcein release from PC : CL 80 : 20 liposomes using BOK AC at the EC_{50} concentration and variable amounts of cBID or (C) increasing concentration of BH3 peptides. Dashed lines represents the maximum calcein release promoted by 100 nM cBID, 0.1 μM full-length BOK \pm 50 nM cBID, or 1 μM of the indicated BH3 peptides. (D) Fraction of nonpermeabilized GUV to cyt. c_{488} (12 kDa) or APC (104 kDa) 60 min after treatment with different combinations of cBID (10 nM), BOK AC (10 nM), BCL- X_L (50 nM), and BAX (20 nM). Bars correspond to mean \pm SEM; $N = 3$. (E) Percentage of filling degree to the indicated fluorescent proteins for each individual vesicle across the indicated treatments. The percentage of GUV on each quadrant is indicated. Statistical differences were calculated with a two-way ANOVA correcting the P -values using the Benjamini–Krieger–Yekutieli method. Shared letters indicate nonsignificant differences with P -values of at least 0.05.

determined their incorporation into the vesicles within 15 min. This narrow time window guaranteed that vesicles filled with these proteins were most likely due to the existence of a preformed pore rather than to newly formed ones. Finally, the samples were imaged

in order to detect whether cyt. c_{488} and APC could also trespass the membrane through the formed pores (Fig. 5A), which would be indicative of cBID/BOK AC creating long-lived pores. Moreover, this experiment provides information about the pore size under

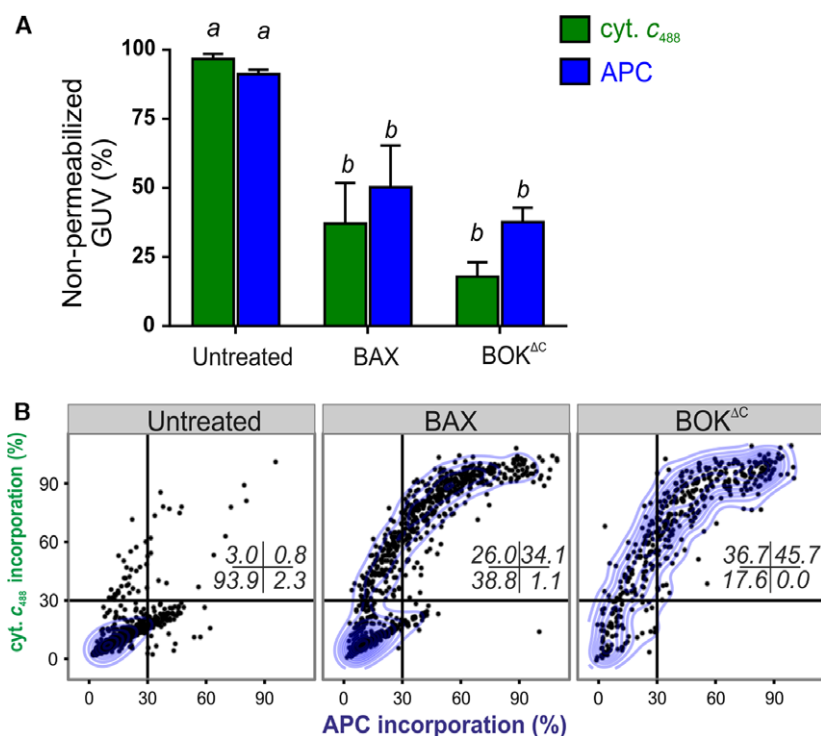


Fig. 4. BOK^{ΔC} can be activated by temperature. (A) Percentage of nonpermeabilized MITOMix-derived GUVs to cyt. *c*₄₈₈ and APC after incubation at 42 °C for 45 min with 20 nM BAX or 10 nM BOK. Bars correspond to mean ± SEM; *N* = 3. (B) Percentage of filling degree to the indicated fluorescent proteins for each individual vesicle across the treatments. The percentage of GUV on each quadrant is indicated. Statistical differences were calculated with a two-way ANOVA correcting the *P*-values using the Benjamini–Krieger–Yekutieli method. Shared letters indicate nonsignificant differences with *P*-values of at least 0.05.

equilibrium conditions and tests the impact of BOK^{ΔC} concentration on the pore size.

The distribution of AF555 incorporation into GUVs was quantified (Fig. 5B). As expected from the experiments shown above, GUV permeabilization positively correlated with the amount of BOK^{ΔC} used. Interestingly, we noticed a decrease of GUVs per area, proportional to the concentration of BOK^{ΔC} (Fig. 5C). We attribute this to the membrane destabilizing impact of the pore formation process, which, combined with the mechanical stress provided while adding the size markers, contribute to GUV destruction. A less pronounced, but still similar effect has been reported for BAX [30]. Afterwards, we focused on GUVs already filled with AF555, which indeed consistently incorporated cyt. *c*₄₈₈ and APC. These results indicate that the initial pores remained permissive and stable during the time of the assay (Fig. 5D,E).

BOK^{ΔC} is inefficient in releasing cyt. *c* from isolated mitochondria

As the membrane activity of BOK^{ΔC} was comparable to that of BAX, we next wanted to determine

whether the BOK^{ΔC} pore-forming activity demonstrated *in vitro* had biological implications in the context of mitochondria. We explored if recombinant BOK^{ΔC} could mediate cyt. *c* release from mitochondria isolated from *Bax*^{-/-}*Bak*^{-/-} mouse embryo fibroblasts (MEF). Of note, and contrary to our findings in artificial lipid vesicles, BOK^{ΔC} was unable to permeabilize these mitochondria, even in the presence of cBID (Fig. 6A). Furthermore, we incubated *Bax*^{-/-}*Bak*^{-/-} mitochondria with BOK^{ΔC} at 43 °C to recapitulate the heat activation process [31]. Surprisingly, and in contrast to BAX, BOK^{ΔC} was again unable to promote MOMP in those mitochondria (Fig. 6B). Strikingly, this lack of activity on mitochondria was not the result of impaired interaction with the membrane, as we clearly detected association of BOK^{ΔC} with crude mitochondrial membranes isolated from *Bok*^{-/-} cells (Fig. 6C). This was also corroborated by sucrose gradient fractionation after coincubation of BOK^{ΔC} with crude BOK-deficient mitochondrial fractions. In this case, BOK^{ΔC} adopted a uniform distribution gradient not restricted to the mitochondria containing fractions, irrespective of the addition of cBID (Fig. 6D).

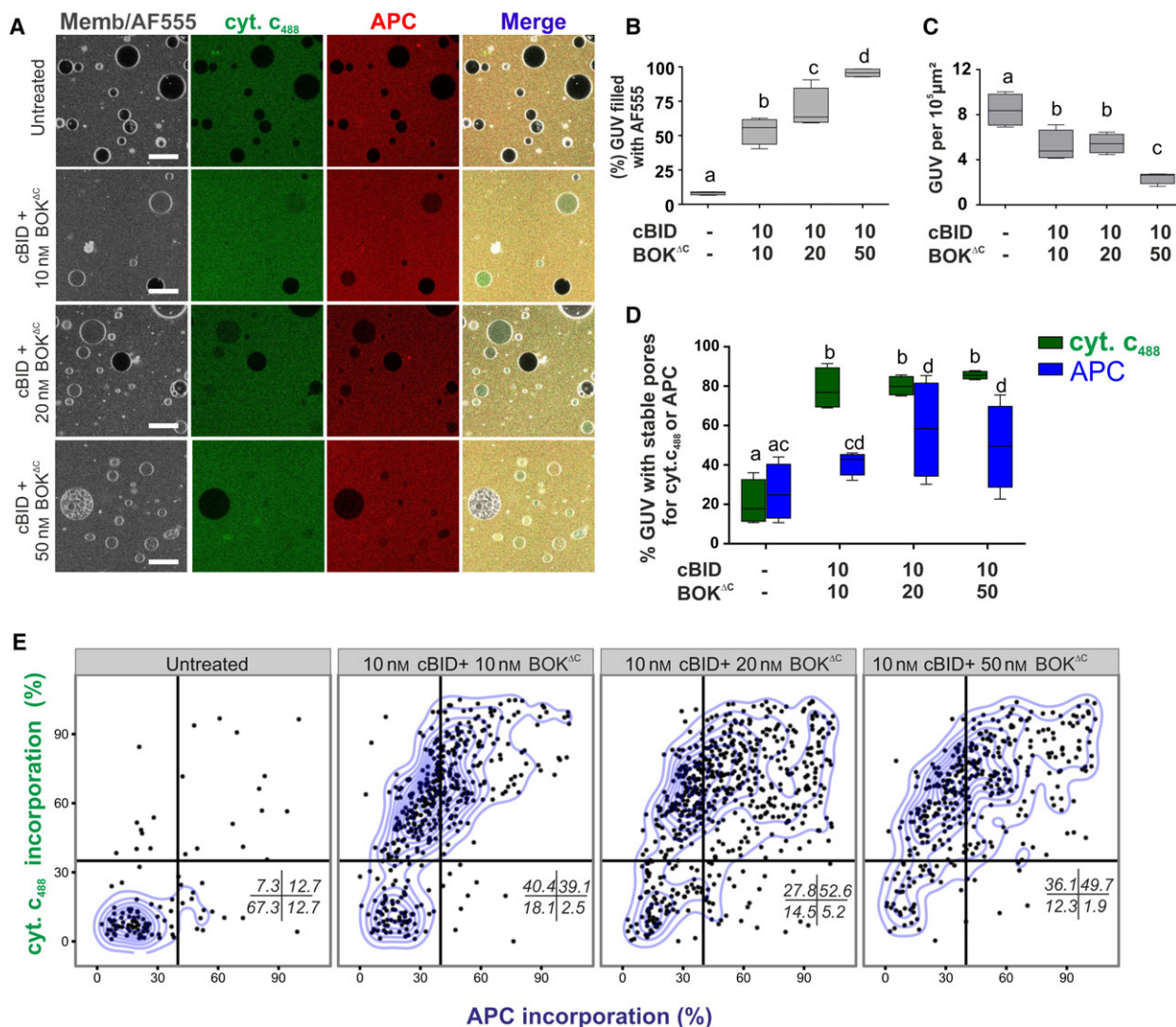


Fig. 5. Pores formed by BOK $^{\Delta C}$ are stable over time. (A) Representative pictures for the MITOmix-made GUV incubated during 45 min with the indicated proteins in the presence of AF555, followed by addition of cyt. c_{488} and APC. Bars represent 50 μm . (B) Determination of the AF555 degree of incorporation into the GUV using a filling threshold of 50%. (C) Number of GUV per area across the treatments. (D) Filling degree to cyt. c_{488} and APC in those GUVs already filled with AF555 (> 50%). (E) Percentage of filling degree to the indicated fluorescent proteins on each individual vesicle across the samples. Whiskers cover 10th–90th percentile; $N = 4$. Statistical differences were calculated with a one-way (B, C) or two-way ANOVA correcting the P -values using the Benjamini–Krieger–Yekutieli method. Shared letters indicate nonsignificant differences with P -values of at least 0.05.

Discussion

BOK remains an enigmatic and controversial protein among the BCL-2 members. In accordance with its sequence homology with BAX/BAK, multiple studies, including our own work, demonstrated that BOK promotes intrinsic apoptosis upon overexpression [11,12,14,34]. However, both BAX/BAK-dependent as well as BAX/BAK-independent mechanisms have been proposed since [12,14,34]. Currently, there is limited evidence for a proapoptotic role for BOK under

physiological and pathophysiological conditions, and several studies even point toward protective roles of BOK in certain tissues or in response to specific stressors [12,13,16–19,34–36].

We describe an approach to purify recombinant BOK from bacteria, combining affinity and ion exchange-based techniques. In our exploratory experiments, we used full-length BOK, and detected comparable pore activity to the truncated protein (data not shown). However, we could not exclude that the

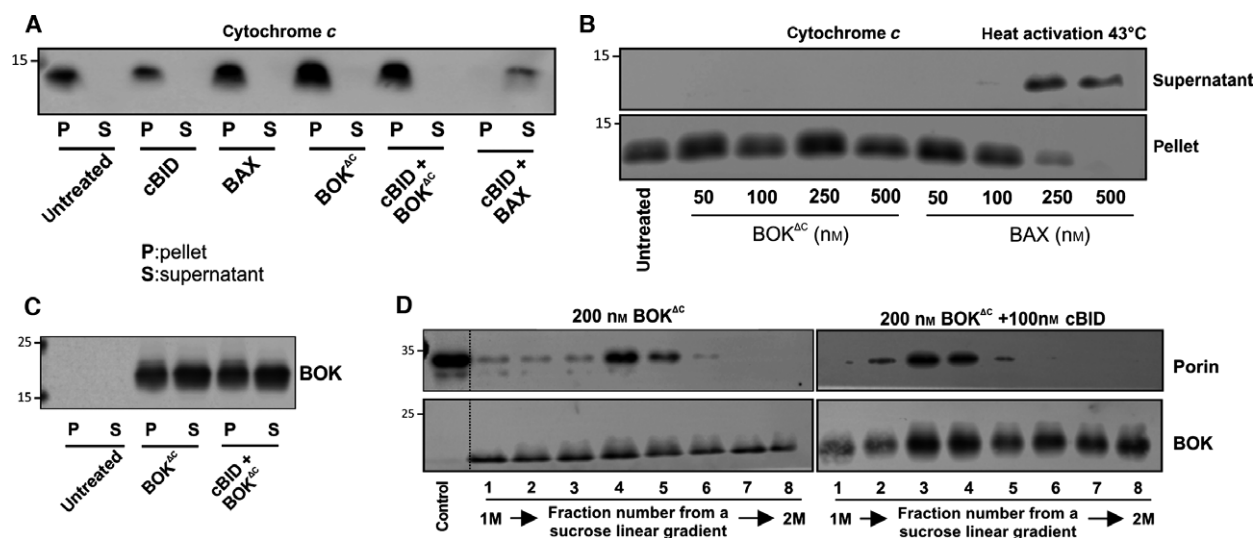


Fig. 6. Binding of BOK^{ΔC} to isolated BAX/BAK-deficient mitochondria is not sufficient for cytochrome *c* release. Mitochondria isolated from *Bax*^{-/-}*Bak*^{-/-} (A, B) or *Bok*^{-/-} (C, D) SV40 MEF were incubated during 1 h at 37 °C (A, C, D) or 43 °C (B) with combinations of 50 nM cBID, 100 nM BOK^{ΔC}, or 100 nM BAX; unless indicated otherwise. The release of cytochrome *c* (A, B) was assessed immediately after the assay by immunoblotting of pellet (mitochondria) and supernatant fractions, respectively. (C) BOK^{ΔC} interacts with membranes in mitochondrial preparation independent of the presence of cBID. (D) BOK^{ΔC} interacts with intracellular membranes not restricted to mitochondria and irrespective of the presence of cBID. Presented data are representative of at least three independent experiments.

insertion of the transmembrane region simply following thermodynamic principles was responsible for this effect. Thus, we decided to use an untagged, truncated version lacking the last 24 amino acids (BOK^{ΔC24}, [12]), which resulted also in higher yields and purity.

Interestingly, BOK seems to predominantly localize to the membranes of the ER, where it interacts with IP3 receptors, and where it is subject to ubiquitylation and proteasomal turnover [12,14,20,21]. In spite of this, addressing the question whether BOK can permeabilize the mitochondrial outer membrane and induce MOMP in a manner similar to BAX/BAK seems absolutely critical to better understand the role and function of BOK. In a recent study, Llambi *et al.* [14] have provided evidence that recombinant BOK (more precisely an 8xHis-tagged, C-terminally truncated version) can have pore-forming activity in liposomes, which, intriguingly, does not seem to require cooperation with activator BH3-only proteins (e.g., tBID). However, the ability to permeabilize membranes has also been reported for other BCL-2 proteins, like BCL-X_L, BCL-2, or cBID, with lack of correlation regarding a direct function in MOMP and therefore caution is advised with the interpretation of simple experiments of liposome permeabilization.

In this work, we analyzed in detail the pore-forming potential of recombinant BOK^{ΔC} in artificial liposomes and isolated mitochondria. We confirmed the recently described ability of BOK^{ΔC} to permeabilize artificial

membranes on its own [14] and demonstrate that the main features of BOK pore activity resemble those of BAX and BAK. The lipid composition of biomembranes strongly defines critical physicochemical properties like overall charge, intrinsic curvature, and fluidity. A concerted interplay of these parameters with membrane proteins guarantees important physiological processes, e.g., membrane fission and fusion, organelle shape, or protein–lipid segregation in microdomains [37]. Our data from calcein assays indicated that BOK^{ΔC} permeabilized vesicles in function of their overall negative charge and greatly depending on the intrinsic curvature of those membranes. This link on lipid composition and activity of BCL-2 proteins has been documented as a key determinant of BAX, BAK, BIM, and BID activities [5,9,10].

Further evaluation of BOK^{ΔC}-mediated pores in GUVs indicated that they have sufficient size to allow the passage of large proteins like cyt. *c* and APC, and that those pores remain stable over time, resembling those described for BAX [23]. This, together with the large dependence on lipid geometry, strongly suggests that the membrane pores induced by BOK are toroidal. As with BAX, our data support the participation of lipids in the pore structure as well as the formation of flexible, undefined pores that reach large sizes and remain open for a long time. Additional studies will be required to elucidate if BOK pores are also tunable in size [30] and correlate with a mixture of BOK

oligomeric species [32], as well as if arc- and/or ring-like assemblies of BOK line the pore walls [38]. Importantly, however, and in contrast to BAX plus cBID, BOK or BOK plus cBID induced pores independently of the presence of BCL-X_L.

Of note, we demonstrate here that cBID, but not its derived BH3-peptide, cooperates with BOK^{ΔC} to induce permeabilization of artificial membranes modeling the mitochondrial lipid composition. This cooperation was noticeable beyond the point of equimolarity between the proteins, suggesting that cBID is less efficient in promoting BOK activity than in activating BAX. This result contrasts with the data provided by Llambi *et al.* [14] who concluded that BOK is constitutively active, independently of the influence of activator BH3-only proteins, or any other BCL-2 protein. While we used untagged BOK^{ΔC}, Llambi *et al.* used an 8xHis-tagged BOK^{ΔC}, which was then artificially aggregated using Ni-NTA. It is conceivable to speculate that Ni-NTA may very strongly activate BOK, thereby masking a possible cooperative effect by BH3-only peptides. Importantly, we further provide evidence that cBID also cooperates with full-length BOK.

We also report that the pore activity of cBID/BOK^{ΔC} is not inhibited by BCL-X_L. This is unexpected, as based on the literature, BCL-X_L should sequester cBID, thereby preventing the activation of BOK^{ΔC}. We speculate that the interaction between cBID and BOK^{ΔC} induces conformational changes hindering the interaction between cBID and BCL-X_L. A direct inhibition of BOK^{ΔC} by BCL-X_L on the other hand seems unlikely, as others and we have failed to show interaction between these two proteins [11,12,39]. Considering the 'helix-loop-helix' secondary structure of BOK and its pore-forming activity, we hypothesized that cBID function could be substituted by administration of heat. The incubation of BOK^{ΔC} and BAX with mildly increased temperatures indeed provided enough energy to induce conformational changes responsible for their insertion in the lipid bilayer. Interestingly, in cells stressed by heat, BAX undergoes conformational changes, translocation to the mitochondria and apoptosis characterized by a significant calcium dyshomeostasis [40]. A thrilling possibility emerging from this stress model is that BOK might be also activated by the treatment, thus compromising the calcium homeostasis in the cell during cell death.

An intriguing result from our work is that, despite of all the above *in vitro* evidence of BOK^{ΔC} being able to permeabilize artificial membranes, we did not find evidence for BOK^{ΔC}-mediated cyt. *c* release from enriched mitochondrial fractions derived from *Bax*^{-/-}/*Bak*^{-/-} MEFs, not even when cBID was added or heat

was provided to the reaction mixture. This result contrasts with reports that BOK can trigger the intrinsic apoptotic pathway independently of BAX/BAK [14,34]. However, neither of those studies provided direct proof of cyt. *c* release by recombinant BOK on isolated mitochondria. Our data indicate that the activity of BOK^{ΔC} in biological membranes might be subjected to important negative regulatory steps or factors overlooked in our assay that deserve further investigation. It remains further possible that, despite its *in vitro* pore-forming potential, BOK^{ΔC} fails to remodel the mitochondria outer membrane in a way compatible with the release of cyt. *c* from the intermembrane space. Additionally, we cannot ignore the possibility that BOK may need its C-terminal tail-anchor for its full activity in mitochondria, despite reports that the C terminus does not seem to be necessary for BAK [31,41] or BAX [42,43] to release cyt. *c* from isolated mitochondria.

Given that BOK does not dominantly localize to mitochondria and that it does not efficiently release cyt. *c* from them when isolated and in the absence of BAX/BAK, we cannot discard the possibility that MOMP induction may not be the main function of BOK. Considering the nature of the effects when BOK interacts with membranes, it seems conceivable that one main function of BOK could be related with the stabilization of regions of high membrane curvature, which may include nonlamellar structures and membrane pores. As most BOK is located at the ER, where it has been shown to interact with IP3R and maybe to play a role in calcium homeostasis, one possibility might be that BOK acts at the ER/mitochondrial contact sites. These sites are responsible for calcium exchange between ER and mitochondria, are enriched in IP3R, and likely involve special membrane structures that allow lipid exchange. The presence of BOK at these sites may also allow their regulation by cBID during apoptosis. Although our work sheds light on the molecular mechanism of BOK at the membrane and opens new research possibilities, additional efforts will be required to connect the mechanism of action of BOK with its biological function.

Taken together, we show that BOK^{ΔC} forms large and stable pores in model membranes, and that BOK^{ΔC} (and likely full-length BOK) activity is cooperatively enhanced by cBID but not blockable by BCL-X_L. However, cyt. *c* release from isolated BAX/BAK-deficient mitochondria by BOK^{ΔC} (with or without cBID) was inefficient compared to BAX/cBID. Although the membrane activity of both proteins in model membranes is very similar, the latter observation clearly distinguishes the properties of BOK^{ΔC} from those of BAX (and BAK).

Experimental procedures

Protein expression and purification

pCMV6 containing the full-length mouse *Bok* cDNA (NM_016778.3) was purchased from Origene (SKU: MC206561, Rockville, MD, USA). The *Bok* CDS was cloned into the *SapI* restriction sites of the pTXB1 plasmid (New England Biolabs, Ipswich, MA, USA), containing the intein–chitin-binding domain tag, according to the manufacturer's instructions and sequences confirmed (Microsynth, Balgach, Switzerland). A truncated version of BOK lacking the C-terminal 24 amino acids (BOK^{ΔC}) was created by PCR using the primers 5'-TGCATCACGGGA GATGCA-3' and 5'-GTGGGAGCGGAAGCCAGGA-3'. A 5 L culture of BL21-CodonPlus (DE3)-RIPL *E. coli* strain (Agilent Technologies, Santa Clara, CA, USA) harboring the pTXB1-BOK^{ΔC} construct was prepared in selective Terrific Broth media (100 μg·mL⁻¹ ampicillin, 30 μg·mL⁻¹ chloramphenicol) and protein expression was induced at 20 °C for 5 h with 1 mM IPTG. The bacterial pellet was collected, resuspended in Chitin Buffer (1 M NaCl, 20 mM Tris/HCl, pH 8.5) supplemented with Complete Protease Inhibitor Cocktail® (Roche Diagnostics AG, Rotkreuz, Switzerland) and disrupted at 11 000 p.s.i in an Emulsiflex-C5 homogenizer (AVESTIN Europe GmbH, Mannheim, Germany). The lysate was cleared and recombinant BOK^{ΔC} captured with chitin beads (New England Biolabs, Hitchin, UK), followed by DTT-induced intein autolysis during 16 h at 4 °C. The protein was eluted, dialyzed, and further purified by a cation-exchange chromatography using a HiTrap SP FF column (GE Healthcare, Europe, Glattbrugg, Switzerland). Purity, yield, and protein identity were assessed by densitometric analysis of Coomassie-stained SDS/PAGE gels using IMAGEJ [44], protein quantification using the Bradford reagent, western blot (using an in-house rabbit monoclonal anti-BOK antibody, RabMab BOK-1-5 [12]), and mass spectrometry, respectively. Protein purity was > 90% (see also Fig. 1B, D), except for studies of the influence of the lipid composition BOK membrane activity (Fig. 2), where a slightly less pure batch of BOK^{ΔC} was used. Cleaved cBID (complex of fragments p7 and p15), BAX, and BCL-X_L were expressed in *E. coli* and purified as previously described [4,23,30].

Preparation of artificial membranes

All the lipids used in this study were purchased from Avanti Polar Lipids (Hamburg, Germany), resuspended in chloroform and mixed at the indicated ratios (w/w). LUVs were prepared as described elsewhere [45]. Briefly, each lipid mixture was vacuum dried and resuspended in a solution of 80 mM calcein, pH 7.0 to a final concentration of 4 mg·mL⁻¹ followed by five cycles of freeze/thawing in liquid nitrogen. The resulting multilamellar vesicles were extruded 31 times

through a 400 μm polycarbonate membrane using a Liposo-Fast manual emulsifier (AVESTIN Europe GmbH). The nonencapsulated calcein was removed from the mixture using a Sephadex-G50 column previously equilibrated with DPBS from Sigma-Aldrich (Buchs, Switzerland). Special lipid mixtures modeling the composition of the mitochondrial membrane (MITOmix; PS : CL : PI : PC : PE, 10 : 8 : 11 : 46 : 25) [23] or the endoplasmic reticulum (ERmix; Sph : PS : PI : PC : PE, 4 : 4 : 10 : 57 : 25) [46] were prepared according to the reported composition. GUVs were prepared as previously described [33]. Shortly, 5 μL of a 1 mg·mL⁻¹ lipid-chloroform solution containing the dye Dil (< 0.05%; Thermo Fisher Scientific, Waltham, MA, USA) was layered in two platinum electrodes, air-dried, and immersed in a Teflon chamber containing 300 mM sucrose. The electrodes were wired to a function generator power source and the GUVs were electro-formed by sequential application of 10 Hz, for 2 h and 2 Hz for 30 min.

Calcein release assay

Calcein-loaded LUVs were incubated with serial dilutions of the recombinant proteins or BH3 peptides corresponding to BIM or BID proteins in a fluorescent-compatible 96-well microtiter plate (NUNC, Wiesbaden, Germany). Calcein release was monitored by fluorescence emission at 520 nm ($\lambda_{\text{excitation}} = 495 \text{ nm}$) during 2 h in an Infinite M200 plate reader (Tecan, Mainz, German). The percentage dye release was calculated as follows:

$$\text{Calcein}_{\text{release}} (\% \text{ of max}) = 100 \times \frac{(F^{\text{Sample}} - F^{\text{Buffer}})}{(F^{\text{TX100}} - F^{\text{Buffer}})},$$

where all the terms refer to the maximum fluorescence registered in the wells incubated with the studied proteins (F^{Sample}), with 0.125% Triton-X100 (F^{TX100}) or DPBS (F^{Buffer}). The maximum values were obtained by curve fitting to a hyperbole, or in those cases where calcein self-quenched due to a massive release, it was assigned to the maximum value before the quenching started. The effective concentration of BOK^{ΔC} was corrected between batches according to the individual EC₅₀ values. The sequences for the BH3 peptides are the following: BID-BH3(IARHLAQVGDMSD), BIM-BH3(IAQLRRIGDEFN).

GUV permeabilization experiments

Giant unilamellar vesicle permeabilization assays were performed according to [23]. Briefly, 70 μL of GUVs made from MITOmix were incubated at 25 °C for 1 h in a casein-coated LabTec chamber (NUNC) containing cyt. *c*₄₈₈, APC, and the studied proteins dissolved in DPBS. The total volume in each reaction chamber is 300 μL. After the incubation time, at least five pictures of each condition

were taken using a LSM710 microscope with a C-Apochromat 40 1.2 water immersion objective (Zeiss, Oberkochen, Germany). A similar setup was prepared for the heat activation of BOK^{ΔC} in GUVs, just setting the reaction temperature to 42 °C for 45 min, before allowing the samples to cool down to RT before the pictures were taken. The evaluation of the pore stability was adapted from Bleicken *et al.* [30]. Shortly, GUVs were incubated for 45 min at RT with or without the indicated BCL-2 proteins in DPBS containing AF555 as an indicator of the permeabilization status of the vesicles. Afterwards, cyt. *c*₄₈₈ and APC were added to the mixture and the pictures were taken 15 min later. For each experiment, the GUVs permeabilization degree to the analyzed dyes was determined using the GUVs detector software available at <http://www.ifib.uni-tuebingen.de/research/garcia-saez/guv-software.html> [47]. The threshold for considering a GUV permeated was arbitrarily set at 30% with the exception of the pore stability assays where it was set up to 50%, 35%, and 40% for AF555, cyt. *c*₄₈₈, and APC, respectively. Data were analyzed using R version 3.2.1 [48] and visualized using the ggplot2 package [49].

Mitochondria isolation

Cell cultures in exponential growth phase of *Bax*^{-/-}*Bak*^{-/-} SV40 large T antigen immortalized mouse embryo fibroblasts (SV40 MEF) were trypsinized, washed with DPBS, and incubated for 15 min in MB buffer [210 mM mannitol, 70 mM sucrose, 1 mM EDTA, 10 mM HEPES pH 7.5 supplemented with Complete Protease Inhibitor Cocktail (Roche)]. The cells were manually disrupted by 18 passages through a 27 G needle, and the debris was removed by centrifugation at 2500 *g* (3 × 5 min). The mitochondria-enriched fraction was obtained by centrifugation for 10 min at 10 000 *g*, resuspended in MB-EGTA buffer (MB buffer with 1 mM EGTA instead of EDTA) and its protein concentration determined by Bradford assay (Biorad, Cressier, Switzerland). The mitochondrial preparations were immediately used for the cyt. *c* release assays.

Cytochrome *c* release assays

Cytochrome *c* release from mitochondria was performed as previously reported [50]. Briefly, 30 μg of mitochondria was incubated with the following protein amounts unless indicated otherwise (100 nM BOK^{ΔC}, 50 nM cBID, 100 nM BAX) in KCL buffer (125 mM KCl, 4 mM MgCl₂, 5 mM KH₂PO₄, 10 mM HEPES pH 7.4, 0.5 mM EGTA) for 60 min at 37 °C. The supernatant was collected and the pellet was washed with KCl buffer, followed by addition of Laemmli buffer. For the experiments using heat-activated BOK^{ΔC}, we proceeded as described by [31] with minor modifications. Shortly, the recombinant proteins were heated at 43 °C for 1 h in the presence of the isolated mitochondria in KCL buffer.

Pellet and supernatant were separated afterwards by centrifugation. The presence of cyt. *c* in the fractions was determined by western blotting using a mouse monoclonal anti-cyt. *c* antibody (BD Biosciences, San Jose, CA, USA, clone 7H8.2C12).

Membrane binding assays

Crude mitochondria preparations from *Bok*^{-/-} SV40 MEF were incubated with the indicated combinations of recombinant proteins (200 nM BOK^{ΔC}, 100 nM cBID) at 37 °C for 1 h. Afterwards the samples were fractionated by centrifugation or linear sucrose gradient (1–2 M). The samples processed by sucrose gradient were ultracentrifuged at 50 000 *g* in a swinging bucket SW41 rotor (Beckman Coulter, Nyon, Switzerland) during 90 min. The gradients were then split into 1 mL fractions and precipitated using methanol/chloroform. The distribution of the recombinant proteins across the gradient was detected by western blotting using the corresponding antibodies: rabbit monoclonal anti-BOK (RabMab BOK-1-5 [12]), rabbit polyclonal anti-BAX (Santa Cruz Biotechnology, Dallas, TX, USA, sc-493), and mouse monoclonal anti-porin (Merck Millipore, Zug, Switzerland, clone 89-173/016).

Acknowledgements

We thank Caroline Stegmüller for the exceptional technical support and Dr Christoph Borner (Freiburg, Germany) for *Bax*^{-/-}*Bak*^{-/-} MEF. This work was supported by the Swiss National Science Foundation (SNF), Grant 310030E150805, part of the D-A-CH initiative from the SNF and the Deutsche Forschungsgemeinschaft (DFG), FOR-2036 (to TK) and the DFG GA1641/2-1 (to AJGS). YFM is a PhD student of the Graduate School of Cellular and Biomedical Sciences of the University of Bern. SB and AJGS were additionally supported by European Research Council (ERC-2012-StG-309966) and SB by the Cluster of Excellence RESOLV (EXC 1069) funded by the DFG.

Author contributions

YFM performed most of the experiments, analyzed data, and wrote the manuscript. SB planned and performed experiments, analyzed data, and wrote the manuscript. KKD and DB performed experiments and analyzed data. AJGS and TK designed the study, planned the experiments, and wrote the manuscript.

Conflict of interest

The authors declare no conflict of interests.

References

- 1 Youle RJ & Strasser A (2008) The BCL-2 protein family: opposing activities that mediate cell death. *Nat Rev Mol Cell Biol* **9**, 47–59.
- 2 Newmeyer DD & Ferguson-Miller S (2003) Mitochondria: releasing power for life and unleashing the machineries of death. *Cell* **112**, 481–490.
- 3 Willis SN, Chen L, Dewson G, Wei A, Naik E, Fletcher JI, Adams JM & Huang DC (2005) Proapoptotic Bak is sequestered by Mcl-1 and Bcl-xL, but not Bcl-2, until displaced by BH3-only proteins. *Genes Dev* **19**, 1294–1305.
- 4 Bleicken S, Classen M, Padmavathi PV, Ishikawa T, Zeth K, Steinhoff HJ & Bordignon E (2010) Molecular details of Bax activation, oligomerization, and membrane insertion. *J Biol Chem* **285**, 6636–6647.
- 5 Chipuk JE, McStay GP, Bharti A, Kuwana T, Clarke CJ, Siskind LJ, Obeid LM & Green DR (2012) Sphingolipid metabolism cooperates with BAK and BAX to promote the mitochondrial pathway of apoptosis. *Cell* **148**, 988–1000.
- 6 Raemy E & Martinou JC (2014) Involvement of cardiolipin in tBID-induced activation of BAX during apoptosis. *Chem Phys Lipids* **179**, 70–74.
- 7 Lucken-Ardjomande S, Montessuit S & Martinou JC (2008) Contributions to Bax insertion and oligomerization of lipids of the mitochondrial outer membrane. *Cell Death Differ* **15**, 929–937.
- 8 Kuwana T, Mackey MR, Perkins G, Ellisman MH, Latterich M, Schneider R, Green DR & Newmeyer DD (2002) Bid, Bax, and lipids cooperate to form supramolecular openings in the outer mitochondrial membrane. *Cell* **111**, 331–342.
- 9 Shamas-Din A, Bindner S, Chi X, Leber B, Andrews DW & Fradin C (2015) Distinct lipid effects on tBid and Bim activation of membrane permeabilization by pro-apoptotic Bax. *Biochem J* **467**, 495–505.
- 10 Raemy E, Montessuit S, Pierredon S, van Kampen AH, Vaz FM & Martinou JC (2016) Cardiolipin or MTCH2 can serve as tBID receptors during apoptosis. *Cell Death Differ* **23**, 1165–1174.
- 11 Hsu SY, Kaipia A, McGee E, Lomeli M & Hsueh AJ (1997) Bok is a pro-apoptotic Bcl-2 protein with restricted expression in reproductive tissues and heterodimerizes with selective anti-apoptotic Bcl-2 family members. *Proc Natl Acad Sci USA* **94**, 12401–12406.
- 12 Echeverry N, Bachmann D, Ke F, Strasser A, Simon HU & Kaufmann T (2013) Intracellular localization of the BCL-2 family member BOK and functional implications. *Cell Death Differ* **20**, 785–799.
- 13 Ke F, Voss A, Kerr JB, O'Reilly LA, Tai L, Echeverry N, Bouillet P, Strasser A & Kaufmann T (2012) BCL-2 family member BOK is widely expressed but its loss has only minimal impact in mice. *Cell Death Differ* **19**, 915–925.
- 14 Llambi F, Wang YM, Victor B, Yang M, Schneider DM, Gingras S, Parsons MJ, Zheng JH, Brown SA, Pelletier S *et al.* (2016) BOK is a non-canonical BCL-2 family effector of apoptosis regulated by ER-associated degradation. *Cell* **165**, 421–433.
- 15 Elsayed MM & Cevc G (2011) The vesicle-to-micelle transformation of phospholipid-cholate mixed aggregates: a state of the art analysis including membrane curvature effects. *Biochim Biophys Acta* **1808**, 140–153.
- 16 Ke F, Bouillet P, Kaufmann T, Strasser A, Kerr J & Voss AK (2013) Consequences of the combined loss of BOK and BAK or BOK and BAX. *Cell Death Dis* **4**, e650.
- 17 Ke F, Grabow S, Kelly GL, Lin A, O'Reilly LA & Strasser A (2015) Impact of the combined loss of BOK, BAX and BAK on the hematopoietic system is slightly more severe than compound loss of BAX and BAK. *Cell Death Dis* **6**, e1938.
- 18 Ray JE, Garcia J, Jurisicova A & Caniggia I (2010) Mtd/Bok takes a swing: proapoptotic Mtd/Bok regulates trophoblast cell proliferation during human placental development and in preeclampsia. *Cell Death Differ* **17**, 846–859.
- 19 D'Orsi B, Engel T, Pfeiffer S, Nandi S, Kaufmann T, Henshall DC & Prehn JH (2016) Bok is not pro-apoptotic but suppresses poly ADP-ribose polymerase-dependent cell death pathways and protects against excitotoxic and seizure-induced neuronal injury. *J Neurosci* **36**, 4564–4578.
- 20 Schulman JJ, Wright FA, Kaufmann T & Wojcikiewicz RJ (2013) The Bcl-2 protein family member Bok binds to the coupling domain of inositol 1,4,5-trisphosphate receptors and protects them from proteolytic cleavage. *J Biol Chem* **288**, 25340–25349.
- 21 Schulman JJ, Wright FA, Han X, Zluhan EJ, Szczesniak LM & Wojcikiewicz RJ (2016) The stability and expression level of Bok are governed by binding to inositol 1,4,5-trisphosphate receptors. *J Biol Chem* **291**, 11820–11828.
- 22 Suzuki M, Youle RJ & Tjandra N (2000) Structure of Bax: coregulation of dimer formation and intracellular localization. *Cell* **103**, 645–654.
- 23 Bleicken S, Wagner C & Garcia-Saez AJ (2013) Mechanistic differences in the membrane activity of Bax and Bcl-xL correlate with their opposing roles in apoptosis. *Biophys J* **104**, 421–431.
- 24 Champion KM, Nishihara JC, Joly JC & Arnott D (2001) Similarity of the *Escherichia coli* proteome upon completion of different biopharmaceutical fermentation processes. *Proteomics* **1**, 1133–1148.
- 25 Wu S, Wan P, Li J, Li D, Zhu Y & He F (2006) Multimodality of pI distribution in whole proteome. *Proteomics* **6**, 449–455.

- 26 Adhikari S, Manthana PV, Sajwan K, Kota KK & Roy R (2010) A unified method for purification of basic proteins. *Anal Biochem* **400**, 203–206.
- 27 Fosnarić M, Bohinc K, Gauger DR, Igljic A, Kralj-Igljic V & May S (2005) The influence of anisotropic membrane inclusions on curvature elastic properties of lipid membranes. *J Chem Inf Model* **45**, 1652–1661.
- 28 Terrones O, Antonsson B, Yamaguchi H, Wang HG, Liu J, Lee RM, Herrmann A & Basanez G (2004) Lipidic pore formation by the concerted action of proapoptotic BAX and tBID. *J Biol Chem* **279**, 30081–30091.
- 29 Bleicken S, Hofhaus G, Ugarte-Urbe B, Schroder R & Garcia-Saez AJ (2016) cBid, Bax and Bcl-xL exhibit opposite membrane remodeling activities. *Cell Death Dis* **7**, e2121.
- 30 Bleicken S, Landeta O, Landajuela A, Basanez G & Garcia-Saez AJ (2013) Proapoptotic Bax and Bak proteins form stable protein-permeable pores of tunable size. *J Biol Chem* **288**, 33241–33252.
- 31 Pagliari LJ, Kuwana T, Bonzon C, Newmeyer DD, Tu S, Beere HM & Green DR (2005) The multidomain proapoptotic molecules Bax and Bak are directly activated by heat. *Proc Natl Acad Sci USA* **102**, 17975–17980.
- 32 Subburaj Y, Cosentino K, Axmann M, Pedrueza-Villalmanzo E, Hermann E, Bleicken S, Spatz J & Garcia-Saez AJ (2015) Bax monomers form dimer units in the membrane that further self-assemble into multiple oligomeric species. *Nat Commun* **6**, 8042.
- 33 Bleicken S & Garcia-Saez AJ (2014) New biophysical methods to study the membrane activity of Bcl-2 proteins. *Methods Mol Biol* **1176**, 191–207.
- 34 Einsele-Scholz S, Malmsheimer S, Bertram K, Stehle D, Johanning J, Manz M, Daniel PT, Gillissen BF, Schulze-Osthoff K & Essmann F (2016) Bok is a genuine multi-BH-domain protein that triggers apoptosis in the absence of Bax and Bak. *J Cell Sci* **129**, 2213–2223.
- 35 Carpio MA, Michaud M, Zhou W, Fisher JK, Walensky LD & Katz SG (2015) BCL-2 family member BOK promotes apoptosis in response to endoplasmic reticulum stress. *Proc Natl Acad Sci USA* **112**, 7201–7206.
- 36 Fernandez-Marrero Y, Ke F, Echeverry N, Bouillet P, Bachmann D, Strasser A & Kaufmann T (2016) Is BOK required for apoptosis induced by endoplasmic reticulum stress? *Proc Natl Acad Sci USA* **113**, E492–E493.
- 37 McMahon HT & Boucrot E (2015) Membrane curvature at a glance. *J Cell Sci* **128**, 1065–1070.
- 38 Salvador-Gallego R, Mund M, Cosentino K, Schneider J, Unsay J, Schraermeyer U, Engelhardt J, Ries J & Garcia-Saez AJ (2016) Bax assembly into rings and arcs in apoptotic mitochondria is linked to membrane pores. *EMBO J* **35**, 389–401.
- 39 Hsu SY & Hsueh AJ (1998) A splicing variant of the Bcl-2 member Bok with a truncated BH3 domain induces apoptosis but does not dimerize with antiapoptotic Bcl-2 proteins in vitro. *J Biol Chem* **273**, 30139–30146.
- 40 Gu ZT, Li L, Wu F, Zhao P, Yang H, Liu YS, Geng Y, Zhao M & Su L (2015) Heat stress induced apoptosis is triggered by transcription-independent p53, Ca(2+) dyshomeostasis and the subsequent Bax mitochondrial translocation. *Sci Rep* **5**, 11497.
- 41 Landeta O, Landajuela A, Gil D, Taneva S, Di Primo C, Sot B, Valle M, Frolov VA & Basanez G (2011) Reconstitution of proapoptotic BAK function in liposomes reveals a dual role for mitochondrial lipids in the BAK-driven membrane permeabilization process. *J Biol Chem* **286**, 8213–8230.
- 42 Priault M, Cartron PF, Camougrand N, Antonsson B, Vallette FM & Manon S (2003) Investigation of the role of the C-terminus of Bax and of tc-Bid on Bax interaction with yeast mitochondria. *Cell Death Differ* **10**, 1068–1077.
- 43 Wieckowski MR, Vyssokikh M, Dymkowska D, Antonsson B, Brdiczka D & Wojtczak L (2001) Oligomeric C-terminal truncated Bax preferentially releases cytochrome c but not adenylate kinase from mitochondria, outer membrane vesicles and proteoliposomes. *FEBS Lett* **505**, 453–459.
- 44 Schneider CA, Rasband WS & Eliceiri KW (2012) NIH Image to ImageJ: 25 years of image analysis. *Nat Methods* **9**, 671–675.
- 45 Garcia-Saez AJ, Coraiola M, Serra MD, Mingarro I, Muller P & Salgado J (2006) Peptides corresponding to helices 5 and 6 of Bax can independently form large lipid pores. *FEBS J* **273**, 971–981.
- 46 Davison SC & Wills ED (1974) Studies on the lipid composition of the rat liver endoplasmic reticulum after induction with phenobarbitone and 20-methylcholanthrene. *Biochem J* **140**, 461–468.
- 47 Hermann E, Bleicken S, Subburaj Y & Garcia-Saez AJ (2014) Automated analysis of giant unilamellar vesicles using circular Hough transformation. *Bioinformatics* **30**, 1747–1754.
- 48 R Core Team (2015) *R: A Language and Environment for Statistical Computing*. R Foundation for Statistical Computing, Vienna, Austria. <http://www.R-project.org/>
- 49 Wickham H (2009) *ggplot2: Elegant Graphics for Data Analysis*. Springer, New York, NY.
- 50 Wilfling F, Weber A, Potthoff S, Vogtle FN, Meisinger C, Paschen SA & Hacker G (2012) BH3-only proteins are tail-anchored in the outer mitochondrial membrane and can initiate the activation of Bax. *Cell Death Differ* **19**, 1328–1336.